Doctoral theses at NTNU, 2020:35

Jing Deng

Optimization of PEG-based membranes and mixed matrix membranes for CO2 capture

Doctoral thesis

Jing Deng

ISBN 978-82-326-4425-4 (printed ver.)
ISBN 978-82-326-4426-1 (electronic ver.)
ISSN 1503-8181

NTNU
Norwegian University of
Science and Technology

Doctoral theses at NTNU, 2020:35

NTNU
Norwegian University of Science and Technology
Thesis for the Degree of
Philosophiae Doctor
Faculty of Natural Sciences
Department of Chemical Engineering

NTNU
Norwegian University of
Science and Technology

Jing Deng

Optimization of PEG-based membranes and mixed matrix membranes for CO2 capture

Thesis for the Degree of Philosophiae Doctor

Trondheim, January 2020

Norwegian University of Science and Technology
Faculty of Natural Sciences
Department of Chemical Engineering

NTNU
Norwegian University of
Science and Technology

NTNU
Norwegian University of Science and Technology

Thesis for the Degree of Philosophiae Doctor

Faculty of Natural Sciences
Department of Chemical Engineering

ISBN 978-82-326-4425-4 (printed ver.)
ISBN 978-82-326-4426-1 (electronic ver.)
ISSN 1503-8181

Doctoral theses at NTNU, 2020:35

Printed by NTNU Grafisk senter

Abstract

To slow down or even realize negative raising rate of the CO_2 atmospheric levels, diminishing the CO_2 emission from diverse large-scale sources has become increasingly urgent. Gas separation membrane technology has long been considered as one of the most promising solution for CO_2 capture due largely to its high energy and cost efficiency, remarkable operational simplicity and reliability and overall environmental compatibility. Polymers have been the major gas separation membrane materials in commercial applications in the past 50 years because of the lower cost and superior processability. However, the performances of current polymeric membranes are still insufficiently to make the membrane process economically comparable to other CO_2 capture technologies (i.e., amine-based absorption). Hence, the objective of this study is to develop a series of highly permeable polymeric membranes for post-combustion CO_2 capture. Two approaches have been employed to achieve this objective.

First of all, cross-linked polyethylene glycol (PEG) membranes with interpenetrating networks have been developed based on click reactions. The single gas permeation results showed that the gas transport properties of the as-prepared membranes are strongly dependent on the cross-linker functionality, the ratio of interpenetrating networks and the length of linear monomers. Within investigated range, the less functionality of cross-linkers results in membranes with higher flexibility, and monomers with longer molecular chain lead to higher CO_2 diffusivity, of which both increase the CO_2 permeability. All the obtained membranes display almost constant CO_2/N_2 ideal selectivity. Moreover, free liquid additives, including low-molecular-weight PEG and several ionic liquids (ILs), have been added into the optimized cross-linked matrix at different loading levels to further enhance gas transport properties. It is found out that the CO_2 permeability greatly increases with the free PEG content, due to the largely enhanced CO_2 diffusivity and the CO_2 solubility. Similar trend has been also obtained for CO_2/N_2 ideal selectivity. The optimization of the polymeric network and the incorporation of free PEG endow significant improvement in CO_2 separation performances: CO_2 permeability rising from 1.54 Barrer to 196.4 Barrer and CO_2/N_2 ideal selectivity rising from 29 to 54, respectively. Furthermore, the effects of adding ILs in cross-linked PEG membranes have also been studied. The characterization results regarding to the material properties and CO_2 separation performances show that the ILs play a different role on the cross-linked PEG membranes, which are greatly affected by the anion. CO_2 permeability firstly decreases at low IL loading (< 20 wt.%) and then increases with further addition of ILs. Further analysis shows that unlike free PEG, the presence of ILs reduces CO_2 diffusivity within the whole studied range. Considering CO_2 solubility, adding ILs into PEG matrix firstly reduces CO_2 solubility at low IL loading, further increasing ILs content may result in an unchanged or higher value, depending on the intrinsic CO_2 affinity of ILs. Hence, the order of increment in CO_2

permeability matches to their CO_2 affinity, which is [Bmim][NTf_2] ≈ [Bmim][TCM] > [Bmim][BF_4]. On the other hand, the CO_2/N_2 selectivity of all cross-linked PEG/IL hybrid membranes decreases with ILs content, regardless of the IL composition and the used cross-linking reactions, mainly because of the intrinsically lower CO_2/N_2 selectivity values of these ILs compared to PEG.

Physically blending zeolitic imidazolate frameworks (ZIFs) particles into polymeric membranes has also been taken as the second approach to improve the membrane performance. Firstly, a series of ZIFs cuboids with controllable thickness have been developed by synthesizing at room temperature in aqueous polymeric solutions, it is found out that the polymeric additives have great effect on the fabricated ZIF's morphologies and properties. Mixed matrix membranes (MMMs) were fabricated by incorporating the obtained ZIF cuboids into Pebax 1657 matrix. The gas separation results show that the addition of ZIFs has positive effects on the overall gas separation performances, due largely to the extra molecular sieving and the increased free volume brought by the ZIFs and the altered polymeric chain packing. The one with the highest thickness (170 nm) exhibits the highest CO_2 permeability (387.2 Barrer, 4.6-fold) with a moderate CO_2/N_2 selectivity (47.1, 2.4-fold) under humidified conditions, compared to the other two analogies. Some of the membrane performance are close to or reach the Robeson upper bound for several gas pairs. Secondly, in addition to the size effects, three ZIFs with different shapes (particle, needle, and leaf) were employed as the fillers in Pebax 2533 to study their influences on the CO_2 separation performance. The gas permeation results show that there exists the optimized ZIFs contents for all Pebax 2533 + ZIFs membranes, which are 10 wt.%, 10 wt.% and 5 wt.% for particle-, needle- and leaf-like ZIFs, respectively. The highest CO_2 permeability obtained from each series are similar, and among them, the performance closest to upper bound in this work is Pebax 2533 + 10 wt.% needle-like ZIF. It is worth mentioning that the leaf-like ZIF suffers severe filler agglomeration and phase separation in membranes at high loading (20 wt.%), but it has comparable gas transport performance to the one containing 10 wt.% needle-like ZIF at lower loading (5 wt.%), which may reduce the cost of membrane materials. Thirdly, two almost identical leaf-like ZIFs with different metal ions have been incorporated into troger base (TB) -based polymers. Despite the similarity in crystal structure and particle morphology of the employed ZIFs, the membranes containing ZIF-L-Co display higher gas permeabilities for all studied gases with similar gas selectivities than TB + ZIF-L-Zn membranes. Combing with the material property results, it is believed that the stiffer Co-N bonds reduce the pore size and thus restrict the transport of big molecules but benefit the small ones. Hence the membranes containing ZIF-L-Co have gained more in H_2 permeability than other gases, which may make these membranes as good candidates for H_2 separation application.

Preface

This thesis is submitted to the Norwegian University of Science and Technology (NTNU) for partial fulfillment of the requirement of the degree of Philosophiae Doctor.

The doctoral work was carried out at the Department of Chemical Engineering, Faculty of Natural Science and Technology, in the period of August 2016 to January 2020. This thesis is supervised by Professor Liyuan Deng.

Acknowledgements

Foremost, I would like to express my sincere gratitude to my supervisor, Professor Liyuan Deng for offering me the opportunity to work in Membrane Research group and the continuous support to my study, research and writing during my whole Ph.D. period. Without her support and guidance through every stage of the process, this journey cannot be finished.

In addition, I would like to thank all the partners in the "PolyMEM" project for the great collaboration in this project and research council of Norway for the funding. Special gratefulness is expressed to Dr. Marius Sandru and Dr. Gina Sandru, for their kind help, valuable advice and following up on the project progress.

My sincere thanks go to Prof. Richard Spontak and his entire group at North Carolina State University for his help and guidance in different but interesting projects, and his entire group for the help I received during my stay as an exchange student. I am also greatly grateful to Dr. Zhongde Dai for his patience to my endless question and time-consuming discussion. His strong work ethic, hard-working, and professionalism have inspired me since the first day we met.

I would like to thank my fellow colleges/friends in the Membrane Research group: Dr. Luca Ansaloni, Dr. Arne Lindbrathen, Dr. Xuezhong He, Mr. Linfeng Lei, Miss Wenqi Xu, Dr. Shamim Haider, Mr. Mahdi Ahmadi, Dr. Maria Teresa Guzman Guitieerrez, Ms. Ragne M Lilleby Helberg, Dr. Gabriel Guerrero Heredia, Mr. Önder Tekinalp, Mr. Saravanan Janakiram, Dr. Mikeal Hammer, and Ms. Gøril Flatberg, for their assistance and support during these years. Moreover, I would like to thank three former master students I have been worked with: Ms. Sandra-Paula Suciu, Mr. JunboYu, and Ms. Alice Busu.

Least but not last, I would like to thank my beloved family and friends for their unconditional love and support through this venture. They ease my anxiety and strengthen my confidence no matter when I needed.

Trondheim, November 2019

Jing Deng

List of Publications

Journal Papers

1. ***Deng, Jing***; Dai, Zhongde; Yan, Jiaqi; Sandru, Marius; Sandru, Eugenia; Spontak, Richard J; Deng, Liyuan; *Facile and solvent-free fabrication of PEG-based membranes with interpenetrating networks for CO_2 separation*, Journal of Membrane Science, 2019, 570, 455
2. ***Deng, Jing***; Yu, Junbo; Dai, Zhongde; Deng, Liyuan; *Cross-linked PEG Membranes of Interpenetrating Networks with ILs as Additives for Enhanced CO_2 Separation*, Industrial & Engineering Chemistry Research, 2019, 58, 13, 5261
3. ***Deng, Jing***; Dai, Zhongde; Deng, Liyuan; *Cross-linked Thiol-ene/Epoxy PEG-based Membranes and the Effects of Ionic Liquids' Addition on CO_2 separation properties*. (Accepted by Journal of Polymer Science)
4. ***Deng, Jing***; Dai, Zhongde; Deng, Liyuan; *Novel MOF nanosheets with tunable thickness and their application in mixed matrix membranes for CO_2 application* (Submitted to Chemistry of Materials)
5. ***Deng, Jing***; Dai, Zhongde; Deng, Liyuan; *Impact of the ZIFs' shape on the CO_2 Separation Performance of MMMs* (To be submitted to ACS Applied Materials & Interfaces)
6. ***Deng, Jing***; Dai, Zhongde; Deng, Liyuan; *H_2-selective Mixed Matrix Membranes Enhanced by 2D MOFs* (Submitted to Journal of Membrane Science)

This thesis is based on the above six papers.

Additional Publications

1. ***Deng, Jing***; Yan, Jiaqi; Tilly, Joseph C; Deng, Liyuan; Mineart, Kenneth P; Spontak, Richard J; *Incorporation of Metallic Species into Midblock-Sulfonated Block Ionomers*, Macromolecular Rapid Communications, 2018, 39, 22, 1800427
2. Dai, Zhongde; ***Deng, Jing***; Peng, Kang-Jen; Liu, Ying-Ling; Deng, Liyuan; *Pebax/PEG Grafted CNT-hybrid Membranes for Enhanced CO_2/N_2 Separation*, Industrial & Engineering Chemistry Research, 2019, 58, 27, 12226
3. Dai, Zhongde; ***Deng, Jing***; Aboukeila, Hesham; Yan, Jiaqi; Ansaloni, Luca; Mineart, Kenneth P; Baschetti, Marco Giacinti; Spontak, Richard J; Deng, Liyuan; *Highly CO_2-permeable membranes derived from a midblock-sulfonated multiblock polymer after submersion in water*, NPG Asia Materials, 2019, 11, 1, 1
4. Dai, Zhongde; ***Deng, Jing***; Yu, Qiang; Helberg, Ragne M Lilleby; Janakiram, Saravanan; Ansaloni, Luca; Deng, Liyuan; *Fabrication and Evaluation of Bio-based Nanocomposite TFC Hollow Fiber Membranes for Enhanced CO_2 capture*, ACS Applied Materials & Interfaces, 2019, 11, 11, 10874
5. Song, Ting; ***Deng, Jing***; Deng, Liyuan; Bai, Lu; Zhang, Xiangping; Zhang, Suojiang; Szabo, Peter; Daugaard, Anders E; *Poly (vinylimidazole-co-butyl acrylate) membranes for CO_2 separation*, Polymer, 2019, 160, 223
6. Dai, Zhongde; ***Deng, Jing***; Ansaloni, Luca; Janakiram, Saravanan; Deng, Liyuan; *Thin-film-composite hollow fiber membranes containing amino acid salts as mobile carriers for CO_2 separation*, Journal of Membrane Science, 2019, 578, 61
7. Dai, Zhongde; Løining, Vilde; ***Deng, Jing***; Ansaloni, Luca; Deng, Liyuan; *Poly (1-trimethylsilyl-1-propyne)-Based Hybrid Membranes: Effects of Various Nanofillers and Feed Gas Humidity on*

CO_2 Permeation, Membranes, 2018, 8, 3, 76

8. Dai, Zhongde; Ottesen, Vegar; ***Deng, Jing***; Helberg, Ragne M Lilleby; Deng, Liyuan; *A Brief Review of Nanocellulose Based Hybrid Membranes for CO_2 Separation*, Fibers, 2019, 7, 5, 40

9. Dai, Zhongde; Aboukeila, Hesham; Ansaloni, Luca; ***Deng, Jing***; Baschetti, Marco Giacinti; Deng, Liyuan; *Nafion/PEG hybrid membrane for CO_2 separation: Effect of PEG on membrane micro-structure and performance*, Separation and Purification Technology, 2019, 214, 67

Conference Presentations

Oral Presentations

1. ***Deng, Jing***; Dai, Zhongde; Deng, Liyuan; *Physically cross-linked PVA/CNC membranes for enhanced CO_2 separation*, Trondheim Conference on CO_2 Capture, Transport and Storage – 10 (TCCS-10), June 2019, Trondheim, Norway;

2. ***Deng, Jing***; Deng, Liyuan; *Membranes are the solution for CO_2 capture*, CLIMIT 2019, January 2019, Oslo, Norway;

3. ***Deng, Jing***; Dai, Zhongde; Sandru, Marius; Deng, Liyuan; *Thiol-ene / epoxy homo-polymerized PEG-based membranes for CO_2 separation*, KIFEE 2018, October 2018, Tromsø, Norway;

4. ***Deng, Jing***; Dai, Zhongde; Sandru, Marius; Deng, Liyuan; *Thiol-ene / epoxy homo-polymerized PEG-based membranes for CO_2 separation*, Euromembrane 2018, June 2018, Valencia, Spain;

5. ***Deng, Jing***; Dai, Zhongde; Yu, Junbo; Sandru, Marius; Deng, Liyuan; *PEG-based membranes with dual cross-linking networks for enhanced CO_2 separation*, The Network Young Membrains 2018, June 2018, Valencia, Spain;

Poster Presentations

1. ***Deng, Jing***; Dai, Zhongde; Busu, Alice; Deng, Liyuan; *Incorporation of polydopamine nanosphere into polyvinyl alcohol composite membranes for CO_2 separation*, Trondheim Conference on CO_2 Capture, Transport and Storage – 10 (TCCS-10), June 2019, Trondheim, Norway;

2. ***Deng, Jing***; Dai, Zhongde; Yu, Junbo; Sandru, Marius; Deng, Liyuan; *PEG-based membranes with dual cross-linking networks for enhanced CO_2 separation*, Euromembrane 2018, June 2018, Spain;

3. ***Deng, Jing***; Sandra Suciu; Dai, Zhongde; Sandru, Marius; Deng, Liyuan; *Cross-linked PTMSP Membrane with Reduced Physical Aging for CO_2 Separation*, Trondheim Conference on CO_2 Capture, Transport and Storage – 9 (TCCS-9), June 20199, Trondheim, Norway

Table of Contents

Symbols and Abbreviations

Symbols	Explanation	Unit
D	diffusivity	cm^2s^{-1}
P	Permeability	Barrer
S	Solubility	$cm^3(STP)cm^{-3}cmHg^{-1}$
T_c	Critical temperature	ºC
T_g	Glass transition temperature	ºC
T_m	Melting temperature	ºC
x	Mole percent of gas in retentate side	-
y	Mole percent of gas in permeate side	-
$\alpha_{i/j}^{ideal}$	Ideal selectivity	-
$\alpha_{i/j}$	Separation factor	-

Abbreviations	Full name
AFM	Atomic force microscopy
ATR	Attenuated total reflectance
DSC	Differential scanning calorimetry
FTIR	Fourier transform infrared
GO	Graphene oxide
MMMs	Mixed matrix membranes
MW	Molecular weight
PTMSP	Poly(1-trimethylsilyl-1-propyne)
PMP	Poly(4-methyl-2-pentyne)
PEG	Poly(ethylene glycol)
PEO	Poly(ethylene oxide)
PEO-PBT	Poly(ethylene oxide)-poly(butylene terephthalate)
PILs	Poly(ionic liquids)
PPO	Poly(propylene oxide)
PTMEO	Poly(tetramethylene oxide)
PTT-b-PEO	Poly(trimethylene terephthalate)-block-poly(ethylene oxide)
PVA	Poly(vinyl alcohol)
PDMS	Polydimethylsiloxane
PI	Polyimide
PIM	Polymers of intrinsic microporosity

PSf	Polysulfone
PVAm	Polyvinyl amine
PU	Polyurethane
SEM	Scanning electron microscope
TGA	Thermal gravimetric analysis
TR	Thermally rearranged
XRD	X-ray diffraction

Part I

Chapter 1

Introduction

Long-term observation has shown that the average global temperature has consistently increased and been already around 1.0 ºC above the pre-industrial level, as shown in **Figure 1 (A)** [1], close the 1.5 ºC target [2, 3]. A special report issued by the Intergovernmental Panel on Climate Change (IPCC) in 2018 has predicted that the global warming of 1.5 ºC is likely to take place if the temperature continues increasing with the current rate. This report suggests that the impacts of passing 1.5 ºC line includes increasing the global average temperature, extreme weather in most inhabited regions and rising sea level [4].

It has been widely accepted that this anthropogenic global warming directly results from the rising atmospheric CO_2 level, as presented in **Figure 1(B)** [5]. The CO_2 in atmosphere prevents heat escaping from the earth and keeps the earth warm. However, the CO_2 emission during the industrial period has excessed the level that the biological system can absorb, and as a result, the CO_2 concentration keeps increasing. The CO_2 concentration in atmosphere passed 400 ppm in 2015, and the increase rate is around 2 ~ 3 ppm / year recently [5]. To prevent the 1.5 ºC scenario, the CO_2 emission should be reduced, and the net emission is suggested to be below zero by 2050, as stated by the Paris agreement [6]. Several strategies that may help cutting down CO_2 emission have been proposed and developed. The most promising ones include improving the current energy conversion efficiency, applying CO_2 capture and storage (CCS) technology and replacing fossil energy with renewable sources [7]. Since fossil energy sources will still occupy the biggest energy market shares in the coming decades, at present time CCS has been widely recognized as a key technology to reduce CO_2 emission and then mitigate global warming [8].

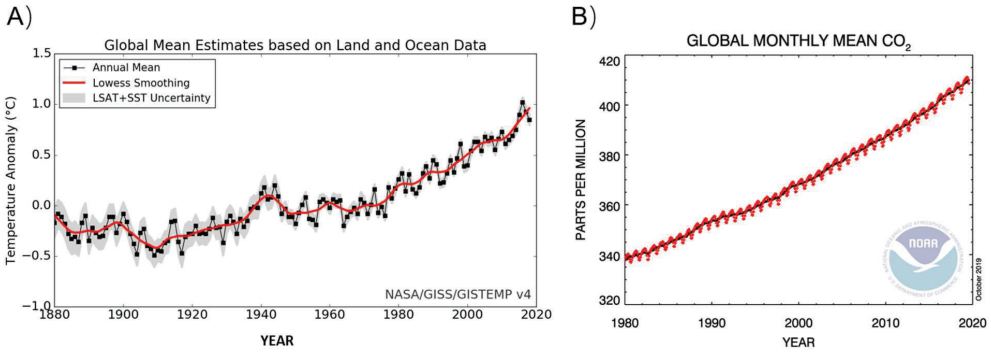

Figure 1.1 A) Global annual mean surface air temperature change with a function of time (1880 to 2020) [1], B) atmospheric CO_2 level changes with time since the 1980s [5]

1.1 CO_2 capture routes

In CCS, the CO_2 produced from power plants or industrial processes could be collected through one of these routes: pre-combustion capture, post-combustion capture and oxyfuel combustion, as shown in **Figure 1.2** [9]. Subsequently, the CO_2 will be transported by ships or pipelines and stored typically in a geological formation.

The post-combustion capture is usually applied in large-scale processes, like power plants, cement kilns and steel production plants, where fossil fuel is burning in air. The CO_2 is captured from the flue gas. The flue gas usually has a total pressure close to atmospheric pressure with a CO_2 concentration of 3 - 15 %, varying in processes [10]. On the other hand, pre-combustion system captures CO_2 before fuel combustion, usually employed in an integrated gasification combined cycle (IGCC) process. Because of the higher CO_2 concentration (ca. 35 %) and pressure (ca. 30 bar) [11], and hence the higher driving force for separation in pre-combustion system, it normally has lower energy consumption compared to the post-combustion process. For oxy-combustion, pure oxygen (> 95%) is used as the combustion atmosphere instead of air. Therefore, the flue gas mainly consists of CO_2 and H_2O, and the flow of fuel gas is relatively lower compared with those in post-combustion or pre-combustion systems.

Other than capturing CO_2 from power-generation sectors, CO_2 could also be potentially captured from several industrial processes with large quantities and low cost. In these cases, the CO_2 is the unwanted compound inside the products, like in nature gas sweetening, or the by-product in some processes, such as iron and steel industry, cement production and ammonia production. It is worth noticing that CO_2 capture in these scenarios may be easier than post-combustion since the CO_2 concentration is higher. For example, the flue gas from steel and cement plants contain 20 % and

15 -30 vol% of CO_2, respectively. Moreover, the post-combustion capture system can be adjusted and applied to these emission sites [12, 13].

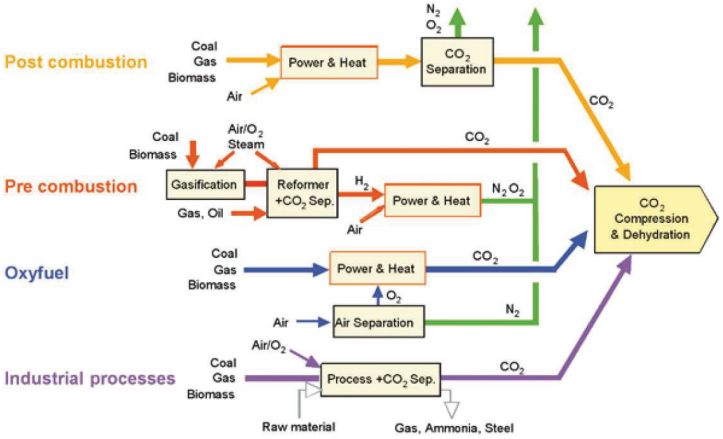

Figure 1.2 Schematic representation of CCS strategies [12].

1.2 CO_2 separation technologies for post-combustion capture

Post-combustion capture has been the hard core for CCS in the coming decades due to its mature engineering and possible retrofit to large-scale emission sources [8, 14, 15]. However, the main obstacle of this process is the low CO_2 partial pressure and the high-volume of the flue gas stream. Moreover, flue gas usually contains a wide variety of contaminants including fly ash, SO_2, NO_x, water, and trace metals. Therefore, robust and highly efficient technologies with considerable capacity are highly required for economically feasible post-combustion CO_2 capture. So far, several technologies have been employed for carbon capture, including absorption, adsorption, membrane and cryogenic process, as shown in Figure 1.3.

Absorption or scrubbing is the most widely studied and preferred technology for carbon capture, as it has been used for industrial gas treatment since 1930 [16]. The flue gas after removal of SO_2 and NO_X will meet the lean solvents, and the CO_2 will be absorbed because of the chemical or physical interaction, but not N_2. Then the CO_2-rich solvent will be regenerated under higher temperature to release the captured CO_2, which will be collected as pure gas for other applications or transportation. There currently exist two types of solvents: chemical solvents, like amine, amino salt and ammonia, and physical solvents, such as Selexol (dimethyl ethers of polyethylene glycol) and Rectisol (methanol) [17]. Among them, the amine-based solvents are the most common ones and have been employed in several large-scale capture systems. However, the amine-based absorption system is greatly costly and energy-intensive. An amine-based system requires around

30% power produced by the plant to remove 90% CO_2 in flue gas, and the CO_2 capture cost is predicted to be around 40 – 100 $/ ton CO_2 [9]. The cost of capturing may be reduced by improving solvents or process configurations [10, 18], but quite limited. Some advanced solvents, such as KS-1, ethyldiethanolamine and ionic liquids (ILs), are more expensive and sensitive to the impurities or process upsets, so the cost may not be reduced [19]. Furthermore, the optimization of process parameters usually results in other issues, such as deteriorating operation flexibility.

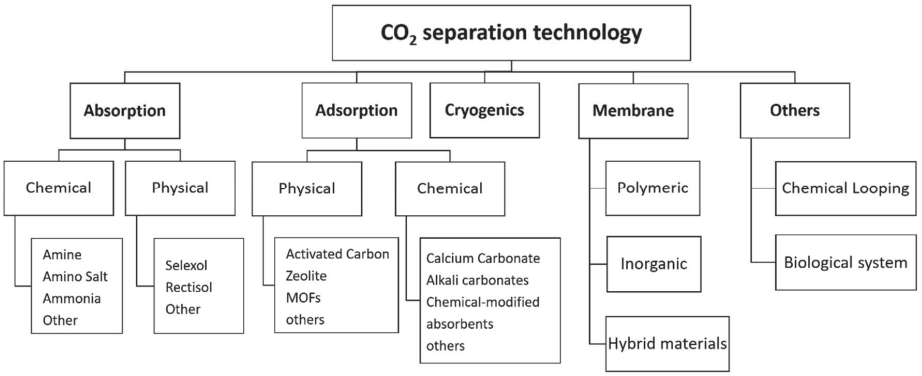

Figure 1.3 CO_2 separation technologies

In addition, other technologies, like adsorption and cryogenic, have also been developing for CO_2 capture in the past decades, but very limited applied for large-scale sites. Adsorption is a technology involving selectively absorbing CO_2 on the surface of absorbents from gas streams by weak intermolecular forces or chemical bonding [20]. Normally pre-treatment is needed before the CO_2 adsorption taking place in the adsorption bed. The CO_2 will be trapped inside the pores of these absorbents until fully loaded. Then the absorbents will be regenerated by increasing temperature (temperature swing adsorption) or reducing pressure (pressure swing adsorption). The released CO_2 will be collected during the regeneration [20, 21].

Different from aforementioned processes, in a cryogenic process, the gas mixture is cooled down and the CO_2 firstly condensates due to its relatively higher vapor temperature. Then the pure CO_2 will be pumped into pipes or gas bottles for further usage [22, 23]. Despite the very high CO_2 purity can be obtained (almost 100 %) and avoided cooling energy for further CO_2 transport, this method is still rarely used in CO_2 capture process because of the very high energy cost, mainly used for creating cryogenic conditions. Additionally, the water in flue gas should be removed before cooling to prevent plugging by ice or the unfavorably significant pressure drop [24].

Integration of this method with other technologies into several hybrid systems, like membrane-cryogenic [22, 25], can be another option. Other technologies, like chemical looping [26, 27], are believed as promising alternatives to the conventional CO_2 capture technologies, but still remained in research level, far beyond the commercialization stage.

Another promising method for CO_2 capture is membrane separation, which has been employed for gas treatment since the 1980s. In a typical membrane process, the gas streams pass along the selective side of the membranes. The preferred compounds for membranes will permeate to another side of the membranes, while the less-permeating compounds are retained at the feed-stream side and exit the membrane modules as the retentate stream. The partial pressure difference of a particular gas across the membranes is the driving force for the permeation process. Therefore, compressing the feed stream or vacuuming the permeate side are usually employed to obtain a higher driving force and thus better separation. Because there is non-phase transition involved in membrane gas separation, the energy needed for membrane separation, and consequently cost for membrane process are much reduced compared to its analogies [28]. It is predicted that energy consumption will reduce >90% if all current thermal-inducing processes are replaced by the membrane processes [29]. Moreover, gas separation membranes have other characteristic advantages, such as environmental-friendly, compact design and operation simplicity [14, 30]. This relatively economical and green technology has attracted widespread attentions in the academicals and industrials, indicating by the number of publications and the related citations, as presented in **Figure 1.4**.

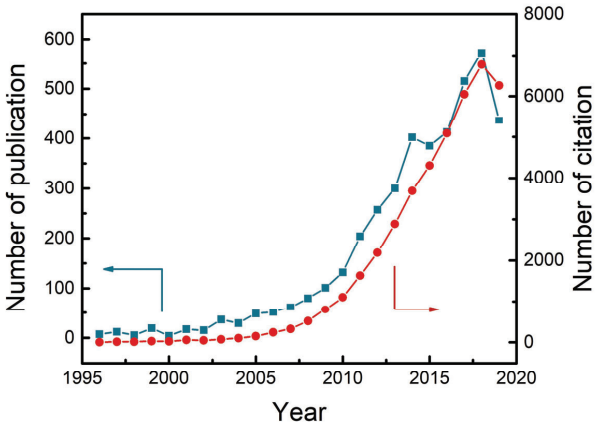

Figure 1.4 Number of annual publications and citation related to the search terms "membrane" AND "CO_2 capture" OR "CO_2 separation" vs year (1996 to 2019).

1.3 Membrane materials for CO_2 separation

Membrane material is the key element for membrane processes. Thus, improving the membrane gas separation performance will enhance the competitiveness of membrane technology. Enormous research efforts have been devoted to developing new membrane materials or making new combinations based on current materials. The membrane materials used for CO_2 separation are generally divided into three categories: polymeric, inorganic and polymer-inorganic hybrid materials.

Polymeric membranes occupy more than 90% market shares of the gas separation membranes, to a large extent due to their superior film-forming ability, processability and good mechanical properties [31]. However, the current polymeric membranes suffer from the trade-off between permeability and selectivity, so-called Robeson upper bound [32], meaning that the highly permeable polymers usually have low selectivity, and *vice versa*. Polymers with higher permeability and /or higher selectivity have been designed and developed based on the related fundamental of polymer and membrane, which mainly revolves around two directions: increasing the free volume of polymeric membranes, leading to a higher gas diffusivity, or enhancing the CO_2 affinity of membrane materials, which benefits the solubility and CO_2/light gas selectivity. The representative candidates for the first one include the polyimide (PI) [33], polymers of intrinsic microporosity (PIM) [34, 35], thermally rearranged (TR) polymers [36, 37], while polyethylene oxide (PEO) or polyethylene glycol (PEG)-based materials [38, 39] and facilitated transport membranes [40] are the typical ones for second approach. Some of the developed high performance membranes have already been fabricated into thin film composite membranes and tested in pre-pilot [41, 42] or even pilot scale [43, 44].

In parallel to the polymeric materials, inorganic membranes are drawn considerable research attentions for their excellent thermal and chemical stability, good chemical resistance and outstanding separation performance. Generally, ceramics, carbon [45, 46], zeolite [47], and metal–organic frameworks [48-50] are the most common membrane materials used for CO_2 separation. Although inorganic membranes offer unique properties, certain aspects still require further improvements, including the mechanical resistance, reproducibility, long-term stability and, more importantly, fabrication costs. Due to these factors, inorganic membranes are not preferred materials for the post-combustion capture, which requires high separation capacity.

In order to overcome the limitations of both polymeric and inorganic membranes materials, hybrid membranes containing these both materials, so-called mixed matrix membranes (MMMs), have been developed, which are usually prepared by imbedding inorganic fillers into polymeric matrices. MMMs have been considered as a solution to combine the advantages from both sides [51-54].

Most of the employed inorganic fillers are porous with suitable pore sizes aiming for its both high gas permeability and high selectivity due to the molecular sieving effects. To date, the research attentions have been mainly devoted to preparing MMMs containing highly permeable / selective inorganic nanomaterials, such as zeolitic imidazolate frameworks (ZIFs), or other two-dimensional (2D) materials, like graphene oxide. Additionally, more and more research works have found that other factors, including the pairing of fillers and polymeric matrix, the interface morphology between two phases and the morphology of fillers or the pores play important roles in the performance of the resultant MMMs. The study of MMMs are still remaining in initial stage, and only a handful of MMMs have been fabricated into compositing membranes, rarely for the large-scale tests.

The current work takes two approaches to enhance the CO_2 separation performances of membranes that are suitable for post-combustion CO_2 capture. The first one revolves around the highly CO_2-philic PEG-based materials, which have high CO_2/light gas selectivity but extremely low gas transport properties as a result of the highly crystalline nature. New cross-linking methods based on highly efficient "click reaction" have been developed to fabricate and optimize the cross-linking PEG-based membranes, which could reduce the crystalline tendency and hence achieve the higher CO_2 permeability. Furthermore, low-molecular-weight additives (free PEG and ILs) have been incorporated into the optimized PEG-based membranes to further improve the gas separation performances. The gas separation performances of these membranes have been systemically evaluated using single gas permeation tests. The materials properties were also studied by various characterization methods.

The second approach is developing ZIF-based MMMs with the focuses on the influences of fillers' morphology (size and shape) and chemical nature of the inorganic fillers on gas separation performances of the resultant MMMs investigated by incorporating various ZIF fillers into different polymeric matrix. The gas separation performances of these resultant membranes have been systemically evaluated by mixed gas permeation or single gas permeation tests under different test conditions. The materials properties were also studied by various characterization methods.

1.4 Research objectives

The primary aim of this research has been to enhance the current membrane separation properties for post-combustion CO_2 capture by: i) developing new cross-linking reactions for PEG-based materials and ii) adding nanofillers into polymeric membranes and studying the effects of filler's morphology on the gas separation performances of the resultant MMMs. The sub-goals for each approach are listed as follows:

1) Cross-linked PEG-based / organic additives membranes
   - To screen proper reactions for cross-linking PEG membranes and the organic additives incorporated into cross-linked PEG membranes;
   - To fabricate the cross-linked PEG membranes based on the chosen cross-linking reactions, as well as the membranes containing organic additives;
   - To characterize the cross-linked PEG / organic additives membranes with various technologies, such as TGA, DSC, XRD and FTIR;
   - To investigate the CO_2 separation performance of developed membranes by single gas permeation tests;
   - To optimize the developed membranes by tuning the cross-linking parameters and organic additives.
2) ZIFs-based mixed matrix membranes
   - To study the influences of the soft templates used in ZIFs preparation on the properties and the morphology of the resultant ZIFs.
   - To fabricate the mixed matrix membranes containing the developed ZIFs.
   - To characterize the developed ZIFs and the mixed matrix membranes with various characterization technologies;
   - To test the CO_2 separation performance of developed membranes by mixed gas permeation tests;
   - To investigate the effects of morphology and chemistry of ZIFs on the material properties of the developed membranes and optimize the developed membranes based on the CO_2 separation performances.

1.5 Outline of this thesis

This thesis consists of two main parts:

Part I contains four chapters to give a general introduction of this thesis. Chapter 1 briefly introduces the background of the global warming and CO_2 emission, CO_2 capture technologies, the research objectives and the outline of this thesis. A general overview of polymeric membranes for gas separation and details literature review of PEG-based membranes and the mixed matrix membranes containing ZIFs are provided in Chapter 2. Chapter 3 includes the technical details in materials, experiments and the characterization methods used in this study. Finally, the conclusions obtained from this research and some suggestions for further work are presented in Chapter 4.

Part II is a collection of six research papers resulted from this work.

Paper 1 reports a new preparation method combining aza-Michael reaction and free radical polymerization for cross-linking PEG membranes. Paper 2 presents the influences of incorporating IL into cross-linked PEG membranes on gas separation properties. Paper 3 focuses on the cross-linked PEG membranes prepared by thiol click reactions and the effects of ILs in this system. Paper 4 reports a facile preparation for a series of new ZIF cuboids with controllable morphology and the effects of ZIF cuboids' thickness on the resultant Pebax + ZIFs membranes. Paper 5 compares the influences of ZIFs with different shapes on the Pebax + ZIFs membranes. Paper 6 reports the incorporation of two leaf-like ZIFs into troger base-based membranes and discusses the impacts of the ZIF's chemistry on the performances of the resultant mixed matrix membranes.

1.6 Main contributions of the papers

- Paper 1. Jing Deng performed most of the experiments and wrote the manuscript, and the tensile tests was conducted by Miss. Jiaqi Yan. The rest of the authors contributed to the manuscript structuring and revision.
- Paper 2. This paper is written by Jing Deng. The experiments were designed and performed by Jing Deng and former master student Junbo Yu, respectively. The rest of the authors contributed to the manuscript structuring and revision.
- Paper 3. Jing Deng performed all the experiments and wrote the manuscript. The rest of the authors contributed to the manuscript structuring and revision.
- Paper 4. Jing Deng performed membrane preparation, the relevant characterization and permeation tests, and wrote the manuscript. Dr. Zhongde Dai proposed the preparation method for synthesizing ZIF cuboids and prepared the ZIF cuboids. Dr. Jingwei Hou performed the XPS tests and related analysis. The rest of the authors contributed to the manuscript structuring and revision.
- Paper 5. Jing Deng performed membrane preparation, the relevant characterization and permeation tests, and wrote the manuscript. Dr. Zhongde Dai prepared the ZIFs employed in this work. The rest of the authors contributed to the manuscript structuring and revision.
- Paper 6. Jing Deng performed membrane preparation, the relevant characterization and permeation tests, and wrote the manuscript. Dr. Zhongde Dai synthesized troger base-based polymers and prepared the ZIFs employed in this work. The rest of the authors contributed to the manuscript structuring and revision.

References

1. *GISS Surface Temperature Analysis* 2019. Available from: https://data.giss.nasa.gov/gistemp/graphs_v4/.

2. V. Masson-Delmotte, P. Zhai, H.O. Pörtner, et al., *Global warming of 1.5°C. An IPCC Special Report on the impacts of global warming of 1.5°C above pre-industrial levels and related global greenhouse gas emission pathways, in the context of strengthening the global response to the threat of climate change, sustainable development, and efforts to eradicate poverty*. 2018, Intergovernmental Panel on Climate Change (IPCC).
3. M. Hulme, *1.5 °C and climate research after the Paris Agreement.* Nature Climate Change, 2016. **6**, 222.
4. W. Zhang, T. Zhou, L. Zou, et al., *Reduced exposure to extreme precipitation from 0.5 °C less warming in global land monsoon regions.* Nature Communications, 2018. **9**(1), 3153.
5. *Trends in Atmospheric Carbon Dioxide*. 2019. Available from: http://www.esrl.noaa.gov/gmd/ccgg/trends/global.html.
6. C.-F. Schleussner, J. Rogelj, M. Schaeffer, et al., *Science and policy characteristics of the Paris Agreement temperature goal.* Nature Climate Change, 2016. **6**, 827.
7. C.o.t.E. Union, *Energy and climate change–elements of the final compromise*. 2008, Council of the European Union Brussels, Belgium.
8. E.S. Rubin, J.E. Davison, and H.J. Herzog, *The cost of CO_2 capture and storage.* Int. J. Greenhouse Gas Control, 2015. **40**, 378-400.
9. T.C. Merkel, H. Lin, X. Wei, et al., *Power plant post-combustion carbon dioxide capture: an opportunity for membranes.* J. Membr. Sci., 2010. **359**(1), 126-139.
10. Y. Wang, L. Zhao, A. Otto, et al., *A Review of Post-combustion CO_2 Capture Technologies from Coal-fired Power Plants.* Energy Procedia, 2017. **114**, 650-665.
11. D.M. D'Alessandro, B. Smit, and J.R. Long, *Carbon dioxide capture: prospects for new materials.* Angew. Chem. Int. Ed., 2010. **49**(35), 6058-6082.
12. B. Metz, O. Davidson, H. De Coninck, et al., *IPCC special report on carbon dioxide capture and storage*. 2005, Intergovernmental Panel on Climate Change.
13. M. Bui, C.S. Adjiman, A. Bardow, et al., *Carbon capture and storage (CCS): the way forward.* Energy Environ. Sci., 2018. **11**(5), 1062-1176.
14. J.D. Figueroa, T. Fout, S. Plasynski, et al., *Advances in CO_2 capture technology—The U.S. Department of Energy's Carbon Sequestration Program.* Int. J. Greenhouse Gas Control, 2008. **2**(1), 9-20.
15. H. Herzog, J. Meldon, and A. Hatton, *Advanced post-combustion CO_2 capture*. 2009, Clean Air Task Force. p. 39.
16. A. Kothandaraman, *Carbon dioxide capture by chemical absorption: a solvent comparison study*, in *Department of Chemical Engineering*. 2010, Massachusetts Institute of Technology Cambridge, Massachusetts, the United State.
17. M. Wang, A. Lawal, P. Stephenson, et al., *Post-combustion CO_2 capture with chemical absorption: A state-of-the-art review.* Chem. Eng. Res. Des., 2011. **89**(9), 1609-1624.
18. G.T. Rochelle, *Conventional amine scrubbing for CO_2 capture*, in *Absorption-Based Post-combustion Capture of Carbon Dioxide*, P.H.M. Feron, Editor. 2016, Woodhead Publishing. p. 35-67.
19. G.T. Rochelle, *Amine Scrubbing for CO_2 Capture.* Science, 2009. **325**(5948), 1652-1654.
20. E.E. Ünveren, B.Ö. Monkul, Ş. Sarıoğlan, et al., *Solid amine sorbents for CO_2 capture by chemical adsorption: A review.* Petroleum, 2017. **3**(1), 37-50.
21. A. Samanta, A. Zhao, G.K. Shimizu, et al., *Post-combustion CO_2 capture using solid sorbents: a review.* Ind. Eng. Chem. Res., 2011. **51**(4), 1438-1463.

22. C.A. Scholes, M.T. Ho, D.E. Wiley, et al., *Cost competitive membrane—cryogenic post-combustion carbon capture.* Int. J. Greenhouse Gas Control, 2013. **17**, 341-348.
23. M. Jensen, *Energy Process Enabled by Cryogenic Carbon Capture*, in *Department of Chemical Engineering*. 2015, Brigham Young University.
24. A. Brunetti, F. Scura, G. Barbieri, et al., *Membrane technologies for CO_2 separation.* J. Membr. Sci., 2010. **359**(1), 115-125.
25. C. Song, Q. Liu, N. Ji, et al., *Alternative pathways for efficient CO_2 capture by hybrid processes—A review.* Renewable and Sustainable Energy Reviews, 2018. **82**, 215-231.
26. M.M. Hossain and H.I. de Lasa, *Chemical-looping combustion (CLC) for inherent CO_2 separations—a review.* Chem. Eng. Sci., 2008. **63**(18), 4433-4451.
27. T. Lockwood, *A compararitive review of next-generation carbon capture technologies for coal-fired power plant.* Energy Procedia, 2017. **114**, 2658-2670.
28. R. Bounaceur, N. Lape, D. Roizard, et al., *Membrane processes for post-combustion carbon dioxide capture: A parametric study.* Energy, 2006. **31**(14), 2556-2570.
29. D.S. Sholl and R.P. Lively, *Seven chemical separations to change the world.* Nature News, 2016. **532**(7600), 435.
30. H.B. Park, J. Kamcev, L.M. Robeson, et al., *Maximizing the right stuff: The trade-off between membrane permeability and selectivity.* Science, 2017. **356**(6343), eaab0530.
31. S. Wang, X. Li, H. Wu, et al., *Advances in high permeability polymer-based membrane materials for CO_2 separations.* Energy Environ. Sci., 2016. **9**(6), 1863-1890.
32. L.M. Robeson, *The upper bound revisited.* J. Membr. Sci., 2008. **320**(1), 390-400.
33. Y. Xiao, B.T. Low, S.S. Hosseini, et al., *The strategies of molecular architecture and modification of polyimide-based membranes for CO_2 removal from natural gas—A review.* Prog. Polym. Sci., 2009. **34**(6), 561-580.
34. S. Yi, B. Ghanem, Y. Liu, et al., *Ultraselective glassy polymer membranes with unprecedented performance for energy-efficient sour gas separation.* Science advances, 2019. **5**(5), eaaw5459.
35. M. Carta, R. Malpass-Evans, M. Croad, et al., *An Efficient Polymer Molecular Sieve for Membrane Gas Separations.* Science, 2013. **339**(6117), 303.
36. H.B. Park, S.H. Han, C.H. Jung, et al., *Thermally rearranged (TR) polymer membranes for CO_2 separation.* J. Membr. Sci., 2010. **359**(1), 11-24.
37. M. Cersosimo, A. Brunetti, E. Drioli, et al., *Separation of CO_2 from humidified ternary gas mixtures using thermally rearranged polymeric membranes.* J. Membr. Sci., 2015. **492**, 257-262.
38. S.L. Liu, L. Shao, M.L. Chua, et al., *Recent progress in the design of advanced PEO-containing membranes for CO_2 removal.* Prog. Polym. Sci., 2013. **38**(7), 1089-1120.
39. H. Lin and B.D. Freeman, *Gas solubility, diffusivity and permeability in poly(ethylene oxide).* J. Membr. Sci., 2004. **239**(1), 105-117.
40. L. Deng, T.-J. Kim, and M.-B. Hägg, *Facilitated transport of CO_2 in novel PVAm/PVA blend membrane.* J. Membr. Sci., 2009. **340**(1), 154-163.
41. Z. Dai, S. Fabio, N. Giuseppe Marino, et al., *Field test of a pre-pilot scale hollow fiber facilitated transport membrane for CO_2 capture.* Int. J. Greenhouse Gas Control, 2019. **86**, 191-200.
42. Y. Han, W. Salim, K.K. Chen, et al., *Field trial of spiral-wound facilitated transport membrane module for CO_2 capture from flue gas.* J. Membr. Sci., 2019. **575**, 242-251.

43. T. Brinkmann, C. Naderipour, J. Pohlmann, et al., *Pilot scale investigations of the removal of carbon dioxide from hydrocarbon gas streams using poly (ethylene oxide)–poly (butylene terephthalate) PolyActive™) thin film composite membranes.* J. Membr. Sci., 2015. **489**, 237-247.
44. H. Lin, Z. He, Z. Sun, et al., *CO_2-selective membranes for hydrogen production and CO_2 capture – Part I: Membrane development.* J. Membr. Sci., 2014. **457**, 149-161.
45. W. Qiu, J. Vaughn, G. Liu, et al., *Hyperaging Tuning of a Carbon Molecular-Sieve Hollow Fiber Membrane with Extraordinary Gas-Separation Performance and Stability.* Angew. Chem. Int. Ed., 2019. **58**(34), 11700-11703.
46. Y. Cao, K. Zhang, O. Sanyal, et al., *Carbon Molecular Sieve Membrane Preparation by Economical Coating and Pyrolysis of Porous Polymer Hollow Fibers.* Angew. Chem. Int. Ed., 2019. **58**(35), 12149-12153.
47. H. Guo, G. Zhu, H. Li, et al., *Hierarchical Growth of Large-Scale Ordered Zeolite Silicalite-1 Membranes with High Permeability and Selectivity for Recycling CO_2.* Angew. Chem. Int. Ed., 2006. **45**(42), 7053-7056.
48. E. Jang, E. Kim, H. Kim, et al., *Formation of ZIF-8 membranes inside porous supports for improving both their H_2/CO_2 separation performance and thermal/mechanical stability.* J. Membr. Sci., 2017. **540**, 430-439.
49. F. Cacho-Bailo, I. Matito-Martos, J. Perez-Carbajo, et al., *On the molecular mechanisms for the H_2/CO_2 separation performance of zeolite imidazolate framework two-layered membranes.* Chem. Sci., 2017. **8**(1), 325-333.
50. A. Huang, Q. Liu, N. Wang, et al., *Bicontinuous Zeolitic Imidazolate Framework ZIF-8@GO Membrane with Enhanced Hydrogen Selectivity.* J. Am. Chem. Soc., 2014. **136**(42), 14686-14689.
51. B. Seoane, J. Coronas, I. Gascon, et al., *Metal-organic framework based mixed matrix membranes: a solution for highly efficient CO_2 capture?* Chem. Soc. Rev., 2015. **44**(8), 2421-2454.
52. M. Galizia, W.S. Chi, Z.P. Smith, et al., *50th Anniversary Perspective: Polymers and Mixed Matrix Membranes for Gas and Vapor Separation: A Review and Prospective Opportunities.* Macromolecules, 2017. **50**(20), 7809-7843.
53. Y. Cheng, Y. Ying, S. Japip, et al., *Advanced Porous Materials in Mixed Matrix Membranes.* Adv. Mater., 2018. **30**(47), 1802401.
54. R. Lin, B. Villacorta Hernandez, L. Ge, et al., *Metal organic framework based mixed matrix membranes: an overview on filler/polymer interfaces.* J. Mater. Chem. A, 2018. **6**(2), 293-312.

Chapter 2

Background and Theory

2.1 Polymeric membranes

It is commonly accepted that polymeric membranes have been and will be the dominating membranes for most of the gas separation applications. Polymers are fabricated into dense membranes, from self-standing membranes for fundamental studies to the composite membranes with a thin selective layer for large scale separations. Therefore, the polymer properties related to gas separation performances will be briefly introduced in this chapter. Also, the gas transport mechanism inside dense polymeric membranes will be discussed. Finally, the state-of-the-art CO_2 separation membranes will be summarized.

2.1.1. Properties of polymers

As the separation performance of a material is greatly affected by both physical and chemical properties, in this section, the polymer properties related to the gas separation performances will be briefly introduced, including the state of polymer, free volume and crystallization.

2.1.1.1 State of polymer

For most polymers, there exists a glassy transition temperature, at a temperature above which the polymer is in the rubbery state, while below which, it becomes the glassy state. The polymeric chains are highly restricted and cannot rotate freely around the main chains in the glassy state. Hence, the polymeric chains in the glassy state are considered as rigid and

restricted. As the temperature increases some minor motions can happen for side chains or a fe se ments of the main chains. When the temperature goes above T_g, the polymeric chains have sufficient energy to overcome the rotational restriction and the interactions between polymeric chains. Thus in the rubbery state the polymers have more feasibility. Remarkable changes can be observed for many physical properties of polymers around T_g, like tensile modulus, specific heat, free volume, and permeability, which will be discussed in this section.

The chemical structure of polymeric chains and the types of intermolecular interactions have great influences on the glassy transition temperature. The chain flexibility is mainly depending on the chemical structures of the main chains. For example, the presence of aromatic groups in the main chains will dramatically increase T_g, while the ones with simple bonds, like -C-C, or -C-O-, have much lower glass transition temperatures. In addition, the side groups also have minor effect on the T_g by aryin the intermolecular distance and the interactions.

2.1.1.2 Free volume theory

Free volume is the space unoccupied by the macromolecules, commonly defined as the differences between the specific volume of polymer and the volume occupied by the molecules. Numerous small spaces between the polymer chains in the amorphous, non-crystalline domain of the materials gives the free volume of these materials. Generally speaking, the free volume is a small percentage (10 – 35%, depending on polymers and the calculation methods) [1] of the total volume, but these spaces are sufficient for the motion of polymeric chain and allowing small molecules passing through.

In the glassy state, the free volume of a specific polymer keeps almost unchanged, as shown in **Figure 2.3**. There exists a sharp change at T_g. Above T_g, the free volume is increasing with the temperature at a constant rate. Based on the understanding of solution-diffusion theory, this increment will result in an enhancement of diffusivity and thus the permeability. However, it may also cause a board free volume element distribution, which may worsen the separation.

It is worth noticing that the free volume of a glass polymer consists of two parts: insufficient packing and the excess free volume due to the restricted chains [1, 2]. For some polymers, like poly(1-trimethylsilyl-1-propyne) (PTMSP), the second part counts a considerably large portion in the total free volume. However, the polymer chains will eventually move to the equilibrium state, suggesting the excess free volume will decrease with time. This phenomenon has been observed in almost all high free volume glassy polymers, such as PTMSP [3, 4], poly(4-methyl-2-pentyne) (PMP) [5, 6], and PIM-1 [7-9], indicated by the decrease of gas permeability with time, which is named as “physical aging”. While for most glassy polymers except these high-free-volume ones, this excess free volume fraction and the loss in their gas permeability with time are negligible.

Some researchers have tried to link the diffusivity or permeability with (fractional) free volume [10, 11]. However, the correlation matches excellently to the experimental data only within similar polymer types [12], not very efficient for different kinds of structures. Moreover, these studies were mainly limited to glassy polymers.

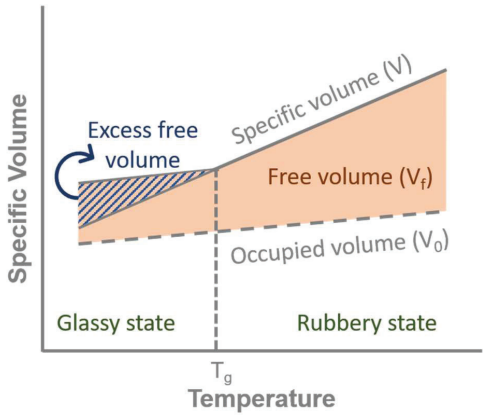

Figure 2.5 Polymer's free volume as a function of temperature. Reproduced from ref. [13].

2.1.1.3 Crystallization

Some polymers have regular structural units or/and very strong intermolecular interactions, such as hydrogen bonding, and the polymeric chains will fold close and form ordered regions, which may grow further to larger structures named crystallites. This behavior is called crystallization, which may happen during cooling from a temperature above melting temperature, mechanical stretching or solvent evaporation. Generally, most polymers are semi-crystalline, consisting both amorphous and crystalline zones. Numerous small crystallites randomly distribute through the polymer and connected by the amorphous domains, as shown in **Figure 2. 4** [14]. The size of crystallites is usually at nanoscale or even smaller, and the shape may be different from case to case.

Therefore, the degree of crystallinity is a very useful index to understand how far it deviates from the amorphous state. The degree of crystallinity of most semi-crystalline polymers is typically within 10 – 80 % [15]. It can be characterized by various approaches [16], but differential scanning calorimetry (DSC) [17-19] and X-ray diffraction (XRD) [20, 21] are the most commonly used two. The typic basis for these measurements is that the apparent polymer is composed of an ideally perfectly ordered crystalline phase and a disordered liquid-like phase [14], which contributes to all overall properties based on their portion. However, it may not be the actual case during research, and hence the values obtained from different technologies may be quite different. In addition, the

direct observation of nanoscale polymer's crystallites by microscopies has been also reported [22, 23]. It is worth noticing that the crystallinity degree cannot reflect any information for the size or shape of crystallites.

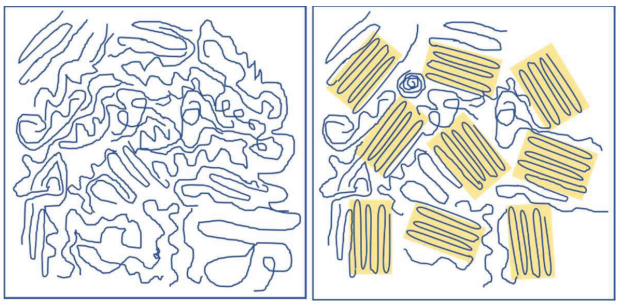

Figure 2.6 Amorphous (left) and semi-crystalline (right) polymer structures.

Crystallization in polymers may cause different behaviors compared with the completely amorphous ones (without crystallization) in plenty of physical and chemical properties. For example, the tensile modulus (one parameter of mechanical properties) is largely influenced by the presence of crystallites, as depicted in **Figure 2.5**. All polymers behave similar at glassy state, suggesting the presence of crystallites has little influence on this mechanical property. However, when the temperature is higher than T_g, the tensile modulus of amorphous polymers decreases dramatically, while the perfect crystalline polymers almost maintain the same level until it reaches the melting temperature (T_m). In the case of the semi-crystalline polymers, the modulus will decrease but with a much lower decreasing rate at rubbery state, which is because that the restricted polymers turn to flexible chains at the point of T_g, while the crystallites remain unchanged under this condition. But all crystallites will disappear at above the melting point, and thus a considerable decrease will be observed at T_m.

Another important physical property largely affected by crystallization is permeation properties. The crystallites are widely accepted as impermeable zones, which shrinks the efficient area for permeation and hence, the overall permeation properties [24, 25]. However, the decrease in permeability does not accompany an increase in selectivity: the selectivity remains the same. Hence, the materials with relatively high crystallinity are generally unfavorable as the selective layer in the composite membranes [26].

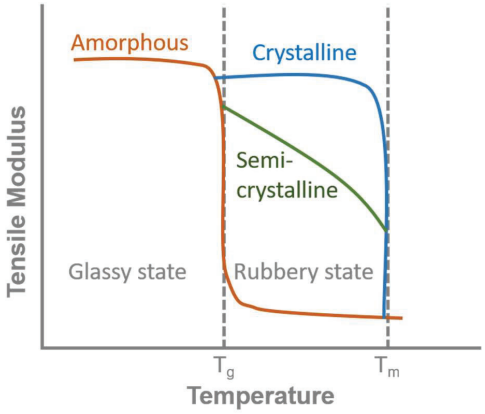

Figure 2.7 Modulus vs temperature curves of amorphous, semi-crystalline and crystalline polymers. Reproduced from Ref. [13].

2.1.2. Gas transport mechanism in dense polymeric membranes

For dense polymeric membranes, there are two major gas transport mechanisms: solution-diffusion and facilitated transport. Generally speaking, the solution-diffusion mechanism exists in all gas transport processes, but the facilitated transport only happens for specified gas-polymer pairs based on the interactions between gas and certain compounds/functional groups in membranes. The most well-known example is the amine-containing membranes for CO_2 separation, which normally display high CO_2 permeability/permeance and CO_2/light gas selectivity [27], as a result of the extra transport route for CO_2.

On the other hand, solution-diffusion theory is the classical mechanism describing how gases transport across most of the polymeric membranes. It is usually believed to consist of five parts: gas diffuses from the bulk of feed streams to membrane surface, being adsorbed at the membrane surface in the feed side, diffuses through membranes, being desorbed on the other membrane surface in the permeate side, and diffuses to the bulk permeate gas. The main three parts, except the diffusion in the feed stream or permeate side, are shown in **Figure 2.1**. The driving force for this process is the partial pressure differences of the penetrant gases across membranes.

Generally speaking, the gas transportation rate (permeability, P) through membranes can be affected by the absorption capacity and diffusion rate inside membranes, defining as the solubility ($S, cm^3(STP)cm^{-3}\ cmHg^{-1}$) and diffusivity ($D, cm^2s^{-1}$), respectively. As a result, permeability is a product of these two factors, as shown in equation (2.1):

$$P_A = S_A \times D_A \tag{2.1}$$

It is worth mentioning that the gas permeability of certain materials is an intrinsic property. Barrer is the most commonly used unit of permeability, 1 Barrer = $10^{-10}\ cm^3(STP)\ cm\ s^{-1}\ cm^{-2}\ cmHg^{-1}$. For multi-layered composite or asymmetric membranes, the permeation rate is usually expressed in terms of permeance, which is defined as P/l. l is the thickness of the selective or the dense layer. The most common unit for permeance is GPU (1 GPU $= 10^{-6} cm^3(STP)\ s^{-1}\ cm^{-2}\ cmHg^{-1}$).

The solubility of gas in polymeric membranes is related to 1) the ease of gas condensation and 2) the interactions between gas molecules and the polymers. The first factor is commonly characterized by the critical temperature of the gas (T_c), which increases with the molecular sizes. The interactions between gas molecules and polymer are usually very small for non-interacting gases, such as H_2, N_2, and CH_4. While for other gases, like CO_2, they could be considerably higher. Therefore, the gas solubility can be enhanced by increasing the gas condensability (or gas size) and/or the interactions of gas molecules with the membrane matrix (suitable gas-polymer pairing).

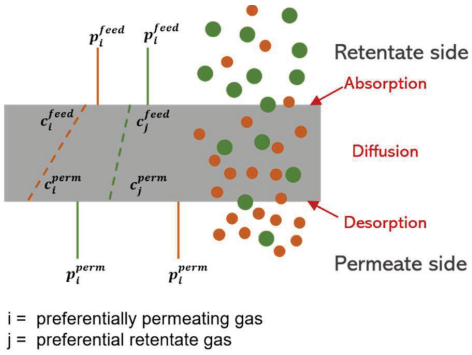

Figure 2.8 Scheme of the solution-diffusion mechanism. Reproduced from Ref. [28, 29]

Gas diffusion is widely accepted to be governed by the membrane's free volume and the size of gas molecules. Free volume elements are considered as the void or unoccupied space in dense polymeric membranes and one of the most important factors affecting gas diffusivity. The amounts, volume and the distribution of these free volume elements have a great influence on gas diffusivity. Incompact packing of polymer chains and the ability for polymer chains to move could offer more efficient diffusion of gas molecules. Furthermore, smaller gas size always results in higher gas diffusivity. As can be seen from Figure 2.2, the gas size has opposite effects on solubility and diffusivity, leading to a complex impact on the gas permeability.

Selectivity reflects the ability of the membranes to separate one gas from another. The ideal selectivity $\alpha_{i/j}^{ideal}$ is the ratio of the two gas permeabilities, as shown in equation (2.2):

$$\alpha_{i/j}^{ideal} = \frac{P_i}{P_j} = \frac{D_i}{D_j} \times \frac{S_i}{S_j} \tag{2.2}$$

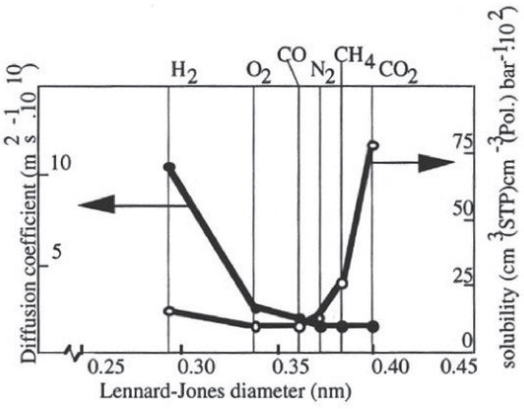

Figure 2.9 Solubility and diffusivity of various gases in natural rubber [13].

Where P_i and P_j are the permeability of the gas i and j in the membrane, respectively.

From this equation, the selectivity is also related to the solubility selectivity (S_i/S_j) and diffusivity selectivity (D_i/D_j). Solubility selectivity refers to the difference in condensability of the penetrant gases and the interactions between penetrate gases and polymeric chains. Diffusivity selectivity arises from the difference in the gas molecule size and the molecule-sieving ability of the polymeric membranes.

In mixed gas separation processes, separation factor ($\alpha_{i/j}$) is a more practical parameter for membrane, which is defined as

$$\alpha_{i/j} = \frac{y_i/x_i}{y_j/x_j} \tag{2.3}$$

Where the y_i and x_i are the mole percent of the gas i in permeate and retentate side, respectively, while y_j and x_j are the mole percent of gas j in permeate and retentate side, respectively.

The separation factor is usually lower than the ideal separation factor, mainly due to the competition and interactions between gases and/or the concentration polarization for some highly permeable materials [30].

2.1.3. Gas separation performance of polymeric membranes

2.1.3.1 Upper bounds

As mentioned before, the two key parameters for a gas separation membrane are the permeability and selectivity. From an engineering perspective, materials with both high permeability and high selectivity are desirable for a higher separation efficiency. However, Robeson has collected and analyzed the performance data of thousands of dense, nonporous polymer membranes, and then qualified a trade-off relationship for different industrial-interesting gas pairs, as shown in **Figure 2.6** [31, 32]. The empirical equation is listed below:

$$\alpha_{A/B} = \beta_{A/B} P_A^{-\lambda_{A/B}} \tag{2.4}$$

Where $\beta_{A/B}$ and $\lambda_{A/B}$ are the empirical parameters.

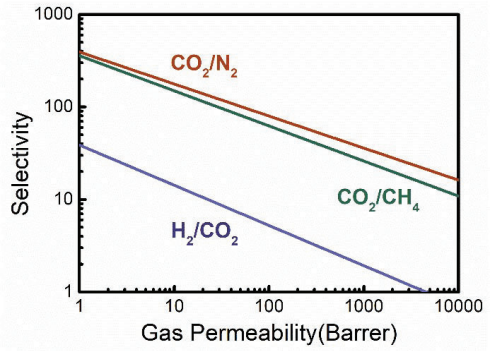

Figure 2.10 Upper bound for different gas pairs. Reproduced from Ref [31].

This equation indicates that the gas permeability on the upper bound increases with inevitably decrease in selectivity. A fundamental theory was proposed later by B.D. Freeman [33]. In this theory, the $\lambda_{A/B}$ is only relying on the gas size, while the other parameter $\beta_{A/B}$is associated to $\lambda_{A/B}$, gas condensability and one adjustable parameter. These results mean that the possibility to alter the slope of upper bound is very low, which is also in agreement with the unchanged slope of the upper bounds reported in 2008 compared to those in 1991 [31, 32]. However, there is some room for improvement by increasing the intercept through changing $\beta_{A/B}$, involving enhancing the solubility selectivity and/or chain stiff with simultaneously increasing free volume [33]. This

theory also suggested that the diffusivity selectivity plays a much greater role for gas selectivity compared with the solubility selectivity, which explains why most of the rubbery polymers are located far under upper bound. This also explains why the upper bound is mainly decided by glassy polymers' performances. It is worth noting that these discussions are only targeting the upper bounds, which are still much higher for many polymeric materials.

2.1.3.2 CO_2 separation performance of current polymeric membranes

Since the 1950's, the major industrial gas separation membranes are derived from cellulose acetate for the removal CO_2 from natural gas. With the development of membranes technology, more advanced membrane materials have been developed, but only a few have processed to pilot-scale tests. Among them, Polaris®, developed by Membrane Technology and Research Inc., is one of the most representative membranes since it has been employed in several large-scale emission sites for flue gas separation [34] or hydrogen separation [35]. With a similar chemical structure, Polyactive® from Helmholtz-Zentrum Geesthacht has also been used in power plants for removing CO_2 from flue gas [36, 37]. Moreover, polyvinyl amine (PVAm) -based facilitated membranes have been tested in a small pilot-scale system for flue gas separation and reported for its long-term stability within 6 months [38, 39].

Although only a few materials have been applied industrially, enormous materials have been developed at the laboratory level, and some of them exhibit excellent separation properties, e.g., the ones surpassing the upper bounds. A brief introduction for these representative membrane materials will be given based on the separation mechanism.

Diffusivity dominated membranes

As predicted by Freeman in 1991, the polymers with stiff chains maintaining selectivity could be an encouraging polymer design approach [40]. After that, great effects have been devoted to developing microporous materials starting with polyacetylenes, such as PTMSP and PMP, well known for the high permeabilites (> 5000 Barrer for CO_2) [41] [42]. The high permeabilities of these glassy polymers mainly come from the large excess free volume, which will disappear over time. Moreover, the selectivities of these polymers are too low to be used in practical applications. Different methods have been used to improve the selectivity and ease the aging issue, such as designing new polymers with various side groups (e.g., CO_2-philic groups, stiff groups or bulky groups) and crosslinking, but the results were not satisfactory [43-46].

In the meantime, incorporation of aromatic groups into polymeric chains have been employed to decrease the mobility of main chains. The aromatic-rich chemical structures have excellent thermal stability and good mechanical properties, which are greatly beneficial as membrane materials. The

spatial linkage configurations, the type of bridging groups and bulkiness, and polarity of pendant groups have been considered as the main consideration factors to improve the polymeric chain rigidity and the free volume, as well as the permeability [47]. By proper molecular design and using suitable aromatic monomers, rigid polyimides (PI) with high gas permeability could be achieved [48]. It has been reported that the presence of CO_2-philic CF_3 group in dianhydride monomers, like 4,4′-(hexafluoroisopropylidene)diphthalic anhydride, enhances not only the stiffness of the chains but also the affinity to CO_2 molecules, resulting in high CO_2 permeability with considerable selectivity [49].

If the stiffness of main chains increases by introducing certain structures with intrinsically inefficient packing, the free volume could be further increased. Due to the special contorted shape and chain rigidity from the ladder polymer chain, a large amount of rotational freedom can be removed from PIM-1, which leads to an inefficiently packed matrix with high free volume elements, typically above 20 % FFV. Thus, PIM membranes exhibit very high gas permeabilities, and the corresponding CO_2 separation performances are generally located above or near the upper bound [50]. After the PIMs were firstly reported by Budd and Mckeown [51, 52], many PIMs with different rigid chains have been synthesized, with the aim of increasing the chain rigidity and inter-chain spacing to improve the gas diffusion [53]. By introducing the extremely rigid spirobifluoren (SBF) unit, PIM-SBF membrane with a CO_2 permeability of up to 13900 Barrer and a CO_2/N_2 of 17.7 was reported [54]. Similar to PTMSP, the non-equilibrium state of PIMs chains also has resulted in significant physical aging issue over time [55].

Furthermore, higher gas diffusivity could be realized by creating selective cavies through thermally rearranging the functionalized PIs [53, 56]. Upon heating at high temperatures (generally > 300 °C) in an inert gas (usually N_2 or Ar), the polymer chain of the precursor polymer will be rearranged into a new rigid structure, which may display rapider gas transport with size sieving separation [57].
The molecular structure of TR polymers could be tuned by changing the chemical structures of precursor and heat treatment protocols to achieve desirable gas separation performance [58]. In addition to PIs, polyamides or polybenzoxazole can also be used as the polymeric precursors for TR membranes. Usually, the gas transport properties of TR polymers are a bit lower than that of PTMSP (10 – 20, 000 Barrer), but higher than their precursors. In addition, TR polymers hold much higher selectivity compared to PTMSP, especially for CO_2/CH_4, (e.g., ~50). Therefore, the overall CO_2 separation performances are always close or exceed the upper bound [56, 59, 60]. It is worth mentioning that the TR membranes have much a higher tolerance to the plasticization, which is greatly attractive as gas separation membranes.

Solubility dominated membranes

Based on the solution - diffusion theory, apart from the diffusivity, another strategy of improving CO_2 permeability is to enhance the CO_2 solubility. Poly(ionic liquids) (PILs), Poly(vinyl alcohol) (PVA), poly(vinyl alcohol) (PVAm) and poly(ethylene oxide) (PEO) are some representative solubility-dominated polymeric membrane materials. The first three materials will be discussed briefly below, while detailed information regarding the PEO or PEG based membranes will be given in section 2.2.

Ionic liquids are salts composing organic cations and inorganic/organic anions. They have been emerged as potential candidates for CO_2 capture and separation owing to their unique and outstanding properties, such as nonvolatility, high CO_2 solubility and selectivity [61, 62]. Soon after ILs was firstly proposed as CO_2 capture medium in 1999 [63], enormous research effects have been devoted to applying ILs into CO_2 separation membrane. ILs have been intensively used in supported ionic liquid membranes, cross-linked ionic liquids membranes, the polymer/ILs membranes, IL-gel membranes, and the membrane absorption systems in the past 20 years. In addition, the chemical structures of ILs are designable, and various ILs with specified functional groups have been developed for gas separation applications, including amino acid-based ILs, amine-based ILs, and protic ILs. Excellent CO_2 separation performances of IL-based membranes have been reported, and some of them have exceeded the upper bound [64, 65]. Despite these advantages, the potentials of ILs-based membranes are still being questioned for their long-term stability and the considerable cost.

PVA is another example of polymers with high CO_2 solubility. Normally, the CO_2 permeability of PVA membranes is very low unless tested at humidified operation conditions. The water vapor from gas streams could swell the PVA chains and then increases the diffusivity resulted from membranes swelling [66]. The presence of H_2O inside membranes could also enhance the CO_2 solubility. Moreover, the current PVA-based membranes are generally blended with other materials, like mobile carriers or hydrophilic additives, which will further improve the CO_2 permeability at humidified conditions. For instance, the introduction of amino acid salts into PVA could result in a 2-fold increment in the CO_2 permeance (399 to 791 GPU) without scarifying CO_2/N_2 selectivity [67]. The water-enhanced membranes process could avoid the dehydration step, which is the prerequisite pre-treatment for other types of membrane materials (e.g., PI).

Apart from the materials of intrinsically high CO_2-philic, the polymers with suitable reactivity with CO_2 could also improve CO_2 transport. In this case, the transport of CO_2 is governed by both solution-diffusion and facilitated transportation mechanism, where the non-interacting gases, such as N_2, H_2, and CH_4, transport only by solution-diffusion mechanism [53]. As a result, high CO_2 selectivity can be achieved without sacrificing gas permeability. PVAm is one of the representative materials in this case. Under humid conditions, CO_2 molecules will dissolve on the surface of a

PVAm membrane, then react with the amine groups and water to form HCO_3^-, achieving a much faster CO_2 permeation compared to a membrane in solution-diffusion mechanism. As a consequence, PVAm membranes showed excellent CO_2 separation performance. [27]. In addition to amine groups, other carriers have also been reported, such as amine acids and ionic liquids, which showed high CO_2 separation performance.

2.2 PEO-based membranes

Ether group is well known for its high CO_2 affinity due to their quadrupolar interactions. Naturally, the polymers composing ether bonds, like PEO, have excellent CO_2 solubility with potentially high CO_2 diffusivity due to its rubber nature. Therefore, the PEO-based membranes should be the ideal candidate for CO_2 separation. However, the CO_2 permeability of the linear PEO membranes (around 12 Barrer) is much lower than expected [24], mainly because of the high tendency of crystallization and the resultant impermeable zones, inhibiting the gas transportation. Theoretical analysis has shown that the strong hydrogen bonding between ethylene oxide units and the resultant intermolecular network are the main reasons for the considerable crystallization, and four PEO chains with 7 repeating EO units in each chain are enough to form a crystallite [68]. Hence, in order to improve the CO_2 permeability by releasing the inhibited crystalline zones, breaking the repeating EO units by 1) copolymerizing with other types of polymeric chains and 2) cross-linking PEO-based monomers or enlarging the distances between two EO units by 3) incorporating liquid additives are the three most efficient approaches.

2.2.1. Copolymerizing with other segments

By copolymerizing PEO with other segments, the tendency of the PEO segment's crystallization could be reduced, benefiting the gas permeation. Aromatic-rich units or the crystalline structures, including polyester [36] [69, 70], polyamide [71, 72], polyimide [73, 74], and polyurea [74, 75], are commonly chosen as the second blocks to reinforce the weak PEO polymeric chains and improve the solvent and thermal stability [76]. The most well-known PEO-based copolymers are two series of commercial polymers with the brand names of Polyactive and Pebax, respectively, which belong to the poly(ester-ester) and poly(ester-amide) family, respectively. Due to the variety of these block copolymers, enormous studies have been conducted to investigate the factors affecting the CO_2 separation performance.

2.2.1.1 PEO segment

One of the most distinguishing features of block copolymers is the phase separation between different segments. In most of the PEO-based copolymers, the PEO segment is the one with lower

T_m, usually close to or even lower than the ambient temperature. Therefore, in the ideal case, the PEO segments can be considered as the amorphous zones embedded with the other zones, which normally is the crystalline one. These hard blocks are widely accepted to have little contribution to gas transport through membranes, which is mainly happen in the amorphous PEO phase. However, due to the high tendency of crystallization of PEO chains, the crystalline PEO may also exist inside the polymer, as shown in **Figure 2.7 (B).** Both crystalline PEO and hard segment crystallite are impermeable to gas. Therefore, in order to improve the gas permeability, the amorphous PEO amount should be increased by increasing the PEO content with very low crystallized PEO chains, which can be achieved through the optimization of the ratio of PEO/other segments and/or PEO segmental length [53, 77]. Metz and co-authors have studied the effects of the PEO segment content and length on the CO_2 separation performance of poly(ethylene oxide)-poly(butylene terephthalate) (PEO-PBT) [69]. It is reported that increasing PEO content from 40 to 75 wt.% could result in an increment in gas permeability from around 30 Barrer to around 130 Barrer. Similar results have been observed by several researchers [72, 78-80]. In addition, CO_2 permeability has been noticed to be positively related to the PEO segment length with a range of 1000 – 5000 g/mol [76]. However, there exist limitations for the maximum content of the PEO block and the length in all PEO-based copolymers, since the high PEO content or long enough PEO chain could cause severe crystallization and then deteriorate the gas transport properties. Peinemann's group has applied a mathematical model to predict the effect of the PEO segmental length and content on the CO_2 permeability based on experimental data [78]. The modelling results show that both the lengths and content of PEO block should be optimized: too high values of these variables result in high crystallization degree with large-size crystallites, while too low PEO content or short PEO block is insufficient for gas transport. Therefore, the one with 2000 g/mol PEO block is chosen with 70 wt.% PEO content for poly(trimethylene terephthalate)-block-poly(ethylene oxide) (PTT-b-PEO), similar to that in Polyactive. The CO_2 permeability reaches 183 Barrer with a CO_2/N_2 selectivity of 51 at 30 °C. In another work from the same group, a range of 2000 – 3500 g/mol for PEO molecular weight (MW) was suggested for PEO-PBT [78]. It is worth mentioning that the optimum PEO segmental length and content vary for different copolymers, which require specific investigation.

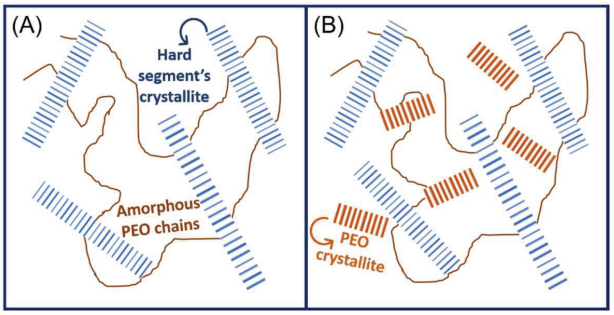

Figure 2.11 Scheme of PEO-based block polymers with (A) fully amorphous or (B) semi-crystalline PEO segments. Reproduced from Ref. [76].

Increasing PEO length and/or content in a moderate range generally leads to positive effects in the CO_2/light gas selectivity. However, some researchers have reported an increased CO_2/He selectivity but a decreased CO_2/N_2 selectivity with increasing PEO content, which is believed due to less phase separation between the PEO and PBT phases [70]. But the increment or decrement is relatively small compared to the values of the selectivity. Moreover, despite the different chemical structure of hard segments or the content or segmental length of PEO, the selectivities of CO_2 over light gas are very similar to each other within different PEO based copolymers (as shown in **Table 2.1**), indicating the separation performance is mainly coming from the amorphous PEO zones.

Considering the fact the crystalline trend increases with the ester group content, researchers replace the PEO chains (partially) by the one with less ester group, like poly(propylene oxide) (PPO) [75, 81-85] or poly(tetramethylene oxide) (PTMEO) [72]. The existence of these units disrupts the regular chain packing and then suppress the crystalline tendency of PEO blocks, leading to the increasing free volume. Compared with the PEO-based membranes, these membranes demonstrated a much higher gas permeability with slightly lower CO_2/light gas selectivity.

2.2.1.2 Second blocks

Apart from the poly(ester-ester) and poly(ester-amide), several permeable units have been chosen recently as the second element to tune the CO_2 separation performance. Tough aromatic-rich units, like polyimide [73, 86-88], have been used to offer mechanical properties instead of the crystalline ones. Okamoto and coworkers conducted a series of research works around poly(ester-imide) more than 10 years ago [87, 89]. It has been reported that the gas permeation is less relevant to the polyimide block. However, due to the mechanical concerns, the polyimide contents are usually required to be relatively high to support the mechanical properties, and hence the gas transport properties are less compatible. Other units, like polysulfone [90, 91] or polycarbonate [92], have been copolymerized with PEO segments. However, the obtained gas permeability is much lower

than that of the poly(ester-amide) membranes [77]. One of the reasons for the low permeability in the above membranes may be the incomplete phase separation due to the good compatibility between these units and PEO, which impedes gas diffusing across the whole membrane.

Recently, Qiao and co-workers fabricated ultrathin thin-film composite (TFC) membranes with a PEO- polydimethylsiloxane (PDMS) selective layer (around 100 nm) based on the continuous assembly of polymers technology [93]. It was achieved by the reaction between the PEO-based macro-crosslinker and the functionalized PDMS gutter layer. The reported CO_2 permeance reaches 1260 GPU with the CO_2/N_2 of over 40. Despite the excellent performance, the feasibility in fabricating defect-free membranes through this method remains doubtful considering the difficulty of this method and the few published papers, all of which are from the same group.

The combination of polyurethane (PU) and PEO has also been proposed and the related work was mainly focused on the optimization of the polyester segments by tuning polyester types and the contents [75, 94, 95]. The reported gas permeability is similar to Polyactive or Pebax, but they are less interested by the industry due to the complex synthesis procedure and hazardous solvents/chemicals. In addition, the mechanical properties of these polymers are not good enough, which may be another issue hindering the upscaling.

In addition to copolymerization, grafting PEO chains onto some current polymers has also been reported recently, and some interesting results have been obtained [96-102]. After grafting PEO side chains to poly(vinyl chloride) (PVC), the CO_2 permeability is promoted from 1.45 Barrer to 100 Barrer with simultaneously increased CO_2/N_2 selectivity [96]. Similar results have been observed by Tiniguchi and co-workers [97, 98]. This significant improvement on CO_2 permeability is mainly because the phase separation between long PEO side chain and the main chain due to their bad compatibility, which promotes gas transport through the more permeable PEO phase.

Based on these discussions, the key factors for improving gas permeability of the PEO-based block copolymers are creating complete phase separation between the amorphous PEO zones and second segments and preventing formation of PEO crystallites. Therefore, the compatibility between the PEO and the second segment is a very important factor: bad compatibility between the PEO segment to the second segment benefits the gas permeability. Attempts have been made to employ mathematical models, like the Maxwell model, to predict these copolymers' behaviors [79, 103]. However, most of them failed or only works for the specificg system, which is less attractive.

Table 2.1 CO_2 separation performance of representative PEO-based block copolymers reported in the literature.

Membranes	P(CO_2) (Barrer)	Selectivity (--)			Test conditions	Ref.
		CO_2/N_2	CO_2/CH_4	CO_2/H_2		
1500PEO77PBT23	115	45.6	17	10.2	30 °C, 0.3 bar single gas	[78]
4000PEO55PBT45	96	43.5	17.1	10.8		
2000PEO70PTT30	183	51	-	10.2	30 °C, 0.3 bar single gas	[79]
2000PEO80PTT20	129	57	-	10.7		
80PTMEO/PA12	221	23.4	-	3.7	35 °C, 10 atm single gas	[72]
53PTMEO/PA12	113	20.4	-	3.5		
55PEO/PA12	120	51.4	-	9.8		
57PEO/PA6	66	56.4	-	7.8		
PEO-ran-PPO-T6T6	447	42.5	13.0	10.2	35 °C, 4 atm single gas	[85]
2700PPG83PU17	190	17	5.5	4.5	35 °C, 2 atm single gas	[75]
2000PEG78PU22	69	29	8.6	5.8		
PEG_{11}-PPG_{16}-PEG_{11}-PU	144	54	-	8.3	25 °C, 4 atm single gas	[94]
XSi-PPU2 (71% PEO)	104	-	20.8	6.9	35 °C, 4 atm single gas	[95]
1900PEO65 PMDA-ODA35	157	-	-	8.5	35 °C, 2 atm single gas	[104]
	179.3	-	-	22.7	35 °C, 4 atm CO_2/H_2 (50/50 vol)	
2000PEO60Pent-PI40	39	46	-	4.1	35 °C, 3 atm single gas	[73]
PCZ-r-PEG	50.7	42.25	-	-	1 bar single gas	[92]
PVC-g-PEO (70 wt% PEO)	100	49	-	-	25 °C, 2 atm CO_2/N_2 (50/50 vol)	[96]
PS-r-PAN-g-PEO (76 wt% PEO)	135	42	-	-	35 °C, 1 atm single gas	[97]

2.2.2. Cross-linking PEO monomers

In addition to copolymerization, another approach to suppress the high crystalline tendency of PEO is cross-linking the short-chain PEO monomers or oligomers. The key point of this process is to create cross-linked but flexible polymeric networks that allow gas to pass through. The polymer chain mobility in these membranes is controlled by the crosslinking density, MW of the monomers (length between cross-linking sites), and the polymer chains/networks. These factors affect the inter-polymer chain spacing and then gas diffusivity. In addition to the polymer design, the reaction types play an important role in the final performance. Hence, studying these factors' effects on the CO_2 separation performance of the resultant membranes are the main topics in this area.

2.2.2.1 Reaction types

Theoretically, cross-linking can be conducted by many different types of reactions. But for this case, there are several aspects that need to be considered, including the efficiency, the availability or possibility of the required functional groups in PEO monomers, and the needed reaction conditions.

Free radical polymerization is the most commonly used cross-linking reaction for PEO-based membranes due to its high conversion efficiency and the abundant acrylate-functionalized PEO monomers. Barrer *et al.* [105] and Hirayama *et al.* [106] have used this reaction to prepare cross-linked PEO membranes using sun lamp and plasma irradiation, respectively, to trigger the reaction between methylacrylate groups. However, these trigger methods did not attract plenty of followers due to the complexity or specified requirements. Later, Freeman and coworkers employed a simple and facile method based on photopolymerization of acrylate-functionalized PEO monomers, which is easier to be triggered than the methylacryate one, and the CO_2 permeability reaches 110 Barrer, almost 10-times higher than that of linear PEO polymer [24, 107]. Afterward, this method has become the most popular cross-linked approach.

Apart from the acrylate, vinyl ether monomers were also utilized based on cationic copolymerization to prepare cross-linked PEO membranes. Excellent gas transport property was obtained, but the obtained membranes were very brittle, which significantly limited its application [108].

In order to exploit the diversity of PEO-containing monomers and avoid the potentially low acrylate conversion, many other cross-linked membrane systems have been developed. For instance, the addition reactions between amino and epoxy groups have been utilized for cross-linking PEO membranes [109-111]. Quan et al. proposed a cross-linking method based on bio-

inspired dopamine and epoxy-functionalized PEO monomers [112]. But the reactions related to dopamine are very complicated, and hence the real cross-linking mechanism still remains unclear. Although amine groups are very reactive, a moderately high temperature (≥ 80 °C) and a relatively long reaction time (≥ 3 h) are needed to complete cross-linking, and some need even more complicated preparation, depending on the monomer reactivity, which is inconvenient for practical applications.

Additionally, the click chemistry has obtained great attention for the advantages, including diverse potential reactions, controllable cross-linking density, high acrylate conversion rate, rapid reaction and low oxygen inhibition [113]. It is worth noting that the click chemistry is a big family, containing more than ten different reactions, like Michael additions [114] and thiol-click relations [115, 116], which provides more opportunity to fabricate PEO-based membranes with different cross-linking structures by employing various monomers/reaction conditions. A series of PEO-based membranes with different cross-linking structures have been fabricated based on radical thiol-ene reactions, which displays improved mechanical properties compared with those made by acrylate polymerization [117]. Moreover, Deng et al. introduced a two-step fabrication based on aza-Michael addition and acrylate homopolymerization for cross-linking PEO membranes [118, 119]. By changing the type of amine- and/or acrylate- and the corresponding monomer ratio, the crosslinking density of the polymeric networks and the CO_2 separation performance of the resultant membranes could be tuned.

Apart from self-standing membranes, Wang and co-workers proposed a cross-linked composite membrane with the selective layer thickness of around 150 nm by using the classical trimesoyl chloride-amine reaction [120]. A PDMS layer was coated firstly on the porous support as the gutter layer to prevent pore penetration. The membranes prepared by longer Jeffamine (ether monomer) display higher CO_2 permeance due to the lower cross-linking density, which is because of not only the longer monomers but also the less available monomers during interfacial polymerization, as a result of the lower diffusion rate of longer monomers. It also leads to lower CO_2/N_2 selectivity and the deterioration at higher operation pressure. Under the same conceptual framework, the membrane prepared by monomers of medium MW exhibits better performance [121].

2.2.2.2 Polymer design

Similar to the situation discussed in Chapter 2.2.1, the number of the continually repeated EO unit, or presented by the MW of these PEO segments, should be limited to a certain value to avoid the potentially forming crystalline PEO. It has been reported that the PEO monomers should not be higher than 1500 g/mol [68]. On the other hand, after cross-linking, the short PEO segments, due to the short PEO monomers, limits the flexibility of the membranes, as well as the free volume and

gas transport properties. Patel et al. cross-linked PEGDA membranes and reported that the CO_2 permeability increases significantly with the number of EO units in PEODA [122]. The longer PEO monomers result in much higher CO_2 diffusivity of the cross-linked membranes compared with those from smaller PEGDA [106]. In addition to the enhancement in gas diffusivity, the EO density in membranes also slightly increases, leading to a simultaneous increment in CO_2 solubility. Therefore, by simply employing longer PEO monomers, the consequent increase in both diffusivity and solubility generates a great increment (~10-fold) in CO_2 permeability. Similar results have been reported in other research works [118, 123].

In addition to the length of the monomers, the monomer types also paly great role in the network configurations and thus, the gas permeability. The commonly employed monomers and the network configurations are presented in **Figure 2.8** and **2.9**. Diacrylate or dimethacrylate monomers are the most intensively employed, which work as bridges in the resultant cross-linking network, as shown in **Figure 2.9 (A)**. Apart from the length of the difunctionalized monomer, their types also play a role on the final performances. With the similar EO unit number, the XLPEGDA membranes have a CO_2 permeability of 110 Barrer, while the CO_2 permeability of the one prepared from BPAEDA is slightly higher (152 Barrer), probably is because that the presence of bulk groups in main chains increases free volume and thus higher gas diffusivity [123].

If incorporating some mono-acrylate or mono-methacrylate functionalized monomers into this network, the monofunctionalized monomers cannot connect to the second polymer chains, and hence behave as flexible side chains. Barrer et al. noticed that the gas permeability increases with the ethyl acrylate (the smallest PEGMEA) content in cross-linked membranes [105]. By connecting this trend with cross-linking density, Freeman et al. designed a series of cross-linked PEGDA/PEGMEA membranes, and the results shows that the CO_2 permeability increases largely and monotonously (from 110 Barrer to 570 Barrer) with the PEGMEA content in membranes (0 to 98.7 wt%). The introduction of PEGMEA decreases T_g, indicating the decrease in cross-linking density. It is believed that increasing PEGMEA content increases the size of free volume elements but has little contribution to their concentration of the free volume elements. But, some research works reported an optimal ratio of PEGDA/PEGMEA in terms of the gas transport properties [124]. In addition, the effects of the PEGMEA's length seems to have some influences on the gas permeability, but less significant than that of PEGDA [123].

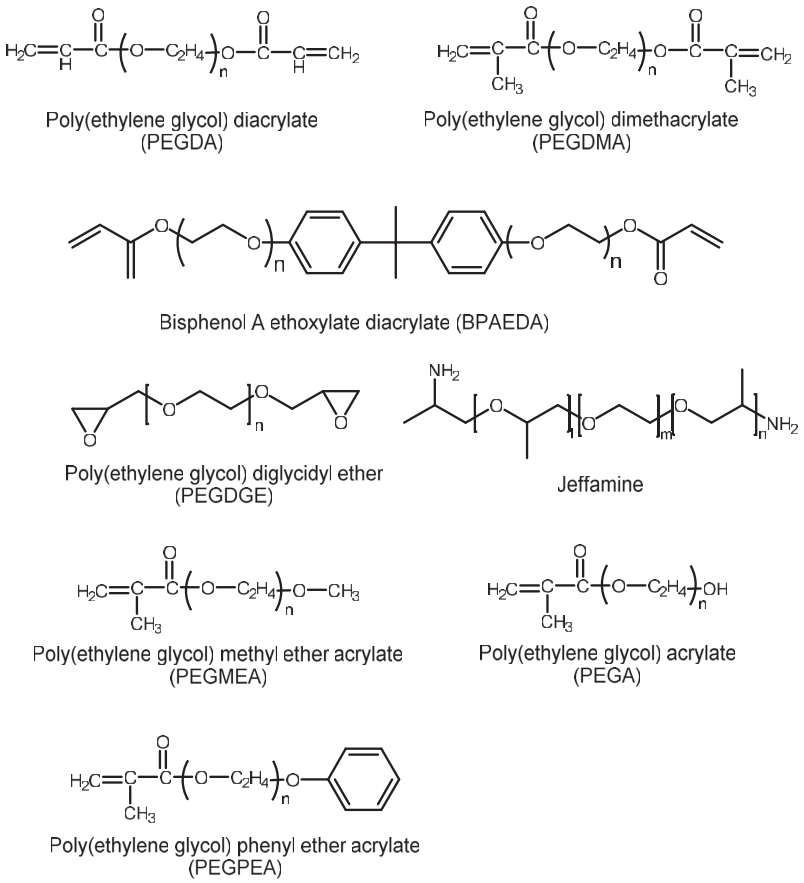

Figure 2.12 The chemical structures of those PEO monomers commonly used for cross-linking PEO membranes

Further studies found that the end groups in the mono-acrylate functionalized monomers play a crucial role in the cross-linked membrane properties and their performances [123, 125]. Kusuma et al. found that when the end groups are methoxy or ethoxy, the introduction of PEGMEA is effective in increasing gas permeability, mainly benefiting from the gains in diffusivity. However, the one with -OH end group displays opposite result, which causes decreasing gas diffusivity and permeability due to the increased hydrogen bonding induced by the -OH end group [125]. Later, the authors also investigated the effects of phenoxy end group, and the results revealed that the addition of phenoxy groups indeed decreases the cross-linking density and increases the free volume. But due to the steric effect of the bulk end group, the flexibility of PEO chains decreases and hence is detrimental for the gas permeability. The membranes with short PEGPEA (n=2)

display a deteriorated CO_2 permeability, while the slightly longer PEGPEA gives more free volume and less harmful effects from the phenoxy group, and as a result, the CO_2 permeability keeps constant [126]. Under the same framework, Freeman's group prepared a series of membranes containing tris-(trimethylsiloxy)silyl groups as the end group of the side chain. This bulk and flexible group increase the free volume by enlarging the size and amount of the element, therefore increasing the CO_2 permeability from 110 Barrer to 800 Barrer. However, the selectivity decreases also because of the changes in free volume [127]. In addition, the gas permeability decreases with the size of the siloxy-based end group, indicating the effects of these bulky end groups [128]. It is worth mentioning that the PEO and Si-based zones are not compatible, which may induce phase separation [129]. Since siloxy-based zones are more permeable than PEO, this incompatibility may be unfavorable to CO_2 selectivity.

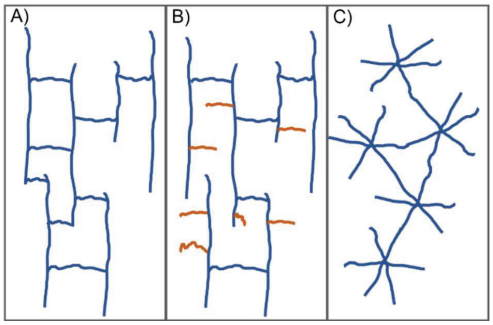

Figure 2.13 The cross-linking network of membrane prepared by A) PEGDA, B) PEGDA + other mono-acrylate monomers, and C) star-like monomers.

Recently, a series of cross-linked PEO membranes have been fabricated based on multi-functionalized monomers [118, 119, 130], which creates a cross-linking network like the one presented in **Figure 2.9 (C)**. It is speculated that this kind of network may be interesting to gas separation due to the different intermolecular packing [131]. Kline and co-workers designed a series of membranes with different network configurations and found out that the network configuration does play a role in the free volume microcavities and thus the gas separation, but very little in terms of selectivity [132]. They also pointed out that this effect is less significant than the one of cross-linking density, which mostly affected by the monomer's molecule weight. Therefore, a proper design should consider both factors. Zhao et al. designed a series of membranes with a three-arm cross-linker as the core and PEGDME as the shell. These membranes display much higher CO_2 permeability (1050 Barrer) than the XLPEGDA one, with similar selectivity, of which the different chain packing and network configuration are believed to be the reason. The authors also found that the short-chain cross-linker should be limited to a small portion in the

preparation receipt, as it might reduce the length between cross-linking sites and increase the stiffness of polymer chains, as well as the network, leading to a sharp decrease of CO_2 permeability and selectivities. The reason for decreasing selectivities probably is connected to the decrease in the ether group content in the as-formed membranes. The same group also optimized the functionality of multi-armed cross-linkers, and the gas permeation results indicate that the too high functionality of cross-linkers may densify the packed chain and result in a lower gas diffusivity and the permeability [133].

Table 2.2 CO_2 separation performance of crosslinked PEO membranes reported in the literature

Membranes	P(CO_2) (Barrer)	Selectivity (-)			Test conditions	Ref
		CO_2/N_2	CO_2/CH_4	CO_2/H_2		
PEGDMA (n=14)	47	68	-	-	25 °C, 0.98 bar single gas	[106]
BPADA (2n=30)	93	63	-	-		
PEGDMA9/PEGMEA9 (90/10)	18.3	68				
PEGDMA14/PEGMEA9 (90/10)	62	69				
PEGDMA23/PEGMEA9 (90/10)	145	66				
PEGDMA69/PEGMEA9 (90/10)	240	56				
PEGDA (n=14)	110	50	18.9	7.3	35 °C, single gas	[107]
PEGMEA (n=8)	570	41	-	12	35 °C, single gas	[134]
PEGDA (20 wt.%)/Tris-A	800	-	~ 5	~ 3	35 °C, single gas	[127]
PEGDMA (50 wt.%) /SiGMA	255	20	6	3.2	35 °C, single gas	[128]
XLBPAEDA (n=15)	152	54	18	7.6	35 °C, single gas	[123]
80/20 BPAEDA15/PEGMEA	198	57	18	8.2		
70/30 BPAEDA15/PEGMEA	221	53	17	8.4		
60/40 BPAEDA15/PEGMEA	261	56	17	9.2		
50/50 BPAEDA15/PEGMEA	300	51	16	9.5		
PEGMEA (70 wt%)/PEGDA	405.7	49.8	-	10.2	35 °C, 3 atm single gas	[124]
PETA (5 wt.%) /PEGMEA	1050	36.5	13.3	-	35 °C, 2 atm single gas	[130]
TMC-EO3	860 [a]	67	-	-	22 °C, 1.1 bar, CO_2/N_2 (15/85)	[120]
TMC-EO21	1310 [a]	33	-	-	22 °C, 5 bar, CO_2/N_2 (15/85)	

TMC-EO14	360 [a]	67.2	-	-	25 °C, CO_2/N_2 (20/80)	[121]
	275 [a]	-	31.6	-	25 °C, CO_2/CH_4 (10/90)	

[a]: CO_2 permeance

2.2.3. Physical blending with low-molecular-weight additives

The third approach to suppress crystalline tendency and improve the gas permeability of PEO-based materials is physical blending with CO_2-philic low-molecular-weight additives, such as low-molecular-weight PEO and ionic liquids. Due to the presence of these additive, the intermolecular distance between EO-rich chains increases, hindering the formation of hydrogen bonding between EO groups and the crystallites.

2.2.3.1 Blending with free PEO

In 2004, Patel *et al.* proposed to embed PEO with a low to medium MW into PEO-based membranes by immersion, and in this early work, the positive impact of free PEO on the CO_2/H_2 selectivity has been mentioned [135]. Inspired by this promising result, Peinemann's group developed a series of blended membranes containing PEO block copolymer and free PEO and systemically studied the effects of added PEO [136-139]. These results firstly show that the addition of free PEO remarkably increases the CO_2 transport properties (up to 8-folds) of both self-standing and composite membranes under various test conditions, indicating the robustness of this approach. Both the structural (increased EO contents) and morphological (increased interchain distance and thus decrease crystallization tendency) properties of the polymeric matrix have been changed by adding free PEO, which enhances both the CO_2 solubility and diffusivity [78]. On the other hand, the gains in CO_2/light gas selectivity have been noticed, although it is less significant, probably due to the same chemical nature of the additives and polymeric matrix.

In addition, various PEO with different terminal groups have been incorporated into this system. It turns out that the gas transport properties are affected by the end groups. Similar to the results in cross-linked membranes, the PEO with methyl ether or butyl ether as end groups are more beneficial than the regular one as higher CO_2 permeability could be obtained. This is explained by these groups could surpass the formation of hydrogen bonding more efficiently [137]. Furthermore, these PEGs induce microphase separation in the blended membranes, which may further enhance the gas diffusivity [137, 139].

Recently, Deng *et al.* investigated the impacts of the MW of free PEO on the Pebax 1074 + PEO membranes with various PEO MW (from 200 to 8000 g/mol) [140]. For the ones containing low-molecular-weight PEO (≤ 600 g/mol), the positive effects of free PEO are similar to the as-

mentioned researches, but the performance of membranes blended with higher MW PEO is temperature-dependent [141]. The crystalline tendency will not be reduced if the added PEO has long chains, which hinders the CO_2 permeability at the temperature below T_m. Once it moves over this critical point, boosted CO_2 permeability could be detected since the crystallites melt.

Notably, the PDMS-PEO blended Pebax® membranes were heterogeneous. Reijerkerk *et al.* hypothesized that the blend membrane prepared using the pristine material with a permeability greater than that of Pebax® may exhibit better performance. Therefore, they blended PDMS-PEG with the specially synthesized poly(ether-amide) of PEO-ran-PPO-T6T6T. The PDMS-PEG blended PEO-ran-PPO-T6T6T membrane exhibited a CO2 permeability of 896 Barrer when the PDMS-PEG content was 50 wt.%. This significantly enhanced permeability confirmed their hypothesis.

By adopting this method into cross-linking, membrane materials with excellent CO_2 separation performance could be realized by incorporating free PEO into cross-linked PEO membranes. There are two main preparation methods for incorporating free PEO into the cross-linked PEO-based membranes: imbedding the PEO into cross-linked membranes by soaking in free PEO-rich media or cross-linking membranes with the presence of the unreactive PEO. The drawback of the first one is the additives' loading cannot be controlled, which is related to the MW of the additives, the immersion condition (temperature, duration solvent, and concentration). Some researchers chose to dissolve additives into a solvent (like ethanol) with higher diffusion rate, which may promote free PEO moving into the cross-linking networks. The MW of free PEO is also a factor needed to be considered: the longer PEO is, the harder it diffuses into the membrane matrix, but more stable it will remain inside membranes. Conversely, in the second preparation method, the free PEO loading could be accurately controlled. However, the presence of unreactive materials reduces the possibility for radical or reactive groups to meet each other and hence the success rate of forming membranes.

Similar to the PEO-based copolymer + free PEO blend membranes, the addition of free PEO improves significantly both CO_2 permeability and CO_2/light gas selectivity of the cross-linked ones, thanks to the lower cross-linking density and thus enlarged interchain distances and reduced crystallinity. Shao *et al.* [124, 142] reported a series of cross-linked PEO + free PEO blending membranes, and more than 7-folds increment in CO_2 (151 to 1301 Barrer) have been achieved with 86% increment in CO_2/H_2 selectivity. In these works, a high free PEO loading (around 50 wt%) was realized by immersing cross-linked membranes into pure PEO and allowing free PEG diffusing into the membranes. It is worth mentioning that in a recent work, Dai et al. has noticed that the relative humidity of the test gas affects the CO_2 permeability and CO_2/light gas selectivity.

The inspiring outcomes from the second method have attract plenty of researchers, and this method has been expanded to other materials [85, 143, 144]. For example, Wessling and co-workers prepared a series of Pebax 1657 membranes blending with PEG-PDMS. Compared to the one with PEG200 (172 Barrer), these additives endow even higher CO_2 permeability (532 Barrer) thanks to the highly permeable PDMS segment [143]. This enhancement is more notable when the matrix changes to another PEO-based block copolymer with higher CO_2 permeability compared with that in Pebax 1657 [85]. Since PDMS is less selective than PEO, these blended membranes display lower CO_2/light gas selectivity.

2.2.3.2 Blending with ionic liquids

Due to the high CO_2-philic nature and their negligible vapor pressures, attempts have been conducted to use ILs as the additives for both PEG-based or cross-linked PEO materials to reduce the crystallinity and improve the CO_2 permeability. Unexpectedly, the addition of ILs does not always lead to positive results in CO_2 permeability. Decreased CO_2/light gas selectivity have been noticed in most relevant studies, as the employed ILs are generally less-selective than PEO. In several works, it is noticed that the addition of ILs decreases the CO_2 permeability at the low loading, which is believed to be because that ILs occupy the free volume and reduced the flexibility of the polymeric chains, judging by the decreased gas diffusivity [145-148]. However, in other Pebax + ILs systems, this decrease is not observed [149], which may be due to the use of different ionic liquids. With increasing loading, the diffusivity increases. In terms of solubility, incorporating ILs generally results in improved values at the low IL loadings, and then keeps at a high level.

It is worth mentioning that the properties of the ionic liquids and PEO-based polymers have huge impacts on the final results. Therefore, the combination should be carefully designed. Due to the different properties of ILs, results may be distinct even the polymers are THE same. Deng et al. prepared Pebax 1657 + ionic liquids membranes with [Bmim][Tf_2N] and [Emim][PF_6] in two works [145, 146]. The ones containing [Bmim][Tf_2N] show a rising trend in CO_2 permeability at higher IL loading, while it is not shown in the membranes with [Emim][PF_6]. This difference may be caused by different compatibility of these ionic liquids with polymeric matrix, which leads to distinct results on diffusion and thus the permeability. In addition to the effects of ionic liquids, the choose of the polymeric matrix also matters. Bernardo et al. added [Bmim][CF_3SO_3] into Pebax 1657 and Pebax 2533, and the effects of this IL are only observed in the Pebax 1657 based membranes (4-fold increase), but not with the Pebax 2533 ones (no changes), of which the reasons are still unclear. But promising results also have been reported [150, 151]. An interesting system consisting of SO/SOS and extremely high amount of [Emim][NTf_2] endows excellent CO_2

separation performance as CO_2 permeability and CO_2/N_2 selectivity increased from 567 to 996 Barrer and from 21.3 to 59.8, respectively [152].

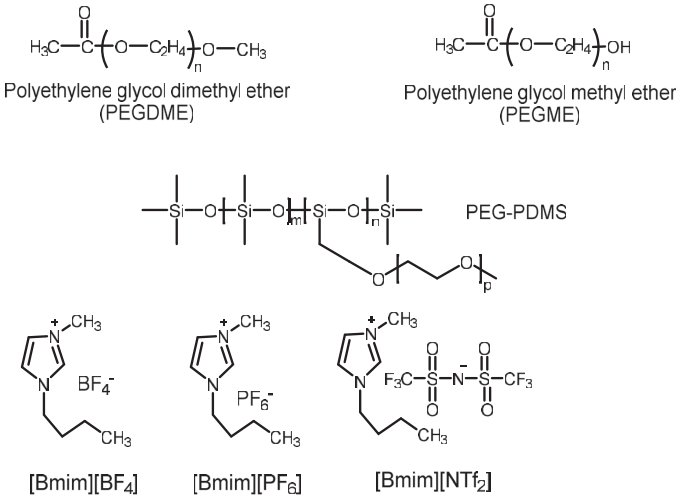

Figure 2.14 The chemical structure commonly used as free additives

Considering the roles of ILs play inside the membranes, incorporating higher CO_2-philic ionic liquids, such as task specific ionic liquids (TSILs), into membranes may be a promising direction to study. The anions of ILs are well-known as a more interesting part for on physical properties and chemical affinity [62]. Hence the researches should be more focused on the functionalization and/or optimization of the anion [151]. Additionally, the polymer + ionic liquid blend materials' microstructure [152, 153], affecting by two individual compounds and the pairing, should be paid more attentions for better understanding of the relationship between the polymers and ionic liquids, and for further improvement of the gas separation properties.

Table 2.3 CO_2 separation performance of PEO-based blended membranes reported in the literature

Membranes	P(CO_2) (Barrer)	Selectivity (-)			Test conditions	Ref
		CO_2/N_2	CO_2/CH_4	CO_2/H_2		
Pebax 1657 + 50wt% PEG200	151	-	-	10.8	25 °C, 1 atm single gas	[136]
PolyActive + 40 wt% PEO	208	48.7	15.8	11.6	30 °C, single gas	[137]
PolyActive + 40 wt% PEG-methyl ether	295	48.7	15.1	12.9		
PolyActive + 40 wt% PEG- butyl ether	400	50.1	12.5	11.8		
PolyActive + 40 wt% PEG-dimethyl ether	430	46.5	14.3	14.6		

PolyActive + 40 wt% PEG-dibutyl ether	750	40	11.2	12.4		
Pebax 1657 + 50 wt% PEG-PDMS	532	36.1	10.8	10.6	35 °C, 4 atm single gas	[143]
1500PEO77PBT23 + 30 wt.% PEO	134	48.7	15.1	10.6	30 °C, single gas	[78]
4000PEO55PBT45 + 50 wt.% PEO	190	47.3	15.9	13.2		
PS-b-PEO-b-PS + 45 % PEG400	86	-	-	4.3	35 °C, 2 atm single gas	[91]
PS-b-PEO-b-PS + 45% PEG4600	17	-	-	2.2		
PEO cross-linked with A-amine + 44 wt% PEGDME	196.4	108.5	7.6	-	R.T., 2 bar single gas	
PEO cross-linked with A-amine + 37.5 wt% PEGDME	180	~ 45 [b]	~ 20 [b]	-	R.T., 2 bar, 90 RH%, CO_2/N_2 (10/90)	[109]
Jeffamine 600 - PEGDGE + 47 wt% PEGDME	1301	-	-	13.0	35 °C, 3.5 atm single gas	[142]
PEGMEA-PEGDA-PEGDME-7-3-10	2980	45.7	-	14.7	35 °C, 3 atm single gas	[124]
XLPEGDA700-PDMS + 40 vol%[emim][NTf_2]	340	31	-	-	40 °C, 1 atm single gas	[150]
Pebax 2533 + 30 wt% TSIL	501[a]	46	-	-	R.T., 1.75 bar, 75RH%[c] CO_2/N_2 (10/90)	[154]
Pebax 1657 + 40 wt% [Emim][PF_6]	86	~ 30 [b]	~ 20 [b]	~ 8 [b]	35 °C, 3 bar single gas	[145]
Pebax 1657 + 40 wt% [Bmim][NTf_2]	286	~ 28 [b]	~ 15 [b]	~ 8 [b]	35 °C, 7 bar single gas	[146]
Pebax 1657 + 80 wt% [Bmim][CF_3SO_3]	~ 300	40	-	-	25 °C, 1 bar single gas	[147]
Pebax 2533 + 80 wt% [Bmim][CF_3SO_3]	~ 250	~ 28	-	-		
SO/SOS + 94 wt% [Emim][NTf_2][d]	996	59.8	-	-	R.T. °C, 4 bar single gas	[152]
XLPEGDA + 40 vol% [Emim][NTf_2]	270	37	-	-		
XLPEGDA + 40 vol% [Emim][dca]	210	60	-	-	30 °C, 1 bar single gas	[150]
XLPEGDA-PDMS + 40 vol% [Emim][NTf_2]	340	31	-	-		
XLPEGDA + 40 vol% [Emim][dca][e]	240	53	-	-		
XLPEGDA + 60 vol% [Emim][NTf_2]	530	31	-	-	30 °C, 1 bar single gas	[151]
PEGDA-TAEA + 44.4 wt% [Bmim][TCM][f]	134.2	49.5	-	-	R.T., 2 bar single gas	[118]

[a]: CO_2 permeance; [b]: Estimated; [c]: R.T. (room temperature), RH: relative humidity

[d]: SO/SOS: polystyrene-b-poly(ethylene oxide) diblock copolymer/polystyrene-b-poly(ethylene oxide)-b-polystyrene triblock copolymer;
[e]: 1-ethyl-3-methylimidazolium dicyanamide
[f]: 1-Butyl-3-methylimidazolium tricyanomethanide

2.2.4. Effect of operation conditions

Apart from the influences of chemical structures of the membranes, operation conditions, including temperatures and pressures, also have great impacts on the obtained performance [71]. Generally speaking, gas permeability decreases almost linearly with reducing test temperature due to the lower gas diffusivity. However, several researchers have observed a steep decrease near the T_m of the PEO segments due to the formation of PEO crystallites [69, 76, 82, 83, 94]. The (PEO-ran-PPO2500/T)$_{10000}$-T6T6T copolymer has a CO_2 permeability of 570 Barrer at 50 °C, but it decreases to 235 Barrer at -10 °C [83]. As mentioned earlier, the T_m of PEO blocks are usually located in 0 - 30 ºC, mainly depending on the composition, which may lead to huge differences in the obtained performance at different test temperatures. When the operating temperature is lower than the T_m of PEO segments, crystallites form and thus reduce the available amorphous PEO zones, correspondingly lower gas permeability. This is the reason that most of the relevant permeation tests have been conducted at 35 ºC to avoid the PEO blocks' crystallization. On the other hand, positive effects have been found in CO_2/N_2 or CO_2/CH_4 selectivity with decreasing temperature, attributed to the prominent size-sieving effect of the crystalline PEO on the diffusivity selectivity [76, 83]. However, reducing temperature has a negligible effect on gas permeability of smaller gases (e.g., H_2), thus decreasing temperature is unfavorable to CO_2/H_2 selectivity [76]. The T_m of the PEO segments are highly related to the PEO segmental length and content. Increasing both PEO segment content and/or length within a proper range can increase the melting temperature of the PEO segments, and thus improve the gas separation performance [69].

The influences of operation pressure on the separation performance of PEO-based block copolymers have also been investigated [36, 71, 72, 82, 143]. It has been reported in different literature that the CO_2 permeability increases with the increasing CO_2 partial pressure, a typical plasticization behavior. The main reason is that there exists strong interactions between CO_2 and polymer chains, the high CO_2concentration inside membranes could swell the polymeric chains and lead to increasing chain flexibility, as well as the free volume [155]. On the other hand, the light gases have much lower solubility compared to CO_2 and plasticization effect, and hence their permeability decreases with the increasing pressure due to the reduced free volume induced. Therefore, the ideal CO_2/light gas selectivity increases with the pressure as well [72, 82]. However, the results obtained from mixed gas permeation tests show te opposite trend. The CO_2-swollen polymeric chains have more flexibility and thus less separation ability, presenting by the decreased

separation factor except for CO_2/H_2. Because H_2 is much smaller, the CO_2/H_2 separation factor still presents positive relation with the pressure, but with a much slower slope compared to the one obtained from the single gas experiment [82]. This effect is also linked to the PEO segment: the plasticization effect is more significant for membranes with higher PEO content. Bondar et al. noticed that the Pebax with higher PEO content suffers more severely at high CO_2 partial pressure [72].

Furthermore, the temperature also affects the separation behavior at different pressure. Wessling's group reported that at low temperatures. CO_2 permeability increases more sharply with the operation pressure, which may be explained by the plasticization [83]. The polymer chains become more flexible at the higher CO_2 transmembrane pressure which offsets the restricted flexibility of PEO zones because of the semi-crystallization at low temperature. Hence, the lower operating temperatures push the performance closer to the upper bound [83], which may be interesting for some applications conducted at low temperatures (like CO_2 separation from natural gas) [82].

2.3 Mixed matrix membranes containing ZIFs

2.3.1. ZIF-based Mixed matrix membranes

In addition to polymer design, incorporating porous inorganic fillers into a polymeric matrix to fabricate mixed matrix membranes (MMMs) has been one of the encouraging and hence intensively studied approaches combining the processability of polymeric substrates and molecular sieving capability of inorganic fillers from both sides. This combination has been predicted to display superior gas separation performance, as shown in **Figure 2.11**, which may exceed the upper bound. Furthermore, the rough inorganic matters also could enhance the polymers with poor mechanical properties. Based on these advantages, numerous research efforts have been put on to developing the MMMs with various polymers and particles and understanding the mechanisms behind [156-158].

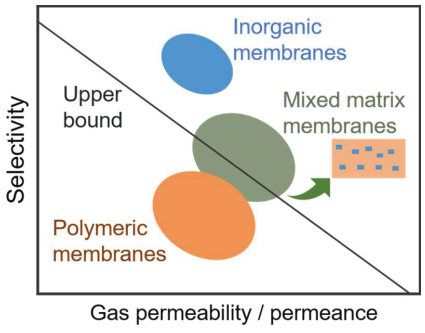

Figure 2.15 The expected performances of mixed matrix membranes. Reproduced from Ref [28]

Among a huge library of inorganic fillers, zeolitic imidazolate framework (ZIFs) have been regarded as a good types of candidates to obtain good compatibility and interaction with polymers because of the organic linkers. With the target as CO_2 separation, the ZIFs with suitable pores could work as molecular seize, which allows the smaller CO_2 (3.3 Å) pass through, but not or less CH_4 (3.8 Å) or N_2 (3.6 Å). Then the CO_2/light gas selectivity could be enhanced by added ZIFs. In addition, these pores also offer more path for CO_2 transport, which may benefit its diffusivity and thus permeability. Therefore, the simultaneous increment in CO_2 permeability and selectivity may be achieved by incorporating suitable ZIFs into the polymeric matrix. The most commonly used ZIFs for this purpose are ZIF-8 with a pore size of 3.4 Å [159], just right for CO_2 separation. It is noteworthy that this method usually is not applied for CO_2-selective hydrogen purification, since the smaller H_2 (2.9 Å) may gain more benefits from the addition of ZIF particles. Hence, this section only covers studies related to CO_2/N_2 and CO_2/CH_4 separation.

Following this concepts, enormous ZIFs-enhanced MMMs have been prepared and studied. In the beginning, the research focuses were mainly on the ZIF + commercial polymer systems, which are usually glassy polymers, including Matrimid [160, 161], polysulfone (PSf) [162] or polyetherimide (like Ultem® 1000 [163]). Almost all researches reported the improved CO_2 permeability after adding ZIFs into polymeric matrices [160, 161]. For the commercial polymers, which usually have CO_2 permeability < 50 Barrer, the incorporation of ZIF particles could realize a several-fold enhancement in CO_2 permeability. For instance, Song et al. prepared a series of Matrimid + ZIF-8 MMMs, and an increase of ~156% in CO_2 permeability has been realized in the one with 30 wt. % ZIF-8 [164]. However, despite these improvements, the values of CO_2 permeability are still much lower than the industry interested performances. Moreover, due to the huge difference in the gas transport properties between these polymers and ZIF particles (usually > 1000 Barrer), the main resistance exists in the polymeric zone and hence it may not be the best option. Koros *et al.* proposed that the more permeable polymers may be more interesting for MMMs [165]. They compared the ZIF-90-based MMMs consisting of various polymers and found that the MMM based on 6FDA-DAM (most permeable polymers in this work) shows the most significant improvement compared to the neat polymer. Later, the incorporation of ZIFs into the highly permeable polymers has become one of the main directions in this area [166-168]. The effects of ZIF nanoparticle in MMMs based on PTMSP [169], PIM-1 [166, 167, 170], PIs [171-173] and TR [174] have been investigated. Compared to the less-permeable polymers, the improvement rate in CO_2 permeability due to the adding ZIFs into these highly permeable systems is less significant (usually within 200% increase), but the real values of CO_2 permeability are much attractive for CO_2 separation, which usually higher than 1000 Barrer. Lately, ZIF particles have also been incorporated into the rubbery polymers, like PEO-based copolymer [175, 176].

These large increments in CO_2 permeability match the previous expectation and are widely accepted as the results of several positive factors. Firstly, the employed ZIFs have a pore size slightly bigger than CO_2, through which CO_2 can pass freely, leading to a great increment in CO_2 diffusivity [171]. For example, in 6FDA-Durene + 20 wt.% ZIF-71 (200nm) membranes, more than 270% increase in CO_2 diffusivity has been documented, which is the main reason for the 240% increment in CO_2 permeability [171]. Moreover, the presence of ZIF particles during membrane preparation also changes the chain packing of the polymeric matrix and may increase the free volume inside MMMs, resulting in positive impacts on the gas diffusivity [164]. Theoretically, this effect should be more notable for glassy polymers, in which polymeric chains have much lower flexibility compared to the rubbery ones [177]. Therefore, in terms of gas permeability, considerable enhancements are usually reported in the ZIF + glassy polymer system. In some works, increasing CO_2 solubility has been observed and is usually ascribed to the interactions of the organic linkers in ZIFs with CO_2 [178, 179].

Table 2.4 CO_2 separation performance of ZIF-based MMMs reported in the literature

Membranes	P(CO_2) (Barrer)	Selectivity (increment) CO_2/N_2	Selectivity (increment) CO_2/CH_4	Test conditions	Ref.
Pebax1657 + 8 wt.% ZIF-7 (30 – 35 nm)/PSf	145 (1.01)	23 (0.64)	64 (1.00)	20 °C, 3.75 or 7.5 bar, single gas	[175]
Pebax1657 + 22 wt.% ZIF-7 (30 – 35 nm)/PSf	111 (0.54)	30 (0.14)	97 (1.85)		
Poly(ether imide) + 7 wt.% ZIF-7	245.9 (1.98)	1.3 (-0.66)	2.3 (-0.49)	35 °C, 2.03 bar, single gas	[179]
Matrimid 5218 + 30 wt.% ZIF-8 (60 nm)	28.72 (2.56)	17.1 (-0.24)	24.9 (-0.29)	22 °C, 4 bar single gas	[164]
PSf + 24 wt.% ZIF-8 (75-105 nm)	24 (3.8)	-	24 (0.04)	35 °C, 2 bar CO_2/CH_4 (1:1)	[162]
SBC [a] + 20 wt% ZIF-8 (nm, annealed)	39.74 (1.95)	22 (0.85)	-	R.T., 2 bar single gas	[180]
SEBS [b] + 30 wt.% ZIF-8 (88 nm)	439.2 (1.57)	10.6 (-0.15)	5.2 (0.21)	35 °C, 3.75 or 7.5 bar, single gas	[181]
SEBS + 30 wt.% ZIF-8 (240 nm)	454.6 (1.66)	12 (-0.03)	5.4 (0.25)		
SEBS + 30 wt.% ZIF-8 (533 nm)	465.4 (1.728)	10.8 (-0.13)	5.2 (0.21)		
PVC-g-POEM [c] + 30 wt% ZIF-8 (206 nm)	687.7 (7.80)	34.9 (0.14)	12.4 (-0.12)	35 °C, single gas	[182]
PIM-1 + 43 vol% ZIF-8 (as-casted)	6300 (0.44)	-	14.7 (0.04)	R.T., 1 bar, single gas	[166]
PIM-1 + 43 vol% ZIF-8 (alcohol-treated)	19350 (0.53)	-	7.3 (-0.57)		
TR + 20 wt. % ZIF-8	947 (1.29)	16.7 (-0.19)	21.9 (-0.03)	35 °C, 1 bar, single gas	[174]

XLPEGDA + 59.8 wt.% ZIF-8	910.8 (1.15)	28.5 (0.17)	9.2 (-0.37)	35 °C, 5 atm, single gas	[183]
XLPEGDA + 67.7 wt.% ZIF-7	1083.7 (1.56)	38.5 (0.17)	12.7 (-0.12)		
Pebax 2533 + 10 wt.% Zn/Ni-ZIF-8	321 (0.97)	42.8 (~ 0.4 [d])	-	30 °C, 2 bar, single gas	[184]
Pebax 2533 + 10 wt.% ZIF-8	266 (0.63)	33.8 (0.13)	-		
Pebax 1657 + 5 wt.% ZIF-8	130 (0.63)	46.4 (-0.12)	18.6 (-0.06)	35 °C, 11 bar, single gas	[185]
Pebax 1657 + 5 wt.% ZIF-67	160 (0.63)	81.0 (0.54)	24.9 (0.26)		
6FDA-DAM + 20 wt% ZIF-11 (0.2 -2 µm)	257.5 (11.5)	-	31.02 (-0.05)	30 °C, 4 bar, single gas	[172]
PIM-1 + 20 wt.% ZIF-67	5206 (0.15)	24.2 (0.20)	16.8 (0.34)	30 °C, 2 bar, single gas	[170]
PIM-1 + 30 wt% ZIF-71	8377.1 (1.54)	18.3 (-0.09)	11.2 (0.10)	35 °C, 3.5 atm, single gas	[167]
UVPIM-1 + 30 wt% ZIF-71	3458.6 (1.80)	26.9 (-0.1)	35.6 (0.04)		
6FDA-Durene + 20 wt% ZIF-71 (30 nm)	2560 (2.1)	13.8 (-0.07)	14.2 (-0.17)	35 °C, 3.5 atm, single gas	[171]
6FDA-Durene + 20 wt% ZIF-71 (200 nm)	2744 (2.41)	13.2 (-0.09)	13.9 (-0.18)		
6FDA-Durene + 20 wt% ZIF-71 (600 nm)	1656 (1.06)	13.5 (-0.08)	14.7 (-0.14)		
6FDA-DAM + 15 wt.% ZIF-90 (0.85 µm)	700 (0.79)	-	37 (0.54)	25 °C, 2 atm CO_2/CH_4 (1:1)	[165]
6FDA-DAM + 15 wt.% ZIF-90 (2.0 µm)	590 (0.51)	-	34 (0.42)		
6FDA-TP + 50 wt% ZIF-90 (79 nm)	63 (2.15)	20 (0.0)	36 (-0.03)	30 °C, 9.5 bar, single gas	[168]
6FDA-DAM + 40 wt.% ZIF-94 (< 500 nm)	2310 (2.0)	22.7	-	25 °C, 2 atm CO_2/N_2 (15:85)	[173]
PSf + 0.037 wt. % ZIF-108 (170 nm)	~ 160 [d] (14)	~ 12 [a] (~ 0.5 [a])	-	6 atm CO_2/N_2 (1:1)	[186]
	~ 180 [d] (> 10)	-	~ 12.5 [d] (~ 0.5 [d])	6 atm CO_2/CH_4 (1:1)	
Pebax 1657+ 5.0 wt.% ZIF-67 nanosheets	139.4 (0.51)	73.2 (0.76)	17.6 (0.45)	25 °C, 1 bar, single gas	[177]
Pebax 1657+ 5.0 wt.% ZIF-67 nanoparticles	95.7 (0.03)	46 (0.10)	12.9 (0.06)		
Pebax 1657+ 5.0 wt.% ZIF-67 microparticles	101.0 (0.09)	45.1 (0.08)	12.8 (0.06)		

[a]: SBC: poly(styrene-co-butadiene)
[b]: SEBS: polystyrene-block-poly(ethylene-ran-butylene)-block-polystyrene
[c]: PVC-g-POEM: poly(vinyl chloride)-g-poly(oxyethylene methacrylate)
[d]: Estimated

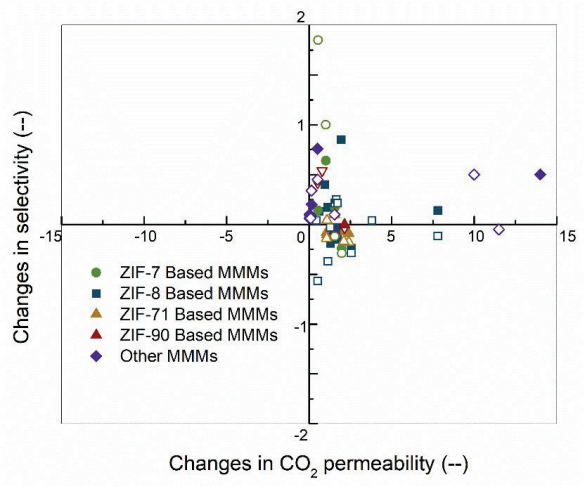

Figure 2.16 The changes of CO_2 permeability vs. the changes of CO_2/N_2 (solid symbols) and CO_2/CH_4 (open symbols) selectivity after adding ZIFs into the polymeric matrix. The results are listed in **Table 2.5**.

However, the CO_2/light gas selectivities were not enhanced greatly as expected [160, 165, 187]. The selectivities only show moderate [161] or even negative improvements [164, 179] in plenty of research works, as displayed in **Figure 2.12**. One of the reasons for it is the gate-opening phenomenon existed in ZIFs, presenting as the molecules bigger than the pores still can pass through the ZIFs, due mainly to the swinging of the $-CH_3$ groups and imidazolate linkers [188]. Therefore, the blocking effects are much lower than expected. But the most severe one is the bad interface between the polymeric matrix and ZIF particles due to the incompatible issue [158, 187, 189, 190]. This incompatibility leads to the non-selective void between polymeric chains the particles, which has been observed by SEM in several reports [191, 192], and as a result, the selectivity deteriorates. This issue will become much severer for further scaling-up, where MMMs work as the selective layer in composite membranes, because of the very thin layer with a thickness of ≤ 1 μm.

Apart from the interface issue, the agglomeration of particles or poor dispersion has been observed from SEM, especially when the filler loading is high, which could result in separation performance deterioration. This problem is usually associated with the poor adhesivity of polymers on the filler surface, which leads to the bad compatibility between fillers and polymers. Some researchers claim that the compatibility between ZIFs and polymers may have been overestimated. In order to overcome it, the selection of polymer and ZIF pairing and the preparation methods should be wisely chosen.

2.3.2. Current modification approach

To address the above-mentioned issues, research attentions have been drawn into understanding how particles affect the performance of the resultant MMMs, modifying the particles' surface or the organic linkers for better compatibility between polymers, adding third compounds, and developing new membrane preparation methods [156, 157, 193].

The properties of polymers and ZIFs are directly associated with the interface morphology of the resultant MMMs as well as the separation performance. Moreover, the polymer matrix determines the lower limitation of CO_2 separation performances, while the added ZIFs affect their improvement, based on the Maxwell equation, in a defect-free MMMs. Hence, a wise pairing has a higher possibility of obtaining better membranes. In terms of ZIF-based MMMs, the ZIFs have been regards as good fillers in some polymers, like polybenzimidazole (PBI), due to the strong interaction [189, 194]. Great improvement has been reported for H_2 separation and pervaporation, but this combination is rarely used for CO_2 separation because of the low CO_2 permeability and selectivity of PBI. Hence, the research interests have been more focused on the ZIFs side.

2.3.2.1 Filler properties

Previously the researchers focused more on the effects of pores inside ZIFs, especially the pore size, or the chemical properties of organic linkers in terms of the compatibility with polymers. However, several recent studies have shown that the filler's geometry may result in distinct performance, even for the same pairing [189]. Generally speaking, MOFs with smaller sizes have higher external surface areas and thus more interfacial areas between polymer and nanoparticles [165, 195, 196]. But on the contrary, larger particles have less trend of particle agglomeration and may benefit the gas transport properties of the resultant membranes [171, 196, 197]. Therefore, the optimization of nanoparticle size should be taken into consideration. Zheng *et al.* prepared a series of MMMs containing Pebax and ZIF-8 nanoparticles with different sizes (40–110 nm) and found out that the larger nanoparticles are preferable for both CO_2 permeability and CO_2/N_2 selectivity, for all studied ZIF-8 loading [197]. It is believed that the presence of larger ZIF-8s in MMMs leads to a higher free volume and thus higher permeability, and the higher specific surface area of ZIF-8 nanoparticles benefits the selectivity. Similar results have been reported in several research works [171, 196], while further increases in particle size may not bring positive results. Japip and co-workers investigate the effects of the filler sizes on the gas separation performances of 6FDA-Durene + ZIF-71 MMMs comprising three different ZIF-71 particle sizes (30, 200, and 600 nm). They found that the ZIF-71 with size $\geq$ 200 nm endows lower CO_2 permeability, mostly due to the lower diffusivity, with similar selectivity [171]. Another study reported the similar results that

smaller ZIF-90 (0.85 μm) gives better results in both CO_2 permeability and selectivities [165].

In addition to the size, the shapes of the particles also play a role in the interface morphology. The most intensively studied particle shape is spherical or close to spherical, which is relatively easy to be fully wrapped by polymeric chains, while the other appearance may result in different situations. Koros et al. predicted that the particles with higher aspect ratio, like sheets, flake or platelet-like, may be more attractive as fillers in MMMs because of the increased permeation difficulty for the rejected gases and thus, the enhanced separation ability. These types of fillers also could offer shortcut path for desired molecules and therefore, elevated flux [156, 198-201]. However, only a few related researches have been reported. Very recently, Feng and co-workers developed several ZIF-67s (200nm nano-particles, 2 μm micro-particles, and nanosheets) and incorporated them into Pebax 1657 to investigate the effect of the ZIF morphology in the performance of the resultant MMMs [177]. The gas permeation results show that a small amount of nanosheet (5 wt.%) endows about 51% increase in CO_2 permeability with simultaneous improved CO_2/N_2 and CO_2/CH_4 selectivities, while other MMMs display nearly unchanged values in both CO_2 permeability and selectivities. The authors speculate that the dispersed ultra-thin nanosheets (~ 4 nm) provides more obstructs for bigger molecules, like CH_4 or even N_2, but not CO_2, since CO_2 can pass through nanosheets directly. However, this theory cannot match with the diffusivity and solubility data in this work, in which the CO_2 diffusivity and solubility improve, but N_2 diffusivity and solubility keep almost unchanged compared to the MMMs with other ZIF-67s. The incorporation of ZIF-67 nanosheets may have only offered more interfacial exchange area and "shortcut" for CO_2 diffusion, not obstructs for bigger molecules. These results match with several works employing other fillers [202, 203].

A recent study compares the effects ZIF-67 and ZIF-8 in the MMMs comprising of Pebax 1657 as the polymeric matrix. Although these two ZIFs have the same organic linkers and crystal morphology, the membranes containing ZIF-67 display higher values in both CO_2 permeability (160 Barrer) and selectivity (CO_2/N_2: 81 and CO_2/CH_4: 25), compared with the one enhanced by ZIF-8 (130 Barrer with reduced selectivity) [185]. Moreover, the direct reasons for improved CO_2 permeabilities are different: adding ZIF-8 increases CO_2 solubility, while added ZIF-67 enhances diffusivity in MMMs. This difference is brought by the effects of metal ion, expressing as the stiffer Co-N bond and smaller pore size. The influences of the metal ions have also been documented in another study, in which the better performances are endowed by the Ni-substituted ZIFs [184].

2.3.2.2 Modification of ZIFs

In addition to the bare ZIFs, functionalized ZIFs with CO_2-philic compounds have been accomplished to offer better compatibility with polymeric matrix and/or stronger interactions with CO_2. Amino-functionalization is the most common one for this target [204-209]. Dong *et al.* modified ZIF-8 by coating a thin layer of polydopamine on the surface and incorporated them into Pebax membranes [204]. An anti-tradeoff behavior was reported in the membranes with coated ZIF-8, which 15 wt.% loading gives 135% and 108% increments in CO_2 permeability and CO_2/N_2 selectivity, respectively, surpassing the upper bound. While adding the pristine ZIF-8 results in a lower increment in CO_2 permeability and reduced CO_2 selectivity compared with the neat polymeric membrane.

Linker-exchange is another direction for post-modification of ZIFs. Previous studies suggest that the ligand dipole moment may be the main criteria of ZIFs' CO_2 solubility, which also may strongly affect the improvement in CO_2 separation performance of the MMMs [210]. In a recent work, the modified ZIF-7 by replacing the organic linker inside ZIF-7 to benzotriazole has been added into poly(ether imide) membranes, which improved permeabilities of all the gas investigated, while adding the neat ZIF-7 led to significant reduction [179]. In addition to functionalized ZIFs, some researchers have also chosen different strategies, such as thermal annealing [180] or etching [208].

In addition to chemical functionalization, changing ZIF's architecture has also been a direction. Recently, hollow or capsule-like ZIFs have been reported as the fillers in MMMs [211-213]. Kim's group fabricated hollow ZIF-8s by several methods and incorporated them into PVC-g-POEM [211, 212]. The as-prepared MMMs display a several-fold increase in CO_2 permeability with moderate selectivity, which is close to the upper bound. Similarly, Hu et al. developed an open-cocoon like ZIF and then embedded it into cross-linked PEO membranes. These ZIFs are considered as "CO_2 transport promoter" and work as low-resistance channels only for CO_2. Therefore, only 10 wt. % loading realized the enhancement of CO_2 permeability from ~ 130 Barrer to ~373 Barrer, with a 15% increase in CO_2/H_2 selectivity and a slight decrease (10%) in CO_2/N_2 selectivity [213].

In the past years, employing porous nanomaterials as the carriers of ZIFs has been a popular method for better filler dispersion and compatibility with polymer. Moreover, this method also combines the advantage from both nanomaterials [214-216]. For example, Dong et al. [214] fabricated MMMs by incorporating ZIF-8/graphene oxide (ZIF-8-GO) composites into Pebax to improve CO_2 separation performance. This composite is designed based on the combination of the high CO_2 solubility (ZIF-8) and the selective barrier (GO). Permeation results show that the interface compatibility of ZIF-8-GO with Pebax and the separation performance of the resultant

MMMs are much better than its parents. Only 6 wt.% filler content endows a CO_2 permeability of 249 Barrer and a CO_2/N_2 selectivity of 47.6.

2.3.2.3 Third compounds

Introduction a third compound, usually liquids, into the polymer + ZIFs binary systems is another promising approach. The third compounds are mainly designed and used for eliminating the interfacial voids [189, 217]. ILs have excellent CO_2 solubility and negligible vapor pressure, and hence have often been utilized as the third compounds in MMMs to ease the interface issue and improve CO_2 affinity of membranes.

Li et al. introduced several ILs into Pebax/ZIF-8 systems by direct blending. Compared to the binary systems, this ternary system displays three-step changes: the CO_2 permeability increase, then decrease, and finally increases with the ILs loading [218]. The ionic liquids first locate at the interfacial defects, then the initial free volumes, and finally expand the interchain distance due to the large amount, which matches the changes in permeability. The positive effects are also reported in the PIL/IL/ZIF systems, where the negative results are not found, which may be because of the different preparation. In these systems, ionic liquids mainly behave like the wetting agent between the ZIF-8 and PIL phases at low loading [219]. Following the same idea, free PEO has also been employed as the third compounds in a recent work [220].

Different preparation methods have been developed, and different effects of ILs are also explored. For example, the ZIFs could work as nanocages for immobilizing ILs, and then be incorporated into the polymeric matrix. Some attempts have been devoted to this approach and found improved performance in the corresponding membranes because of the high CO_2 solubility of ILs. In this regard, higher CO_2 selectivity and better mechanical properties have been reported compared with the one only containing ZIF particles, suggesting the better compatibility between IL-loaded ZIF and polymeric matrix and the favorable interface [221]. However, due to the occupied pores in ZIFs, the CO_2 permeability of the ternary is lower than the binary system. An obvious cavity-occupying effect of ILs in the cages was observed, which led to a decrease in the effective cage size of ZIF-8. This cavity-occupying effect, also reported in other work [222], has been observed, expressed as the decrease in the effective cage of ZIF-8 (from 1.12 to 0.59 nm) based on N_2 adsorption results.

2.3.2.4 Novel preparation methods

The preparation methods have a great influence on the MMMs morphology. For example, the agglomeration of fillers may happen during solvent evaporation when the viscosity of membrane

solution is too low, or the dispersion of fillers inside membranes solution is very poor. The most widely used preparation method is priming one, in which the polymers are gradually added into the filler/solvent suspension, so that the fillers could be coated by a thin layer of polymer at the first stage. Moreover, the stress at polymer/filler interface could be reduced, and as a result, better polymer/filler interaction. However, this process is still not sufficient to eliminate the formation of agglomeration in some cases. Some novel preparation methods have been proposed to obtain better dispersion and interface between polymer and fillers.

Blending ZIFs with the polymerizable monomers and then cross-linking these monomers at the presence of ZIF particles. Since the fillers are well surrounded by the small molecules, the interface issue between these ZIFs and the formed polymer chains are largely eliminated. To date, this method is only valid for PIL/ZIF and cross-linked PEO/ZIF systems [219, 223]. For these two classes of polymers, the glass transition temperatures are lower than room temperature, and hence the interface defects are further reduced because of the flexible chains. Furthermore, the addition of free liquid additives, like ILs or PEGs, is usually accompanied, which further reduces the possibility of generating interfacial void. Additionally, extra interaction may also be introduced within ZIFs and polymers by careful design. Xiang et al. functionalized ZIF-7 with amine groups by in-situ substituting 2-aminobenzimidazol into ZIF-7 and then mixed with PEO monomers to form MMMs. Compared to the neat ZIF-7, this developed MMM displays both better CO_2 permeability and selectivity. The improvement was believed as a result of the enlarged aperture size of functionalized ZIF-7 and the chelating effect between Zn^{2+} (ZIF-7's metal ions) and ester groups [223].

Recently, a recent work developed a bottom-up approach combining in-situ formation of ZIFs with cross-linking PEO networks. The precursors were pre-dispersed with PEO monomers, following by a thermal treatment, in which cross-linking PEO networks were achieved with simultaneously formation of ZIF particles. The MMMs with a ZIF loading of 67.7 wt% was realized. Excellent CO_2 separation performances with a CO_2 permeability of 1083.7 Barrer and CO_2/N_2 and CO_2/CH_4 selectivity of 38.5 and 12.7, respectively, have been documented, surpassing the upper bound for CO_2/N_2 pairing [183].

References

1. R.W. Baker, *Membrane technology and applications*. 2012: John Wiley & Sons.
2. R.P. White and J.E.G. Lipson, *Polymer Free Volume and Its Connection to the Glass Transition.* Macromolecules, 2016. **49**(11), 3987-4007.
3. G. Consolati, I. Genco, M. Pegoraro, et al., *Positron annihilation lifetime (PAL) in poly [1-(trimethyl-silyl) propine](PTMSP): Free volume determination and time dependence of permeability.* J. Polym. Sci., Part B: Polym. Phys., 1996. **34**(2), 357-367.

4. L. Starannikova, V. Khodzhaeva, and Y. Yampolskii, *Mechanism of aging of poly [1-(trimethylsilyl)-1-propyne] and its effect on gas permeability.* J. Membr. Sci., 2004. **244**(1-2), 183-191.
5. A. Morisato, Z. He, and I. Pinnau, *Mixed-Gas Permeation Properties and Physical Aging of Poly(4-methyl-2-pentyne)*, in *Polymer Membranes for Gas and Vapor Separation*. 1999, American Chemical Society. p. 56-67.
6. K. Nagai, A. Sugawara, S. Kazama, et al., *Effects of physical aging on solubility, diffusivity, and permeability of propane and n-butane in poly (4-methyl-2-pentyne).* J. Polym. Sci., Part B: Polym. Phys., 2004. **42**(12), 2407-2418.
7. R.R. Tiwari, J. Jin, B. Freeman, et al., *Physical aging, CO_2 sorption and plasticization in thin films of polymer with intrinsic microporosity (PIM-1).* J. Membr. Sci., 2017. **537**, 362-371.
8. P.M. Budd, N.B. McKeown, B.S. Ghanem, et al., *Gas permeation parameters and other physicochemical properties of a polymer of intrinsic microporosity: Polybenzodioxane PIM-1.* J. Membr. Sci., 2008. **325**(2), 851-860.
9. P.M. Budd, N.B. McKeown, and D. Fritsch, *Free volume and intrinsic microporosity in polymers.* J. Mater. Chem., 2005. **15**(20), 1977-1986.
10. Y. Kobayashi, K. Haraya, S. Hattori, et al., *Evaluation of polymer free volume by positron annihilation and gas diffusivity measurements.* Polymer, 1994. **35**(5), 925-928.
11. A. Thran, G. Kroll, and F. Faupel, *Correlation between fractional free volume and diffusivity of gas molecules in glassy polymers.* J. Polym. Sci., Part B: Polym. Phys., 1999. **37**(23), 3344-3358.
12. C. Aitken, W. Koros, and D.R. Paul, *Effect of structural symmetry on gas transport properties of polysulfones.* Macromolecules, 1992. **25**(13), 3424-3434.
13. J. Mulder, *Basic principles of membrane technology*. 1996, the Netherlands: Kluwer Academic Publishers.
14. S. Kavesh and J. Schultz, *Meaning and measurement of crystallinity in polymers: A review.* Polym. Eng. Sci., 1969. **9**(5), 331-338.
15. G.W. Ehrenstein and R.P. Theriault, *Polymeric Materials: Structure, Properties, Applications*. 2001: Hanser Publishers.
16. A. Kljun, T.A. Benians, F. Goubet, et al., *Comparative analysis of crystallinity changes in cellulose I polymers using ATR-FTIR, X-ray diffraction, and carbohydrate-binding module probes.* Biomacromolecules, 2011. **12**(11), 4121-4126.
17. Y. Kong and J.N. Hay, *The measurement of the crystallinity of polymers by DSC.* Polymer, 2002. **43**(14), 3873-3878.
18. A.P. Gray, *Polymer crystallinity determinations by DSC.* Thermochim. Acta, 1970. **1**(6), 563-579.
19. Y. Kong and J. Hay, *The enthalpy of fusion and degree of crystallinity of polymers as measured by DSC.* Eur. Polym. J., 2003. **39**(8), 1721-1727.
20. Z. Mo and H. Zhang, *The degree of crystallinity in polymers by wide-angle x-ray diffraction (WAXD).* J. Macromol. Sci., Polym. Rev., 1995. **35**(4), 555-580.
21. A. Lopez-Rubio, B.M. Flanagan, E.P. Gilbert, et al., *A novel approach for calculating starch crystallinity and its correlation with double helix content: A combined XRD and NMR study.* Biopolymers, 2008. **89**(9), 761-768.
22. Y. Tong, Y. Lin, S. Wang, et al., *A study of crystallisation of poly (ethylene oxide) and polypropylene on graphene surface.* Polymer, 2015. **73**, 52-61.

23. C.J. Takacs, N.D. Treat, S. Krämer, et al., *Remarkable Order of a High-Performance Polymer.* Nano Lett., 2013. **13**(6), 2522-2527.
24. H. Lin and B.D. Freeman, *Gas solubility, diffusivity and permeability in poly(ethylene oxide).* J. Membr. Sci., 2004. **239**(1), 105-117.
25. J.G.A. Bitter, *Effect of crystallinity and swelling on the permeability and selectivity of polymer membranes.* Desalination, 1984. **51**(1), 19-35.
26. S. Kanehashi, A. Kusakabe, S. Sato, et al., *Analysis of permeability; solubility and diffusivity of carbon dioxide; oxygen; and nitrogen in crystalline and liquid crystalline polymers.* J. Membr. Sci., 2010. **365**(1), 40-51.
27. L. Deng, T.-J. Kim, and M.-B. Hägg, *Facilitated transport of CO_2 in novel PVAm/PVA blend membrane.* J. Membr. Sci., 2009. **340**(1), 154-163.
28. H.B.T. Jeazet, C. Staudt, and C. Janiak, *Metal–organic frameworks in mixed-matrix membranes for gas separation.* Dalton Transactions, 2012. **41**(46), 14003-14027.
29. J. Yao and H. Wang, *Zeolitic imidazolate framework composite membranes and thin films: synthesis and applications.* Chem. Soc. Rev., 2014. **43**(13), 4470-4493.
30. Z. Dai, L. Ansaloni, and L. Deng, *Recent advances in multi-layer composite polymeric membranes for CO_2 separation: A review.* Green Energy Environ., 2016. **1**(2), 102-128.
31. L.M. Robeson, *The upper bound revisited.* J. Membr. Sci., 2008. **320**(1), 390-400.
32. L.M. Robeson, *Correlation of separation factor versus permeability for polymeric membranes.* J. Membr. Sci., 1991. **62**(2), 165-185.
33. B.D. Freeman, *Basis of permeability/selectivity tradeoff relations in polymeric gas separation membranes.* Macromolecules, 1999. **32**(2), 375-380.
34. L.S. White, K.D. Amo, T. Wu, et al., *Extended field trials of Polaris sweep modules for carbon capture.* J. Membr. Sci., 2017. **542**, 217-225.
35. H. Lin, Z. He, Z. Sun, et al., *CO_2-selective membranes for hydrogen production and CO_2 capture–Part II: Techno-economic analysis.* J. Membr. Sci., 2015. **493**, 794-806.
36. T. Brinkmann, C. Naderipour, J. Pohlmann, et al., *Pilot scale investigations of the removal of carbon dioxide from hydrocarbon gas streams using poly (ethylene oxide)–poly (butylene terephthalate) PolyActive™) thin film composite membranes.* J. Membr. Sci., 2015. **489**, 237-247.
37. J. Pohlmann, M. Bram, K. Wilkner, et al., *Pilot scale separation of CO_2 from power plant flue gases by membrane technology.* Int. J. Greenhouse Gas Control, 2016. **53**, 56-64.
38. M.B. Hägg, A. Lindbråthen, X. He, et al., *Pilot Demonstration-reporting on CO_2 Capture from a Cement Plant Using Hollow Fiber Process.* Energy Procedia, 2017. **114**, 6150-6165.
39. M. Sandru, T.-J. Kim, W. Capala, et al., *Pilot Scale Testing of Polymeric Membranes for CO_2 Capture from Coal Fired Power Plants.* Energy Procedia, 2013. **37**, 6473-6480.
40. J.D. Figueroa, T. Fout, S. Plasynski, et al., *Advances in CO_2 capture technology—The U.S. Department of Energy's Carbon Sequestration Program.* Int. J. Greenhouse Gas Control, 2008. **2**(1), 9-20.
41. Y. Hu, M. Shiotsuki, F. Sanda, et al., *Synthesis and Properties of Indan-Based Polyacetylenes That Feature the Highest Gas Permeability among All the Existing Polymers.* Macromolecules, 2008. **41**(22), 8525-8532.
42. L. Shao, J. Samseth, and M.-B. Hägg, *Crosslinking and stabilization of nanoparticle filled PMP nanocomposite membranes for gas separations.* J. Membr. Sci., 2009. **326**(2), 285-292.

43. T. Masuda, *Substituted polyacetylenes.* J. Polym. Sci., Part A: Polym. Chem., 2007. **45**(2), 165-180.
44. Y. Ichiraku, S.A. Stern, and T. Nakagawa, *An Investigation of the High Gas-Permeability of Poly (1-Trimethylsilyl-1-Propyne).* J. Membr. Sci., 1987. **34**(1), 5-18.
45. S.D. Kelman, S. Matteucci, C.W. Bielawski, et al., *Crosslinking poly (1-trimethylsilyl-1-propyne) and its effect on solvent resistance and transport properties.* Polymer, 2007. **48**(23), 6881-6892.
46. S.D. Bazhenov, I.L. Borisov, D.S. Bakhtin, et al., *High-permeance crosslinked PTMSP thin-film composite membranes as supports for CO_2 selective layer formation.* Green Energy Environ., 2016. **1**(3), 235-245.
47. Y. Xiao, B.T. Low, S.S. Hosseini, et al., *The strategies of molecular architecture and modification of polyimide-based membranes for CO_2 removal from natural gas—A review.* Prog. Polym. Sci., 2009. **34**(6), 561-580.
48. M. Langsam, *Polyimides for gas separation*, in *Polyimides*. 2018, CRC Press. p. 697-742.
49. A. Brunetti, F. Scura, G. Barbieri, et al., *Membrane technologies for CO_2 separation.* J. Membr. Sci., 2010. **359**(1), 115-125.
50. Y. Yampolskii, *Polymeric gas separation membranes.* Macromolecules, 2012. **45**(8), 3298-3311.
51. P.M. Budd, K.J. Msayib, C.E. Tattershall, et al., *Gas separation membranes from polymers of intrinsic microporosity.* J. Membr. Sci., 2005. **251**(1–2), 263-269.
52. P.M. Budd, B.S. Ghanem, S. Makhseed, et al., *Polymers of intrinsic microporosity (PIMs): robust, solution-processable, organic nanoporous materials.* Chem. Commun., 2004(2), 230-231.
53. S. Wang, X. Li, H. Wu, et al., *Advances in high permeability polymer-based membrane materials for CO_2 separations.* Energy Environ. Sci., 2016. **9**(6), 1863-1890.
54. C.G. Bezzu, M. Carta, A. Tonkins, et al., *A Spirobifluorene-Based Polymer of Intrinsic Microporosity with Improved Performance for Gas Separation.* Adv. Mater., 2012. **24**(44), 5930-5933.
55. X. Ma, B. Ghanem, O. Salines, et al., *Synthesis and effect of physical aging on gas transport properties of a microporous polyimide derived from a novel spirobifluorene-based dianhydride.* Acs Macro Lett., 2015. **4**(2), 231-235.
56. H.B. Park, C.H. Jung, Y.M. Lee, et al., *Polymers with Cavities Tuned for Fast Selective Transport of Small Molecules and Ions.* Science, 2007. **318**(5848), 254-258.
57. S. Kim and Y.M. Lee, *Rigid and microporous polymers for gas separation membranes.* Prog. Polym. Sci., 2015. **43**, 1-32.
58. H.B. Park, S.H. Han, C.H. Jung, et al., *Thermally rearranged (TR) polymer membranes for CO_2 separation.* J. Membr. Sci., 2010. **359**(1), 11-24.
59. J.I. Choi, C.H. Jung, S.H. Han, et al., *Thermally rearranged (TR) poly(benzoxazole-co-pyrrolone) membranes tuned for high gas permeability and selectivity.* J. Membr. Sci., 2010. **349**(1–2), 358-368.
60. S.H. Han, J.E. Lee, K.-J. Lee, et al., *Highly gas permeable and microporous polybenzimidazole membrane by thermal rearrangement.* J. Membr. Sci., 2010. **357**(1–2), 143-151.
61. S. Zeng, X. Zhang, L. Bai, et al., *Ionic-Liquid-Based CO_2 Capture Systems: Structure, Interaction and Process.* Chem. Rev., 2017. **117**(14), 9625-9673.

62. Z. Dai, R.D. Noble, D.L. Gin, et al., *Combination of ionic liquids with membrane technology: A new approach for CO_2 separation.* J. Membr. Sci., 2016. **497**, 1-20.
63. L. Blanchard, D. Hancu, E. Beckman, et al., *Ionic liquid/CO_2 biphasic systems: new media for green processing.* Nature, 1999. **399**(1), 28-29.
64. H.Z. Chen, P. Li, and T.-S. Chung, *PVDF/ionic liquid polymer blends with superior separation performance for removing CO_2 from hydrogen and flue gas.* Int. J. Hydrogen Energy, 2012. **37**(16), 11796-11804.
65. S. Kasahara, E. Kamio, T. Ishigami, et al., *Effect of water in ionic liquids on CO_2 permeability in amino acid ionic liquid-based facilitated transport membranes.* J. Membr. Sci., 2012. **415**, 168-175.
66. L. Deng and M.-B. Hägg, *Swelling behavior and gas permeation performance of PVAm/PVA blend FSC membrane.* J. Membr. Sci., 2010. **363**(1), 295-301.
67. Z. Dai, J. Deng, L. Ansaloni, et al., *Thin-film-composite hollow fiber membranes containing amino acid salts as mobile carriers for CO_2 separation.* J. Membr. Sci., 2019. **578**, 61-68.
68. J. Liu, X. Hou, H.B. Park, et al., *High -performance polymers for membrane CO_2/N_2 separation.* Chem. - Eur. J., 2016. **22**(45), 15980-15990.
69. S. Metz, M. Mulder, and M. Wessling, *Gas-permeation properties of poly (ethylene oxide) poly (butylene terephthalate) block copolymers.* Macromolecules, 2004. **37**(12), 4590-4597.
70. Z. Luo, L. Zhang, and J. Jiang, *Atomistic insight into micro-phase separation and gas diffusion in PEO–PBT multiblock copolymers.* Mol. Simul., 2013. **39**(11), 902-907.
71. J.H. Kim, S.Y. Ha, and Y.M. Lee, *Gas permeation of poly(amide-6-b-ethylene oxide) copolymer.* J. Membr. Sci., 2001. **190**(2), 179-193.
72. V. Bondar, B.D. Freeman, and I. Pinnau, *Gas transport properties of poly (ether -b -amide) segmented block copolymers.* J. Polym. Sci., Part B: Polym. Phys., 2000. **38**(15), 2051-2062.
73. S. Luo, K.A. Stevens, J.S. Park, et al., *Highly CO_2-Selective Gas Separation Membranes Based on Segmented Copolymers of Poly(Ethylene oxide) Reinforced with Pentiptycene-Containing Polyimide Hard Segments.* ACS Appl. Mater. Interfaces, 2016. **8**(3), 2306-2317.
74. X. Solimando, J. Babin, C. Arnal-Herault, et al., *Highly selective multi-block poly(ether-urea-imide)s for CO_2/N_2 separation: Structure-morphology-properties relationships.* Polymer, 2017. **131**, 56-67.
75. H. Li, B.D. Freeman, and O.M. Ekiner, *Gas permeation properties of poly(urethane-urea)s containing different polyethers.* J. Membr. Sci., 2011. **369**(1), 49-58.
76. D. Husken, T. Visser, M. Wessling, et al., *CO_2 permeation properties of poly(ethylene oxide)-based segmented block copolymers.* J. Membr. Sci., 2010. **346**(1), 194-201.
77. S.L. Liu, L. Shao, M.L. Chua, et al., *Recent progress in the design of advanced PEO-containing membranes for CO_2 removal.* Prog. Polym. Sci., 2013. **38**(7), 1089-1120.
78. A. Car, C. Stropnik, W. Yave, et al., *Tailor-made Polymeric Membranes based on Segmented Block Copolymers for CO_2 Separation.* Adv. Funct. Mater., 2008. **18**(18), 2815-2823.
79. W. Yave, A. Szymczyk, N. Yave, et al., *Design, synthesis, characterization and optimization of PTT-b-PEO copolymers: A new membrane material for CO_2 separation.* J. Membr. Sci., 2010. **362**(1), 407-416.

80. S. Armstrong, B. Freeman, A. Hiltner, et al., *Gas permeability of melt-processed poly(ether block amide) copolymers and the effects of orientation.* Polymer, 2012. **53**(6), 1383-1392.
81. A.C. Ijzer, A. Arun, S.R. Reijerkerk, et al., *Synthesis and properties of hydrophilic segmented block copolymers based on poly(ethylene oxide)-ran-poly(propylene oxide).* J. Appl. Polym. Sci., 2010. **117**(3), 1394-1404.
82. S.R. Reijerkerk, K. Nijmeijer, C.P. Ribeiro, et al., *On the effects of plasticization in CO_2/light gas separation using polymeric solubility selective membranes.* J. Membr. Sci., 2011. **367**(1), 33-44.
83. S.R. Reijerkerk, A.C. Ijzer, K. Nijmeijer, et al., *Subambient Temperature CO_2 and Light Gas Permeation Through Segmented Block Copolymers with Tailored Soft Phase.* ACS Appl. Mater. Interfaces, 2010. **2**(2), 551-560.
84. S.R. Reijerkerk, A. Arun, R.J. Gaymans, et al., *Tuning of mass transport properties of multi-block copolymers for CO_2 capture applications.* J. Membr. Sci., 2010. **359**(1), 54-63.
85. S.R. Reijerkerk, M. Wessling, and K. Nijmeijer, *Pushing the limits of block copolymer membranes for CO_2 separation.* J. Membr. Sci., 2011. **378**(1), 479-484.
86. I. Kammakakam, S. Nam, and T.-H. Kim, *PEG–imidazolium-functionalized 6FDA–durene polyimide as a novel polymeric membrane for enhanced CO_2 separation.* RSC Adv., 2016. **6**(37), 31083-31091.
87. K.-i. Okamoto, N. Umeo, S. Okamyo, et al., *Selective Permeation of Carbon Dioxide over Nitrogen through Polyethyleneoxide-Containing Polyimide Membranes.* Chem. Lett., 1993(2), 225-228.
88. G.K. Kline, Q. Zhang, J.R. Weidman, et al., *PEO-rich semi-interpenetrating polymer network (s-IPN) membranes for CO_2 separation.* J. Membr. Sci., 2017. **544**, 143-150.
89. M. Yoshino, K. Ito, H. Kita, et al., *Effects of hard-segment polymers on CO_2/N_2 gas-separation properties of poly (ethylene oxide)-segmented copolymers.* J. Polym. Sci., Part B: Polym. Phys., 2000. **38**(13), 1707-1715.
90. H.W. Kim and H.B. Park, *Gas diffusivity, solubility and permeability in polysulfone–poly(ethylene oxide) random copolymer membranes.* J. Membr. Sci., 2011. **372**(1), 116-124.
91. N.P. Patel and R.J. Spontak, *Gas-Transport and Thermal Properties of a Microphase-Ordered Poly(styrene-b-ethylene oxide-b-styrene) Triblock Copolymer and Its Blends with Poly(ethylene glycol).* Macromolecules, 2004. **37**(8), 2829-2838.
92. R. Patel, S.J. Kim, D.K. Roh, et al., *Synthesis of amphiphilic PCZ-r-PEG nanostructural copolymers and their use in CO_2/N_2 separation membranes.* Chem. Eng. J., 2014. **254**, 46-53.
93. Q. Fu, J. Kim, P.A. Gurr, et al., *A novel cross-linked nano-coating for carbon dioxide capture.* Energy Environ. Sci., 2016. **9**(2), 434-440.
94. A.P. Isfahani, M. Sadeghi, K. Wakimoto, et al., *Enhancement of CO_2 capture by polyethylene glycol-based polyurethane membranes.* J. Membr. Sci., 2017. **542**, 143-149.
95. R. Gharibi, A. Ghadimi, H. Yeganeh, et al., *Preparation and evaluation of hybrid organic-inorganic poly(urethane-siloxane) membranes with build-in poly(ethylene glycol) segments for efficient separation of CO_2/CH_4 and CO_2/H_2.* J. Membr. Sci., 2018. **548**, 572-582.
96. S.H. Ahn, J.A. Seo, J.H. Kim, et al., *Synthesis and gas permeation properties of amphiphilic graft copolymer membranes.* J. Membr. Sci., 2009. **345**(1), 128-133.

97. I. Taniguchi, K. Kinugasa, S. Egashira, et al., *Preparation of well-defined hyper-branched polymers and the CO_2 separation performance.* J. Membr. Sci., 2016. **502**, 124-132.
98. I. Taniguchi, N. Wada, K. Kinugasa, et al., *A strategy to enhance CO_2 permeability of well-defined hyper-branched polymers with dense polyoxyethylene comb graft.* J. Membr. Sci., 2017. **535**, 239-247.
99. Y.V. Ivanova, G.A. Shandryuk, D. Roizard, et al., *Synthesis of polyvinyltrimethylsilane-graft-poly(ethylene glycol) copolymers and properties of gas-separating membranes formed on their basis.* Polym. Sci. Ser. B, 2014. **56**(3), 282-289.
100. M. Karunakaran, M. Kumar, R. Shevate, et al., *CO_2-Philic Thin Film Composite Membranes: Synthesis and Characterization of PAN-r-PEGMA Copolymer.* Polymers, 2017. **9**(7).
101. J.H. Lee, J.P. Jung, E. Jang, et al., *CO2-philic PBEM-g-POEM comb copolymer membranes: Synthesis, characterization and CO_2/N_2 separation.* J. Membr. Sci., 2016. **502**, 191-201.
102. J.P. Jung, C.H. Park, J.H. Lee, et al., *Room-temperature, one-pot process for CO_2 capture membranes based on PEMA-g-PPG graft copolymer.* Chem. Eng. J., 2017. **313**, 1615-1622.
103. M. Minelli, M. Giacinti Baschetti, D.T. Hallinan, et al., *Study of gas permeabilities through polystyrene-block-poly(ethylene oxide) copolymers.* J. Membr. Sci., 2013. **432**, 83-89.
104. H. Chen, Y. Xiao, and T.-S. Chung, *Synthesis and characterization of poly (ethylene oxide) containing copolyimides for hydrogen purification.* Polymer, 2010. **51**(18), 4077-4086.
105. R. Barrer, J. Barrie, and P.-L. Wong, *The diffusion and solution of gases in highly crosslinked copolymers.* Polymer, 1968. **9**, 609-627.
106. Y. Hirayama, Y. Kase, N. Tanihara, et al., *Permeation properties to CO_2 and N_2 of poly(ethylene oxide)-containing and crosslinked polymer films.* J. Membr. Sci., 1999. **160**(1), 87-99.
107. H. Lin, T. Kai, B.D. Freeman, et al., *The Effect of Cross-Linking on Gas Permeability in Cross-Linked Poly(Ethylene Glycol Diacrylate).* Macromolecules, 2005. **38**(20), 8381-8393.
108. T. Sakaguchi, F. Katsura, A. Iwase, et al., *CO_2-permselective membranes of crosslinked poly (vinyl ether) s bearing oxyethylene chains.* Polymer, 2014. **55**(6), 1459-1466.
109. Z. Dai, L. Ansaloni, D.L. Gin, et al., *Facile fabrication of CO_2 separation membranes by cross-linking of poly (ethylene glycol) diglycidyl ether with a diamine and a polyamine-based ionic liquid.* J. Membr. Sci., 2017. **523**, 551-560.
110. S. Li, X. Jiang, Q. Yang, et al., *Effects of amino functionalized polyhedral oligomeric silsesquioxanes on cross-linked poly(ethylene oxide) membranes for highly-efficient CO_2 separation.* Chem. Eng. Res. Des., 2017. **122**, 280-288.
111. L. Shao, S. Quan, X.-Q. Cheng, et al., *Developing cross-linked poly(ethylene oxide) membrane by the novel reaction system for H_2 purification.* Int. J. Hydrogen Energy, 2013. **38**(12), 5122-5132.
112. S. Quan, S. Li, Z. Wang, et al., *A bio-inspired CO_2-philic network membrane for enhanced sustainable gas separation.* J. Mater. Chem. A, 2015. **3**(26), 13758-13766.
113. D. Fournier, R. Hoogenboom, and U.S. Schubert, *Clicking polymers: a straightforward approach to novel macromolecular architectures.* Chem. Soc. Rev., 2007. **36**(8), 1369-1380.

114. B.D. Mather, K. Viswanathan, K.M. Miller, et al., *Michael addition reactions in macromolecular design for emerging technologies.* Prog. Polym. Sci., 2006. **31**(5), 487-531.
115. C.E. Hoyle and C.N. Bowman, *Thiol–Ene Click Chemistry.* Angew. Chem. Int. Ed., 2010. **49**(9), 1540-1573.
116. C.E. Hoyle, A.B. Lowe, and C.N. Bowman, *Thiol-click chemistry: a multifaceted toolbox for small molecule and polymer synthesis.* Chem. Soc. Rev., 2010. **39**(4), 1355-1387.
117. L. Kwisnek, J. Goetz, K.P. Meyers, et al., *PEG Containing Thiol–Ene Network Membranes for CO_2 Separation: Effect of Cross-Linking on Thermal, Mechanical, and Gas Transport Properties.* Macromolecules, 2014. **47**(10), 3243-3253.
118. J. Deng, J. Yu, Z. Dai, et al., *Cross-linked PEG Membranes of Interpenetrating Networks with ILs as Additives for Enhanced CO_2 Separation.* Ind. Eng. Chem. Res., 2019. **58**(13), 5261-5268.
119. J. Deng, Z. Dai, J. Yan, et al., *Facile and solvent-free fabrication of PEG-based membranes with interpenetrating networks for CO_2 separation.* J. Membr. Sci., 2019. **570**, 455-463.
120. S. Li, Z. Wang, C. Zhang, et al., *Interfacially polymerized thin film composite membranes containing ethylene oxide groups for CO_2 separation.* J. Membr. Sci., 2013. **436**, 121-131.
121. A.A. Salih, C. Yi, H. Peng, et al., *Interfacially polymerized polyetheramine thin film composite membranes with PDMS inter-layer for CO_2 separation.* J. Membr. Sci., 2014. **472**, 110-118.
122. N.P. Patel, A.C. Miller, and R.J. Spontak, *Highly CO_2-Permeable and -Selective Membranes Derived from Crosslinked Poly(ethylene glycol) and Its Nanocomposites.* Adv. Funct. Mater., 2004. **14**(7), 699-707.
123. J.J. Richards, M.K. Danquah, S. Kalakkunnath, et al., *Relation between structure and gas transport properties of polyethylene oxide networks based on crosslinked bisphenol A ethoxylate diacrylate.* Chem. Eng. Sci., 2009. **64**(22), 4707-4718.
124. X. Jiang, S. Li, and L. Shao, *Pushing CO_2-philic membrane performance to the limit by designing semi-interpenetrating networks (SIPN) for sustainable CO_2 separations.* Energy Environ. Sci., 2017. **10**(6), 1339-1344.
125. V.A. Kusuma, B.D. Freeman, M.A. Borns, et al., *Influence of chemical structure of short chain pendant groups on gas transport properties of cross-linked poly(ethylene oxide) copolymers.* J. Membr. Sci., 2009. **327**(1), 195-207.
126. V.A. Kusuma, S. Matteucci, B.D. Freeman, et al., *Influence of phenoxy-terminated short-chain pendant groups on gas transport properties of cross-linked poly(ethylene oxide) copolymers.* J. Membr. Sci., 2009. **341**(1), 84-95.
127. V.A. Kusuma, B.D. Freeman, S.L. Smith, et al., *Influence of TRIS-based co-monomer on structure and gas transport properties of cross-linked poly(ethylene oxide).* J. Membr. Sci., 2010. **359**(1), 25-36.
128. V.A. Kusuma, G. Gunawan, Z.P. Smith, et al., *Gas permeability of cross-linked poly(ethylene-oxide) based on poly(ethylene glycol) dimethacrylate and a miscible siloxane co-monomer.* Polymer, 2010. **51**(24), 5734-5743.
129. V.A. Kusuma, E.A. Roth, W.P. Clafshenkel, et al., *Crosslinked poly(ethylene oxide) containing siloxanes fabricated through thiol-ene photochemistry.* J. Polym. Sci., Part A: Polym. Chem., 2015. **53**(13), 1548-1557.
130. H. Zhao, X. Ding, P. Yang, et al., *A novel multi-armed and star-like poly(ethylene oxide) membrane for CO2 separation.* J. Membr. Sci., 2015. **489**, 258-263.

131. Y. Yin, L. Yang, M. Yoshino, et al., *Synthesis and Gas Permeation Properties of Star-like Poly(ethylene oxide)s Using Hyperbranched Polyimide as Central Core.* Polym. J., 2004. **36**(4), 294-302.
132. G.K. Kline, J.R. Weidman, Q. Zhang, et al., *Studies of the synergistic effects of crosslink density and crosslink inhomogeneity on crosslinked PEO membranes for CO_2-selective separations.* J. Membr. Sci., 2017. **544**, 25-34.
133. H. Zhao, C. Kang, X. Ding, et al., *The effect of cross-linkers with multi-armed structures on gas transport properties in star-like poly (ethylene oxide) polymers.* Sep. Sci. Technol., 2018. **53**(1), 154-160.
134. H. Lin, E.V. Wagner, J.S. Swinnea, et al., *Transport and structural characteristics of crosslinked poly(ethylene oxide) rubbers.* J. Membr. Sci., 2006. **276**(1), 145-161.
135. N.P. Patel and R.J. Spontak, *Mesoblends of Polyether Block Copolymers with Poly(ethylene glycol).* Macromolecules, 2004. **37**(4), 1394-1402.
136. A. Car, C. Stropnik, W. Yave, et al., *Pebax®/polyethylene glycol blend thin film composite membranes for CO_2 separation: Performance with mixed gases.* Sep. Purif. Technol., 2008. **62**(1), 110-117.
137. W. Yave, A. Car, S.S. Funari, et al., *CO_2-Philic Polymer Membrane with Extremely High Separation Performance.* Macromolecules, 2010. **43**(1), 326-333.
138. W. Yave, A. Car, K.-V. Peinemann, et al., *Gas permeability and free volume in poly(amide-b-ethylene oxide)/polyethylene glycol blend membranes.* J. Membr. Sci., 2009. **339**(1), 177-183.
139. W. Yave, A. Car, and K.-V. Peinemann, *Nanostructured membrane material designed for carbon dioxide separation.* J. Membr. Sci., 2010. **350**(1), 124-129.
140. S. Feng, J. Ren, D. Zhao, et al., *Effect of poly(ethylene glycol) molecular weight on CO_2/N_2 separation performance of poly(amide-12-b-ethylene oxide)/poly(ethylene glycol) blend membranes.* Journal of Energy Chemistry, 2019. **28**, 39-45.
141. S. Feng, J. Ren, K. Hua, et al., *Poly(amide-12-b-ethylene oxide)/polyethylene glycol blend membranes for carbon dioxide separation.* Sep. Purif. Technol., 2013. **116**, 25-34.
142. S. Quan, Y.P. Tang, Z.X. Wang, et al., *PEG-Imbedded PEO Membrane Developed by a Novel Highly Efficient Strategy Toward Superior Gas Transport Performance.* Macromol. Rapid Commun., 2015. **36**(5), 490-495.
143. S.R. Reijerkerk, M.H. Knoef, K. Nijmeijer, et al., *Poly(ethylene glycol) and poly(dimethyl siloxane): Combining their advantages into efficient CO_2 gas separation membranes.* J. Membr. Sci., 2010. **352**(1), 126-135.
144. S. Feng, J. Ren, D. Zhao, et al., *CO_2-philic polyether-block-amide/glycerol triacetate blend membranes: gas-permeation performance, thermal stability, and storage stability.* J. Appl. Polym. Sci., 2019. **136**(23), 47620.
145. Y. Qiu, J. Ren, D. Zhao, et al., *Blend membranes of poly(amide-6-b-ethylene oxide)/[Emim][PF6] for CO2 separation.* Sep. Purif. Technol., 2017. **179**, 309-319.
146. Y. Qiu, J. Ren, D. Zhao, et al., *Poly(amide-6-b-ethylene oxide)/[Bmim][Tf_2N] blend membranes for carbon dioxide separation.* Journal of Energy Chemistry, 2016. **25**(1), 122-130.
147. P. Bernardo, J.C. Jansen, F. Bazzarelli, et al., *Gas transport properties of Pebax®/room temperature ionic liquid gel membranes.* Sep. Purif. Technol., 2012. **97**, 73-82.
148. S. Magana, G. Sudre, F. Gouanvé, et al., *Influence of the film-forming process on the nanostructuration of Pebax®/1-ethyl-3-methylimidazolium triflate ionic liquid:*

Consequences on the thermal, mechanical, gas, and water transport properties. J. Polym. Sci., Part B: Polym. Phys., 2017. **55**(10), 778-788.
149. E. Ghasemi Estahbanati, M. Omidkhah, and A. Ebadi Amooghin, *Preparation and characterization of novel Ionic liquid/Pebax membranes for efficient CO_2/light gases separation.* Journal of Industrial and Engineering Chemistry, 2017. **51**, 77-89.
150. V.A. Kusuma, M.K. Macala, J. Liu, et al., *Ionic liquid compatibility in polyethylene oxide/siloxane ion gel membranes.* J. Membr. Sci., 2018. **545**, 292-300.
151. V.A. Kusuma, M.K. Macala, J.S. Baker, et al., *Cross-Linked Poly(ethylene oxide) Ion Gels Containing Functionalized Imidazolium Ionic Liquids as Carbon Dioxide Separation Membranes.* Ind. Eng. Chem. Res., 2018. **57**(34), 11658-11667.
152. D.B. Wijayasekara, M.G. Cowan, J.T. Lewis, et al., *Elastic free-standing RTIL composite membranes for CO_2/N_2 separation based on sphere-forming triblock/diblock copolymer blends.* J. Membr. Sci., 2016. **511**, 170-179.
153. Z. Dai, L. Ansaloni, J.J. Ryan, et al., *Nafion/IL hybrid membranes with tuned nanostructure for enhanced CO_2 separation: effects of ionic liquid and water vapor.* Green Chem., 2018. **20**(6), 1391-1404.
154. Z. Dai, L. Bai, K. Hval, et al., *Pebax®/TSIL blend thin film composite membranes for CO_2 separation.* Sci. China. Chem., 2016. **59**(1674-7291), 538.
155. J.S. Chiou, J.W. Barlow, and D.R. Paul, *Plasticization of glassy polymers by CO_2.* J. Appl. Polym. Sci., 1985. **30**(6), 2633-2642.
156. M. Galizia, W.S. Chi, Z.P. Smith, et al., *50th Anniversary Perspective: Polymers and Mixed Matrix Membranes for Gas and Vapor Separation: A Review and Prospective Opportunities.* Macromolecules, 2017. **50**(20), 7809-7843.
157. B. Seoane, J. Coronas, I. Gascon, et al., *Metal-organic framework based mixed matrix membranes: a solution for highly efficient CO_2 capture?* Chem. Soc. Rev., 2015. **44**(8), 2421-2454.
158. T.-S. Chung, L.Y. Jiang, Y. Li, et al., *Mixed matrix membranes (MMMs) comprising organic polymers with dispersed inorganic fillers for gas separation.* Prog. Polym. Sci., 2007. **32**(4), 483-507.
159. K.S. Park, Z. Ni, A.P. Côté, et al., *Exceptional chemical and thermal stability of zeolitic imidazolate frameworks.* Proceedings of the National Academy of Sciences, 2006. **103**(27), 10186-10191.
160. M.J.C. Ordoñez, K.J. Balkus, J.P. Ferraris, et al., *Molecular sieving realized with ZIF-8/Matrimid® mixed-matrix membranes.* J. Membr. Sci., 2010. **361**(1), 28-37.
161. S. Basu, A. Cano-Odena, and I.F.J. Vankelecom, *MOF-containing mixed-matrix membranes for CO_2/CH_4 and CO_2/N_2 binary gas mixture separations.* Sep. Purif. Technol., 2011. **81**(1), 31-40.
162. H.B. Tanh Jeazet, S. Sorribas, J.M. Román-Marín, et al., *Increased Selectivity in CO_2/CH_4 Separation with Mixed-Matrix Membranes of Polysulfone and Mixed-MOFs MIL-101(Cr) and ZIF-8.* Eur. J. Inorg. Chem., 2016. **2016**(27), 4363-4367.
163. Y. Dai, J.R. Johnson, O. Karvan, et al., *Ultem®/ZIF-8 mixed matrix hollow fiber membranes for CO_2/N_2 separations.* J. Membr. Sci., 2012. **401-402**, 76-82.
164. Q. Song, S. Nataraj, M.V. Roussenova, et al., *Zeolitic imidazolate framework (ZIF-8) based polymer nanocomposite membranes for gas separation.* Energy Environ. Sci., 2012. **5**(8), 8359-8369.

165. T.-H. Bae, J.S. Lee, W. Qiu, et al., *A High-Performance Gas-Separation Membrane Containing Submicrometer-Sized Metal–Organic Framework Crystals.* Angew. Chem. Int. Ed., 2010. **49**(51), 9863-9866.
166. A.F. Bushell, M.P. Attfield, C.R. Mason, et al., *Gas permeation parameters of mixed matrix membranes based on the polymer of intrinsic microporosity PIM-1 and the zeolitic imidazolate framework ZIF-8.* J. Membr. Sci., 2013. **427**, 48-62.
167. L. Hao, K.-S. Liao, and T.-S. Chung, *Photo-oxidative PIM-1 based mixed matrix membranes with superior gas separation performance.* J. Mater. Chem. A, 2015. **3**(33), 17273-17281.
168. Q. Zhang, S. Luo, J.R. Weidman, et al., *Preparation and gas separation performance of mixed-matrix membranes based on triptycene-containing polyimide and zeolite imidazole framework (ZIF-90).* Polymer, 2017. **131**, 209-216.
169. Z. Dai, V. Løining, J. Deng, et al., *Poly(1-trimethylsilyl-1-propyne)-Based Hybrid Membranes: Effects of Various Nanofillers and Feed Gas Humidity on CO_2 Permeation.* Membranes, 2018. **8**(3).
170. X. Wu, W. Liu, H. Wu, et al., *Nanoporous ZIF-67 embedded polymers of intrinsic microporosity membranes with enhanced gas separation performance.* J. Membr. Sci., 2018. **548**, 309-318.
171. S. Japip, Y. Xiao, and T.-S. Chung, *Particle-Size Effects on Gas Transport Properties of 6FDA-Durene/ZIF-71 Mixed Matrix Membranes.* Ind. Eng. Chem. Res., 2016. **55**(35), 9507-9517.
172. M. Safak Boroglu and A.B. Yumru, *Gas separation performance of 6FDA-DAM-ZIF-11 mixed-matrix membranes for H_2/CH_4 and CO_2/CH_4 separation.* Sep. Purif. Technol., 2017. **173**, 269-279.
173. M. Etxeberria-Benavides, O. David, T. Johnson, et al., *High performance mixed matrix membranes (MMMs) composed of ZIF-94 filler and 6FDA-DAM polymer.* J. Membr. Sci., 2018. **550**, 198-207.
174. J.S. Kim, S.J. Moon, H.H. Wang, et al., *Mixed matrix membranes with a thermally rearranged polymer and ZIF-8 for hydrogen separation.* J. Membr. Sci., 2019. **582**, 381-390.
175. T. Li, Y. Pan, K.-V. Peinemann, et al., *Carbon dioxide selective mixed matrix composite membrane containing ZIF-7 nano-fillers.* J. Membr. Sci., 2013. **425-426**, 235-242.
176. V. Nafisi and M.-B. Hägg, *Development of dual layer of ZIF-8/PEBAX-2533 mixed matrix membrane for CO_2 capture.* J. Membr. Sci., 2014. **459**, 244-255.
177. S. Feng, M. Bu, J. Pang, et al., *Hydrothermal stable ZIF-67 nanosheets via morphology regulation strategy to construct mixed-matrix membrane for gas separation.* J. Membr. Sci., 2020. **593**, 117404.
178. K. Díaz, L. Garrido, M. López-González, et al., *CO_2 Transport in Polysulfone Membranes Containing Zeolitic Imidazolate Frameworks As Determined by Permeation and PFG NMR Techniques.* Macromolecules, 2010. **43**(1), 316-325.
179. B.A. Al-Maythalony, A.M. Alloush, M. Faizan, et al., *Tuning the Interplay between Selectivity and Permeability of ZIF-7 Mixed Matrix Membranes.* ACS Appl. Mater. Interfaces, 2017. **9**(39), 33401-33407.
180. W.-H. Lai, G.-L. Zhuang, H.-H. Tseng, et al., *Creation of tiny defects in ZIF-8 by thermal annealing to improve the CO_2/N_2 separation of mixed matrix membranes.* J. Membr. Sci., 2019. **572**, 410-418.

181. W.S. Chi, S. Hwang, S.-J. Lee, et al., *Mixed matrix membranes consisting of SEBS block copolymers and size-controlled ZIF-8 nanoparticles for CO2 capture.* J. Membr. Sci., 2015. **495**, 479-488.
182. W.S. Chi, S.J. Kim, S.-J. Lee, et al., *Enhanced Performance of Mixed-Matrix Membranes through a Graft Copolymer-Directed Interface and Interaction Tuning Approach.* ChemSusChem, 2015. **8**(4), 650-658.
183. L. Ma, F. Svec, Y. Lv, et al., *In situ bottom–up growth of metal–organic frameworks in a crosslinked poly(ethylene oxide) layer with ultrahigh loading and superior uniform distribution.* J. Mater. Chem. A, 2019. **7**(35), 20293-20301.
184. X. Zhang, T. Zhang, Y. Wang, et al., *Mixed-matrix membranes based on Zn/Ni-ZIF-8-PEBA for high performance CO_2 separation.* J. Membr. Sci., 2018. **560**, 38-46.
185. S. Meshkat, S. Kaliaguine, and D. Rodrigue, *Comparison between ZIF-67 and ZIF-8 in Pebax® MH-1657 mixed matrix membranes for CO_2 separation.* Sep. Purif. Technol., 2020. **235**, 116150.
186. Y. Ban , Y. Li, Y. Peng , et al., *Metal-Substituted Zeolitic Imidazolate Framework ZIF-108: Gas-Sorption and Membrane-Separation Properties.* Chemistry – A European Journal, 2014. **20**(36), 11402-11409.
187. B. Zornoza, B. Seoane, J.M. Zamaro, et al., *Combination of MOFs and zeolites for mixed - matrix membranes.* ChemPhysChem, 2011. **12**(15), 2781-2785.
188. M.E. Casco, Y.Q. Cheng, L.L. Daemen, et al., *Gate-opening effect in ZIF-8: the first experimental proof using inelastic neutron scattering.* Chem. Commun., 2016. **52**(18), 3639-3642.
189. R. Lin, B.V. Hernandez, L. Ge, et al., *Metal organic framework based mixed matrix membranes: an overview on filler/polymer interfaces.* J. Mater. Chem. A, 2018. **6**(2), 293-312.
190. R. Mahajan, R. Burns, M. Schaeffer, et al., *Challenges in forming successful mixed matrix membranes with rigid polymeric materials.* J. Appl. Polym. Sci., 2002. **86**(4), 881-890.
191. S. Basu, A. Cano-Odena, and I.F.J. Vankelecom, *Asymmetric Matrimid®/[$Cu_3(BTC)_2$] mixed-matrix membranes for gas separations.* J. Membr. Sci., 2010. **362**(1), 478-487.
192. A. Ehsani and M. Pakizeh, *Synthesis, characterization and gas permeation study of ZIF-11/Pebax® 2533 mixed matrix membranes.* Journal of the Taiwan Institute of Chemical Engineers, 2016. **66**, 414-423.
193. R. Lin, B. Villacorta Hernandez, L. Ge, et al., *Metal organic framework based mixed matrix membranes: an overview on filler/polymer interfaces.* J. Mater. Chem. A, 2018. **6**(2), 293-312.
194. T. Yang, Y. Xiao, and T.-S. Chung, *Poly-/metal-benzimidazole nano-composite membranes for hydrogen purification.* Energy Environ. Sci., 2011. **4**(10), 4171-4180.
195. I.l. Ayas, L. Yilmaz, and H. Kalipcilar, *The gas permeation characteristics of ternary component mixed matrix membranes prepared using ZIF-8 with a large range of average particle size.* Ind. Eng. Chem. Res., 2018. **57**(47), 16041-16050.
196. J. Sánchez-Laínez, B. Zornoza, S. Friebe, et al., *Influence of ZIF-8 particle size in the performance of polybenzimidazole mixed matrix membranes for pre-combustion CO_2 capture and its validation through interlaboratory test.* J. Membr. Sci., 2016. **515**, 45-53.
197. W. Zheng, R. Ding, K. Yang, et al., *ZIF-8 nanoparticles with tunable size for enhanced CO_2 capture of Pebax based MMMs.* Sep. Purif. Technol., 2019. **214**, 111-119.

198. M. Zhao, Y. Huang, Y. Peng, et al., *Two-dimensional metal–organic framework nanosheets: synthesis and applications.* Chem. Soc. Rev., 2018. **47**(16), 6267-6295.
199. M. Ahmadi, S. Janakiram, Z. Dai, et al., *Performance of mixed matrix membranes containing porous two-dimensional (2D) and three-dimensional (3D) fillers for CO_2 separation: a review.* Membranes, 2018. **8**(3), 50.
200. J.R. Johnson and W.J. Koros, *Utilization of nanoplatelets in organic–inorganic hybrid separation materials: Separation advantages and formation challenges.* Journal of the Taiwan Institute of Chemical Engineers, 2009. **40**(3), 268-275.
201. S. Kim, E. Shamsaei, X. Lin, et al., *The enhanced hydrogen separation performance of mixed matrix membranes by incorporation of two-dimensional ZIF-L into polyimide containing hydroxyl group.* J. Membr. Sci., 2018. **549**, 260-266.
202. T. Rodenas, I. Luz, G. Prieto, et al., *Metal–organic framework nanosheets in polymer composite materials for gas separation.* Nat. Mater., 2014. **14**, 48.
203. A. Sabetghadam, B. Seoane, D. Keskin, et al., *Metal organic framework crystals in mixed-matrix membranes: impact of the filler morphology on the gas separation performance.* Adv. Funct. Mater., 2016. **26**(18), 3154-3163.
204. L. Dong, M. Chen, X. Wu, et al., *Multi-functional polydopamine coating: simultaneous enhancement of interfacial adhesion and CO_2 separation performance of mixed matrix membranes.* New J. Chem., 2016. **40**(11), 9148-9159.
205. R. Ding, W. Zheng, K. Yang, et al., *Amino-functional ZIF-8 nanocrystals by microemulsion based mixed linker strategy and the enhanced CO_2/N_2 separation.* Sep. Purif. Technol., 2019, 116209.
206. A. Atash Jameh, T. Mohammadi, and O. Bakhtiari, *Preparation of PEBAX-1074/modified ZIF-8 nanoparticles mixed matrix membranes for CO_2 removal from natural gas.* Sep. Purif. Technol., 2020. **231**, 115900.
207. Y. Gao, Z. Qiao, S. Zhao, et al., *In situ synthesis of polymer grafted ZIFs and application in mixed matrix membrane for CO_2 separation.* J. Mater. Chem. A, 2018. **6**(7), 3151-3161.
208. W. Zhu, X. Li, Y. Sun, et al., *Introducing hydrophilic ultra-thin ZIF-L into mixed matrix membranes for CO_2/CH_4 separation.* RSC Adv., 2019. **9**(40), 23390-23399.
209. S. Cong, Q. Shen, M. Shan, et al., *Enhanced permeability in mixed matrix membranes for CO_2 capture through the structural regulation of the amino-functionalized Co/ZIF-8 heterometallic nanoparticles.* Chem. Eng. J., 2019, 123137.
210. H. Amrouche, S. Aguado, J. Pérez-Pellitero, et al., *Experimental and Computational Study of Functionality Impact on Sodalite–Zeolitic Imidazolate Frameworks for CO_2 Separation.* The Journal of Physical Chemistry C, 2011. **115**(33), 16425-16432.
211. S. Hwang, W.S. Chi, S.J. Lee, et al., *Hollow ZIF-8 nanoparticles improve the permeability of mixed matrix membranes for CO_2/CH_4 gas separation.* J. Membr. Sci., 2015. **480**, 11-19.
212. J.H. Lee, H.T. Kwon, S. Bae, et al., *Mixed-matrix membranes containing nanocage-like hollow ZIF-8 polyhedral nanocrystals in graft copolymers for carbon dioxide/methane separation.* Sep. Purif. Technol., 2018. **207**, 427-434.
213. L. Hu, J. Cheng, Y. Wang, et al., *Open-cocoon zeolitic imidazolate framework nanoparticles introduce low-resistance path for CO_2 transport in crosslinked poly(ethylene oxide) membrane.* Sep. Purif. Technol., 2019. **217**, 299-306.

214. L. Dong, M. Chen, J. Li, et al., *Metal-organic framework-graphene oxide composites: A facile method to highly improve the CO_2 separation performance of mixed matrix membranes.* J. Membr. Sci., 2016. **520**, 801-811.
215. B. Chen, C. Wan, X. Kang, et al., *Enhanced CO_2 separation of mixed matrix membranes with ZIF-8@GO composites as fillers: Effect of reaction time of ZIF-8@GO.* Sep. Purif. Technol., 2019. **223**, 113-122.
216. S. Anastasiou, N. Bhoria, J. Pokhrel, et al., *Metal-organic framework/graphene oxide composite fillers in mixed-matrix membranes for CO_2 separation.* Mater. Chem. Phys., 2018. **212**, 513-522.
217. X. Guo, Z. Qiao, D. Liu, et al., *Mixed-matrix membranes for CO_2 separation: role of the third component.* J. Mater. Chem. A, 2019.
218. M. Li, X. Zhang, S. Zeng, et al., *Pebax-based composite membranes with high gas transport properties enhanced by ionic liquids for CO_2 separation.* RSC Adv., 2017. **7**(11), 6422-6431.
219. L. Hao, P. Li, T. Yang, et al., *Room temperature ionic liquid/ZIF-8 mixed-matrix membranes for natural gas sweetening and post-combustion CO_2 capture.* J. Membr. Sci., 2013. **436**, 221-231.
220. M. Barooah and B. Mandal, *Synthesis, characterization and CO_2 separation performance of novel PVA/PG/ZIF-8 mixed matrix membrane.* J. Membr. Sci., 2019. **572**, 198-209.
221. H. Li, L. Tuo, K. Yang, et al., *Simultaneous enhancement of mechanical properties and CO_2 selectivity of ZIF-8 mixed matrix membranes: Interfacial toughening effect of ionic liquid.* J. Membr. Sci., 2016. **511**, 130-142.
222. Y. Ban, Z. Li, Y. Li, et al., *Confinement of Ionic Liquids in Nanocages: Tailoring the Molecular Sieving Properties of ZIF-8 for Membrane-Based CO_2 Capture.* Angew. Chem. Int. Ed., 2015. **54**(51), 15483-15487.
223. L. Xiang, L. Sheng, C. Wang, et al., *Amino-Functionalized ZIF-7 Nanocrystals: Improved Intrinsic Separation Ability and Interfacial Compatibility in Mixed-Matrix Membranes for CO_2/CH_4 Separation.* Adv. Mater., 2017. **29**(32), 1606999.

Chapter 3

Materials and Experimental

3.1 Materials

General chemicals

Pentaerythritol triacrylate (PEG3A, 298 g/mol), pentaerythritol tetraacrylate (PEG4A, 352 g/mol), 1-hydroxylcyclohexyl phenyl ketone (HCPK, 204 g/mol), PEGDA with different molecular weights (250, 575 and 700 g/mol), tris(2-aminoethyl)amine (TAEA), Jeffamine ED-600 (500 g/mol) and poly(ethylene glycol) dimethyl ether (PEGDME, ca. 500 g/mol) were all purchased from Sigma Aldrich, Germany. Dipentaerythritol hexaacrylate (PEG5A, 578 g/mol) was obtained from Abcr GmbH, Germany.

Three ionic liquids, 1-butyl-3-methylimidazolium bis(trifluoromethylsulfonyl) imide ([Bmim][NTf_2], 98%), 1-butyl-3-methylimidazolium tetrafluoroborate ([Bmim][BF_4], 98%), and 1-butyl-3-methylimidazolium hexafluorophosphate ([Bmim][PF_6], 98%) were obtained from Sigma-Aldrich, Germany. 1-Butyl-3-methylimidazolium tricyanomethanide ([Bmim][TCM], 98%) was ordered from Iolitec, Germany.

$Zn(NO_3)_2 \cdot 6H_2O$ and 2-methylimidazole (Hmim) were ordered from Sigma, Norway. PVA (Mn 30000 – 70000 g/mol, 72000 g/mol, 85000 – 124000 g/mol and 89000-98000 g/mol, 99% hydrolyzed) and polyethylene glycol (400 g/mol, PEG 400) were ordered from Sigma, Germany. Tolidine, dimethoxymethane (DMM), trifluoroacetic acid (TA), ammonium hydroxide solution (28%) and methylpyrrolidone (NMP) were also bought from Sigma. Pebax 1657 and 2533 pellets were ordered from Arkema, France. Ethanol (96%) and methanol were ordered from VWR, Norway.

The N_2, CH_4, CO_2, H_2 (99.999%), and the mixed gas (10 vol% CO_2 in N_2) used in gas permeation tests were provided by AGA, Norway. All chemicals were used as-received without further purification.

3.2 Synthesis of Polymer, ZIFs particles and membrane preparation

Cross-linked PEG membranes

Cross-linked PEG membranes were fabricated by UV-induced cross-linking reactions, similar to that described elsewhere [1-3]. A brief description of the reaction scheme is illustrated in **Figure 3.1**. Multiple functionalized cross-linkers, linear monomers, free liquid-like additives (PEGDME or ILs) and 0.01–0.1 wt% HCPK were mixed in a glass vial and stirred for several minutes to ensure uniform mixing. The mass ratio of additives ($W_{additive}$) was calculated based on Equation 3.1.

$$W_{additive} = \frac{m_{additive}}{m_{cross-linker} + m_{linear\ monomers}} \times 100\% \quad (3.1)$$

Where $m_{additive}$, $m_{cross-linker}$ and $m_{linear\ monomers}$ are the mass of additives, cross-linker and linear monomers, respectively.

After mixing, the mixture was sandwiched between two quartz plates separated by spacers to control the membrane thickness. The solution was photopolymerized under a UV lamp (UVLS-28, Ultra-Violet Products Ltd.) with a wavelength of 365 nm for 2 h. The resultant membranes were evaluated by various characterization methods and permeation tests.

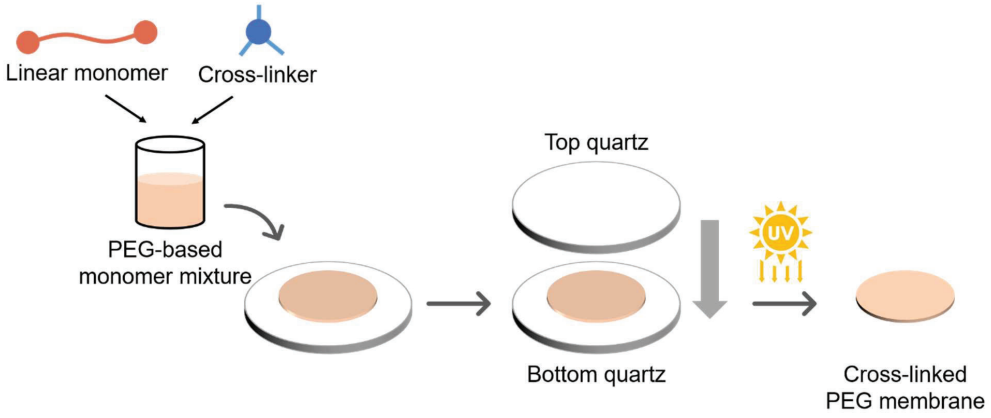

Figure 3.17 Schematic representative for preparation of cross-linked PEG membranes.

TB polymer synthesis

The TB polymer was synthesized based on a procedure reported previously [4, 5]. The polymerization reaction is shown in **Scheme 3.1**. Under a N_2 atmosphere, 20 g o-Tolidine and 36 g DMM were mixed in a 500 mL three-necked flask, which was placed in an ice-water bath. 200 ml trifluoroacetic acid (TFA) was added drop-wisely into the mixture within 30 min. The mixture was stirred under ambient condition for 48 h. Thereafter, the polymerization was stopped by slowly pouring the solution into 2 L aqueous ammonium hydroxide solution (5 wt. %). The obtained polymer was washed with excess DI water until the pH close to 7. The polymer was then dried in a vacuum oven for 12 hours at 80 °C. The polymer was further purified by dissolving it in NMP (~10 wt.%) and re-precipitate it in methanol for 2 times. Finally, the polymer was dried in vacuum oven for 12 hours at 80 °C.

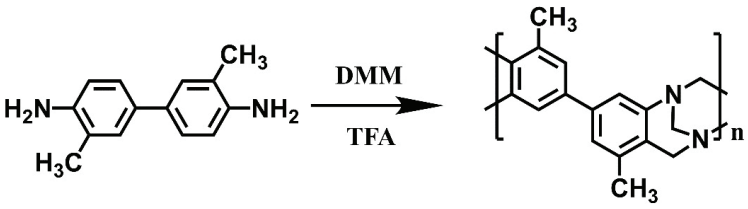

Scheme 3.1 The polymerization of TB polymer.

ZIF particle preparation

The preparation of ZIF particles is similar to the method developed by Wang's group [6]. 0.59 g $Zn(NO_3)_2$•$6H_2O$ and 1.30 g Hmim were dissolved in 40 mL deionized water or 1 wt.% polymer solution, respectively, and then the two solutions were mixed with stirring at room temperature for 3 h. For the preparation of ZIF-L-Co, 0.7275g $Co(NO_3)_2$•$6H_2O$ and 2.4025g Hmim was dissolved in two glass bottles with 50 mL DI water, before the two solution were mixed and the mixture was further stirred for another 30 min. White ZIF-L-Zn and purple ZIF-L-Co were obtained by filtrating the solution using a vacuum filtration assembly (VWR) equipped with a PVDF filter membrane (pore size of 0.65 μm). The obtained ZIF particles were further washed with DI water for several times and finally dried in a vacuum oven for 12 hours at 60 °C.

MMMs preparation

In this work, MMMs were prepared through a knife-casting method similar to the literature [7]. The solvent, the polymeric concentration and the drying temperatures were adjustable depending on the polymer employed in each study. Take Pebax 1657 based MMMs as example, the Pebax 1657 polymer was dissolved in EtOH/H_2O mixture (70/30 vol%) with reflux at 80 °C for ~ 3 hours with a concentration of 8 wt.%. The Pebax 1657 solution was mixed with the desired amount of ZIF-C aqueous dispersion under stirring for at least 6 hours. The mixture was then casted on a Teflon plate using a casting knife (PA-4302, BYK-CHEMIE GMBH, Germany) with a wet gap of ~ 600 μm. The casted membrane was then placed in a ventilated oven at 40 °C for at least 6 hours. After the membrane was removed from the Teflon plates, it was dried in a vacuum oven at 60 °C for at least 6 hours before further characterization.

3.3 Characterization techniques

3.3.1. Fourier transform infrared (FTIR) spectroscopy

FTIR spectroscopy is one of the most powerful tools for the determination of functional group in materials (solid, liquid and gas) together with possible intermolecular bonds between the compounds in the studied materials. In a typical FTIR tests, the IR beam generated by certain sources passes through the investigated materials and then will be collected by the detector. The FTIR spectrum originates from the differences between the raw IR beam and the one detected by the detector. Therefore, the obtained FTIR spectrum can provide useful information regarding to the chemical bonds inside the investigated materials, based on the fact that different bonds absorb light at different wavelengths.

In this study, FTIR was used to detect the vibration characteristics of chemical functional groups in the studied materials. A Thermo Nicolet Nexus FTIR spectrometer with a smart endurance reflection cell was used to obtain the FTIR spectra of the investigated materials with a wavelength range of 500 - 4000 cm^{-1}. The obtained spectrum is the average of 16 scans. The attenuated total reflectance (ATR) technique has been employed using a diamond crystal.

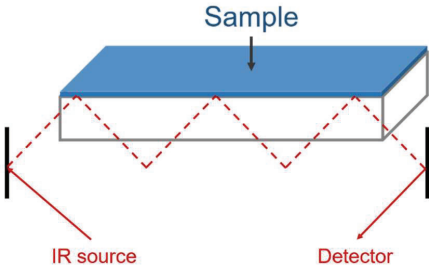

Figure 3.18 Schematics of FTIR analysis with the ATR mode

3.3.2. Thermo-gravimetric analysis (TGA)

Thermo-gravimetric analysis (TGA) is a thermal analysis method by studying the mass change of a material with a function of temperature (with constant heating rate) or time (with constant temperature and / or constant mass loss), as shown in **Figure 3.3**. Some information related to the physical and chemical properties of the studied materials can be obtained from the TGA results.

In this study, the TGA is used to investigate the thermal stability of the materials in terms of the decomposition temperature and decomposition behavior. A thermo-gravimetric analyser (TGA, NETZSCH-Gerätebau GmbH) was used. Samples of 10 - 20 mg were placed in the crucibles and heated from room temperature to up to 800°C with a heating rate of 10 °C /min. Nitrogen was used as both the balance and sweep gas, with flow rates of 10 and 60 mL/min, respectively.

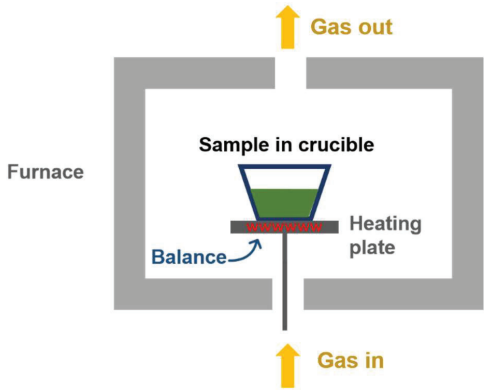

Figure 3.19 Schematics of TGA.

3.3.3. Differential scanning calorimetry (DSC)

Differential scanning calorimetry (DSC) is a thermo-analytical technique, in which the difference in the amount of heat required to increase or decrease the temperature of a sample and reference is measured as a function of temperature. The temperatures of both the sample and the reference pans are maintained at the same level throughout the experiment. The difference in the required heat of the sample pan and reference pan reflects the thermos-properties of the investigated materials, as illustrated in **Figure 3.4**. The reference sample should have a well-defined heat capacity over the range of temperatures to be scanned. Generally, air is used as the reference.

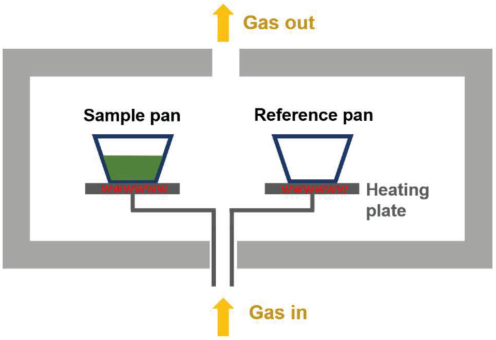

Figure 3.20. Schematics of DSC.

In the present work, the thermal properties of various materials were investigated using a DSC (DSC 214 Polyma, NETZSCH-Gerätebau GmbH). A sample of about 10 - 20 mg was put in an aluminum pan covered with a proper lid. The sample and reference (a standard empty pan with cover) were heated at a rate of 10 ºC/min under an N_2 atmosphere in the DSC furnace. A plot of

temperature versus heat flow (w/g) is obtained which was analyzed to obtain the glass transition temperature and / or melting temperature of the investigated polymers.

3.3.4. Scanning electron microscope (SEM)

A scanning electron microscope (SEM) is one of the most useful electron microscopes that produce images of various samples, including particles and membranes. As shown in **Figure 3.5**, in a SEM, a beam of electrons produced by the filament goes through electromagnetic fields and lenses and finally hits the sample, which can be detected by detectors.

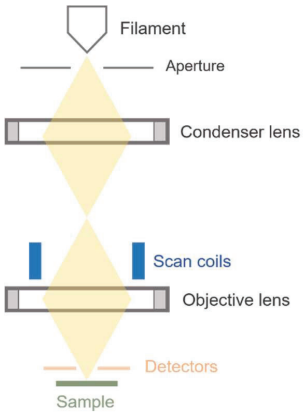

Figure 3.21 Schematics of SEM.

In this work, SEM was used to study the morphological characteristics of particles and membranes, including both surface and cross-section images. A Hitachi S3400 scanning electron microscope (Hitachi) was used. Samples of the membrane cross-section were prepared by freeze-fracturing in liquid nitrogen. The samples were mounted on a sample holder and coated with a thin gold layer (1 min for two times) for better electrical conductivity.

3.3.5. Atomic force microscopy (AFM)

AFM has been considered one of the highest resolution microscopies, that can offer the information about nanoscale material (in the nanometer or even few angstrom range). In addition to the high resolution, it has much low requirement on the space for guiding the beam (by creating a vacuum) and the sample conductivity, and thus does not need to stain/coat samples with other materials. Tapping is the most common mode to obtain AFM images for regular solid materials or liquid samples, as presented in **Figure 3.6**.

In the current work, the topography of ZIF-C nanosheets was characterized by an AFM (Dimension Icon, Bruker) using ScanAsyst mode. The as-prepared nanosheets were dispersed in ethanol and dried on cover glasses for AFM analysis.

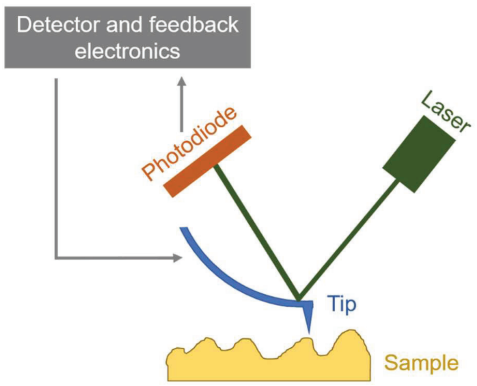

Figure 3.22 Schematics of AFM with the tapping mode.

3.3.6. X-ray diffraction (XRD)

XRD is a nondestructive technique for characterizing crystalline or semi-crystalline materials. It provides detailed information about the crystallographic structure, chemical composition, and physical properties of materials. X-ray diffraction peaks are produced by constructive interference of a monochromatic beam of X-rays scattered at specific angles from each set of lattice planes in a sample. The peak intensities and locations are determined by the atomic positions within the lattice planes, as shown in **Figure 3.7** [8].

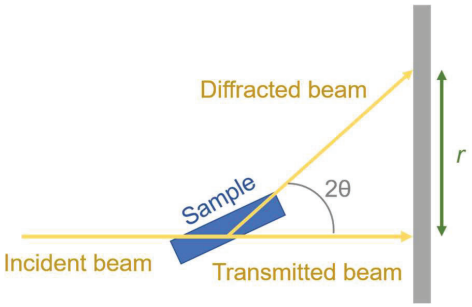

Figure 3.23 Schematics of XRD.

In the current work, the crystallinity of the prepared ZIF materials and resultant membranes was analyzed by a Bruker D8 A25 DaVinci X-ray Diffractometer (Bruker) with

characteristic wavelength λ=1.54 Å (Cu Kα radiation). The scans were taken in the 2θ range from 5° to 75°.

3.3.7. N_2 adsorption

For porous material, especially porous nanoparticles, the surface area contains not only the external but also internal surface area, which could be very useful information indicating the pore size and / or the porosity of the studied materials. The most frequently employed characterization technique to obtain surface area of nanomaterials is N_2 adsorption based on Brunauer-Emmett-Teller (BET) theory. Consequently, the obtained surface area is called the BET area.

In this work, a Tristar II 3020 (Micromeritics Instruments, USA) was used for N_2 sorption isotherms at 77 K. Before the measurements, ZIF samples were degassed at room temperature overnight under vacuum.

3.3.8. Water uptake

Water-uptake tests were conducted to evaluate the hydrophilicity of the membranes, as well as their swelling capacities. Membrane samples were dried by heating in vacuum oven at 60 ºC overnight prior to the water uptake tests. These samples were then placed in a closed container saturated with water vapor (100% relative humidity) at ambient temperature. The subsequent increase in weight was measured at different time intervals until it was stabilized. The water uptake (W_{H_2O}) of membranes was calculated by

$$W_{H_2O} = \frac{m_w - m_d}{m_d} \times 100\% \tag{3.2}$$

Where m_w and m_d are the weights of water-swollen and dried membranes, respectively. Water uptake of the membranes was estimated from the average W_{H_2O} value of two samples with an error lower than 10%.

3.3.9. Rheological test

For polymer solution with a certain concentration, its viscosity is usually positively related to the molecular weight of the polymer. For instance, during polymerization, the viscosity of the polymer solution increases with the length of the polymer chains, which also can be considered as the molecular weight of the polymer, because the longer chains have more resistance for friction compared to the small compounds. Therefore, viscosity could be used to measure the polymer's molecular weight qualitatively.

In the current work, the viscosity of liquid samples was measured by rheological tests performed on a Thermal Scientific HR-2 instrument, as shown in **Figure 3.8**. Samples were interrogated in a parallel-plate geometry with a 1 mm gap size at shear rates ranging from 1 to 100 s^{-1} at 20 °C.

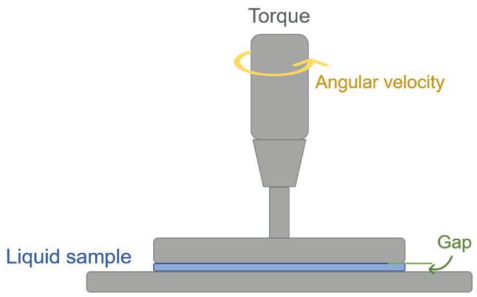

Figure 3.24 Schematics of rheometer with parallel plate system.

3.3.10. Tensile test

Tensile test, or known as tension test, is one of the most fundamental and common methods for characterizing the bulk mechanical properties. In a typical tensile test, tensile (pulling) force is applied to a material and its response to a certain stress is measured and recorded. In this way, several mechanical properties, including Young's modulus, toughness and elongation, could be obtained.

The bulk mechanical properties of the membranes in this work were investigated by performing quasistatic uniaxial tensile tests on an Instron Universal Machine 5943. Samples measuring ~500 μm thick were cut into strips measuring 4.0 cm x 1.0 cm with a CO_2 laser on a Universal Laser VLS3.50 system. The samples were strained at a crosshead speed of 10 mm/min. Each membrane thickness was the average of 5 measurements.

3.4 Gas permeation

3.4.1. Single gas permeation test

The single gas permeation results were obtained from a constant volume and variable pressure single gas permeation setup, as shown in **Figure 3.9**.

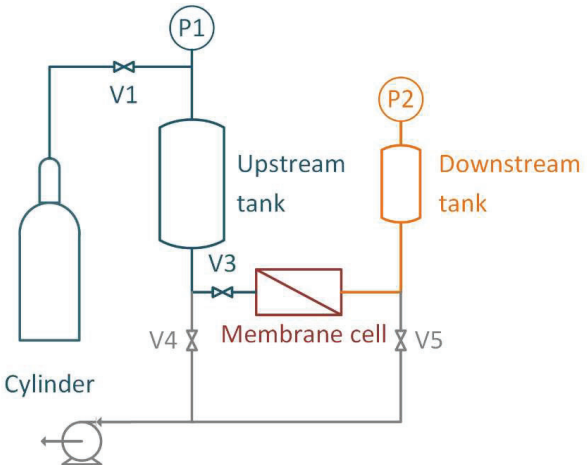

Figure 3.25 Scheme of single gas permeation setup. P1 and P2 are the pressure indicator for the upstream side with a range of 1 – 10 bar and the downstream side with a range of 0 – 100 mbar, respectively.

The gas permeability is calculated based on the Equation 3.3:

$$P = \left[\left(\frac{dp_d}{dt}\right)_{t\to\infty} - \left(\frac{dp_d}{dt}\right)_{leak}\right] \cdot \frac{V_d}{A \cdot R \cdot T} \cdot \frac{l}{(p_u - p_d)} \tag{3.3}$$

where P is the permeability, p_d and p_u represent the downstream and upstream pressure, respectively, t refers to time, V_d is the downstream volume, A means the effective membrane area, R and T are the ideal gas constant and temperature, and l is the membrane thickness, respectively. The leakage rate dp_d/dt was measured by isolating the membrane cell at vacuum condition with air for a certain period. The thicknesses of all membranes were measured by an ABS Digimatic Indicator from Mitutoyo (Suzhou, China). The average thicknesses were given based on more than 10 measurements for each membrane. The permeability was the average values obtained based on, at least, 2 samples with a relative error of less than 10%.

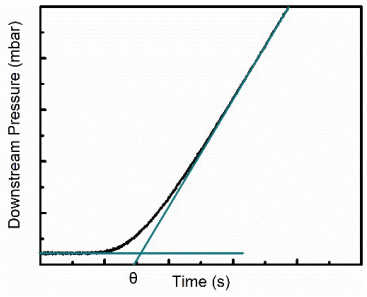

Figure 3.26 The analysis using time-lag method.

Furthermore, the diffusion coefficient (D) was evaluated using the time-lag method according to Equation 3.4:

$$D = \frac{l^2}{6\theta} \tag{3.4}$$

where θ corresponds to the time from the start of the measurement to the time when the steady state is achieved in permeation tests, as shown in **Figure 3.10**.

Accompanying solubility (S) values were calculated from the permeability and diffusivity assuming the solution-diffusion mechanism apply in the Fickian regime, as shown in equation (3.5):

$$S = \frac{P}{D} \tag{3.5}$$

The ideal selectivity α_{CO_2/N_2} was calculated using Equation 3.6:

$$\alpha_{CO_2/N_2} = \frac{P_{CO_2}}{P_{N_2}} \tag{3.6}$$

3.4.2. Mixed gas permeation tests

The mixed gas separation performances were measured using a constant pressure/variable flow method [7, 9]. Before the permeation test, all the membrane samples were carefully evacuated to remove previously dissolved species. The gas separation performance was investigated by measuring the steady state flux of two components in a mixed gas stream permeating through the membrane, where all the process variables such as pressure, the relative humidity (RH) of the gases, the gas flow rate, temperature and gas composition were continuously and simultaneously

registered by a Lab View program. A mixed gas with the composition of 10% CO_2/90% N_2 was used as a feed gas and CH_4 was used as a sweep gas. The composition of the permeate gas was analyzed continuously by a micro GC Agilent 3000. All the mixed gas permeation experiments were performed at room temperature with a feed pressure of 2 bar and a sweep pressure of 1.05 bar if not particularly mentioned. The detailed mixed gas permeation setup is shown in **Figure 3. 11**. The relative humidity of the feed and sweep gas can be controlled by adjusting the flow rate of the dry and wet flow.

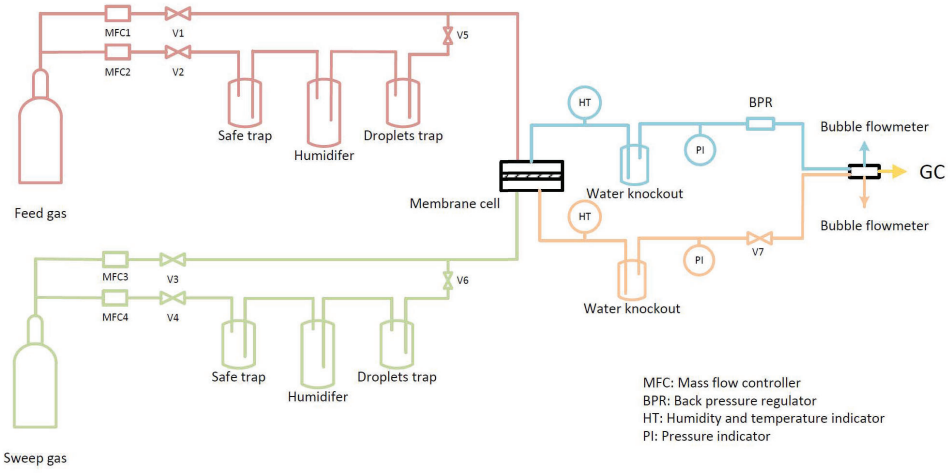

Figure 3.27 Scheme of humidified mixed gas permeation.

The permeability coefficient (P_i) of the *i*th penetrant species can be calculated from Equation 3.7:

$$P_i = \frac{N_{perm}(1 - y_{H_2O})y_i}{A(p_{i,feed} - p_{i,perm})} \quad (3.7)$$

where N_{perm} is the total permeate flow measured by a bubble flow meter , y_{H_2O} refers to the molar fraction of water in the permeate flow (calculated according to the relative humidity value and the vapor pressure at the tested temperature), y_i is the molar fraction of the gas *i* in the permeate flow (%), and $p_{i,feed}$ and $p_{i,perm}$ stand out the partial pressures of the gas *i* in feed and permeate streams, respectively. A is the effective membrane area. In the present work, the gas permeability is expressed in the unit of Barrer (1 Barrer = 10^{-10}cm^3(STP)*cm*cm^{-2}*s^{-1}*cmHg^{-1}). The separation factor was determined from Equation (3.8):

$$\alpha_{AB} = \frac{y_A/y_B}{x_A/x_B} \quad (3.8)$$

y_A and y_B are the mole ratio of gas *A* and *B* in the permeate stream, while x_A and x_B are the mole ratio of gas *A* and *B* in the feed side.

Reference

1. Z. Dai, L. Ansaloni, D.L. Gin, et al., *Facile fabrication of CO_2 separation membranes by cross-linking of poly (ethylene glycol) diglycidyl ether with a diamine and a polyamine-based ionic liquid.* J. Membr. Sci., 2017. **523**, 551-560.
2. G. González, X. Fernández-Francos, À. Serra, et al., *Environmentally-friendly processing of thermosets by two-stage sequential aza-Michael addition and free-radical polymerization of amine–acrylate mixtures.* Polym. Chem., 2015. **6**(39), 6987-6997.
3. L. Kwisnek, J. Goetz, K.P. Meyers, et al., *PEG Containing Thiol–Ene Network Membranes for CO_2 Separation: Effect of Cross-Linking on Thermal, Mechanical, and Gas Transport Properties.* Macromolecules, 2014. **47**(10), 3243-3253.
4. Y.F. Fan, C. Li, X.S. Zhang, et al., *Troger's base mixed matrix membranes for gas separation incorporating NH_2-MIL-53(Al) nanocrystals.* J. Membr. Sci., 2019. **573**, 359-369.
5. S.S. Zhao, J.Y. Liao, D.F. Li, et al., *Blending of compatible polymer of intrinsic microporosity (PIM-1) with Troger's Base polymer for gas separation membranes.* J. Membr. Sci., 2018. **566**, 77-86.
6. R. Chen, J. Yao, Q. Gu, et al., *A two-dimensional zeolitic imidazolate framework with a cushion-shaped cavity for CO_2 adsorption.* Chem. Commun., 2013. **49**(82), 9500-9502.
7. Z. Dai, J. Deng, K.-J. Peng, et al., *Pebax/PEG Grafted CNT Hybrid Membranes for Enhanced CO_2/N_2 Separation.* Ind. Eng. Chem. Res., 2019. **58**(27), 12226-12234.
8. R. Kohli, *Chapter 3 - Methods for Monitoring and Measuring Cleanliness of Surfaces*, in *Developments in Surface Contamination and Cleaning*, R. Kohli and K.L. Mittal, Editors. 2012, William Andrew Publishing: Oxford. p. 107-178.
9. Z. Dai, H. Aboukeila, L. Ansaloni, et al., *Nafion/PEG hybrid membrane for CO_2 separation: Effect of PEG on membrane micro-structure and performance.* Sep. Purif. Technol., 2019. **214**, 67-77.

Chapter 4

Summary and suggestions for further work

4.1 Summary and conclusions

The main objective of this work has been to develop highly permeable polymeric membranes for post-combustion CO_2 capture. Two approaches have been employed to realize this objective: chemically cross-linking PEO monomers based on click reactions and physically incorporating new ZIF particles into polymeric membranes. From the results, it can be concluded that:

1) chemically cross-linking PEO monomers based on click reactions

- The selected click reactions: aza-Michael, thiol-ene and thiol-epoxy, show excellent feasibility for fabricating cross-linking PEO membranes with facile preparation methods and tunable network structure.
- Two cross-linking methods have been developed for fabricating cross-linked PEO membranes with dual cross-link networks: the two-step cross-linking method combined aza-Michael addition and acrylate polymerization and the one-pot method comprising thiol-ene and thiol-epoxy.
- The length of linear monomers and the functionality of the multi-functional cross-linker have great influence on the gas permeability of the resultant membranes. Within the range studied in this work, the longer linear monomers and less functional cross-linkers endow higher CO_2 permeability with almost unchanged CO_2/N_2 selectivity.
- The addition of free PEGDME into cross-linked PEO membranes yields a significantly enhanced CO_2 permeability without sacrificing the CO_2/N_2 selectivity, which is mainly attributed by the increase in CO_2 diffusivity.
- The incorporation of free ILs has different impacts, which are greatly affected by the anion types. The changes of CO_2 permeability depend on the content of ILs, which decreases at low IL loading (< 20 wt. %) and then increases with increasing ILs content. The order of

CO_2 permeability of IL-containing membranes matches with their CO_2 affinity: [Bmim][NTf_2] ≈ [Bmim][TCM] > [Bmim][BF_4]. The selectivity of the resultant membranes decreases with the addition of ILs for all investigated ILs, probably resulted from the less-selective nature of selected ILs compared to PEO.

- For cross-linked PEO/IL membranes, further analysis reveals that the presence of ILs tends to reduce the gas diffusivity in the range of investigated additive loading, while the CO_2 solubility firstly decreases and then increases or keeps unchanged with increasing ILs content, depending on the ILs' composition.

2) Physically incorporation ZIF particles with various morphologies into polymeric membranes

- A simple preparation method for new ZIF with controllable morphology (cuboids with different thickness, needles and particles) in diluted polymer solution at room temperature has been proposed. Different polymers and their molecular weights have strong influences on the shape and the size of synthesized ZIF nanomaterials, as well as the material properties.
- During the growth of ZIFs, the polymer additives are selectively attached on the surface of the ZIF crystals and inhibit the growth of the crystal along certain directions, by which the shape and the size of these nanosheets can be manipulates. This speculation has been confirmed by FTIR and TGA results.
- The ZIF cuboids with different thicknesses have been incorporated into Pebax 1657.It is found out that for all ZIF-Cs, both CO_2 permeability and CO_2/N_2 selectivity increases with the ZIF-Cs loading. However, the thickest ZIF-C is the most efficient nanofiller in promoting CO_2 transport properties compared to its thinner counterparts, mainly because of the selective adsorption of CO_2 inside the ZIF-C nanosheets. The highest CO_2 permeability (387.2 Barrer) with a CO_2/N_2 selectivity of 47.1 is obtained from the Pebax + 20% ZIF-C 85-124 MMM under fully humidified conditions.
- To further study the impact of the filler's morphology, the ZIF particles with different shapes (particles, needles and leaves) have been embedded within the Pebax 2533 matrix. The leaf-like ZIF has a higher agglomeration tendency compared to the other two. Surprising, the effect of these ZIFs on the CO_2 permeation results are similar: CO_2 permeability firstly increasing and then decreasing with increasing ZIF loading. The optimized ZIFs loadings are 10 wt.% for particle- and needle- like ZIFs, while 5 wt.% for leaf-like ZIF. The leaf-like ZIF endows the highest CO_2 permeability followed by the needle- and particle- like ZIF, but the order for CO_2/N_2 selectivity is the opposite. The shapes with higher aspect ratio may cause more voids inside MMMs due to the imperfect

wrap by polymeric matrix, resulting in higher gas transport properties with lower selectivity.

- Two leaf-like ZIFs based on different metal ions (ZIF-L-Zn and ZIF-L-Co) have been added into TB polymers to study the metal ion's effects. Because of the stiffer Co-N bond, the ZIF-L-Co may have a smaller efficient size than ZIF-L-Zn, indicated by the much lower N_2 adsorption amount. Hence, the H_2 separation performance could benefit more from the ZIF-L-Co instead of the ZIF-L-Zn, judging from the both higher H_2 permeability and H_2 selectivities.

4.2 Recommendation for future work

In order to further study the structure-property of the cross-linked PEO-based membranes and ZIF-based MMMs and then improve their separation performance, more studied are suggested based on the results obtained from the current work:

- New cross-linking methods based on more efficient reactions with moderate reaction conditions may be developed to achieve different cross-linking network structure;
- The influences of cross-linking network structure on the gas separation performance can be further investigated by more advanced analytic techniques;
- More CO_2-philic liquid, such as amine-functionalized ILs into cross-linking PEO membranes, may be used as the additives in PEO-based membranes, to further improve CO_2 solubility and potentially enhance CO_2 diffusivity;
- The long-term stability of the blend cross-linked PEO-based membranes with liquid additives (e.g., free PEO and ILs) blend membranes should be studied;
- New methods to fabricate PEO membranes into thin-film-composite membranes should be explored.
- New porous inorganic fillers with different morphologies should be used as the inorganic phase in MMMs. The impacts on the morphology of inorganic phase on the interface morphology inside MMMs and the gas separation performance of MMMs need more in-depth discussion;
- The effects of fillers' morphologies on gas separation performances can be integrated into the current mathematical models for MMMs.
- New polymeric materials with better compatibility with nanofillers and processability for MMMs fabrication should be developed.

Part II

Paper I

Facile and solvent-free fabrication of PEG-based membranes with interpenetrating networks for CO_2 separation

This paper is published in
Journal of Membrane Science
2019, 570–571, 455–463

Journal of Membrane Science 570–571 (2019) 455–463

Contents lists available at ScienceDirect

Journal of Membrane Science

journal homepage: www.elsevier.com/locate/memsci

Facile and solvent-free fabrication of PEG-based membranes with interpenetrating networks for CO_2 separation

Jing Deng[a], Zhongde Dai[a], Jiaqi Yan[b], Marius Sandru[c], Eugenia Sandru[c], Richard J. Spontak[b,d], Liyuan Deng[a,*]

[a] Department of Chemical Engineering, Norwegian University of Science and Technology, 7491 Trondheim, Norway
[b] Department of Chemical and Biomolecular Engineering, North Carolina State University, Raleigh, NC 27695, USA
[c] Department of Polymer Particles and Surface Chemistry, SINTEF Industry, 7034 Trondheim, Norway
[d] Department of Materials Science and Engineering, North Carolina State University, Raleigh, NC 27695, USA

ARTICLE INFO

Keywords:
Polymer cross-linking
Poly(ethylene glycol)
Interpenetrating networks
Aza-Michael addition
CO_2 separation membrane

ABSTRACT

For nearly two decades, membranes derived from polyethers have served as promising candidate materials for CO_2 separation. Due to the inherent tendency of high-molecular-weight poly(ethylene oxide) (PEO) to crystallize and thus reduce its CO_2 permeability, prior studies have focused on membranes produced from low-molecular-weight poly(ethylene glycol) (PEG). In this work, a novel series of cross-linked PEG-based membranes composed of interpenetrating polymer networks has been generated through the use of amine-terminated Jeffamine and multiple acrylate-functionalized cross-linkers in a facile, solvent-free, two-stage reaction. Evidence of cross-linked interpenetrating polymer networks formed by aza-Michael addition and acrylate polymerization is confirmed by real-time fourier-transform infrared spectroscopy. In addition, we systematically investigate the thermal stability, mechanical properties and water sorption of these multicomponent membranes. Corresponding CO_2 and N_2 transport properties, evaluated by single-gas permeation tests, are found to depend on both the chemical nature of the cross-linkers and the ratio of the interpenetrating networks. Moreover, free PEG dimethyl ether has been added into the optimized cross-linked matrix at different loading levels to further enhance gas-transport properties.

1. Introduction

Escalating atmospheric CO_2 levels are related closely to accelerating global warming, rising sea levels and growing deterioration of typical weather patterns. To address these worrisome concerns, the development of CO_2-capture technologies designed to reduce CO_2 emission from diverse power generation sources has become increasingly urgent [1–4]. Gas-separation membranes have long been considered as a viable solution for CO_2 capture due largely to their relatively low cost, high operational simplicity and reliability, high energy efficiency, and overall environmental compatibility [2,5–10]. For nearly 50 years, polymeric membranes have enjoyed the biggest share of the gas-separation membrane market because of the lower cost and superior processability of organic, compared to inorganic membranes [11]. However, the performance of polymeric membranes is generally limited by the trade-off between gas permeability and selectivity [12], which means that highly permeable membranes usually possess low selectivity and vice-versa. Recently, several emerging polymeric materials and material classes have attracted tremendous attention due to their unique ability to surpass this trade-off, the so-called Robeson upper bound, between selectivity and permeability [12]. Examples of these exceptional materials or their membranes include polymers of intrinsic microporosity (PIMs) [13–15], thermal rearrangement (TR) membranes [16–18], poly(ethylene glycol) (PEG) or poly(ethylene oxide) (PEO) membranes [19–21], and polymers endowed with specific chemical moieties to serve as carriers for facilitated gas transport [22–24]. Of particular interest here, polyether-based membranes generally possess a high intrinsic affinity towards CO_2 [10,25]. Since high-molecular-weight PEO is semi-crystalline, however, CO_2 permeability is compromised by an increase in diffusive tortuosity and a reduction in CO_2 solubility [26]. To overcome this drawback, low-molecular-weight PEG has been cross-linked [20] and/or blended with various additives to concurrently improve mechanical integrity and separation performance [25,27].

Typical processes developed to generate gas-separation membranes are often limited to solvent-based methods, such as dip-coating, spin-

* Corresponding author.
E-mail address: liyuan.deng@ntnu.no (L. Deng).

https://doi.org/10.1016/j.memsci.2018.10.031
Received 29 August 2018; Received in revised form 1 October 2018; Accepted 9 October 2018
Available online 16 October 2018
0376-7388/

coating and solution-casting [11]. The potential toxicity and large volumes of organic solvents employed in membrane production provide an ongoing impetus to explore more environment-friendly preparation approaches [28,29]. For instance, a solvent-free method, such as thermal [21,30] or UV [19] reactive coupling of end-functionalized PEG, has become increasingly more attractive in membrane fabrication [20,27]. Freeman and co-workers [19,31,32] have reported that UV photopolymerization of acrylate-endcapped PEG oligomers could be used to generate amorphous membranes in which the CO_2 permeability substantially increased. Furthermore, they have demonstrated that the cross-link density of such membranes can be controllably varied by adjusting the water or PEG methyl ether acrylate (PEGMEA) level in pre-polymer solutions [19]. Similarly, multicomponent membranes composed of PEG diacrylate (PEGDA), PEGMEA and PEG dimethyl ether (PEGDME) exhibit an unprecedentedly high CO_2 permeability [20]. Recently, additional strategies have been proposed to improve gas-transport properties by incorporating nanoparticles through physical blending and/or chemical bonding [33–35]. A fundamental shortcoming of UV cross-linking is, however, that the free radicals generated during acrylate polymerization are sensitive to atmospheric O_2 trapped in the polymer solutions, thereby resulting in undesirable oxygen inhibition and incomplete reaction [36]. Reduction of O_2 in the reacting solution therefore requires the use of an oxygen-free glove box or a dry N_2 atmosphere. To avoid this complication, Kwisnek et al. [37,38] have incorporated multifunctional thiols into acrylate-functionalized cross-linked PEG membranes to exploit the O_2 tolerance of thiol-based radicals. The resultant thiol-modified membranes possess a lower cross-link density due to a different polymerization mechanism, but enhanced gas-transport [37] and mechanical [38] properties.

In addition to free-radical polymerization, other preparation methods have also been used to form chemically cross-linked polymeric networks/membranes on the basis of diverse PEG-based monomers/oligomers. For instance, Shao et al. [39] have prepared cross-linked amorphous PEG membranes from the ring-opening reaction of epoxy by amine-terminated Jeffamine and report a slightly enhanced CO_2 permeability of 180 Barrer and a CO_2/N_2 selectivity of 58. They have also employed the reaction between bio-inspired dopamine and epoxy-functionalized PEG oligomer to fabricate dopamine/PEG membranes at elevated temperatures [40]. In addition, introduction of low-molecular-weight PEGDME could greatly improve gas-transport performance. Dai et al. [41] have investigated cross-linked PEG-based membranes produced from the reaction between diamine or diamine-functional ionic liquids and PEG diglycidyl ether (PEGDGE) and possessing a CO_2 permeability of ~ 200 Barrer after free PEGDGE is incorporated into the cross-linked network. It is noteworthy that all these reactions require a moderately high temperature (≥ 80 °C) and a relatively long reaction time (≥ 3 h) to complete cross-linking, and some reactions need even more complicated preparation [39,40], which is inconvenient for practical applications. Thus, the development of a facile, rapid and highly effective cross-linking system that employs relatively mild reaction conditions is desirable for the fabrication of PEG-based membranes.

Due to its mild reaction conditions and the absence of unwanted by-products, aza-Michael addition constitutes one of the most important reactions in organic chemistry and is crucial in the materials design of functional silicone intermediates [42], biomaterial functionalization [43] and the surface modification of membranes or nanoparticles [42,44]. Here, we demonstrate that this reaction can likewise be applied to the preparation of novel PEG-based membranes for gas separations. Generally speaking, the aza-Michael addition refers to the addition reaction of a primary or secondary amine to an electron-deficient molecule, such as an acrylate [45–47]. Ramis and co-workers [45,48] have proposed a dual-curing and solvent-free procedure for thermosets on the basis of aza-Michael addition (using an acrylate-amine) and acrylate photopolymerization under atmospheric conditions. The formation of tertiary amines by aza-Michael addition effectively prevents oxygen inhibition during free-radical acrylate polymerization. Moreover, the properties of the final material are tunable for diverse requirements by using different monomer species and formulation specifications. This observation is in agreement with the observations of Yang and co-workers [46,49]. That is, by tuning the composition, monomers and reaction conditions, the network topology, swellability and other properties of the aza-Michael addition product (e.g., shape memory, environmental protection and structured surfaces) could be readily modulated.

In this work, a series of PEG-based membranes developed exclusively for CO_2 separation have been generated from aza-Michael addition and free-radical acrylate polymerization and consist of interpenetrating polymer networks. A cross-linked acrylate-amine network forms quickly at ambient temperature, while residual acrylate groups are photopolymerized under UV radiation. The cross-link density can be controlled by the choice of cross-linker at different compositions, and addition of a PEG-based oligomer serves to induce network swelling and improve gas transport. The chemical structure, thermal properties and single-gas permeation of the resultant membranes are investigated here by various characterization techniques.

2. Experimental

2.1. Materials

Pentaerythritol triacrylate (PEG3A, 298 g/mol), pentaerythritol tetraacrylate (PEG4A, 352 g/mol), 1-hydroxylcyclohexyl phenyl ketone (HCPK, 204 g/mol), Jeffamine ED-600 (500 g/mol) and PEGDME (*ca.* 500 g/mol) were all purchased from Sigma Aldrich. Dipentaerythritol hexaacrylate (PEG5A, 578 g/mol) was obtained from Abcr. All chemicals were used as-received without further purification. The chemical structures of these monomer species are displayed in Fig. 1.

2.2. Membrane preparation

Membranes were fabricated by a two-stage cross-linking reaction similar to that described elsewhere [19,45]. A brief description of the reaction scheme, illustrated in Fig. 2, is presented here. Multiple acrylate-functionalized cross-linkers, free PEGDME and 0.01–0.1 wt% HCPK were combined in a glass vial for several minutes to ensure uniform mixing. The mass ratio of PEGDME (W_{PEGDME}) was calculated from

$$W_{PEGDME} = \frac{m_{PEGDME}}{m_{Cross-linker}} \times 100\% \quad (1)$$

A known amount of Jeffamine was added to the mixture under vigorous stirring to promote complete reaction. The mole ratio of cross-linkers and Jeffamine was calculated on the basis of acrylate groups to N-H bonds. The mixture was then transferred to a vacuum oven to remove the likelihood of bubbles. Afterwards, the solution was sandwiched between two quartz plates separated by spacers to control the membrane thickness. The solution was photopolymerized under a UV lamp (UVLS-28, Ultra-Violet Products Ltd.) with a wavelength of 365 nm for 2 h. The resultant membranes were evaluated by various characterization methodologies and permeation tests. In this work, all membranes are systematically designated as "Cross-linker-Jeffamine-X-X" according to the constituent species and the ratio of acrylate-containing cross-linker to amine-terminated monomer. For example, the PEG3A-J-6-1 membrane consists of PEG3A and Jeffamine with 6 PEG3A acrylate groups per Jeffamine N-H bond.

2.3. Membrane characterization

A Thermo Nicolet Nexus Fourier-transform infrared (FTIR) spectrometer with an attenuated total reflectance (ATR) cell equipped with

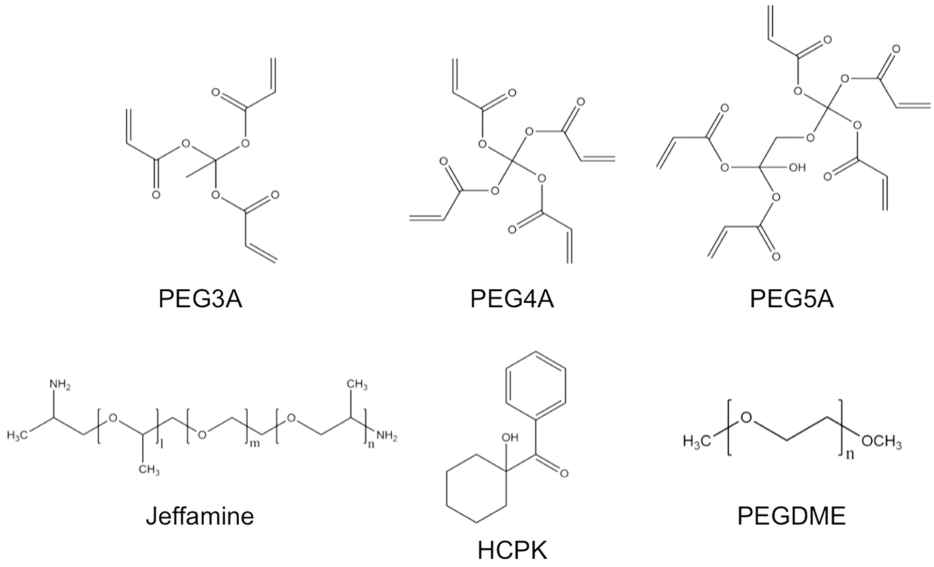

Fig. 1. Chemical structures of the monomers and cross-linkers employed in this study: PEG3A, PEG4A, PEG5A, Jeffamine, HCPK and PEGDME.

a diamond crystal was used to collect chemical spectra from all the membranes in this study. To monitor the real-time reaction between cross-linker and Jeffamine, the Marco-Real protocol was employed: a drop of mixture solution containing cross-linker and Jeffamine was placed on the diamond crystal, heated to 30 °C and covered by a glass Petri dish. Spectra were recorded every 1.5 min over the course of 1 h under isothermal conditions. The viscosity of liquid samples was measured by rheological tests performed on a Thermal Scientific HR-2 instrument. Samples were interrogated in a parallel-plate geometry with a 1 mm gap size at shear rates ranging from 1 to 100 s^{-1} at 20 °C. The thermal stability of the membranes was interrogated by thermogravimetric analysis (TGA) performed on a Thermal Scientific Q500 instrument. Approximately 10–20 mg samples were heated in a ceramic crucible from ambient temperature to 700 °C at a constant heating rate of 10 °C/min under N_2 to prevent thermo-oxidative degradation of the membranes. The bulk mechanical properties of the membranes were investigated by performing quasistatic uniaxial tensile tests on an Instron Universal Machine 5943. Samples measuring ~ 500 μm thick

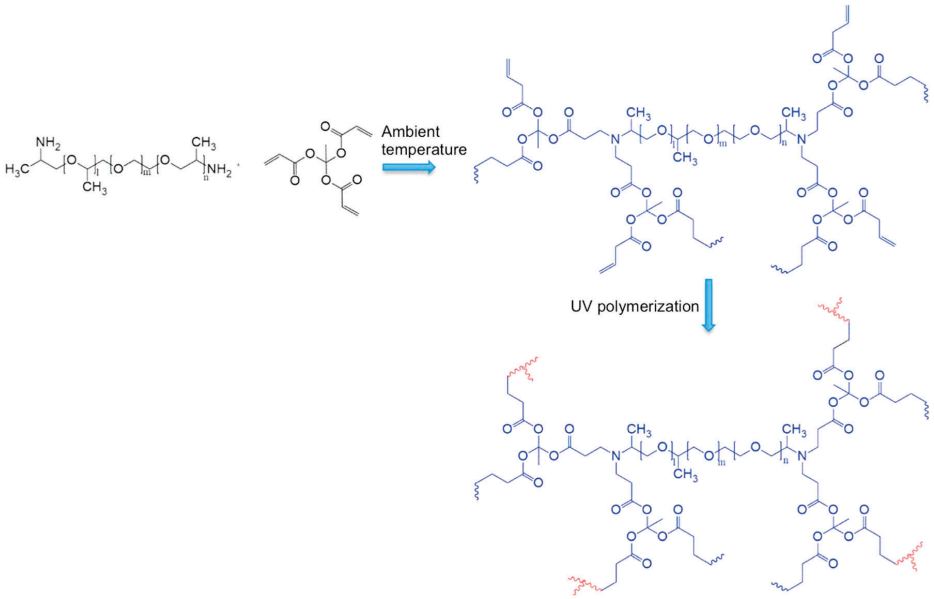

Fig. 2. Schematic illustration of a portion of the PEG3A-Jeffamine interpenetrating network.

were cut into strips measuring 4.0 cm x 1.0 cm with a CO_2 laser on a Universal Laser VLS3.50 system. The samples were strained at a crosshead speed of 10 mm/min. Each membrane thickness was discerned as the average of 5 measurements. Water-uptake tests were conducted to evaluate the hydrophilicity of the membranes, as well as their swellability. Membrane specimens were placed in a closed container saturated with water vapor at ambient temperature. The subsequent increase in weight was measured until it stabilized. The water uptake (W_{H2O}) of membranes was calculated by

$$W_{H_2O} = \frac{W_f - W_0}{W_0} \times 100\% \quad (2)$$

where W_f is the final (stabilized) specimen weight and W_0 represents the initial weight.

In this work, the gas permeability (P) of either CO_2 or N_2 through the membranes was measured by the constant-volume variable-pressure method according to

$$P = \left[\left(\frac{dp_d}{dt} \right)_{t \to \infty} - \left(\frac{dp_d}{dt} \right)_{t \to leak} \right] \bullet \frac{V_d}{A \bullet R \bullet T} \bullet \frac{l}{(p_u - p_d)} \quad (3)$$

where p_d and p_u identify the downstream and upstream gas pressures, respectively, and t is time. Here, V_d is the downstream volume, A corresponds to the effective permeation area of membrane, R is the universal gas constant, T denotes absolute temperature, and l is the membrane thickness. The leakage rate of the gas permeation setup $(dp_d/dt)_{t \to leak}$ was measured from the increase in downstream pressure relative to vacuum over time. Membrane thicknesses were measured by a Digitix II thickness gauge. Average thicknesses were averaged from more than 10 measurements for each membrane. All gas permeation experiments were performed using an upstream pressure of 2 bar (absolute) at ambient temperature. For each membrane, the reported permeabilities were the average of measurements acquired from at least two specimens. The ideal CO_2/N_2 selectivity was calculated from the ratio of gas permeabilities *viz.*

$$\alpha_{ij} = \frac{P_i}{P_j} \quad (4)$$

Furthermore, the diffusion coefficient (D) was evaluated by the time-lag method during single-gas permeation tests from

$$D = \frac{l^2}{6 \bullet \theta} \quad (5)$$

where θ corresponds to the time from the start of the measurement to the time when steady state is achieved in permeation tests. Accompanying solubility (S) values were calculated from the permeability and diffusivity assuming applicability of the solution-diffusion mechanism in the Fickian regime so that

$$S = \frac{P}{D} \quad (6)$$

3. Results and discussion

3.1. Cross-linking mechanism

To confirm the aza-Michael addition between acrylate and amine groups, we have performed real-time FTIR-ATR analysis of mixtures composed of Jeffamine and PEG3A. Since the amine content in Jeffamine is relatively low, the peak corresponding to the -NH_2 group (at 3100–3500 cm^{-1}) is imperceptible, in which case changes in the acrylate group are used to follow the reaction. The intensity of the peaks corresponding to the -C=C- stretching band (at 1637 cm^{-1}) and the =C-H band (at 1408 and 808 cm^{-1}) are observed to decrease significantly with increasing time in Fig. 3, thereby confirming that the acrylate groups are consumed. Considering that the amine is the only functional group that is capable of reacting with the acrylate and that acrylate cannot self-react rapidly in the absence of catalyst in the present system, this result confirms the reaction between Jeffamine and PEG3A. In addition, the peak intensities related to the C=C and =C-H bonds decrease sharply at early measurement times but become less time-dependent as the reaction progresses, in agreement with the typical kinetics characteristic of a step-growth mechanism such as aza-Michael polymerization [50]. The PEG3A is first expected to react rapidly with Jeffamine to form star-like oligomers, which subsequently react with each other and grow to build a cross-linked network. As mentioned earlier, this reaction proceeds much more slowly during real-time measurement (without constant stirring) when compared to the reaction under film preparation conditions. In addition to these real-time FT-IR results, the increase in viscosity of this mixture from 0.56 to 5.32 Pa·s after 1 h while stirred at ambient condition further confirms that the amines in Jeffamine react with the acrylate groups on the PEG3A cross-linker.

The effect of aza-Michael addition is also apparent from the spectra of the final membranes, as evidenced in Fig. 4. A signal corresponding to residual –C=C- bonds remains in FT-IR spectra acquired from PEG3A or PEG3A-J membranes with sufficient irradiation (2 h instead of the regular 90 s – 3 min [31]), indicating incomplete conversion of acrylate. The peak intensity of acrylate in these final membranes decreases upon addition of Jeffamine. These observations could result from several considerations. First, the cross-linkers used in this works are multifunctional, in which case considerable steric hindrance might yield isolated C=C groups during the cross-linking reaction. In addition, oxygen inhibition might also contribute to the low conversion of acrylate during homopolymerization [36]. Addition of Jeffamine with longer chains is anticipated to increase the distance between cross-linking sites and reduce steric hindrance. Moreover, the aza-Michael addition overcomes oxygen inhibition of free-radical acrylate polymerization to achieve higher acrylate conversion. Lastly, as the concentration of Jeffamine is increased, typical peaks associated with the ether and methyl groups (at 1102 and 2867 cm^{-1}, respectively) corresponding to Jeffamine become more conspicuous in the FTIR spectra, suggesting an increase in the fraction of ethylene glycol units, which is further expected to benefit CO_2 transport and improve CO_2 separation performance.

3.2. Bulk properties

The thermal stability of PEG3A-J and PEG3A membranes has been investigated by TGA (*cf.* Fig. 5). These results reveal that all the membranes investigated here exhibit single-stage thermal decomposition, with the decomposition temperature varying between 300 and 400 °C, depending on the formulation details. An increase in amine content is, however, accompanied by a progressive reduction in the thermal stability of the PEG3A-J membranes. This behavior is attributed to the intrinsic properties of the C-C and C-N bonds, since C-N bonds are known to be less thermally stable than C-C bonds [45]. Although these results demonstrate that the thermal stability of acrylate/amine-based membranes is compromised upon addition of amine, all the membranes possess sufficient thermal stability for CO_2 separation membranes intended for use in post-combustion and natural-gas sweetening, which are normally operated at temperatures below 80 °C. It is worth mentioning here that differential scanning calorimetry was also conducted on the resultant membranes. No distinct glass transition temperatures (T_gs) are, however, observed over the range from -150–150 °C, suggesting that either the expected T_g is lower than the test temperature (the reported T_g of the cross-linked PEG membrane is usually < 0 °C) or the heat change associated with the T_g of these membranes is undetectable by this characterization method. For this reason, these results are not reported in this work. Since these membranes must likewise possess sufficient mechanical resilience, the mechanical properties of PEG3A-J and PEG3A membranes have been evaluated by quasistatic uniaxial tensile testing (according to ASTM

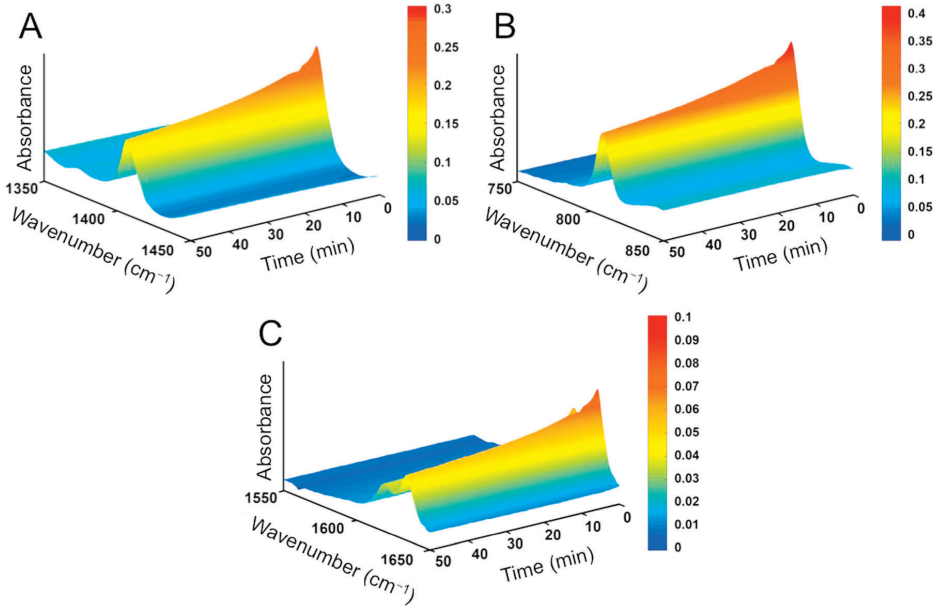

Fig. 3. Real-time FTIR spectra of a PEG3A/Jeffamine reaction mixture with 1:1 w/w ratio collected over three different regions (in cm^{-1}): (A) 750–850, (B) 1350–1450 and (C) 1550–1650.

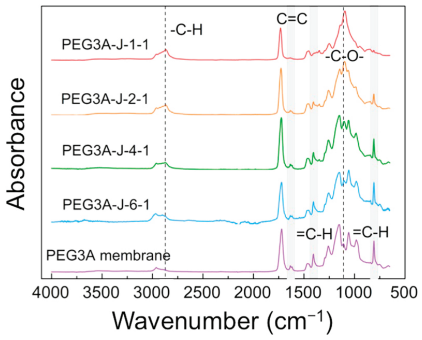

Fig. 4. FTIR spectra of PEG3A and four PEG3A-J membranes varying in Jeffamine content (labeled and color-coded). Specific spectral peaks discussed in the text are highlighted. (For interpretation of the references to color in this figure legend, the reader is referred to the web version of this article).

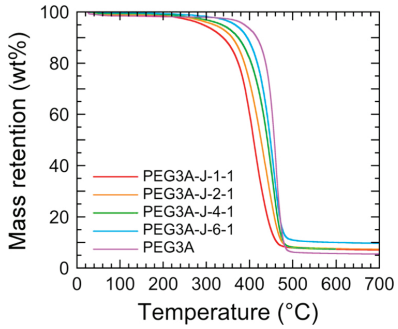

Fig. 5. Mass retention measured by TGA and presented as a function of temperature for PEG3A and four PEG3A-J membranes varying in Jeffamine content (color-coded). (For interpretation of the references to color in this figure legend, the reader is referred to the web version of this article).

D882-1223 and displayed in Fig. 6**A**). All the membranes undergo catastrophic failure over a relatively narrow strain range (< 13%) with only PEG3A-J-1-1 displaying evidence of elastomeric behavior. From these strain-stress curves, the PEG3A-J membranes are found to be less brittle compared to the neat PEG3A membranes, and an increase in Jeffamine content promotes an increase in the maximum strain and a corresponding reduction in tensile strength. The tensile modulus, which quantifies the stiffness of a solid material [51] and is calculated from either the initial slope of the stress-strain curve or the stress measured at 2% strain, is observed in Fig. 6**B** to decrease with increasing Jeffamine fraction. Tensile strength values, identified as the maximum stresses observed in Fig. 6**A** and included in Fig. 6**B**, indicate a slight maximum, but does not change appreciably, with increasing Jeffamine content. Also included in the inset of Fig. 6**B** are the elongation-at-break (discerned at the tensile strength) and the relative fracture toughness (measured from the area under each stress-strain curve and normalized with respect to the value determined for PEG3A). We therefore conclude that the PEG3A-J membranes become softer (lower tensile modulus) and weaker (lower tensile strength) but more stretchable (larger maximum strain) and tougher (larger fracture toughness) as the N-H/acrylate ratio is systematically increased. These changes are believed to be due to the longer chains afforded by the addition of Jeffamine.

Gas-separation performance can be significantly improved by the presence of water vapor for hydrophilic membranes such as polyvinylamine [52,53], poly(acrylic acid) [54], poly(vinyl alcohol) [55,56], and ionic liquid-containing membranes [57–59]. Several factors could be responsible for such improvement: enhanced polymer chain mobility, highly permeable water-swollen regions or facilitated transport arising from specific functional moieties. For comparison, we examine the effect of water sorption on the present membrane

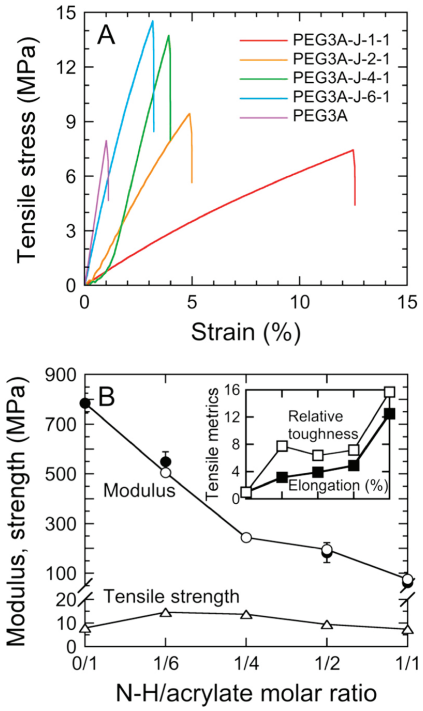

Fig. 6. (A) Quasistatic uniaxial tensile tests measured from PEG3A-J and four PEG3A membranes varying in Jeffamine content (color-coded). (B) Moduli measured from the initial slope up to 1% strain (•) or the stress value at 2% strain (○), as well as the tensile strength (Δ) determined from the maximum stress, of the data displayed in (A) as functions of the N-H/acrylate molar ratio. Included in the inset are the maximum strain (or elongation, in %) and relative fracture toughness (labeled). The solid lines in (B) serve to connect the data. (For interpretation of the references to color in this figure legend, the reader is referred to the web version of this article).

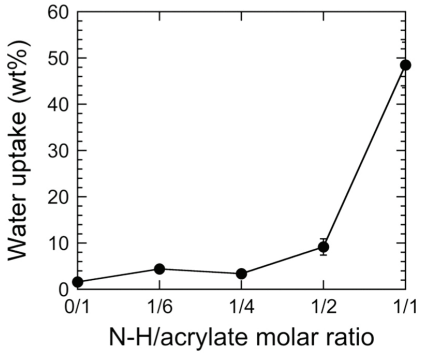

Fig. 7. Water uptake presented as a function of N-H/acrylate molar ratio for PEG3A and four PEG3A-J membranes varying in Jeffamine content. The solid lines serves to connect the data.

materials. Fig. 7 displays water uptake results measured from the PEG3A-J membranes at ambient temperature and immediately reveals that these membranes with different interpenetrating networks exhibit different hydrophilicity levels. The extremely low water uptake (< 2 wt%) of the parent PEG3A membrane is a direct consequence of its high cross-link density. Water uptake increases slightly upon addition of Jeffamine, ultimately resulting in 48.5 wt% for PEG3A-J-1-1, which does not contain interpenetrating networks connected by C-C and C-N bonds. Since C-C bonds are less hydrophilic than C-N bonds, the existence of more C-C bonds in the PEG3A-J-1–2 membrane reduces its bulk hydrophilicity, as reflected by its lower water uptake of 9.2 wt% in Fig. 7.

3.3. Permeability considerations

To ascertain the influence of cross-linker functionality on the gas-separation performance, cross-linked PEG membranes have been prepared from three cross-linking agents possessing different functional groups (PEG3A, PEG4A and PEG5A) at a constant N-H:acrylate ratio of 1:4. The single-gas transport properties of these membranes have been tested at ambient temperature with a feed pressure of 2.0 bar and a vacuum level of 1 mbar on the permeate side. The CO_2 and N_2 permeabilities of these membranes, as well as the corresponding CO_2/N_2 ideal selectivities, are presented in Table 1. Theoretically, an increase in the fraction of acrylate groups contained in the cross-linkers is expected to generate membranes with a higher cross-link density and lower gas permeability, which agrees with the N_2 permeability of these membranes. The CO_2 permeability of PEG5A-J-4-1 appears to increase slightly relative to PEG4A-J-4-1, but this difference lies within the range of experimental uncertainty. A similar trend applies to the CO_2 diffusivity, which is also complicated by experimental uncertainty. Taken together, these results suggest that gas permeability decreases (or at least does not change significantly) as the number of acrylate groups in the cross-linkers is increased. Due largely to the dependence of N_2 permeability on cross-linker functionality, the CO_2/N_2 ideal selectivity increases with increasing acrylate content, a result of higher cross-link density, as evidenced by the combination of a nearly unchanged CO_2 solubility and a reduced CO_2 diffusivity. Because of such high cross-link density, all membranes display relatively low gas permeability and moderate CO_2/N_2 selectivity. To improve gas-transport properties, we have chosen the PEG3A cross-linker for further study in this work.

The effect of dual cross-linked networks on the gas-separation performance of PEG3A-J membranes is interrogated by systematically varying the ratio between N-H and acrylate groups. In Fig. 8**a**, CO_2 permeability and CO_2/N_2 ideal selectivity values are provided as functions of the N-H/acrylate molar ratio. While the CO_2 permeability of cross-linked PEG3A is low (≈1.56 Barrer) and the corresponding CO_2/N_2 selectivity is about 29, introduction of the cross-linked N-H/amine network enhances CO_2 permeability and becomes more effective with increasing N-H/acrylate ratio. Since N_2 permeability likewise increases with increasing N-H/acrylate ratio, the CO_2/N_2 ideal selectivity is only marginally improved to just under 40 and then remains relatively constant. Since the CO_2-philic groups in both PGE3A and Jeffamine are ether groups and cross-linked PEG-based membranes are typically rubbery at ambient temperature, these two materials are reasonably expected to possess similar CO_2/N_2 ideal selectivities (40 ~ 60) as those of PEG-based materials. The reason for CO_2 permeability enhancement in the PEG3A-J membranes is related to either the diffusivity or solubility of CO_2 in the membranes. These values, calculated from Eqs. (5) and (6), respectively, are included in Fig. 8**b**. The CO_2 diffusivity displays a monotonic increase as the N-H/acrylate ratio is increased, indicating that the acrylate/amine cross-linked network becomes increasingly less dense, which is responsible for promoting a 5-time increase in CO_2 diffusivity relative to that in the neat acrylate cross-linked membrane and for following the same trend as membrane stiffness (according to the tensile modulus in Fig. 6). As mentioned earlier, Jeffamine possesses a longer chain than PEG3A, which extends the distance between cross-link sites and generates a more flexible network, resulting in a higher CO_2 diffusivity. On the other hand, CO_2

Table 1
The effect of different cross-linkers on gas-separation performance.

Membrane	P_{CO2} (Barrer)	CO_2 diffusivity (10^{-8} cm^2/s)	CO_2 solubility (10^{-8} cm^2/s)	P_{N2} (Barrer)	CO_2/N_2 ideal selectivity
PEG3A-J-4-1	3.73 ± 0.50	1.30 ± 0.30	2.96 ± 0.30	0.10 ± 0.03	36.5 ± 6.0
PEG4A -J-4-1	1.94 ± 0.31	0.58 ± 0.05	3.36 ± 0.23	0.05 ± 0.01	38.7 ± 9.2
PEG5A-J-4-1	2.68 ± 0.47	0.88 ± 0.15	3.05 ± 0.004	0.04 ± 0.02	46.7 ± 8.2

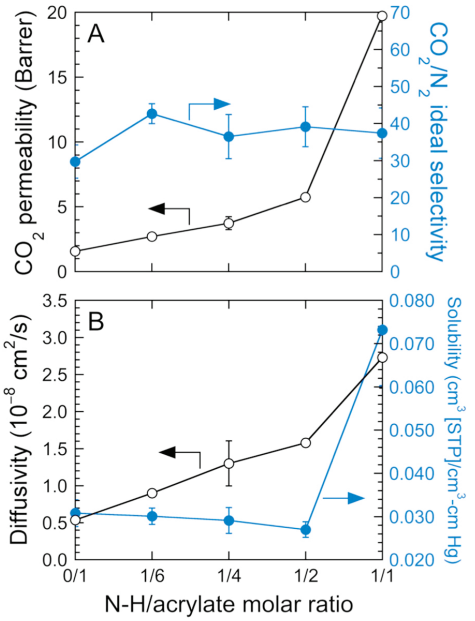

Fig. 8. (A) CO_2 permeability and CO_2/N_2 ideal selectivity as functions of the N-H/acrylate ratio (color-coded). (B) Corresponding CO_2 diffusivity and CO_2 solubility values of the PEG3A and PEG3A-J membranes (similarly color-coded). The solid lines serve to connect the data. (For interpretation of the references to color in this figure legend, the reader is referred to the web version of this article).

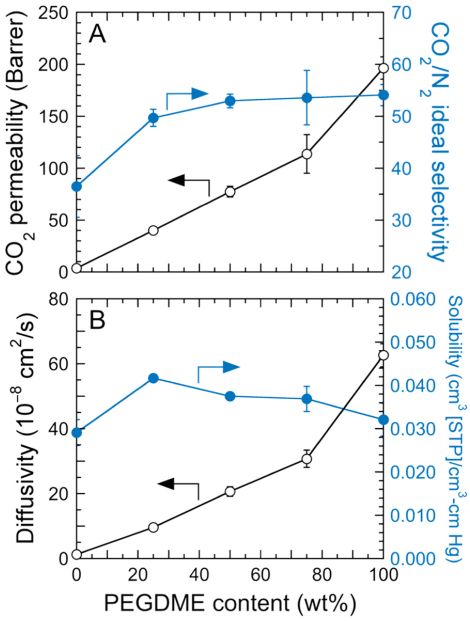

Fig. 9. (A) CO_2 permeability and CO_2/N_2 ideal selectivity as functions of PEGDME content in the PEG3A-J-4–1 membrane (color-coded). (B) Corresponding CO_2 diffusivity and CO_2 solubility values of the same PEGDME-containing membranes (similarly color-coded). The solid lines serve to connect the data. (For interpretation of the references to color in this figure legend, the reader is referred to the web version of this article).

solubility initially displays a slight reduction (very close to experimental uncertainty) from 0.031 to 0.027 cm^3(STP)/(cm^3-cm Hg) as the N-H/acrylate ratio is increased from 0:1 to 1:2. A decrease in CO_2 solubility over this range could be due to the lower CO_2 affinity for propylene oxide relative to ethylene oxide [60–62]. Further increasing the N-H/acrylate ratio to 1:1 promotes a considerably higher CO_2 solubility of 0.073 cm^3(STP)/(cm^3-cm Hg) in the PEG3A-J-1-1 membrane. This sudden increase is attributed to the positive effect of the presence of additional C-N bonds.

A low-molecular-weight PEG additive (PEGDME) has been incorporated into the PEG3A-J membranes to further improve gas-separation performance. The PEG3A-J-4-1 membrane is selected for this analysis due to its promising mechanical stability. Both CO_2 permeability and CO_2/N_2 ideal selectivity are shown as functions of PEGDME content in Fig. 9**a**. As expected, the CO_2 permeability systematically increases with increasing PEGDME loading level, from 3.7 Barrer in the PEGDME-free membrane to 196.4 Barrer in the membrane with 100% PEGDME incorporation. The CO_2/N_2 ideal selectivity increases with increasing PEGDME content up to ≈ 50 wt% PEGDME and then remains constant. Corresponding values of the CO_2 diffusivity and solubility in PEG3A-J-PEGDME membranes are also provided in Fig. 9**b**. By

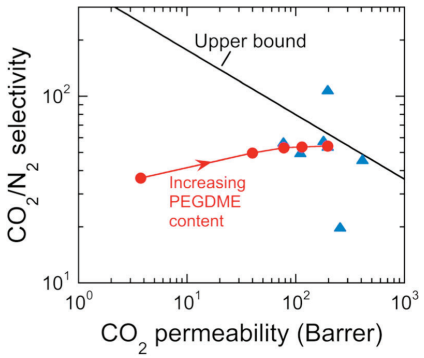

Fig. 10. Values of CO_2 permeability and CO_2/N_2 selectivity evaluated here from the PEG3A-J-4–1 membrane at several PEGDME loading levels (●). Comparable data gleaned from the literature and listed in Table 2 are included for comparison (▲). The solid line through the data serves as a guide for the eye, whereas the line identifying the Robeson upper bound is labeled.

Table 2
CO_2/N_2 separation performance of cross-linked PEG-based membranes measured in this work and reported elsewhere.

Membrane	P_{CO2} (Barrer)	CO_2/N_2 selectivity	Reference
XLPEGDA[a]	110	50	[19]
Poly(TEGMVE:VEEM)[b]	410	46	[61]
PEGDMA/SiGMA copolymers	255	20	[62]
Thiol-containing PEG	77	57	[37]
PEG cross-linked with A-amine (80% free PEGDME)	196	108	[41]
PEGDGE cross-linked with Jeffamine	180	58	[39]
PEG-Jeffamine (100% free PEGDME)	196	54	This work

[a] Cross-linked PEGDA (molecular weight: 743 g/mol).
[b] TEGMVE: [2-(2-(2-methoxyethoxy)ethoxy)ethyl vinyl ether), VEEM: 2-(2-vinyloxyethoxy)ethyl methacrylate.

increasing the PEGDME content, the CO_2 diffusivity increases monotonically, while the CO_2 solubility fluctuates most likely within the range of experimental uncertainty. The similarity of CO_2 solubilities measured for membranes with and without added PEGDME is explained by the comparable affinity of PEG-based material for CO_2. Therefore, the increase in CO_2 permeability due to the addition of PEGDME is mainly attributed to the increase in CO_2 diffusivity, whereas the CO_2/N_2 ideal selectivity relates to the CO_2 solubility. The increase in CO_2 diffusivity with PEGDME level could be explained by two effects. Addition of low-molecular-weight CO_2-philic species in the membrane is expected to form fast diffusion zones so that CO_2 molecules will migrate more readily through these regions [41,60]. Moreover, the presence of PEGDME during membrane formation can alternatively lead to larger distances between cross-link sites, resulting in larger unobstructed gas-transport pathways. The overall performance of the membranes prepared and examined in this study, as well as the state-of-the-art PEG-based membranes, are compared in the Robeson trade-off plot provided in Fig. 10. Detailed data from selected literature sources are likewise listed in Table 2. As is evident from these comparisons, the gas-separation performance of PEG3A-J-PEGDME membranes approaches the upper bound and becomes comparable to other recently reported PEG-based membranes prepared by common solvent evaporation methods.

4. Conclusions

In this work a series of PEG-based materials with interpenetrating polymeric networks has been synthesized and fabricated into membranes for CO_2 separation. The preparation procedure is based on a facile and solvent-free two-stage cross-linking process based on aza-Michael addition and acrylate photopolymerization. Results from FTIR spectroscopy confirm the cross-linking mechanisms and indicate the existence of dual cross-link networks. The thermal stability of all the membranes indicates that these membranes become less stable with increasing amine content but are nonetheless suitable for CO_2 separation processes. Addition of Jeffamine softens and toughens the membranes by introducing longer polymer chains and improving the flexibility of the cross-linked network. An amine-induced increase in water uptake confirms that the hydrophilic properties of the membranes are improved by incorporation of Jeffamine. Although not investigated here, this dependence might benefit CO_2 separation under humid conditions. Three multi-acrylate functionalized cross-linkers have been reacted with Jeffamine. Single-gas permeation results confirm that cross-linkers with fewer acrylate groups induce lower cross-link densities and better gas-transport properties. Cross-linked PEG membranes possessing a high N-H/acrylate ratio display a high CO_2 permeability. Incorporation of free PEGDME in the optimized membrane yields a significantly enhanced CO_2 permeability that is largely attributed to an increase in CO_2 diffusivity without sacrificing the CO_2/N_2 ideal selectivity. Overall, this two-stage cross-linking method constitutes a straightforward and effective solvent-free route to prepare self-standing cross-linked PEG-based membranes with excellent CO_2 separation performance. In addition, the results reported herein have established that the molecular, transport and bulk properties of these membranes are all highly tunable, which affords practical advantages for feasible membrane preparation under environmentally-benign conditions.

Acknowledgments

This work was supported at the Norwegian University of Science & Technology and SINTEF Industry by the Research Council of Norway, Norway through the CLIMIT program (POLYMEM project, No. 254791) and at North Carolina State University by the Nonwovens Institute, USA.

References

[1] H. Yang, Z. Xu, M. Fan, R. Gupta, R.B. Slimane, A.E. Bland, I. Wright, Progress in carbon dioxide separation and capture: a review, J. Environ. Sci. 20 (2008) 14–27.
[2] D.M. D'Alessandro, B. Smit, J.R. Long, Carbon dioxide capture: prospects for new materials, Angew. Chem. Int. Ed. 49 (2010) 6058–6082.
[3] S. Zeng, X. Zhang, L. Bai, X. Zhang, H. Wang, J. Wang, D. Bao, M. Li, X. Liu, S. Zhang, Ionic-liquid-based CO_2 capture systems: structure, interaction and process, Chem. Rev. 117 (2017) 9625–9673.
[4] C.E. Powell, G.G. Qiao, Polymeric CO_2/N_2 gas separation membranes for the capture of carbon dioxide from power plant flue gases, J. Membr. Sci. 279 (2006) 1–49.
[5] M. Galizia, W.S. Chi, Z.P. Smith, T.C. Merkel, R.W. Baker, B.D. Freeman, 50th anniversary perspective: polymers and mixed matrix membranes for gas and vapor separation: a review and prospective opportunities, Macromolecules 50 (2017) 7809–7843.
[6] S. Kim, Y.M. Lee, High performance polymer membranes for CO_2 separation, Curr. Opin. Chem. Eng. 2 (2013) 238–244.
[7] X. Zhang, B. Singh, X. He, T. Gundersen, L. Deng, S. Zhang, Post-combustion carbon capture technologies: energetic analysis and life cycle assessment, Int. J. Greenh. Gas. Control 27 (2014) 289–298.
[8] M.-.B Hägg, L. Deng, Membranes in gas separation, Handbook of Membrane Separations: Chemical, Pharmaceutical, Food, and Biotechnological Applications, CRC Press, Boca Raton, FL, 2015, pp. 143–180.
[9] Z. Dai, R.D. Noble, D.L. Gin, X. Zhang, L. Deng, Combination of ionic liquids with membrane technology: a new approach for CO_2 separation, J. Membr. Sci. 497 (2016) 1–20.
[10] S. Wang, X. Li, H. Wu, Z. Tian, Q. Xin, G. He, D. Peng, S. Chen, Y. Yin, Z. Jiang, Advances in high permeability polymer-based membrane materials for CO_2 separations, Energy Environ. Sci. 9 (2016) 1863–1890.
[11] Z. Dai, L. Ansaloni, L. Deng, Recent advances in multi-layer composite polymeric membranes for CO_2 separation: a review, Green. Energy Environ. 1 (2016) 102–128.
[12] L.M. Robeson, The upper bound revisited, J. Membr. Sci. 320 (2008) 390–400.
[13] M. Carta, R. Malpass-Evans, M. Croad, Y. Rogan, J.C. Jansen, P. Bernardo, F. Bazzarelli, N.B. McKeown, An efficient polymer molecular sieve for membrane gas separations, Science 339 (2013) 303–307.
[14] N.B. McKeown, P.M. Budd, K.J. Msayib, B.S. Ghanem, H.J. Kingston, C.E. Tattershall, S. Makhseed, K.J. Reynolds, D. Fritsch, Polymers of intrinsic microporosity (PIMs): bridging the void between microporous and polymeric materials, Chem.- Eur. J. 11 (2005) 2610–2620.
[15] P.M. Budd, N.B. McKeown, B.S. Ghanem, K.J. Msayib, D. Fritsch, L. Starannikova, N. Belov, O. Sanfirova, Y. Yampolskii, V. Shantarovich, Gas permeation parameters and other physicochemical properties of a polymer of intrinsic microporosity: polybenzodioxane PIM-1, J. Membr. Sci. 325 (2008) 851–860.
[16] H.B. Park, C.H. Jung, Y.M. Lee, A.J. Hill, S.J. Pas, S.T. Mudie, E. Van Wagner, B.D. Freeman, D.J. Cookson, Polymers with cavities tuned for fast selective transport of small molecules and ions, Science 318 (2007) 254–258.
[17] H.B. Park, S.H. Han, C.H. Jung, Y.M. Lee, A.J. Hill, Thermally rearranged (TR) polymer membranes for CO_2 separation, J. Membr. Sci. 359 (2010) 11–24.
[18] S.H. Han, N. Misdan, S. Kim, C.M. Doherty, A.J. Hill, Y.M. Lee, Thermally rearranged (TR) polybenzoxazole: effects of diverse Imidization routes on physical properties and gas transport behaviors, Macromolecules 43 (2010) 7657–7667.
[19] H. Lin, T. Kai, B.D. Freeman, S. Kalakkunnath, D.S. Kalika, The effect of cross-linking on gas permeability in cross-linked poly(ethylene glycol diacrylate), Macromolecules 38 (2005) 8381–8393.
[20] X. Jiang, S. Li, L. Shao, Pushing CO_2-philic membrane performance to the limit by designing semi-interpenetrating networks (SIPN) for sustainable CO_2 separations, Energy Environ. Sci. 10 (2017) 1339–1344.
[21] N.P. Patel, A.C. Miller, R.J. Spontak, Highly CO_2-permeable and selective polymer nanocomposite membranes, Adv. Mater. 15 (2003) 729–733.
[22] L. Deng, T.-J. Kim, M.-B. Hägg, Facilitated transport of CO_2 in novel PVAm/PVA blend membrane, J. Membr. Sci. 340 (2009) 154–163.
[23] J. Liao, Z. Wang, C. Gao, S. Li, Z. Qiao, M. Wang, S. Zhao, X. Xie, J. Wang, S. Wang, Fabrication of high-performance facilitated transport membranes for CO_2

separation, Chem. Sci. 5 (2014) 2843–2849.
[24] J. Zou, W.S.W. Ho, CO_2-selective polymeric membranes containing amines in crosslinked poly(vinyl alcohol), J. Membr. Sci. 286 (2006) 310–321.
[25] S.L. Liu, L. Shao, M.L. Chua, C.H. Lau, H. Wang, S. Quan, Recent progress in the design of advanced PEO-containing membranes for CO_2 removal, Prog. Polym. Sci. 38 (2013) 1089–1120.
[26] H. Lin, B.D. Freeman, Gas solubility, diffusivity and permeability in poly (ethylene oxide), J. Membr. Sci. 239 (2004) 105–117.
[27] S. Wang, X. Li, H. Wu, Z. Tian, Q. Xin, G. He, D. Peng, S. Chen, Y. Yin, Z. Jiang, Advances in high permeability polymer-based membrane materials for CO_2 separations, Energy Environ. Sci. 9 (2016) 1863–1890.
[28] G. Szekely, M.F. Jimenez-Solomon, P. Marchetti, J.F. Kim, A.G. Livingston, Sustainability assessment of organic solvent nanofiltration: from fabrication to application, Green Chem. 16 (2014) 4440–4473.
[29] A. Figoli, T. Marino, S. Simone, E. Di Nicolò, X.M. Li, T. He, S. Tornaghi, E. Drioli, Towards non-toxic solvents for membrane preparation: a review, Green. Chem. 16 (2014) 4034–4059.
[30] N.P. Patel, A.C. Miller, R.J. Spontak, Highly CO_2-permeable and-selective membranes derived from crosslinked poly (ethylene glycol) and its nanocomposites, Adv. Funct. Mater. 14 (2004) 699–707.
[31] H. Lin, B.D. Freeman, Gas and vapor solubility in cross-linked poly(ethylene glycol diacrylate), Macromolecules 38 (2005) 8394–8407.
[32] H. Lin, E.V. Wagner, J.S. Swinnea, B.D. Freeman, S.J. Pas, A.J. Hill, S. Kalakkunnath, D.S. Kalika, Transport and structural characteristics of crosslinked poly(ethylene oxide) rubbers, J. Membr. Sci. 276 (2006) 145–161.
[33] X. Jiang, S. Li, S. He, Y. Bai, L. Shao, Interface manipulation of CO_2-philic composite membranes containing designed UiO-66 derivatives towards highly efficient CO_2 capture, J. Mater. Chem. A 6 (2018) 15064–15073.
[34] N.C. Su, Z.P. Smith, B.D. Freeman, J.J. Urban, Size-dependent permeability deviations from Maxwell's model in hybrid cross-linked poly(ethylene glycol)/silica nanoparticle membranes, Chem. Mater. 27 (2015) 2421–2429.
[35] J. Kim, Q. Fu, K. Xie, J.M. Scofield, S.E. Kentish, G.G. Qiao, CO_2 separation using surface-functionalized SiO_2 nanoparticles incorporated ultra-thin film composite mixed matrix membranes for post-combustion carbon capture, J. Membr. Sci. 515 (2016) 54–62.
[36] S.C. Ligon, B. Husár, H. Wutzel, R. Holman, R. Liska, Strategies to reduce oxygen inhibition in photoinduced polymerization, Chem. Rev. 114 (2013) 557–589.
[37] L. Kwisnek, S. Heinz, J.S. Wiggins, S. Nazarenko, Multifunctional thiols as additives in UV-cured PEG-diacrylate membranes for CO_2 separation, J. Membr. Sci. 369 (2011) 429–436.
[38] L. Kwisnek, J. Goetz, K.P. Meyers, S.R. Heinz, J.S. Wiggins, S. Nazarenko, PEG containing thiol–ene network membranes for CO_2 separation: effect of cross-linking on thermal, mechanical, and gas transport properties, Macromolecules 47 (2014) 3243–3253.
[39] L. Shao, S. Quan, X.-Q. Cheng, X.-J. Chang, H.-G. Sun, R.-G. Wang, Developing cross-linked poly(ethylene oxide) membrane by the novel reaction system for H_2 purification, Int. J. Hydrog. Energy 38 (2013) 5122–5132.
[40] S. Quan, S. Li, Z. Wang, X. Yan, Z. Guo, L. Shao, A bio-inspired CO_2-philic network membrane for enhanced sustainable gas separation, J. Mater. Chem. A 3 (2015) 13758–13766.
[41] Z. Dai, L. Ansaloni, D.L. Gin, R.D. Noble, L. Deng, Facile fabrication of CO_2 separation membranes by cross-linking of poly (ethylene glycol) diglycidyl ether with a diamine and a polyamine-based ionic liquid, J. Membr. Sci. 523 (2017) 551–560.
[42] A. Genest, D. Portinha, E. Fleury, F. Ganachaud, The aza-Michael reaction as an alternative strategy to generate advanced silicon-based (macro) molecules and materials, Prog. Polym. Sci. 72 (2017) 61–110.
[43] W. Cheng, D. Wu, Y. Liu, Michael addition polymerization of trifunctional amine and acrylic monomer: a versatile platform for development of biomaterials, Biomacromolecules 17 (2016) 3115–3126.
[44] C.-Y. Liu, C.-J. Huang, Functionalization of polydopamine via the aza-Michael reaction for antimicrobial interfaces, Langmuir 32 (2016) 5019–5028.
[45] G. González, X. Fernández-Francos, À. Serra, M. Sangermano, X. Ramis, Environmentally-friendly processing of thermosets by two-stage sequential aza-Michael addition and free-radical polymerization of amine–acrylate mixtures, Polym. Chem. 6 (2015) 6987–6997.
[46] J. Wang, H. He, R.C. Cooper, H. Yang, In situ-forming polyamidoamine dendrimer hydrogels with tunable properties prepared via aza-Michael addition reaction, ACS Appl. Mater. Interfaces 9 (2017) 10494–10503.
[47] O. Konuray, X. Fernández-Francos, X. Ramis, À. Serra, State of the art in dual-curing acrylate systems, Polymers 10 (2018) 178.
[48] A.O. Konuray, X. Fernández-Francos, À. Serra, X. Ramis, Sequential curing of amine-acrylate-methacrylate mixtures based on selective aza-Michael addition followed by radical photopolymerization, Eur. Polym. J. 84 (2016) 256–267.
[49] J. Wang, G.S. Williamson, I. Lancina, G. Michael, H. Yang, Mildly cross-linked dendrimer hdrogel prepared via aza-Michael adition reaction for tpical bimonidine dlivery, J. Biomed. Nanotechnol. 13 (2017) 1089–1096.
[50] D. Fournier, R. Hoogenboom, U.S. Schubert, Clicking polymers: a straightforward approach to novel macromolecular architectures, Chem. Soc. Rev. 36 (2007) 1369–1380.
[51] S. Luo, Q. Zhang, T.K. Bear, T.E. Curtis, R.K. Roeder, C.M. Doherty, A.J. Hill, R. Guo, Triptycene-containing poly(benzoxazole-co-imide) membranes with enhanced mechanical strength for high-performance gas separation, J. Membr. Sci. 551 (2018) 305–314.
[52] L. Deng, M.-B. Hägg, Swelling behavior and gas permeation performance of PVAm/PVA blend FSC membrane, J. Membr. Sci. 363 (2010) 295–301.
[53] S. Zhao, Z. Wang, Z. Qiao, X. Wei, C. Zhang, J. Wang, S. Wang, Gas separation membrane with CO_2-facilitated transport highway constructed from amino carrier containing nanorods and macromolecules, J. Mater. Chem. A 1 (2013) 246–249.
[54] Y. Zhao, W.W. Ho, Steric hindrance effect on amine demonstrated in solid polymer membranes for CO_2 transport, J. Membr. Sci. 415 (2012) 132–138.
[55] M. Saeed, S. Rafiq, L.H. Bergersen, L. Deng, Tailoring of water swollen PVA membrane for hosting carriers in CO_2 facilitated transport membranes, Sep. Purif. Technol. 179 (2017) 550–560.
[56] L. Deng, M.-B. Hägg, Fabrication and evaluation of a blend facilitated transport membrane for CO_2/CH_4 separation, Ind. Eng. Chem. Res. 54 (2015) 11139–11150.
[57] S. Kasahara, E. Kamio, T. Ishigami, H. Matsuyama, Effect of water in ionic liquids on CO_2 permeability in amino acid ionic liquid-based facilitated transport membranes, J. Membr. Sci. 415 (2012) 168–175.
[58] Z. Dai, L. Ansaloni, J.J. Ryan, R.J. Spontak, L. Deng, Nafion/IL hybrid membranes with tuned nanostructure for enhanced CO_2 separation: effects of ionic liquid and water vapor, Green. Chem. 20 (2018) 1391–1404.
[59] Z. Dai, L. Bai, K.N. Hval, X. Zhang, S. Zhang, L. Deng, Pebax®/TSIL blend thin film composite membranes for CO_2 separation, Sci. China Chem. 59 (2016) 538–546.
[60] N.P. Patel, C.M. Aberg, A.M. Sanchez, M.D. Capracotta, J.D. Martin, R.J. Spontak, Morphological, mechanical and gas-transport characteristics of crosslinked poly (propylene glycol): homopolymers, nanocomposites and blends, Polymer 45 (2004) 5941–5950.
[61] T. Sakaguchi, F. Katsura, A. Iwase, T. Hashimoto, CO_2-permselective membranes of crosslinked poly(vinyl ether)s bearing oxyethylene chains, Polymer 55 (2014) 1459–1466.
[62] V.A. Kusuma, G. Gunawan, Z.P. Smith, B.D. Freeman, Gas permeability of cross-linked poly(ethylene-oxide) based on poly(ethylene glycol) dimethacrylate and a miscible siloxane co-monomer, Polymer 51 (2010) 5734–5743.

Paper II

Cross-Linked PEG Membranes of Interpenetrating Networks with Ionic Liquids as Additives for Enhanced CO_2 Separation

This paper is published in
Industrial & Engineering Chemistry Research
2019, 58, 5261−5268

I&EC research
Industrial & Engineering Chemistry Research

Article

Cite This: Ind. Eng. Chem. Res. 2019, 58, 5261−5268

pubs.acs.org/IECR

Cross-Linked PEG Membranes of Interpenetrating Networks with Ionic Liquids as Additives for Enhanced CO_2 Separation

Jing Deng, Junbo Yu, Zhongde Dai, and Liyuan Deng*

Department of Chemical Engineering, Norwegian University of Science & Technology, 7491 Trondheim, Norway

Supporting Information

ABSTRACT: Polyethylene glycol (PEG)-based membranes have recently been reported with excellent CO_2 separation performances. However, the commonly exhibited high crystallinity may deteriorate the gas permeation properties in this type of membrane. In this work, a two-stage cross-linking method was employed to fabricate PEG membranes with interpenetrating networks to reduce the crystallinity. Ionic liquids (ILs) were incorporated into the resultant membranes to further increase CO_2 diffusivity and the CO_2 affinity of the membranes. By increasing the length of the PEG-based acrylate monomers and optimizing the ratio of the amine-functionalized cross-linker to the acrylate monomers, we significantly enhanced the CO_2 permeability of the resultant membranes (from 0.6 to 85.0 Barrer) with slightly increased CO_2/N_2 selectivity. Four conventional ILs (i.e., [Bmim][BF_4], [Bmim][PF_6], [Bmim][NTf_2] and [Bmim][TCM]) with different anions were added into the optimized cross-linked PEG membranes. The addition of ILs endows superior gas transport properties at high loadings, and the [Bmim][TCM] gives the best CO_2 separation performance of the membranes; CO_2 permeability of up to 134.2 Barrer with the CO_2/N_2 selectivity of 49.5 was documented. The anions in ILs were found contributing the most in promoting the CO_2 permeation, and the higher CO_2 affinity endows the better CO_2 separation performance in the resultant membranes.

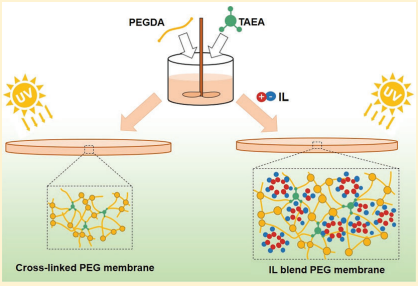

1. INTRODUCTION

The membrane-based CO_2 capture technology, especially the use of polymeric membranes, has attracted widespread interest for its remarkable advantages, including low operation cost, high energy efficiency, easy scale-up or scale-down, and small footprint.[1] However, the CO_2 separation properties of current polymeric membrane materials are still not sufficient to make membrane technology competitive to the mature amine-absorption processes. According to the solution-diffusion mechanism involved in most polymeric membranes, two approaches could be taken to improve the separation performance of a polymeric membrane: to increase the CO_2 solubility (such as by introducing CO_2-philic moieties) or/and CO_2 diffusivity (e.g., through enlarging the free volume of the membrane matrices).[2,3] For the first approach, the ether group (−C−O−) is a well-known functional group with high CO_2-philicity; hence, polymers containing plenty of ether groups, such as polyethylene glycol (PEG, or also called polyethylene oxide (PEO) at a high molecular weight), are expected to possess excellent CO_2 separation performance.[2,4−6]

However, the pristine PEO membranes were reported exhibiting very low CO_2 permeability (∼10 Barrer),[7] most probably due to its high crystallinity resulting from its abundant ethylene oxide (EO) groups and the strong hydrogen bonding, which impedes gas transport through the membranes. It is reported that the formation of crystalline zones in PEO polymers requires 4 chains containing 7 EO units,[3] and therefore the crystallinity could be suppressed via cross-linking PEG monomers with short chains by disrupting the repetition of EO units. Following this idea, Lin et al. reported that by simply cross-linking PEG diacrylate (PEGDA), the CO_2 permeability of the membrane increases by ∼10-fold without sacrificing the CO_2 selectivity.[8] The significantly reduced crystallinity and thus increased amorphous PEG phase release the restricted crystalline zone for gas diffusion, resulting in greatly improved CO_2 transport properties.

In addition, the length of the EO units or PEG monomers, which can be simply presented by their molecular weight (MW), is critical in determining the crystallinity and thus the final gas transport properties of the PEG-based membranes, as long polymer chains may result in increased crystalline zones. However, after cross-linking, the membranes prepared by monomers of long chains are more flexible and have more free volume for gas diffusion. Patel et al. cross-linked PEGDA membranes and reported that the CO_2 permeability increases significantly with the number of EO units in PEGDA.[9] The longer PEG monomers would result in much higher CO_2 diffusivity after cross-linking compared with those made by shorter chains.[10] In addition to the enhancement in gas

Received: January 14, 2019
Revised: March 8, 2019
Accepted: March 14, 2019
Published: March 14, 2019

DOI: 10.1021/acs.iecr.9b00241
Ind. Eng. Chem. Res. 2019, 58, 5261−5268

diffusivity, the EO density in membranes also slightly increases, leading to a simultaneous increment in CO_2 solubility. Hence, by simply employing longer PEG monomers, the consequent increase in both diffusivity and solubility generates a great increment (~10-fold) in CO_2 permeability. However, crystalline phases may form by monomers with the chain length of >1500 g/mol;[3] hence, cross-linking with monomers of too long PEG chains may not be able to suppress efficiently the high crystallinity of the PEG polymers. On the other hand, cross-linking with monomers of short chains results in high cross-linking density, leading to a low free volume of the polymer and low gas permeation. It is thus important to investigate the effects of the chain length in cross-linked PEG-based membranes to optimize the gas separation performance of the membranes.

The incorporation of low-molecular-weight "free" PEG into the PEG-based membranes has also been widely reported as an effective approach to reduce the crystallinity and increase the chain flexibility (and thus the free volume) of the polymers, which enhances the gas transport properties in membranes without sacrificing their CO_2 selectivity.[11,12] Similarly, the addition of ionic liquids (ILs) has been reported in improving the CO_2 permeability of membranes made by crystalline polymers.[13−18] ILs have been widely reported as CO_2-philic additives to improve the CO_2 separation performance of membranes in recent years,[13,19] especially for membranes of highly crystalline[15,16,20] or highly cross-linked polymers.[21,22] The addition of ILs may reduce the crystallinity and increase the CO_2 diffusivity, therefore increasing the CO_2 permeation properties greatly. Moreover, the high CO_2 affinity and the extremely low vapor pressure of ILs are the additional advantages as additives. Bara et al.[23] added only 20 mol % [Bmim][NTf_2] into the poly(RTIL) membrane, and the CO_2 permeability obtained remarkable enhancement (~4-fold) with a slight improvement in CO_2/N_2 selectivity (33%) compared with that of the pristine poly(RTIL) membrane. The addition of low-viscosity [Emim][$B(CN)_4$] endows an excellent CO_2 permeability of 1778 Barrer (0.74 Barrer in its analogue), and this great increment is mainly contributed by the increase in CO_2 diffusivity.[15] In addition, the tunable chemical structures of ILs bring in more possibilities to improve the membrane properties for diverse requirements.[24] However, some research works reported that the addition of ILs into polymeric materials did not result in the expected gain in gas permeability.[25,26] It is believed that the compatibility between ILs and the polymeric matrices have a decisive influence on the final performance.

Despite the similar role between ILs and PEG materials, the combination of these two approaches has rarely been reported in CO_2 separation membranes. In this work, the incorporation of ILs into the cross-linked PEG-based membranes has been systemically investigated. First, a series of cross-linked PEG-based membranes with interpenetrating polymeric networks were fabricated through a facile, two-stage cross-linking method based on aza-Michael addition and acrylate homopolymerization.[27,28] The cross-linking density of the resultant PEG membranes was optimized by controlling the molecular weight of the acrylate-functionalized PEG-based monomer and the ratio of amine cross-linkers to acrylate monomers. The influences on the chemical structure, thermal properties, phase transition behavior, crystalline trend and gas permeation properties were studied by various characterization techniques. Moreover, four conventional ILs with the same cation $[Bmim]^+$ but different anions were incorporated into the optimized cross-linked PEG membranes, and their influences on the material properties and the gas separation performance were systemically investigated.

2. EXPERIMENT

2.1. Materials. PEGDA with different molecular weights (250, 575 and 700 g/mol), tris(2-aminoethyl)amine (TAEA), 1-hydroxycyclohexyl phenyl ketone (HCPK) and three ionic liquids 1-butyl-3-methylimidazolium bis(trifluoromethylsulfonyl)imide ([Bmim][NTf_2], 98%), 1-butyl-3-methylimidazolium tetrafluoroborate ([Bmim][BF_4], 98%), and 1-butyl-3-methylimidazolium hexafluorophosphate ([Bmim][PF_6], 98%) were purchased from Sigma-Aldrich, Germany. 1-Butyl-3-methylimidazolium tricyanomethanide ([Bmim][TCM], 98%) was ordered from Iolitec, Germany. The N_2 and CO_2 (99.999%) used in the single gas permeation test were provided by AGA, Norway. The chemical structures of the above-mentioned chemicals are depicted in Figure 1.

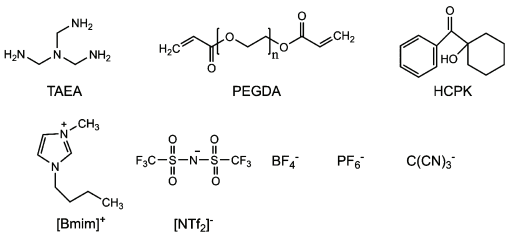

Figure 1. Chemical structures of all chemicals used in the current work.

2.2. Membrane Preparation. The cross-linked PEG membranes were prepared through a two-stage method similar to that reported in the literature.[11,27,28] For the readers' convenience, a brief description is presented below. First, monomer PEGDA, the desired amount of ionic liquids, and photoinitiator HCPK (0.01−0.1 wt % of PEGDA) were magnetically mixed inside a glass vial for 30 min at room temperature (RT). Then a proper amount of the cross-linker TAEA was added into the resultant homogeneous mixture and magnetically stirred (~30 min, RT) to ensure a complete reaction (aza-Michael addition) between amine and acrylate. Afterward, the mixtures were degassed in a vacuum oven for a few minutes at RT to remove the possible bubbles. The mixture was then poured onto a clean quartz plate and sandwiched by using a second quartz plate on the top. The plates were separated by spacers to control the membrane thickness (200−250 μm). The liquid mixture was exposed under UV light with a wavelength of 365 nm for 2 h (UVLS-28, Ultra-Violet Products Ltd., UK) for the homopolymerization of excess acrylate. After irradiation, the cross-linked membranes were transferred to a vacuum oven overnight at 60 °C before further characterization. These membranes were evaluated by various characterization methods and permeation tests. The mass ratio of ILs is defined as the mass of ionic liquid over PEGDA, as shown in eq 1:

$$W_{IL} = \frac{m_{IL}}{m_{PEGDA}} \times 100\% \quad (1)$$

DOI: 10.1021/acs.iecr.9b00241
Ind. Eng. Chem. Res. 2019, 58, 5261−5268

Scheme 1. Schematic Representation of the Two-Stage Procedure for Preparing the Cross-Linked TAEA-PEGDA Membrane

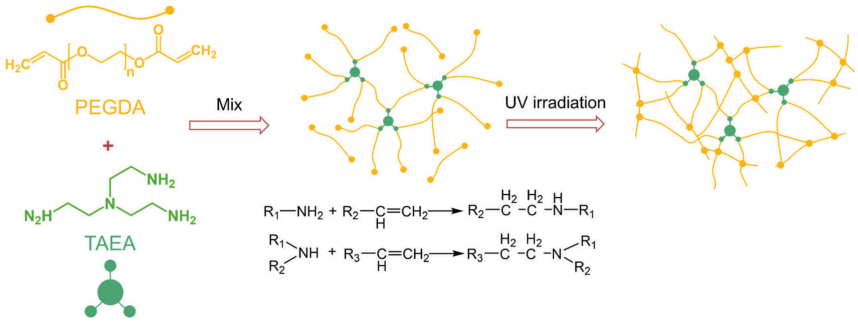

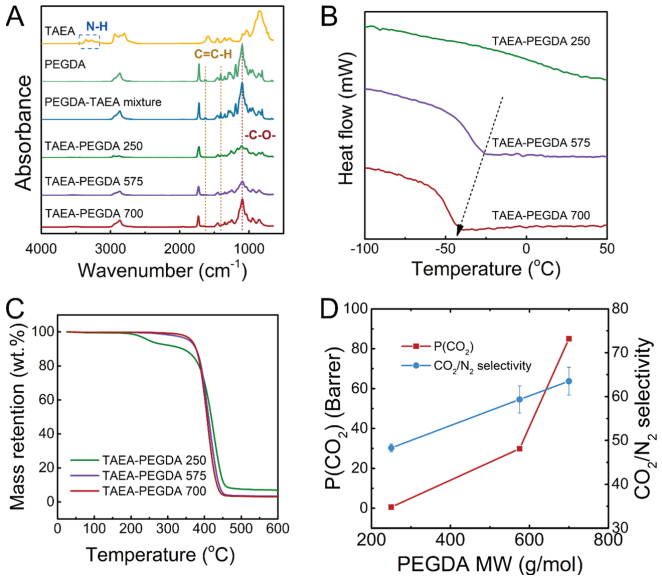

Figure 2. (A) FT-IR spectra, (B) DSC curves, (C) TGA results of PEGDA, TAEA and TAEA-PEGDA membranes, and (D) gas permeation results of TAEA-PEGDA membranes prepared by PEGDA of different MWs (250, 575, and 700 g/mol) with the same N−H/acrylate ratio of 1:6.

In this work, the cross-linked PEG membranes are systematically designated as "TAEA-PEGDA *XX-X-X*" according to the ratio of amine-containing cross-linker (TAEA) to acrylate-terminated monomer (PEGDA with a molecular weight of *XX* g/mol). For example, the TAEA-PEGDA 700-1-6 membrane consists of TAEA and PEGDA (MW 700 g/mol) with one N−H bond from TAEA and six acrylate groups from PEGDA 700.

2.3. Characterization. A Thermo Nicolet Nexus Fourier-transform infrared spectrometer (FT-IR, Oslo, Norway) with an attenuated total reflectance (ATR) cell equipped with a diamond crystal was used to collect the FT-IR spectra for all the membranes. Spectra were averaged over 16 scans at a wavenumber resolution of 4 cm^{-1} in the range 650−4000 cm^{-1}. Small membrane samples were employed for FTIR tests, and at least two spectra were collected for each membrane for the reproducibility and the uniformity of the membranes.

The thermal stability of the membranes was interrogated by thermogravimetric analysis (TGA) performed on a Thermal Scientific Q500 instrument. Approximately 10−20 mg samples were heated in a ceramic crucible from 25 to 700 °C at a constant heating rate of 10 °C/min under N_2 to prevent thermo-oxidative degradation of the samples.

A differential scanning calorimeter (DSC, DSC 214 Polyma, NETZSCH-Gerätebau GmbH, Germany) was used to investigate the phase transition behavior of all membranes. Samples with around 10 mg were collected in a standard aluminum pan covered by a fitting lid and heated at the rate of 10 °C/min under a N_2 atmosphere. Two cycles have been applied for the DSC tests, and the curves from the second cooling run are used for further analysis.

The crystallinity of all membrane samples was examined by X-ray diffraction analysis (XRD) using a Bruker D8 A25 DaVinci X-ray diffractometer (Cambridge, UK). The XRD patterns were recorded from 5° to 70°.

2.4. Gas Permeation Test. The gas permeability (P) of both CO_2 and N_2 through the membranes was measured by

DOI: 10.1021/acs.iecr.9b00241
Ind. Eng. Chem. Res. 2019, 58, 5261−5268

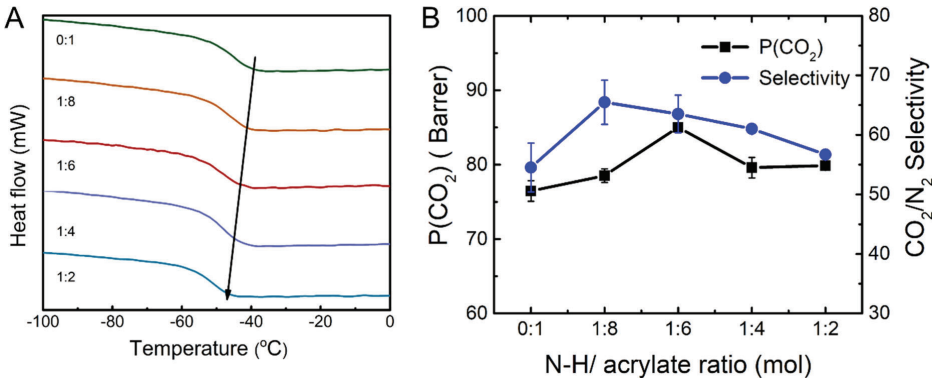

Figure 3. (A) DSC results and (B) gas permeation results of TAEA-PEGDA 700 membranes of different N−H/acrylate ratios.

the constant-volume variable-pressure method, which can be calculated based on eq 2:

$$P = \left[\left(\frac{\mathrm{d}p_\mathrm{d}}{\mathrm{d}t}\right)_{t\to\infty} - \left(\frac{\mathrm{d}p_\mathrm{d}}{\mathrm{d}t}\right)_{t\to\mathrm{leak}}\right]\frac{V_\mathrm{d}}{ART}\frac{l}{p_\mathrm{u} - p_\mathrm{d}} \tag{2}$$

where p_d and p_u identify the downstream and upstream gas pressures, respectively, and t is time. Here, V_d is the downstream volume, A corresponds to the effective permeation area of the membrane, R is the universal gas constant, T denotes absolute temperature, and l is the membrane thickness. The leakage rate of the gas permeation setup $(\mathrm{d}p_\mathrm{d}/\mathrm{d}t)_{t\to\mathrm{leak}}$ was measured from the increase in pressure relative to a vacuum over time. Membrane thicknesses were measured by an ABS Digimatic Indicator (Mitutoyo, Japan). The thicknesses were averaged from more than 10 measurements for each membrane after permeation tests. All gas permeation experiments were performed using an upstream pressure of 2 bar (absolute) at room temperature. For each membrane, the reported permeabilities were the average of measurements acquired from at least two specimens. The ideal CO_2/N_2 selectivity was calculated from the ratio of gas permeabilities in accord with

$$\alpha_{ij} = \frac{P_i}{P_j} \tag{3}$$

3. RESULTS AND DISCUSSION

3.1. Effect of PEGDA Molecular Weight. In this work, the effect of the length, or more precisely, MW, of the monomer PEGDA was systematically investigated. PEGDA of three different MWs (250, 575 and 700 g/mol) has been employed to fabricate the membranes with dual cross-linking networks based on the aza-Michael reaction and the homopolymerization of excess acrylate, as shown in Scheme 1. It is worth mentioning that the MW of PEGDA is limited to <1000 g/mol to reduce the formation of the crystalline phases. FI-TR analysis was employed to examine the monomers (PEGDA and TAEA), the product of the aza-Michael reaction (the mixture of PEGDA and TAEA with excess PEGDA), and the formed membranes (the ratio of N−H/acrylate is 1:6) to confirm the two above-mentioned reactions. As can be seen in Figure 2A, the peaks related to amine groups (~3366 and 3265 cm^{-1}) disappear after mixing, and the peaks corresponding to acrylate (1635 and 1407 cm^{-1}) clearly show a reduced trend. These results imply that the amine and part of the acrylate react (aza-Michael addition) and form an N−H/acrylate cross-linking network because of the multifunctionalized TAEA. After UV irradiation, however, the remaining acrylate is hardly observed in all spectra of the formed membranes, regardless of the MW of the used PEGDA, due to the homopolymerization of acrylate, which is known for the ability to build cross-linking networks. Therefore, the network built by acrylate homopolymerization as well as the interpenetrating structures inside the resultant membranes can be confirmed.

According to the characterization results, it is clear that the PEGDA MW affects the properties of the resultant polymers. From the FT-IR spectra, the peak intensity of ether groups (around 1100 cm^{-1}) increases significantly with the increasing MW of PEGDA, which is reasonable since longer PEGDA contains more EO units. Figure 2B shows that the glass transition temperature (T_g) of the resultant membranes decreases largely with the increasing PEGDA MW due to the longer and more flexible polymer chains in the cross-linked membranes. The T_g of the membranes with PEGDA 250 is not observed in this work, which may be because of the highly restricted polymer chains caused by the high cross-linking density. Moreover, as shown in Figure 2C, membranes containing long PEGDA chains (PEGDA 575 and 700) possess good thermal stability with one-step decomposition starting at ~360 °C, while the membrane with PEGDA 250 has the two-stage decomposition behavior, and the first decomposition begins at ~200 °C due to the unreacted monomers. The reactions involving the short PEGDA chains (PEGDA 250) are incredibly rapid, forming a highly cross-linked polymer network that may block the further diffusion of the monomer PEGDA 250, and thus some PEGDA 250 may stay as free monomer or form oligomers inside the polymer matrix.

The CO_2 and N_2 permeabilities of the resultant membranes were measured by single gas permeation tests, and the CO_2/N_2 ideal selectivity was calculated, as presented in Figure 2D. It is worth mentioning that the errors of the CO_2 permeability are very low (in most cases <5% of the average value); hence, the error bars are almost invisible in Figure 2C. Detailed permeation data can be found in Table S1. As expected, the CO_2 permeability increases significantly (from 0.6 to 85.0

DOI: 10.1021/acs.iecr.9b00241
Ind. Eng. Chem. Res. 2019, 58, 5261−5268

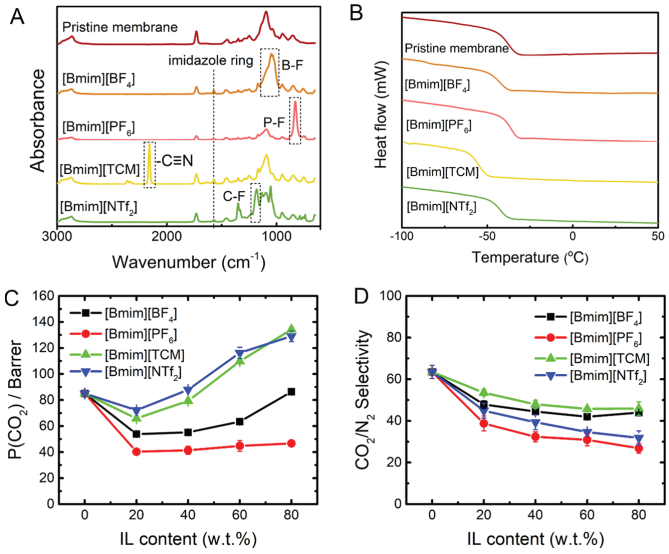

Figure 4. (A) FT-IR spectra, (B) DSC curves of blend membranes with 80% IL loading, (C) CO_2 permeability, and (D) CO_2/N_2 selectivity of four IL blend membranes as a function of ionic liquid content.

Barrer) with the increasing MW of PEGDA, consistent with the characterization analysis regarding the increasing free volume and CO_2 affinity of the membrane materials with the increment in PEGDA MW. In addition, the increasing distance between the two cross-linking sites, because of the longer PEGDA monomer, results in looser cross-linking networks (lower cross-linking density), leading to a more permeable membrane. Furthermore, the increasing ether content in the membrane from longer PEGDA monomers provides enhanced CO_2 affinity of the membrane and thus the improved CO_2 transport properties. These CO_2 permeation results are in agreement with Patel's work.[9] The CO_2/N_2 ideal selectivity also obtains a notable increment (from 48.3 to 63.5), which is similar to the reported value of PEG-based material in the literature.[2−4] The increase in the CO_2/N_2 selectivity is believed contributed by the more ethylene units in the membrane matrix, as shown in the FT-IR results. Therefore, PEGDA 700 is chosen as the reactant monomer for further investigation.

3.2. Effect of N−H/Acrylate Ratio. The chemistry nature and the cross-linking density of the resultant membranes are tunable through changing the composition of the dual cross-linking networks (presented by the N−H bond/acrylate group ratio).[27,28] A higher N−H/acrylate ratio (N−H bond in TAEA to the acrylate in PEGDA) in the reactants implies that more TAEA will react with PEGDA, and then less PEGDA will be left for the homopolymerization step. Therefore, the effects of the N−H/acrylate ratio are investigated with regard to the network structure and thus membrane properties.

DSC, TGA, XRD, FI-IR, and gas permeation tests were performed to investigate the effects of the N−H/acrylate ratio on various properties of the resultant PEG-based polymers of interpenetrating networks from PEGDA700. Figure 3A presents the DSC curves of different N−H/acrylate ratios. As it can be seen, the T_g decreases with the increasing N−H/acrylate ratio, indicating enhanced chain mobility of the cross-linked polymers with increasing N−H/acrylate ratio. In addition, the TGA analysis (Figure S1) shows that all TAEA-PEGDA700 membranes display sufficient thermal stability (T_{onset} > 200 °C) for most of the CO_2 separation applications. Most importantly, the XRD results (Figure S2) suggest that the interpenetrating networks are amorphous according to the broad XRD peaks (around 21°) at all studied N−H/acrylate ratios, confirming that the tendency to become highly crystalline in PEG polymer has been suppressed. The FT-IR spectra of the membranes of different N−H/acrylate ratios are given in Figure S3. A higher N−H/acrylate ratio means more C−N and fewer C−C bonds, which should be able to examine by FT-IR. However, the C−N has a similar frequency with C−C bonds in all cases. The FT-IR spectra of all TAEA-PEGDA 700 membranes are nearly identical despite the different N−H/acrylate ratio. Nevertheless, at all N−H/acrylate ratios, all amine and acrylate disappear in the FT-IR spectra of the membranes (Figure S3), suggesting that both groups have fully reacted either in the aza-Michael reaction or in the acrylate homopolymerization step.

The effect of N−H/acrylate ratio on CO_2 separation performance of the resultant membranes has been evaluated, and the results are shown in Figure 3B. The CO_2 permeability increases from 76.5 ± 1.4 to 85.0 ± 0.4 Barrer at the N−H/acrylate ratio of 1:6 and then maintains at a lower level of ∼79.0 Barrer with a higher N−H/acrylate ratio. A similar trend is also observed in the CO_2/N_2 ideal selectivity: the selectivity increases from around 54.5 to 65.5 after adding a small amount of TAEA and then decreases to 57.0 with further increasing N−H/acrylate ratio, which is in the same range with the reported selectivity of PEG-based membranes (40−60).[4] Theoretically, different cross-linking networks have different architecture structures and therefore different gas transport properties. However, the CO_2 permeability values of the membranes with N−H/acrylate of 0:1 and 1:1 are nearly the

DOI: 10.1021/acs.iecr.9b00241
Ind. Eng. Chem. Res. 2019, 58, 5261−5268

same, suggesting that these two networks have similar CO_2 transport properties despite the different network structures (star-like for the TAEA-PEGDA network and parallel for pristine cross-linked PEGDA).[28] This similar CO_2 permeation performance may be due to the rubbery nature of PEG chains and the same building unit PEGDA in both membranes. It is evident that the interpenetration of the chains affects the structure of both networks and results in more free volume for gas transport, leading to the increased CO_2 permeability. On the other hand, the CO_2/N_2 selectivity of these membranes is not significantly influenced by changing the N−H/acrylate ratio. Hence, among the range of N−H/acrylate ratios studied in this work, the TAEA-PEGDA 700 membrane with an N−H/acrylate ratio of 1:6 was selected for further investigation due to its highest CO_2 permeability and higher CO_2/N_2 selectivity compared with the pristine membrane. It is worth mentioning that the tertiary amine is the product of the aza-Michael addition used to build the interpenetrated network in the resultant membranes, which cannot function as CO_2 carriers due to the missing accessible N−H bonds and especially the absence of water vapor in the current test conditions.

3.3. IL Blend Membrane. In this work, four conventional ILs with different anions (i.e., [Bmim][BF_4], [Bmim][PF_6], [Bmim][TCM] and [Bmim][NTf_2]) were incorporated into the optimized cross-linked PEG-based membranes to study the influences of the IL addition on the membrane properties and the CO_2 separation performance. The FT-IR spectra of the pristine PEG membrane synthesized in this work and membranes containing four ILs (80% IL loading) are presented in Figure 4A, showing clear peaks corresponding to their respective anions and the imidazole ring ($[Bmim]^+$) in all blend membranes. The information about related peaks is given as follows: 1051 cm^{-1} (B−F stretching of $[BF_4]^-$), 830 cm^{-1} (P−F stretching of $[PF_6]^-$), 2156 cm^{-1} (−C≡N stretching of $[TCM]^-$), 1181 cm^{-1} (C−F stretching of $[NTf_2]^-$) and 1571 cm^{-1} (C−C vibration of the imidazole ring). It is also observed that the intensities of the peaks mentioned above are stronger than those related to the polymer chains in all IL blend membranes, which indicates a considerably high loading of ILs in the membrane matrix, suggesting that the cross-linked PEG membranes have the capability of possessing a high amount of ILs. In addition, with increasing ILs content, the peaks of ILs become more evident in the spectra of the blend membranes (Figure S7), suggesting that the ILs existed in membrane matrix do increase as expected. Compared with the pristine cross-linked PEGDA membrane (Figure S6), different decomposition behaviors of the membranes containing ILs (i.e., starting point of decomposition and the decomposition rate) were observed, also indicating the existence of the ILs inside the blend membranes.

Generally speaking, T_g decreases with adding low-molecular-weight additives into the polymer,[3,16] while a lower T_g usually indicates enhanced gas permeation properties. The T_gs of the cross-linked PEG membranes incorporated with four selected ILs have been evaluated by DSC, as shown in Figure 4B. T_gs of the membranes containing [Bmim][BF_4], [Bmim][TCM], and [Bmim][NTf_2] decrease with increasing IL content, indicating more flexible polymeric chains with the addition of ILs. In addition, the membranes containing different ILs show distinct values of T_g with the same IL loading (80 wt %): −57.1, −58.9, and −66.9 °C for membranes containing [Bmim][BF_4], [Bmim][NTf_2] and [Bmim][TCM], respectively, compared with −53.5 °C of the pristine membrane. This order is consistent with the values of the neat ILs. Additionally, only one T_g can be observed for each blend membrane, indicating the successful blending of ILs into the cross-linked PEG matrix. However, the trend of decreasing in T_g is less obvious in the membranes containing [Bmim][PF_6] compared with those containing other ILs, as shown in Figure S4, despite the much lower T_g value of the neat IL. This difference may be ascribed to the intermolecular interactions, e.g., hydrogen bonding or Coulombic and van der Waals interactions between $[PF_6]^-$ and PEG polymer chains, which compensates for the decreasing trend of T_g after adding ILs.[29] It is worth mentioning that the melting or crystallinity peaks of the four pure ILs are not observed in the spectra of the blend membranes, implying that ILs have been homogeneously mixed with the polymeric matrix. The incorporation of ILs into cross-linked PEG membranes also reduces its original crystallinity, proved by broader and less sharp peaks in XRD curves (Figure S5).

The gas transport properties of the IL blend membranes have been measured by single gas permeation tests, and the results are presented in Figure 4C. The CO_2 permeabilities of the membranes with four ILs decrease after adding a small amount of ILs (e.g., 20 wt %), which may be because ILs occupy the initial free volume of cross-linked PEG membranes, resulting in a decreased diffusivity and therefore lower permeability.[30] With more ILs added into the membranes, the CO_2 permeability increases with the IL loading except for [Bmim][PF_6]. For example, the membranes with 80 wt % [Bmim][TCM] have an ∼2-fold increment in CO_2 permeability (134.2 Barrer) from the membrane with 20 wt % IL content (65.8 Barrer). Several reasons could be responsible for the influence of the IL loading. First, the presence of ILs during polymerization may lead to an increase in the free volume[11] and thus a higher gas diffusivity. Additionally, gases transport more easily through IL zone than a solid polymer matrix and therefore permeate faster with more ILs inside the membranes. Moreover, the high affinity of ILs toward CO_2 enhances the CO_2 solubility, which also contributes to the increment of the CO_2 permeability.

Different ILs have different influences in the gas transport properties of the membranes. The cross-linked membranes with the addition of [Bmim][NTf_2] and [Bmim][TCM] show the highest CO_2 permeability, followed by that with [Bmim][BF_4], while the value of the membranes containing [Bmim][PF_6] is located at the bottom. The CO_2 permeability of the first two series of IL blend membranes is high as expected, since they are well-known for the good CO_2 absorption properties. But the enhancement in CO_2 permeability by the two ILs is believed following different mechanisms: the high affinity of $[NTf_2]^-$ to CO_2, mainly resulting from the plentiful fluoride atoms in the anion,[31] may increase the CO_2 solubility, while the low viscosity of $[TCM]^-$ may have less transport resistance for CO_2 penetrating and hence an increased diffusivity.[32] For the case of [Bmim][BF_4], less fluorination in the anions leads to a lower van der Waals force between the anions and CO_2 and thus a lower CO_2 solubility and permeability than $[NTf_2]^-$. Unexpectedly, the membranes containing $[PF_6]^-$ show a notable decrease in CO_2 permeability, even lower than that of the least CO_2-philic compound $[BF_4]^-$, which could be related to the interactions between $[PF_6]^-$ ions with the ethylene oxide groups.

DOI: 10.1021/acs.iecr.9b00241
Ind. Eng. Chem. Res. 2019, 58, 5261−5268

It is worth mentioning that the CO_2/N_2 selectivity of these four ILs blend membranes decreases with the increasing ILs loading, as shown in Figure 4D. This result is ascribed to the relatively lower CO_2/N_2 selectivity of these conventional ILs (20−30) compared with that of PEG-based materials (40−60). Therefore, the incorporation of conventional ILs into PEG-based materials shows lower CO_2 selectivity. A different order has been observed for ideal CO_2/N_2 selectivity of the ILs blend membranes, which is $[TCM]^-$ > $[BF_4]^-$ > $[NTf_2]^-$ > $[PF_6]^-$. The highest selectivity of ILs blend membranes (45.9) comes from the high intrinsic CO_2/N_2 selectivity of cyanide-based anions, which is larger than that of the fluorinated ones,[33,34] and the more fluoro groups ILs possess, the higher the N_2 permeability and thus the lower CO_2/N_2 selectivity membranes have.[34] Hence, the membrane with $[BF_4]^-$ has a higher selectivity than that with $[NTf_2]^-$, and the interactions between $[PF_6]^-$ and polymeric matrix results in the lowest selectivity.

4. CONCLUSION

In this work, four conventional ILs were incorporated in PEG-based membranes with interpenetrating networks based on aza-Michael addition and acrylate homopolymerization. The study of the effect of the monomer PEGDA's MW on the material properties and CO_2 separation performance shows that longer PEGDA leads to better thermal stability and gas transport properties. The CO_2 permeability was around a 144-time increment (from 0.6 to 85.0 Barrer) with a simultaneously increased CO_2/N_2 selectivity (from 48.3 to 63.5) when longer PEGDA is used (700 g/mol) instead of the short one (250 g/mol). The improvement in the CO_2 separation performance of the membranes is found from the outcome of the increasing numbers of ethylene oxide units and more flexible polymer chains inside the membranes.

Membranes with different N−H/acrylate ratios show different CO_2 separation performance. The CO_2 permeability increases and then decreases with the increasing N−H/acrylate ratio. The membrane with the best CO_2 separation performance is the one with a N−H/acrylate ratio of 1:6.

The incorporation of ILs improves the gas transport properties of the cross-linked PEG-based membranes by the enhanced CO_2 affinity from ILs. The CO_2 permeability of the membrane changes with the addition of ILs and the changes depend on the content of ILs, which decreases with ILs addition at low loading (<20 wt %) and then increases with the increasing ILs content. The addition of more CO_2-philic ILs leads to a higher CO_2 permeability in the order $[Bmim][NTf_2]$ ≈ [Bmim][TCM] > $[Bmim][BF_4]$. The further addition of $[Bmim][PF_6]$ into the membrane displays no increase in CO_2 permeation, hence, the CO_2 permeability stays at a lower level compared with that of the pristine membrane. However, with a large increase in CO_2 permeability, a constant decrement in CO_2/N_2 selectivity was observed. The more CO_2-philic ILs, such as amine-functionalized ILs, may endow better CO_2 separation performance with higher CO_2 permeability and selectivity due to the higher CO_2 affinity, which may be further studied.

■ ASSOCIATED CONTENT

Supporting Information

The Supporting Information is available free of charge on the ACS Publications website at DOI: 10.1021/acs.iecr.9b00241.

TGA, FTIR, and XRD results of TAEA-PEGDA700 membranes with different N−H ratios; XRD, TGA, and DSC results of the blend membranes with different ILs (PDF)

■ AUTHOR INFORMATION

Corresponding Author

*(L.D.) E-mail deng@nt.ntnu.no, Tel +47 73594112.

ORCID

Jing Deng: 0000-0003-3680-3799
Zhongde Dai: 0000-0002-3558-5403
Liyuan Deng: 0000-0003-4785-4620

Notes

The authors declare no competing financial interest.

■ ACKNOWLEDGMENTS

This work was supported by the Research Council of Norway through the CLIMIT program (No. 254791).

■ REFERENCES

(1) Hägg, M.-B.; Deng, L. Membranes in gas separation. In *Handbook of Membrane Separations: Chemical, Pharmaceutical, Food, and Biotechnological Applications*; CRC Press: Boca Raton, FL, 2015; pp 143−180.

(2) Wang, S.; Li, X.; Wu, H.; Tian, Z.; Xin, Q.; He, G.; Peng, D.; Chen, S.; Yin, Y.; Jiang, Z.; Guiver, M. D. Advances in high permeability polymer-based membrane materials for CO_2 separations. *Energy Environ. Sci.* **2016**, *9* (6), 1863−1890.

(3) Liu, J.; Hou, X.; Park, H. B.; Lin, H. High-performance polymers for membrane CO_2/N_2 separation. *Chem. - Eur. J.* **2016**, *22* (45), 15980−15990.

(4) Liu, S. L.; Shao, L.; Chua, M. L.; Lau, C. H.; Wang, H.; Quan, S. Recent progress in the design of advanced PEO-containing membranes for CO_2 removal. *Prog. Polym. Sci.* **2013**, *38* (7), 1089−1120.

(5) Kusuma, V. A.; Matteucci, S.; Freeman, B. D.; Danquah, M. K.; Kalika, D. S. Influence of phenoxy-terminated short-chain pendant groups on gas transport properties of cross-linked poly (ethylene oxide) copolymers. *J. Membr. Sci.* **2009**, *341* (1−2), 84−95.

(6) Wang, Y.; Li, H.; Dong, G.; Scholes, C.; Chen, V. Effect of Fabrication and Operation Conditions on CO_2 Separation Performance of PEO−PA Block Copolymer Membranes. *Ind. Eng. Chem. Res.* **2015**, *54* (29), 7273−7283.

(7) Lin, H.; Freeman, B. D. Gas solubility, diffusivity and permeability in poly (ethylene oxide). *J. Membr. Sci.* **2004**, *239* (1), 105−117.

(8) Lin, H.; Kai, T.; Freeman, B. D.; Kalakkunnath, S.; Kalika, D. S. The effect of cross-linking on gas permeability in cross-linked poly(ethylene glycol diacrylate). *Macromolecules* **2005**, *38* (20), 8381−8393.

(9) Patel, N. P.; Miller, A. C.; Spontak, R. J. Highly CO_2-permeable and-selective membranes derived from crosslinked poly (ethylene glycol) and its nanocomposites. *Adv. Funct. Mater.* **2004**, *14* (7), 699−707.

(10) Hirayama, Y.; Kase, Y.; Tanihara, N.; Sumiyama, Y.; Kusuki, Y.; Haraya, K. Permeation properties to CO_2 and N_2 of poly (ethylene oxide)-containing and crosslinked polymer films. *J. Membr. Sci.* **1999**, *160* (1), 87−99.

(11) Dai, Z.; Ansaloni, L.; Gin, D. L.; Noble, R. D.; Deng, L. Facile fabrication of CO_2 separation membranes by cross-linking of poly (ethylene glycol) diglycidyl ether with a diamine and a polyamine-based ionic liquid. *J. Membr. Sci.* **2017**, *523*, 551−560.

(12) Yave, W.; Car, A.; Peinemann, K.-V. Nanostructured membrane material designed for carbon dioxide separation. *J. Membr. Sci.* **2010**, *350* (1−2), 124−129.

(13) Dai, Z.; Noble, R. D.; Gin, D. L.; Zhang, X.; Deng, L. Combination of ionic liquids with membrane technology: A new approach for CO_2 separation. *J. Membr. Sci.* **2016**, *497*, 1−20.
(14) Bara, J. E.; Noble, R. D.; Gin, D. L. Effect of "Free" Cation Substituent on Gas Separation Performance of Polymer−Room-Temperature Ionic Liquid Composite Membranes. *Ind. Eng. Chem. Res.* **2009**, *48* (9), 4607−4610.
(15) Chen, H. Z.; Li, P.; Chung, T.-S. PVDF/ionic liquid polymer blends with superior separation performance for removing CO_2 from hydrogen and flue gas. *Int. J. Hydrogen Energy* **2012**, *37* (16), 11796−11804.
(16) Dai, Z.; Bai, L.; Hval, K. N.; Zhang, X.; Zhang, S.; Deng, L. Pebax®/TSIL blend thin film composite membranes for CO_2 separation. *Sci. China: Chem.* **2016**, *59* (5), 538−546.
(17) Dai, Z.; Ansaloni, L.; Ryan, J. J.; Spontak, R. J.; Deng, L. Nafion/IL hybrid membranes with tuned nanostructure for enhanced CO_2 separation: effects of ionic liquid and water vapor. *Green Chem.* **2018**, *20* (6), 1391−1404.
(18) Kusuma, V. A.; Macala, M. K.; Baker, J. S.; Hopkinson, D. Cross-Linked Poly(ethylene oxide) Ion Gels Containing Functionalized Imidazolium Ionic Liquids as Carbon Dioxide Separation Membranes. *Ind. Eng. Chem. Res.* **2018**, *57* (34), 11658−11667.
(19) Gao, H.; Bai, L.; Han, J.; Yang, B.; Zhang, S.; Zhang, X. Functionalized ionic liquid membranes for CO_2 separation. *Chem. Commun.* **2018**, *54* (90), 12671−12685.
(20) Deng, J.; Bai, L.; Zeng, S.; Zhang, X.; Nie, Y.; Deng, L.; Zhang, S. Ether-functionalized ionic liquid based composite membranes for carbon dioxide separation. *RSC Adv.* **2016**, *6* (51), 45184−45192.
(21) Zhou, J.; Mok, M. M.; Cowan, M. G.; McDanel, W. M.; Carlisle, T. K.; Gin, D. L.; Noble, R. D. High-permeance room-temperature ionic-liquid-based membranes for CO_2/N_2 separation. *Ind. Eng. Chem. Res.* **2014**, *53* (51), 20064−20067.
(22) Bara, J. E.; Hatakeyama, E. S.; Gabriel, C. J.; Zeng, X.; Lessmann, S.; Gin, D. L.; Noble, R. D. Synthesis and light gas separations in cross-linked gemini room temperature ionic liquid polymer membranes. *J. Membr. Sci.* **2008**, *316* (1), 186−191.
(23) Bara, J. E.; Hatakeyama, E. S.; Gin, D. L.; Noble, R. D. Improving CO_2 permeability in polymerized room-temperature ionic liquid gas separation membranes through the formation of a solid composite with a room-temperature ionic liquid. *Polym. Adv. Technol.* **2008**, *19* (10), 1415−1420.
(24) Zeng, S.; Zhang, X.; Bai, L.; Zhang, X.; Wang, H.; Wang, J.; Bao, D.; Li, M.; Liu, X.; Zhang, S. Ionic-liquid-based CO_2 capture systems: structure, interaction and process. *Chem. Rev.* **2017**, *117* (14), 9625−9673.
(25) Kusuma, V. A.; Macala, M. K.; Liu, J.; Marti, A. M.; Hirsch, R. J.; Hill, L. J.; Hopkinson, D. Ionic liquid compatibility in polyethylene oxide/siloxane ion gel membranes. *J. Membr. Sci.* **2018**, *545*, 292−300.
(26) Bernardo, P.; Jansen, J. C.; Bazzarelli, F.; Tasselli, F.; Fuoco, A.; Friess, K.; Izák, P.; Jarmarová, V.; Kačírková, M.; Clarizia, G. Gas transport properties of Pebax®/room temperature ionic liquid gel membranes. *Sep. Purif. Technol.* **2012**, *97*, 73−82.
(27) González, G.; Fernández-Francos, X.; Serra, À.; Sangermano, M.; Ramis, X. Environmentally-friendly processing of thermosets by two-stage sequential aza-Michael addition and free-radical polymerization of amine−acrylate mixtures. *Polym. Chem.* **2015**, *6* (39), 6987−6997.
(28) Deng, J.; Dai, Z.; Yan, J.; Sandru, M.; Sandru, E.; Spontak, R. J.; Deng, L. Facile and solvent-free fabrication of PEG-based membranes with interpenetrating networks for CO_2 separation. *J. Membr. Sci.* **2019**, *570*−*571*, 455−463.
(29) Trivedi, S.; Pandey, S. Interactions within a [Ionic Liquid + Poly(ethylene glycol)] Mixture Revealed by Temperature-Dependent Synergistic Dynamic Viscosity and Probe-Reported Microviscosity. *J. Phys. Chem. B* **2011**, *115* (22), 7405−7416.
(30) Kanehashi, S.; Kishida, M.; Kidesaki, T.; Shindo, R.; Sato, S.; Miyakoshi, T.; Nagai, K. CO_2 separation properties of a glassy aromatic polyimide composite membranes containing high-content 1-butyl-3-methylimidazolium bis (trifluoromethylsulfonyl) imide ionic liquid. *J. Membr. Sci.* **2013**, *430*, 211−222.
(31) Lei, Z.; Dai, C.; Chen, B. Gas Solubility in Ionic Liquids. *Chem. Rev.* **2014**, *114* (2), 1289−1326.
(32) Kim, J. E.; Kim, H. J.; Lim, J. S. Solubility of CO_2 in ionic liquids containing cyanide anions:$[C_2mim][SCN]$, $[C_2mim][N(CN)_2]$ and $[C_2mim][C(CN)_3]$. *Fluid Phase Equilib.* **2014**, *367*, 151−158.
(33) Scovazzo, P.; Kieft, J.; Finan, D. A.; Koval, C.; DuBois, D.; Noble, R. Gas separations using non-hexafluorophosphate $[PF6]^-$ anion supported ionic liquid membranes. *J. Membr. Sci.* **2004**, *238* (1), 57−63.
(34) Mahurin, S. M.; Lee, J. S.; Baker, G. A.; Luo, H.; Dai, S. Performance of nitrile-containing anions in task-specific ionic liquids for improved CO_2/N_2 separation. *J. Membr. Sci.* **2010**, *353* (1), 177−183.

DOI: 10.1021/acs.iecr.9b00241
Ind. Eng. Chem. Res. 2019, 58, 5261−5268

Paper III

Synthesis of Cross-linked PEG/IL Blend Membrane via One-pot Thiol-ene/epoxy Chemistry

This paper has been accepted by
Journal of Polymer Science

Synthesis of Cross-linked PEG/IL Blend Membrane via One-pot Thiol-ene/epoxy Chemistry

Jing Deng, Zhongde Dai, Liyuan Deng*

Department of Chemical Engineering, Norwegian University of Science and Technology, 7491 Trondheim, Norway

Correspondence to: Liyuan Deng (deng@nt.ntnu.no)

ABSTRACT

Polyethylene glycol (PEG)-based membranes have obtained considerable attentions for CO_2 separation for their promising CO_2 separation performance and excellent thermal/chemical resistance. In this work, a one-pot thiol-ene/epoxy reaction was used to prepare cross-linked PEG-based and PEG/ionic liquids (ILs) blend membranes. Four ILs of the same cation $[Bmim]^+$ with different anions ($[BF_4]^-$, $[PF_6]^-$, $[NTf_2]^-$, and $[TCM]^-$) were chosen as the additives. The chemical structure, thermal properties, hydrophilicity and permeation performance of the resultant membranes were investigated to study the ILs' effects. An increment in CO_2 permeability (~34%) was obtained by optimizing monomer ratios and thus the cross-linking network structures. Adding ILs into optimized PEG matrix shows distinct influence in CO_2 separation performance depending on the anions' types, due to the different CO_2 affinity and compatibility with PEG matrix. Among these ILs, $[Bmim][NTf_2]$ was found the most effective in enhancing CO_2 transport by simultaneously increasing the solubility and diffusivity of CO_2.

KEYWORDS: Epoxy resin; thiol click; cross-linked poly(ethylene glycol); ionic liquids; CO_2 separation

INTRODUCTION

Epoxy resins, or called polyepoxides, are a class of polymers formed by monomers or oligomers containing epoxy groups,[1] usually with the presence of cross-linkers, such as amines. The excellent chemical and thermal resistance, good mechanical properties and notable adhesion of epoxy resins allow them to play important roles in various industrial applications, such as coating, reinforcement,[2,3] and adhesives [4-7] Recently, several groups have expanded these materials to gas separation, especially as CO_2 separation membranes, thanks to the facile and rapid cross-linking, tunable chemical structure and the presence of secondary amines. [8-11] In addition, the used epoxy monomers are mainly focused on polyethylene glycol (PEG)-based materials, which have been considered as one of the most promising materials to overcome the trade-off between gas permeability and selectivity of the polymeric membranes,[12] due to the high CO_2 solubility and solubility selectivity. [13,14]

A series of cross-linked PEG membranes based on the epoxy-amine reaction for CO_2 capture have been reported.[8,15-21] Thanks to the CO_2-philic ethylene oxide (EO) units, the CO_2 permeability of the neat cross-linked PEG membranes reaches 180 Barrer with high CO_2/light gas selectivity.[8] Compared with the PEG membranes formed by the classical acrylate homopolymerization, membranes prepared by using the epoxy-amine reaction exhibit around 60% higher CO_2 permeability, [13] due probably to the more flexible cross-linking network. Similarly, Patil and coworkers employed diamine Jeffamine and a low-molecular-weight epoxy

monomer (145 g/mol) to prepare PEG-based membranes with promising CO_2 separation performance. Further analysis found out that higher gas permeability can be obtained by decreasing cross-linking density (increased diffusivity), which can be accomplished by increasing the monomer length, [11,22] or adding low-molecular-weight CO_2-philic additives into the cross-linked membranes. In the first case, however, due to the highly crystalline trend between long PEG chains, the maximum monomer molecular weight is suggested to be limited within ~ 1000 to 1500 g/mol. [14,23,24] The increased monomer molecular weight seriously hinders the cross-linking reactivity, therefore higher reaction temperature or longer reaction time is required. For examples, Lu *et al.* used the three-stage curing method involving a pre-cured stage at 80 °C for 3 h, followed by another 2 h at 100 °C and lastly 0.5 h at 120 °C. [8] Even with low-molecular-weight amine functionlization cross-linkers, the prepartion was still complicated compared to other cross-linking mechanisms, [16,25] like the UV-induced acrylate homopolymerzation.

Physically blending with low-molecular-weight additives is another widely-used approach to enhance the gas transport properties of PEG-based membranes. With the presence of the liquid additives, the concentration of reactive functional groups inside monomer mixture is further diluted, which increases the difficulty to complete the reaction. To address this issue, Shao et al. employed a two-step method to incorporate free-PEG into the cross-linked PEG membranes, where the PEG membranes were prepared via a thermal-induced epoxy-amine reaction, then the membranes were immersed into aqueous PEG solution to obtain the PEG-imbedded membranes.[15,25] A CO_2 permeability of up to 1301 Barrer has been reported accompanied with a CO_2/H_2 selectivity of 13 after imbedding free PEG into the cross-linked PEG membranes, which makes it very promising for various CO_2 separation applications. However, the multi-stage membrane preparation procedure is rather time-consuming, at least 4 days was used to obtain one batch of membranes. Besides, the amount of free liquid additives inside membranes may not be controlled precisely, making it challenging for the membrane up-scaling and industrial applications. Moreover fast membrane preparation method is of great importance to promote the industrial potential of the PEG-based membranes.

Thiol-epoxy is well-known for its more controllable cross-linking density, high reaction rate, and moderate reaction condition. [26,27] In this work, a one-pot synthesis method using thiol-epoxy reaction was developed to fabricate cross-linked PEG-based membranes with the presence of ionic liquids (ILs) as liquid additives. Another classical thiol-click reaction, thiol-ene, was also used to study the effects of the cross-linking reactions. Ionic liquids, the salt containing organic cation and inorganic/organic anion, which usually have a melting point lower than 100 °C, have been well accepted as membrane additives to improve the CO_2 permeation properties for the high CO_2 solubility. Various studies have incorporated highly CO_2-philic "free" ILs into polymeric membranes, and the results shows that the presence of ILs greatly enhances the CO_2 separation performance of highly crystallized polymers or cross-linked polymers, such as poly(ionic liquids) [10,28] or PEG-based polymers [24,29-32]. In addition, the numberless combinations of various anions and cations and ILs' negligible vapor pressure offers the great opportunity for further improvement and excellent long-term stability. [33,34] Therefore,

based on the literature study, the addition of ILs was taken as an approach to improve the CO_2 permeation in the cross-linked membranes. In order to study the effect of the ILs of different anions, four ILs in a series with the same cation $[Bmim]^+$, 1-butyl-3-methylimidazolium), but different anions were selected and incorporated into the optimized cross-linked PEG-based polymeric matrix. Fourier transform infrared spectroscopy (FTIR), thermogravimetric analysis (TGA), differential scanning calorimetry (DSC) and water uptake experiments were conducted to study the chemical structure and evaluate the thermal properties and hydrophilicity of the resultant membranes. The CO_2 and N_2 transport properties of the aforementioned membranes were test to investigate the effect of the cross-linked network structure and the addition of ILs in the CO_2 separation performance.

EXPERIMENTAL

Material

Poly(ethylene glycol) diacrylate (Mn ≈ 700) (PEGDA), trimethylolpropane tris(3-mercaptopropionate) (3T), poly(ethylene glycol) diglycidyl ether (Mn ≈ 500) (PEGDGE) and 1-Hydroxycyclohexyl phenyl ketone (HCPK) were purchased from Sigma Aldrich, Steinheim, Germany. 1-Butyl-3-methylimidazolium tetrafluoroborate ([Bmim][BF_4]), 1-butyl-3-methylimidazolium hexafluorophosphate ([Bmim][PF_6]), and 1-butyl-3-methylimidazolium bis(trifluoromethanesulfonyl)imide ([Bmim][NTf_2]) were also obtained from Sigma Aldrich, Steinheim, Germany. 1-Butyl-3-methylimidazolium tricyanomethanide ([Bmim][TCM]) was bought from Iolitec, Germany. The pure gases (N_2 and CO_2) used for gas separation performance evaluation were provided by AGA, Trondheim, Norway. All chemicals were used as received and their chemical structures are shown in **FIGURE 1**.

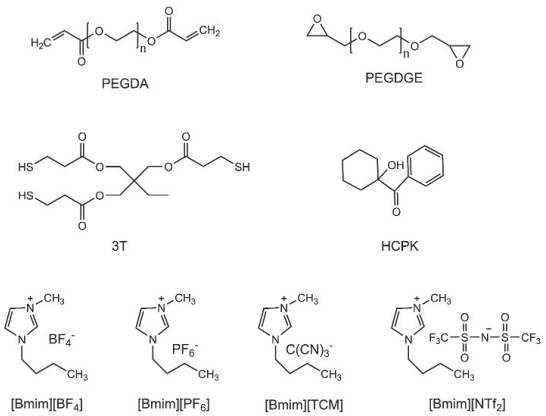

FIGURE 1. The chemical structure of PEGDA, PEGDGE 3T and four ILs used in this work

Membrane preparation

Membranes were fabricated by a cross-linking method similar with those in literatures [25,35] (**FIGURE 2**). A brief description is presented below to the readers' convenience: PEGDA, PEGDGE, equivalent cross-linker 3T (mole ratio), a calculated amount of ILs, and 0.01-0.1w.t. % HCPK were mixed in a glass vial for a few minutes. The content of ILs w_{IL} (%) is calculated based on the mass ratio of IL to the total membrane mass in equation (1):

$$w_{IL} = \frac{m_{IL}}{m_{PEGDGE} + m_{PEGDA} + m_{3T} + m_{IL}} \quad (1)$$

The well-mixed membrane solution was transferred into a vacuum oven to remove the bubbles. After that, the solution was sandwiched between two quartz plates separated by a spacer to control the thickness of membranes (~ 200 µm). UV irradiation with a wavelength of 365 nm (UVLS-28, Ultra-Violet Products Ltd., Cambridge, UK) was then applied to the membrane solution. To ensure a complete reaction, the time of UV

cross-linking is set as 1 h. The resultant self-standing membranes were obtained for further characterization and permeation test.

In this work, all membranes without ILs are systematically named according to the mole ratio of three monomers. For example, the "1-0.25-1.25" presents the membrane with 0.25 mole PEGDGE per 1 mole PEGDA and the 1.25 mol thiol groups, which needs 0.4745 g PEGDGE and 0.1786 g 3T per gram PEGDA. Then 1.6531 g IL is required to prepare this membrane with 50 w.t.% ILs.

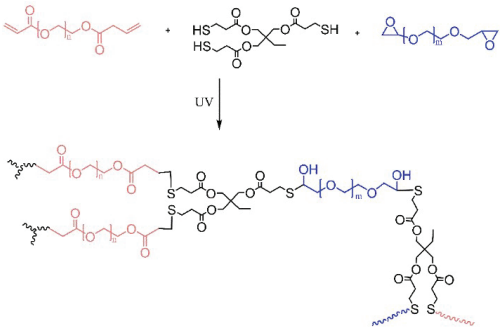

FIGURE 2. The cross-linking reactions used in this work

Characterization

A Thermo Nicolet Nexus FTIR spectrometer (NicoletTM iSTM 50, Thermo Fisher, Oslo, Norway) with a smart endurance reflection cell was used to study the chemical structure of the resultant membranes and reactants in this work. All membranes or reactants were scanned in the range of 650 - 4000 cm^{-1}.

Thermal stabilities of these investigated membranes were tested by a thermogravimetric analyzer (TGA, TG 209 F1 Libra, NETZSCH, Selb, Germany). Around 10-20 mg samples were used in a typical TGA test, with a temperature range of 25 ~ 700 °C and a heating rate of 10 °C/min. N_2 is employed to prevent oxidation of samples. In addition, a differential scanning calorimeter (DSC, DSC 214 Polyma, NETZSCH, Selb, Germany) was used to investigate the glass transition temperature of the resultant membranes and reactant. Samples of around 10 mg were collected in a standard aluminum pan covered by a proper lid and heated at the rate of 10 °C/min under N_2 atmosphere.

Water uptake tests of the membrane samples were employed to evaluate the hydrophilicity of membranes. To completely remove the moisture, all membrane samples were vacuumed at 40 °C overnight. Dried samples with known weights were placed in a water desiccator at room temperature. The weights of these membrane samples were measured with a certain interval until they were stabilized. The water uptake (w_{H2O}) was calculated using equation 2:

$$w_{H2O} = \frac{w_f - w_0}{w_0} \times 100\% \qquad (2)$$

where w_f and w_0 are the weight of the wet sample and dried sample, respectively.

Gas permeation test

Gas permeation tests were conducted at room temperature with a feed pressure of 2 bar to evaluate the CO_2 and N_2 transport properties by the constant-volume variable-pressure method. The permeability (P) of CO_2 or N_2 were calculated by equation 3.

$$P = \left[\left(\frac{dp_d}{dt}\right)_{t\to\infty} - \left(\frac{dp_d}{dt}\right)_{leak}\right] \cdot \frac{V_d}{A \cdot R \cdot T} \cdot \frac{l}{(p_u - p_d)} \qquad (3)$$

where *P* is the permeability, p_d and p_u represent the downstream and upstream pressure, respectively, t refers to the time, V_d is the downstream volume, *A* means the effective permeation area of the membrane, *R* and *T* are the ideal gas constant and temperature, and *l* is

the thickness of the membrane, respectively. The leakage rate dp_d/dt was measured by isolating the membrane cell at vacuum condition with air for a certain period. The thicknesses of all membranes were measured by an ABS Digimatic Indicator from Mitutoyo (Suzhou, China). The average thicknesses were given based on more than 10 measurements for each membrane. The permeability was the average values obtained based on, at least, 2 samples with a relative error of less than 10%.

The ideal selectivity α_{CO_2/N_2} was calculated using equation 4:

$$\alpha_{CO_2/N_2} = \frac{P_{CO_2}}{P_{N_2}} \quad (4)$$

Furthermore, the diffusivity (*D*) was determined by the time-lag (ϑ) method from the single gas permeation test, and the calculation equation is shown below:

$$D = \frac{l^2}{6 \cdot \theta} \quad (5)$$

The solubility (*S*) was calculated by the permeability (*P*) and the diffusivity (*D*) based on the solution-diffusion mechanism:

$$S = \frac{P}{D} \quad (6)$$

RESULTS AND DISCUSSION

Membrane preparation

Self-standing cross-linked PEGDA-PEGDGE-3T membranes were obtained after 1 hour UV irradiation. The four different ILs ([Bmim][PF_6], [Bmim][TCM], [Bmim][NTf_2], and [Bmim][BF_4], and the resultant membranes were also well formed, except the one containing [Bmim][BF_4] (as shown in **FIGURE 3**). The mixture containing [Bmim][BF_4] gels rapidly (< 10 mins) under atmospheric condition, even without the presence of UV or photo-initiator, suggesting that the $[BF_4]^-$ anion probably accelerates or catalyzes either thiol-ene or thiol-epoxy reaction. Since this gelation is too fast to prepare a proper membrane, the membrane containing [Bmim][BF_4] was not further characterized.

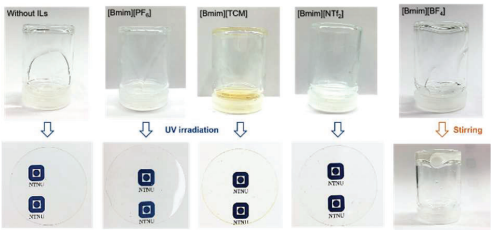

FIGURE 3. The pre-polymer mixture and the formed membranes of PEGDA-PEGDGE-3T membrane (1-0.25-1.25), and the blend membranes with ILs.

Material properties

The FTIR analysis was employed to confirm the thiol-ene and thiol-epoxy reactions between PEGDA, PEGDGE and the cross-linker. The spectra of cross-linker, PEGDA and the resultant membrane (1-0-1) are presented in **FIGURE 4** (A). The reactive thiol (2570 cm^{-1} for S-H) and acrylate groups (1630 cm^{-1} for C=C, 1410 and 830 cm^{-1} for H-C=) are clear in the spectra of cross-linker and PEGDA, respectively, but all of them disappear in the spectra of the resultant membranes. After the reaction, the peaks assigned to C-S bond shifts to the right side (1144 cm^{-1} to 1100 cm^{-1}), which is in agreement to the literature.[36] In addition, the other peak of PEGDA at around 850 cm^{-1} becomes boarder and bigger in the resulted membranes , which may be overlapped with the peak related with the newly formed C-S bond. [37] These results suggest that the acrylate reacts with thiol and forms C-S groups under the experiment conditions, confirming the completion of the thiol-ene reaction. On the

other hand, in addition to the change of acrylate and thiol groups, the peak for epoxy (~ 904 cm^{-1}) has also disappeared in all PEGDA-PEGDGE-3T membranes, suggesting that the epoxy groups are consumed by the thiol groups, which is the only possible reactant in the system. Considering that the newly formed bonds in thiol-ene and thiol-epoxy are exactly the same, to distinguish between them via FTIR spectra is impossible and unnecessary. Hence, the membranes with different PEGDGE/PEGDA ratio have identical spectra, as present in **FIGURE 4. (C)**.

Since three different ILs have been embedded into the cross-linked PEG membranes, the states of ILs inside the membranes may be different, which influence the membrane properties and separation performance. The membranes with ILs were characterized by FTIR analysis, taking membranes containing 50% IL as samples, as shown in **FIGURE 4** (D). The FTIR spectra of the pristine membrane without ILs and the neat ILs are also given as a comparison. The ILs used in this work have the same cation $[Bmim]^+$ (1-butyl-3-methylimidazolium), which has characteristic peaks around 1570 cm^{-1} and 1460 cm^{-1} relating to imidazolium ring. [38] These two peaks are evident in the resultant membranes with different anions. The peaks of anions are also observed in the corresponding membranes at 832 cm^{-1} (PF_6^- asymmetric stretch), 1059 cm^{-1} (S=O bending), and 1200-1130 cm^{-1} (C–F stretching) of NTf_2^- [30] and 2165 cm^{-1} of TCM^-, [39] confirming that the added ILs are embedded in the cross-linked PEG matrix. Moreover, no new peaks are found in the FTIR spectra of the blend membranes, indicating that these three ILs do not have any chemical reactions with the PEG-based monomers or the resultant polymer matrix. ILs only work as a physical additive in the investigated membranes.

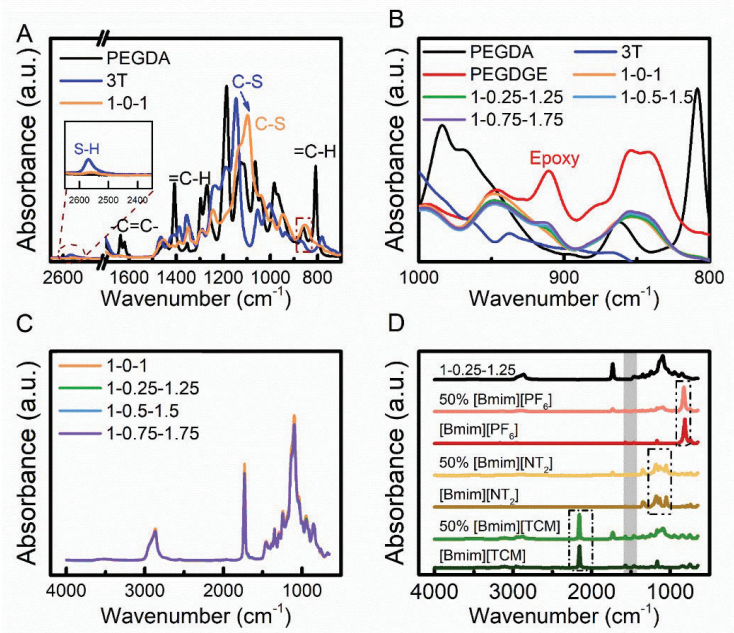

FIGURE 4. The FTIR spectrum of (A) 3T, PEGDA and PEGDA-PEGDGE-3T (1-0-1) membranes, (B) PEGDA, PEGDGE, 3T and PEGDA-PEGDGE-3T membranes with a different ratio at 1000 – 800 cm-1, (C) PEGDA-

PEGDGE-3T membranes with a different ratio, and (D) membrane without ILs, membrane with 50% ILs and the pure ILs.

The thermal stabilities of all resultant membranes in this work were studied by TGA, as shown in **FIGURE 5**. The PEGDA-3T (1-0-1) membrane shows a one-stage decomposition behavior, starting at 320 °C, while the membranes containing PEGDGE decompose at a lower temperature, and the more PEGDGE it contains, the more easily it decomposes. For the membrane containing the highest amount of PEGDGE (1-0.75-1.75), a two-stage decomposition behavior is observed; the first decomposition begins at 155 °C and the second one appears at around 300 °C, as can be seen in the insert in **FIGURE 5** (A). The weight loss during the first stage is up to 5 w.t.%, which may be a small amount of unreacted PEGDGE due to the less reactive thiol-epoxy under experimental conditions in this work.

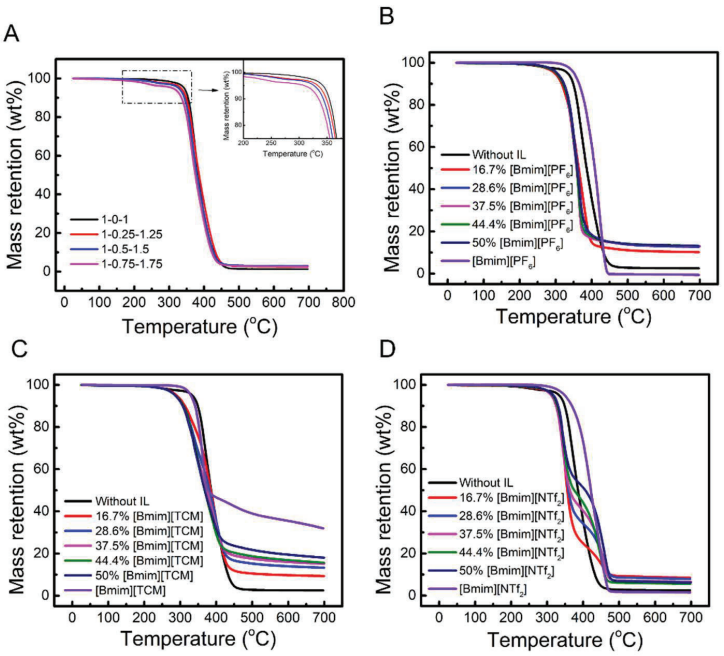

FIGURE 4. The thermal stabilities of cross-linked PEG membranes with different PEGDA/PEGDGE ratio (A), [Bmim][PF_6]-containing blend membranes (B), [Bmim][TCM]-containing blend membranes (C) and the [Bmim][NTf_2]-containing blend membranes (D) with different IL loading.

The thermal stabilities of the optimized cross-linked PEG membranes (represented by 1-0.25-1.25), three IL-containing blend membranes and the corresponding ILs are displayed in **FIGURE 5** (B)-(D). Interestingly, although pure ILs and cross-linked PEG membranes start decomposing around 300 °C, all the blend membranes decompose at a lower temperature (around 270 °C). The reason may be ascribed to the weakened hydrogen bonding between PEG polymer chains [8,14] due to the presence of ILs inside the membranes. The [Bmim][PF_6]-containing

membranes have one-stage decomposition curves, probably due to the strong interactions between [Bmim][PF_6] and polymeric matrix at high temperature conditions. Differently, the blend membranes composing [Bmim][TCM] also have similar decomposition behavior but with a slower decomposition rate, and that is because of the overlapping decomposition temperature range of their parents. On the other hand, the decomposition curves of the membrane with [Bmim][NTf_2] are close to that of [Bmim][NTf_2] at high temperature (≥ 430 °C), especially for those with higher IL loading, proving the existence of [Bmim][NTf_2]. These results show that the membranes containing PEGDGE may not be suitable for a high-temperature process (≥ 150 °C). Generally, most CO_2 separation membrane processes are operated at a temperature range of up to 80 °C, so these resultant membranes have satisfactory thermal stabilities for this application.

As the glass transition temperature of polymers (T_g) is the temperature polymer chains change from "restricted" to "flexible", for gas separation, a lower T_g of a membrane generally indicates a higher gas permeation property. To investigate the effect of the IL addition on T_g of the resultant membranes, a DSC analysis was conducted. The obtained curves are shown in **FIGURE 6**, and the T_gs were presented in **TABLE 1**.

Despite the nearly identical FTIR spectra of all the cross-linked PEGDA-PEGDGE-3T membranes, the T_gs of these membranes show a clear difference, which decreases with the increasing PEGDGE content, implying that the cross-linked network structures of these membranes may be different. As for the one containing [Bmim][PF_6], T_gs of the blend membranes show no evident difference regardless of the much lower T_g of the neat IL [Bmim][PF_6], which may result from the interaction of [Bmim][PF_6] with PEG-based polymer chains. Another reason may be that the presence of [Bmim][PF_6] has little effect on the T_g of matrix, and similar results have been reported in literature. [29,40] On the other hand, the blend membranes with [Bmim][TCM] or [Bmim][NTf_2] display a decreasing trend of T_g with the increasing IL loading, possibly due to the lower value of these two ILs and the increasing chain movement with the presence of ILs. The decrease in T_g may imply an enhanced polymer chain flexibility and thus improved gas transport properties.

DSC curves can also indicate the miscibility of components in blend membranes. From FIGURE 6, it is clear that, in the blend membranes with [Bmim][PF_6], the melting and crystallization peaks of the IL disappear, suggesting that the [Bmim][PF_6] has homogeneously dispersed within the cross-linked PEG polymeric matrix. On the contrary, these peaks are visible in the DSC curves of the blend membranes containing [Bmim][NTf_2], which suggests the formation of a [Bmim][NTf_2] phase in the cross-linked PEG matrix. The hydrophobic feature of [Bmim][NTf_2] may have induced a phase separation with the hydrophilic PEG-based polymer chains as reported in the literature. [41] Nevertheless, the ILs domain regions have been reported to have a positive effect on gas transport properties; [42] hence the cross-linked PEG membrane integrated with [Bmim][NTf_2] may still be interesting for gas separation. In the case of [Bmim][TCM], neither the melting and crystallization peaks of pure IL nor its analogy blend membranes are observed.

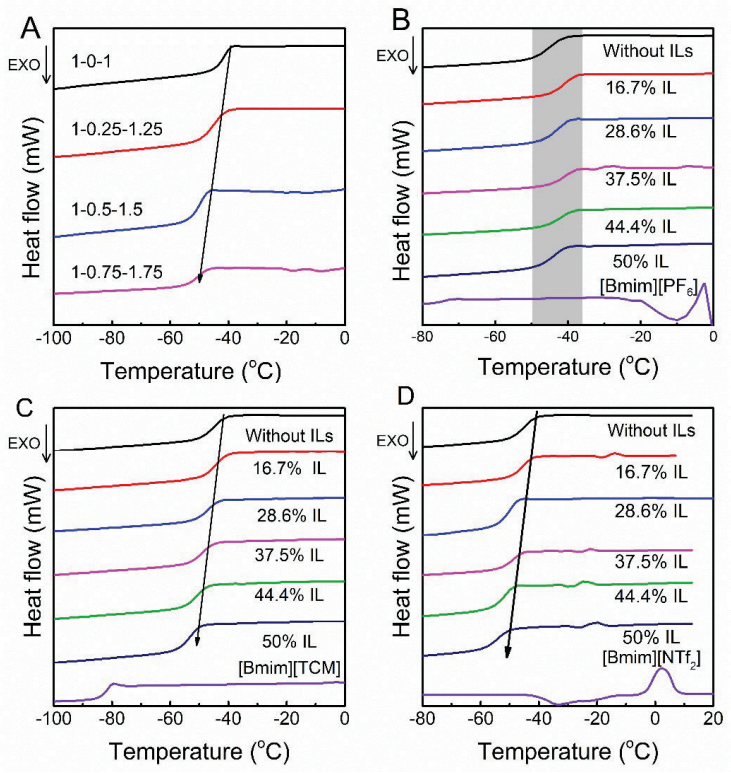

FIGURE 5. The DSC curves of cross-linked PEG membranes with different PEGDA/PEGDGE ratio (A), [Bmim][PF_6]-containing blend membranes (B), [Bmim][NTf_2]-containing blend membranes (C) and the [Bmim][TCM]-containing blend membranes (D) with different IL loading

TABLE 1. The T_g of membranes presented in the **FIGURE 6**.

Membranes	T_g (°C)
1-0-1	-44.7
1-0.25-1.25	-49.8
1-0.5-1.5	-53.4
1-0.75-1.75	-55.7
[Bmim][PF_6]-containing Membranes	
0% [Bmim][PF_6]	-49.8
16.7% [Bmim][PF_6]	-45.5
28.6% [Bmim][PF_6]	-46.6
37.5% [Bmim][PF_6]	-45.2
44.4% [Bmim][PF_6]	-46.6
50% [Bmim][PF_6]	-48.9
Pure [Bmim][PF_6]	-75.9
[Bmim][TCM]-containing Membranes	
0% [Bmim][TCM]	-49.8
16.7% [Bmim][TCM]	-48.3
28.6% [Bmim][TCM]	-51.6
37.5% [Bmim][TCM]	-53.3
44.4% [Bmim][TCM]	-55.2
50% [Bmim][TCM]	-57.6
Pure [Bmim][TCM]	-84.3
[Bmim][TCM]-containing Membranes	
0% [Bmim][NTf_2]	-49.8
16.7% [Bmim][NTf_2]	-48.2
28.6% [Bmim][NTf_2]	-49.5
37.5% [Bmim][NTf_2]	-52.4
44.4% [Bmim][NTf_2]	-55.7
50% [Bmim][NTf_2]	-58.2
Pure [Bmim][NTf_2]	-87.5

The water uptake experiments were conducted at room temperature for all resultant membranes. The weight gains of the membrane samples with time are presented in **FIGURE 7**. It is clear that all cross-linked PEGDA-PEGDGE-3T membranes have water uptakes of around 40 w.t.%, and the PEGDGE/PEGDA ratio seems not to display a significant effect on the material hydrophilicity. Considering that both monomers are PEG-based materials, it is reasonable to assume that the resultant networks have similar hydrophilicity.

However, the blend membranes containing different ILs present a different water uptake and generally, decrease with the increasing IL amount, especially at the low IL loading range. **FIGURE 7 B-D** presents the water uptake of various IL contents in the cross-linked membrane (1-0.25-1.25). As it can be seen, when the ILs amount is over 37.5 w.t.%, the change of the water uptake becomes nearly negligible. Since the ILs used in this work are more hydrophobic compared with the PEG-based materials, the initial trend of declining in water uptake is expected. When the loading of ILs inside membranes reaches a certain level (> 37.5 w.t.%), the apparent hydrophilicities of the membranes reduce to the intrinsic values of the ILs; hence the water uptake of the membranes remains nearly constant with the further increase of the IL amount.

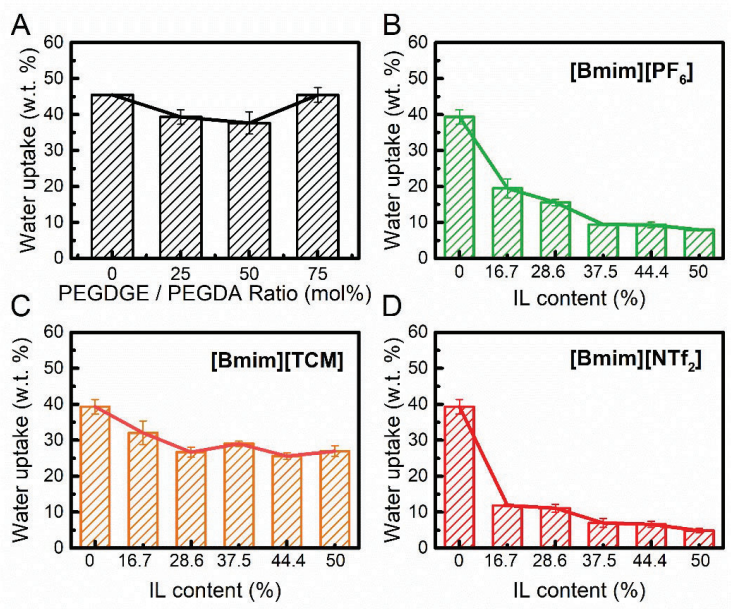

FIGURE 6. The water uptake of cross-linked PEG membranes with different PEGDA/PEGDGE ratio (A), [Bmim][PF_6]-containing blend membranes (B), [Bmim][TCM]-containing blend membranes (C) and the [Bmim][NTf_2]-containing blend membranes (D) with different IL loading.

Based on the chemical structures, the hydrophilicities of the studied ionic liquids should be different and follow the order: TCM^- > PF_6^- >NTf_2^-. The water uptake of the blend membranes follows the same order as the neat ILs, as can be seen in **FIGURE 7**. The

[Bmim][TCM]-containing membranes have the highest water uptake of around 30 w.t.%, and those containing [Bmim][PF_6] have around 10 w.t.%, and those with the addition of [Bmim][NTf_2] present only 6 w.t.%. Therefore, despite the hydrophilic nature of the cross-linked PEG polymer, membranes containing the ILs become less hydrophilic.

Gas permeation properties

Effect of PEGDGE addition

The CO_2 and N_2 permeation properties of the PEGDGE-PEGDA-3T membranes were tested by single gas permeation tests at a feed pressure of 2 bar and room temperature to study the effect of PEGDGE addition. The CO_2 permeability, ideal CO_2/N_2 selectivity, and the gas diffusivity and solubility of the PEGDGE-PEGDA-3T membranes with different PEGDGE/PEGDA ratio are presented in **FIGURE 8**.

The CO_2 permeability increases from 100.3 to 134.2 Barrer with a nearly unchanged CO_2/N_2 selectivity of around 67 by adding a small amount of PEGDGE (1-0.25-1.25), which may be explained by the disturbance of the cross-linked PEG network due to the addition of the PEGDGE, leading to a rearranged cross-linking network and enhanced gas transport properties. The increase in diffusivities of CO_2 and N_2 (as shown in **FIGURE 8 (B))** also suggests the increase in the free volume of the cross-linked PEG membranes. However, the CO_2 permeabilities and gas diffusivities decrease with the further increasing PEGDGE/PEGDA ratio. This trend is believed to be caused by the reduced overall chain length between the cross-linked sites since PEGDGE has shorter polymer chains (around 8 ethylene oxide units) compared to those of PEGDA (around 13 ethylene oxide units). On the other hand, the solubility of CO_2 and N_2 in the PEGDGE-PEGDA-3T membranes are rising with the increasing PEGDGE/PEGDA ratio, which can be explained by the similar chemical structure of PEGDGE and PEGDA, especially the same CO_2-philic groups (ethylene oxide units). Therefore, the cross-linked networks with higher PEGDGE/PEGDA ratio become more rigid (less diffusive) with nearly unaffected CO_2 solubility. The CO_2/N_2 selectivity slightly decreases with the increasing amount of PEGDGE in membranes, but the value (56 - 66) is still reasonably high and within the range of the inherent selectivity of typical PEG-based membranes. [8] Since the membrane containing the lowest amount of PEGDGE (1-0.25-1.25) holds the highest CO_2 permeability and CO_2/N_2 selectivity, it is chosen as the optimized polymeric matrix for further study.

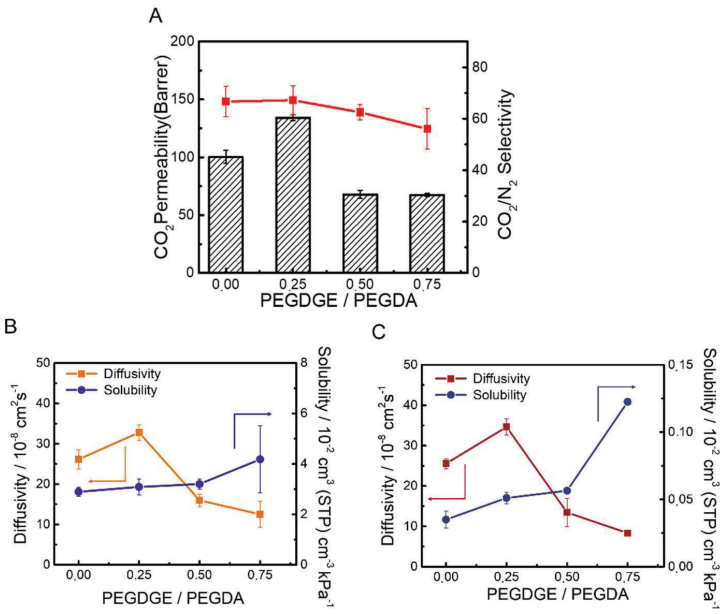

FIGURE 7. The CO_2 permeability, CO_2/N_2 selectivity (A), the diffusivity and solubility of CO_2 (B) and the diffusivity and solubility of N_2 (C) of PEGDA-PEGDGE-3T membranes with different PEGDA/PEGDGE mole ratio

Effects of IL addition

Gas permeation tests of the cross-linked PEG membranes (1-0.25-1.25) containing different ILs were performed to evaluate the effects of IL addition, as presented in **FIGURE 9**. It is clearly seen that ILs with different anions show distinguishing effects on the gas permeation properties. At low IL-loading (< 37.5 %), CO_2 permeabilities of the IL-blend membranes with [Bmim][BF_4] or [Bmim][TCM] decrease. Based on the solution-diffusion theory, the permeability is governed by diffusivity and solubility. From the diffusivity and solubility results, the reason for this drop in CO_2 permeability may be the decreased diffusivity with increasing IL-loading, as it is believed that a small amount of ILs occupies the original void of the pristine polymeric membrane. [41,43] The solubility of these two series of membranes also decreases when 16.7 w.t.% IL is added, followed by an unaltered trend, and it may be because of the relatively lower CO_2 solubility of ILs, compared with the pure PEG-based material. [44] Interestingly, the CO_2 permeability with [Bmim][NTf_2] displays a plateau in the same IL-loading range because of the much higher CO_2 solubility of the resultant membranes than that of others and the offset to the decrease in diffusivity. The higher CO_2 solubility could be explained by the higher CO_2 affinity of $[NTf_2]^-$ (more CO_2-philic fluorine atom) in agreement with the observation of CO_2 absorption using ILs as absorbents. [45]

At higher IL loadings, the changes in $P(CO_2)$, $D(CO_2)$ and $S(CO_2)$ of the resultant membranes containing different ILs display distinctive trends. For example, CO_2 permeability of the membranes with [Bmim][PF_6] keeps constant even at a high IL-loading (i.e., 37.5 – 50 w.t.%), so

do its diffusivity and solubility, suggesting that further adding [Bmim][PF_6] contributes little to these properties. On the other hand, membranes with [Bmim][TCM] or [Bmim][NTf_2] display enhanced CO_2 permeability at higher IL-loading. However, the reasons responsible for these improvements are quite different: for [Bmim][TCM]-containing membranes, the increased CO_2 solubility (from 3.40×10^{-2} to 5.58×10^{-2} $cm^3(STP)cm^{-3}kPa^{-1}$) is the major contributor for the gain in CO_2 permeability since the CO_2 diffusivity remains unchanged. In the case of membranes with [Bmim][NTf_2] (≥ 37.5 w.t.% IL loading), the increment in CO_2 permeability is the product of the simultaneously increased CO_2 solubility (1.90-fold) and diffusivity (3.22-fold) compared to the one containing 37.5 w.t.% [Bmim][NTf_2]. The increased CO_2 diffusivity is considered as the benefit of micro-phase separation (shown in DSC results), leading to more IL-rich micro-zones and thus lower transport resistance for gas transport. As a result, the membranes with highest [Bmim][NTf_2] amount have the highest CO_2 permeability of 187.9 Barrer in this work compared to those containing [Bmim][PF_6] (53.7 Barrer) and [Bmim][TCM] (117.7 Barrer).

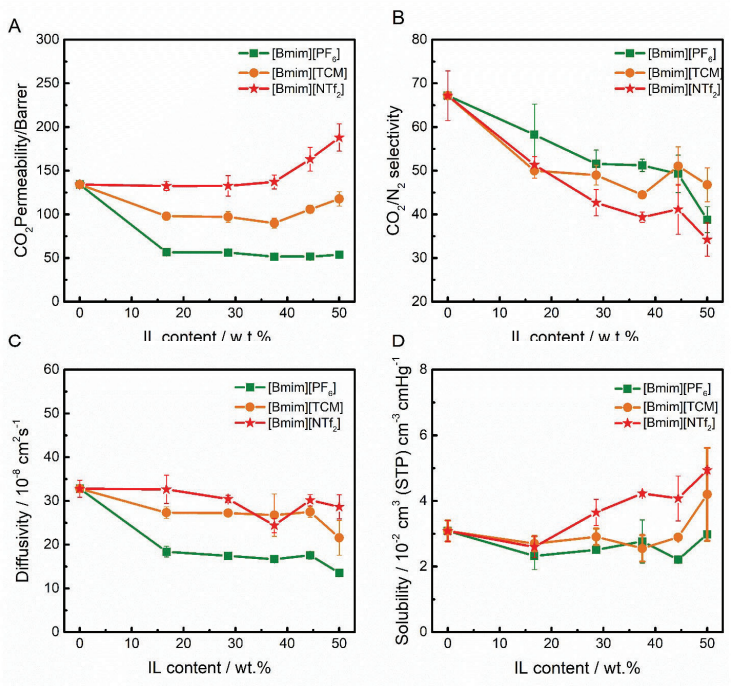

FIGURE 8. The CO_2 permeability (A), CO_2/N_2 selectivity (B), the CO_2 diffusivity (C) and CO_2 solubility (D) of three IL blend membranes with different IL loading.

Hence, the change in CO_2 permeability of the blend membrane with different ILs follows different patterns. Initial adding ILs (< 37.5 w.t.%) leads to a decrease in CO_2 diffusivity, while solubility is affected by the CO_2 affinity of ILs, and thus the resulting permeability may be decreased or unchanged. The further addition of IL shows little effect on the diffusivity, while with

more additive loading, the influence of ILs in CO_2 solubility becomes the key parameter. The most CO_2-philic anion ($[NTf_2]^-$) renders the most enhanced S(CO_2), followed by the $[TCM]^-$ (due to the interaction between cayno-functionalized anion and CO_2 [46]), and the $[PF_6]^-$. This order is agreed with the order of P(CO_2) and the absorption capability of these ILs for CO_2 capture. [47] It is worth mentioning that, in case of the membranes containing [Bmim][NTf_2], the micro-phase separation between [Bmim][NTf_2] and cross-linked PEG chains increases the D(CO_2) and thus enhances P(CO_2) more.

In terms of CO_2 selectivity, all apparent values of the membranes containing ILs are lower than the pristine one. For instance, the CO_2/N_2 selectivity of membranes with 50% IL loading are within 30-50: [Bmim][NTf_2] (34.2), [Bmim][TCM] (46.8) and [Bmim][PF_6] (38.8), while the pristine membrane has a CO_2/N_2 selectivity of 67.2. This decrease may be explained by the relatively low CO_2/N_2 selectivity of the physical-adsorption ILs (around 20-30) [44] compared with PEG-based materials (around 40-60). [8] Another possible reason is that ILs may act as the plasticizers in cross-linked PEG membranes, which could lower CO_2 selectivity. [43] In addition, different anions have distinct effects on CO_2/N_2 selectivity. Generally speaking, in this work, the order of CO_2/N_2 selectivity with a low IL amount (≤ 37.5%) in membranes is $[PF_6]^- \approx [TMC]^- > [NTf_2]^-$; with more IL being incorporated, those containing $[TMC]^-$ move to the first in this order. The positive effects of $[TMC]^-$ in CO_2 selectivity (mainly due to the interaction between CO_2 and cyano) [42,48] are believed to be the highest value obtained in this work. The instinct of its high affinity towards CO_2 explains the excellent CO_2 selectivity in high IL loadings. [Bmim][PF_6]-containing membranes have a relatively high CO_2 selectivity, which may be because that the interaction between $[PF_6]^-$ and polymeric matrix slows down the decreasing trend of CO_2 selectivity. The data in high IL loading suggest that it may further decrease with increasing IL. On the other hand, the considerable decrease in CO_2 selectivity of [Bmim][NTf_2] could be caused by the micro-phase separation of IL and polymeric matrix; gas mainly passes through the IL zones, leading to the apparent selectivity close to the values of pure [Bmim][NTf_2] (around 20-30).

CONCLUSIONS

In the present work, cross-linked PEG-based membranes and PEG/ILs blend membranes were fabricated using one-pot thiol-ene/epoxy click chemistry. The cross-linking reactions were confirmed by FT-IR analysis. The cross-linked PEG-membrane were systematically evaluated using various characterization methods. The monomer ratios were optimized to enhance gas transport properties. Up to 50 w.t. % of ILs can be incorporated into the PEG/ILs blend membranes. The anions in ILs have significant effects in membrane structure and hence the gas separation performance. PEG membranes containing [Bmim][NTf_2] shows the highest CO_2 permeability due to the high CO_2 affinity of $[NTf_2]^-$ anion and the possible micro-separation in the membranes. On the other hand, the addition of [Bmim][TCM] is more beneficial for increasing CO_2 solubility than diffusivity, while the [Bmim][PF_6] has a negative influence on both CO_2 solubility and diffusivity.

The fabrication of the cross-linked PEG/IL membranes via the one-pot thiol-ene/epoxy click chemistry is a facile and fast method. The pairing of ILs and polymer has significant influences on the membrane material properties as well as the CO_2 separation performance. The properties of final materials are tunable by various PEG monomers and ILs, which may be

practical and advantageous for feasible optimization of the blend membranes. Even the performance in this work was not greatly improved by the addition of physical-absorption ILs in this work, the addition of more CO_2-selective ILs (e.g., a chemical-absorption type of IL with CO_2/N_2 selectivity of > 40) may be a promising approach worthy of further research to promote the CO_2 permeability and the selectivity of PEG-based membranes simultaneously.

CONFLICTS OF INTEREST

There are no conflicts to declare.

ACKNOWLEDGEMENT

This work is supported by the Research Council of Norway through the CLIMIT program ("POLYMEM" project, No. 254791).

REFERENCE AND NOTES

1. Lipic, P. M.; Bates, F. S.; Hillmyer, M. A., J. Am. Chem. Soc. 120, 8963 1998.
2. Zhu, J.; Peng, H. Q.; Rodriguez-Macias, F.; Margrave, J. L.; Khabashesku, V. N.; Imam, A. M.; Lozano, K.; Barrera, E. V., Adv. Funct. Mater. 14, 643 2004.
3. Yamaguchi, A.; Hashimoto, T.; Kakichi, Y.; Urushisaki, M.; Sakaguchi, T.; Kawabe, K.; Kondo, K.; Iyo, H., J. Polym. Sci., Part A: Polym. Chem. 53, 1052 2015.
4. Furutani, M.; Kakinuma, A.; Arimitsu, K., J. Polym. Sci., Part A: Polym. Chem. 56, 237 2018.
5. Makiuchi, N.; Sudo, A.; Endo, T., J. Polym. Sci., Part A: Polym. Chem. 53, 2569 2015.
6. Bomze, D.; Knaack, P.; Koch, T.; Jin, H.; Liska, R., J. Polym. Sci., Part A: Polym. Chem. 54, 3751 2016.
7. Wang, Y.; Kimura, M.; Sudo, A.; Endo, T., J. Polym. Sci., Part A: Polym. Chem. 54, 2611 2016.
8. Liu, S. L.; Shao, L.; Chua, M. L.; Lau, C. H.; Wang, H.; Quan, S., Prog. Polym. Sci. 38, 1089 2013.
9. McDanel, W. M.; Cowan, M. G.; Chisholm, N. O.; Gin, D. L.; Noble, R. D., J. Membr. Sci. 492, 303 2015.
10. McDanel, W. M.; Cowan, M. G.; Carlisle, T. K.; Swanson, A. K.; Noble, R. D.; Gin, D. L., Polymer 55, 3305 2014.
11. Patil, P. N.; Roilo, D.; Brusa, R. S.; Miotello, A.; Checchetto, R., Polymer 58, 130 2015.
12. Robeson, L. M., J. Membr. Sci. 320, 390 2008.
13. Lin, H.; Freeman, B. D., Macromolecules 38, 8394 2005.
14. Liu, J.; Hou, X.; Park, H. B.; Lin, H., Chem. Eur. J. 22, 15980 2016.
15. Quan, S.; Tang, Y. P.; Wang, Z. X.; Jiang, Z. X.; Wang, R. G.; Liu, Y. Y.; Shao, L., Macromol. Rapid Commun. 36, 490 2015.
16. Quan, S.; Li, S.; Wang, Z.; Yan, X.; Guo, Z.; Shao, L., J. Mater. Chem. A 3, 13758 2015.
17. Li, S.; Jiang, X.; Yang, Q.; Shao, L., Chem. Eng. Res. Des. 122, 280 2017.
18. Quan, S.; Li, S. W.; Xiao, Y. C.; Shao, L., INT. J. GREENH. GAS CON. 56, 22 2017.
19. Jiang, X.; Li, S.; He, S.; Bai, Y.; Shao, L., J. Mater. Chem. A 6, 15064 2018.
20. Li, S.; Jiang, X.; Yang, X.; Bai, Y.; Shao, L., J. Membr. Sci. 570-571, 278 2019.
21. Jiang, X.; He, S.; Li, S.; Bai, Y.; Shao, L., J. Mater. Chem. A 7, 16704 2019.
22. Roilo, D.; Patil, P. N.; Brusa, R. S.; Miotello, A.; Checchetto, R., Polymer 113, 147 2017.
23. Patel, N. P.; Miller, A. C.; Spontak, R. J., Adv. Funct. Mater. 14, 699 2004.
24. Deng, J.; Yu, J.; Dai, Z.; Deng, L., Ind. Eng. Chem. Res. 58, 5261 2019.
25. Dai, Z.; Ansaloni, L.; Gin, D. L.; Noble, R. D.; Deng, L., J. Membr. Sci. 523, 551 2017.
26. Hoyle, C. E.; Lowe, A. B.; Bowman, C. N., Chem. Soc. Rev. 39, 1355 2010.
27. Jin, K.; Wilmot, N.; Heath, W. H.; Torkelson, J. M., Macromolecules 49, 4115 2016.
28. Bara, J. E.; Gin, D. L.; Noble, R. D., Ind. Eng. Chem. Res. 47, 9919 2008.
29. Dai, Z.; Bai, L.; Hval, K. N.; Zhang, X.; Zhang, S.; Deng, L., Sci. China. Chem. 59, 538 2016.

30. Li, M.; Zhang, X.; Zeng, S.; Gao, H.; Deng, J.; Yang, Q.; Zhang, S., RSC Advances 7, 6422 2017.
31. Fam, W.; Mansouri, J.; Li, H.; Chen, V., J. Membr. Sci. 537, 54 2017.
32. Kusuma, V. A.; Macala, M. K.; Liu, J.; Marti, A. M.; Hirsch, R. J.; Hill, L. J.; Hopkinson, D., J. Membr. Sci. 545, 292 2018.
33. Fujii, K.; Makino, T.; Hashimoto, K.; Sakai, T.; Kanakubo, M.; Shibayama, M., Chem. Lett. 44, 17 2014.
34. Karunakaran, M.; Villalobos, L. F.; Kumar, M.; Shevate, R.; Akhtar, F. H.; Peinemann, K.-V., J. Mater. Chem. A 5, 649 2017.
35. Lin, H.; Freeman, B. D., Macromolecules 38, 8394 2005.
36. Zhao, Y.; Zhang, X.; He, Y.; Liu, N.; Tan, T.; Liang, C., Materials 10, 1158 2017.
37. Wei, B.; Ouyang, L.; Liu, J.; Martin, D. C., J. Mater. Chem. B 3, 5028 2015.
38. Im, J.; Cho, S. D.; Kim, M. H.; Jung, Y. M.; Kim, H. S.; Park, H. S., Chem. Commun. 48, 2015 2012.
39. Kuroda, D. G.; Singh, P. K.; Hochstrasser, R. M., J. Phys. Chem. B 117, 4354 2012.
40. Ito, A.; Yasuda, T.; Ma, X.; Watanabe, M., Polym. J. 49, 671 2017.
41. Bernardo, P.; Jansen, J. C.; Bazzarelli, F.; Tasselli, F.; Fuoco, A.; Friess, K.; Izák, P.; Jarmarová, V.; Kačírková, M.; Clarizia, G., Sep. Purif. Technol. 97, 73 2012.
42. Chen, H. Z.; Li, P.; Chung, T.-S., Int. J. Hydrogen Energy 37, 11796 2012.
43. Kanehashi, S.; Kishida, M.; Kidesaki, T.; Shindo, R.; Sato, S.; Miyakoshi, T.; Nagai, K., J. Membr. Sci. 430, 211 2013.
44. Dai, Z.; Noble, R. D.; Gin, D. L.; Zhang, X.; Deng, L., J. Membr. Sci. 497, 1 2016.
45. Zeng, S.; Zhang, X.; Bai, L.; Zhang, X.; Wang, H.; Wang, J.; Bao, D.; Li, M.; Liu, X.; Zhang, S., Chem. Rev. 117, 9625 2017.
46. Tomé, L. C.; Marrucho, I. M., Chem. Soc. Rev. 45, 2785 2016.
47. Lei, Z.; Dai, C.; Chen, B., Chem. Rev. 114, 1289 2013.
48. Tomé, L. C.; Isik, M.; Freire, C. S.; Mecerreyes, D.; Marrucho, I. M., J. Membr. Sci. 483, 155 2015.

GRAPHICAL ABSTRACT

Jing Deng, Zhongde Dai, Liyuan Deng*

Thiol-click reactions-based Cross-linked PEG /Ionic Liquid blended membranes

In this arcticle, a series of cross-linked PEG-based membranes has been developed and optimized based on two classical thiol-click reactions. In addition, four ionic liquids have been incorporated into the optimzied membranes to understand their influences on the material properties and gas separation performance.

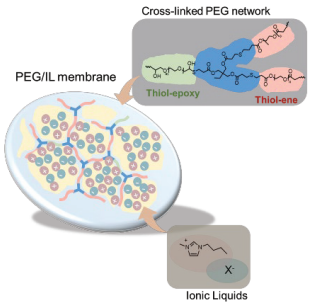

Morphologically tunable MOF nanosheets in mixed matrix membranes for CO_2 separation

This paper has been submitted to

Chemistry of Materials

Paper IV

Morphologically tunable MOF nanosheets in mixed matrix membranes for CO_2 separation

Jing Deng[†1], Zhongde Dai[†1], Jingwei Hou[2] and Liyuan Deng[*1]

AUTHOR ADDRESS

[1] Department of Chemical Engineering, Norwegian University of Science and Technology Trondheim, 7491, Norway.

Email: deng@nt.ntnu.no

[2] School of Chemical Engineering, Faculty of Engineering, Architecture and Information Technology, the University of Queensland, Brisbane, Queensland, Australia

† These authors contributed equally

ABSTRACT: This study first develops a facile method to synthesize zeolitic imidazolate framework cuboid (ZIF-C) nanosheets with tunable thickness from 70 nm to 170 nm from an aqueous polymer solution. The obtained ZIF-C nanosheets were characterized by various techniques, including X-Ray Crystallography (XRD), Scanning Electron Microscope (SEM), Atomic Force Microscopy (AFM), Fourier-Transform Infrared (FTIR) Spectroscopy, X-ray Photoelectron Spectroscopy (XPS), N_2 adsorption and Thermogravimetric analysis (TGA), to understand their compositional and structural properties. The synthesized ZIF-Cs nanosheets with different thickness were further applied as nanofillers to prepare Pebax-based mixed matrix membranes (MMMs) to study the effect of the morphology on membrane properties and CO_2/N_2 separation performances under different relative humidity conditions. Results reveal that the incorporation of these ZIF-Cs simultaneously enhances CO_2 permeability and CO_2/N_2 selectivity in the mixed matrix membranes. In addition, MMMs with the thickest ZIF-C nanosheet presents better performance. A CO_2 permeability of 387.2 Barrer accompanied with a CO_2/N_2 selectivity of 47.1 has been documented, nearly doubled in CO_2 permeability with slightly increased selectivity compared with membranes containing thinner nanosheets.

INTRODUCTION

Owing to the intrinsic porous structures, metal–organic frameworks (MOFs), a class of crystalline materials constituted of metal ions/clusters linked by organic ligands, have drawn extensive attentions in diverse fields during the past decades, such as energy storage, catalysis and separation/storage.[1-4] The nanoscale caves with tunable sizes (from angstrom to nanometre range), high surface area and adjustable surface make them promising as molecular sieving materials to overcome the trade-off relationship[5] between permeability and selectivity of traditional polymeric membranes, which also known as the Robeson Upper bound.[3, 6-8] Therefore, enormous effort has been devoted to developing new MOFs and MOF-based membranes aiming for enhanced separation performances.[9-13]

Incorporating MOFs into polymeric membranes to fabricate mixed matrix membranes (MMMs) is one of the most studied approaches considering the combination of the processability of polymeric substrates and the molecular sieving capability of MOFs, the advantages from both sides.[2, 14, 15] For instance, Bae et al. reported that the addition of submicrometer zeolitic imidazolate framework (ZIF)-90 into 6FDA-DAM realized around 85% and 61% increment in CO_2 permeability (from 390 to 720 Barrer) and CO_2/CH_4 selectivity, respectively.[16] In another work reported by Hwang et al., the CO_2 permeability benefits an 8.9-fold enhancement (70 to 623 Barrer), with a slight loss in selectivity.[17] This significant gain in CO_2 permeation is contributed by the increased CO_2 diffusivity from the hollow structure of fillers, the pore inside ZIF-C crystals, and the enhanced solubility from the imidazole organic linkers.

Despite these greatly improvements, the performances of the majority of the MMMs are still far below the theoretically predicted values.[1, 3, 8, 18-21] Among various reasons, the filler geometry is a crucial factor affecting the interfacial morphology between fillers and the polymer matrix.[22] Sphere [23, 24] is the most common shape of the fillers used in MMMs. Researchers have found that the size of fillers has a significant influence on the final performance of MMMs. As a rule of thumb, MOFs with smaller sizes have higher external surface areas, and thus, larger interfacial areas between polymer and nanoparticles can be anticipated. However, the fabrication of highly crystalline MOF nanoparticles is thermal-dynamically unfavourable and technically challenging. On the other hand, the tendency of agglomeration for small particles is more significant than their larger analogies, leading to poor filler dispersion.[25-27] Therefore, the optimization of nanoparticle size should be taken into consideration. Zheng *et al.* prepared a series of MMMs containing Pebax and ZIF-8 nanoparticles with different sizes (40 – 110 nm) and found out that the larger nanoparticles are preferable for both CO_2 permeability and CO_2/N_2 selectivity, with the studied ZIF-8 loadings.[27] It is believed that the presence of

larger ZIF-8s in MMMs leads to a higher free volume and thus higher permeability, and the higher specific surface area of ZIF-8 nanoparticles benefits the selectivity. Similar results have been reported in several research works,[25, 26] but further increases in particle size may not bring positive results; the visible sedimentation of particles inside membranes and the voids between fillers and polymer matrix were observed in MMMs containing 10 wt.% MIL-53(Al) particles with a size of 3.2 μm. [28]

Very recently, MOFs with a higher aspect ratio, such as sheet-, flake-, or platelet-like MOFs, have been considered as potentially more promising fillers due to the increased permeation resistance for rejected gas (and hence the enhanced separation factor) as well as the shortcut path for desired molecules (and therefore the elevated flux).[21, 23, 29-31] However, only limited literature can be found applying MOF nanosheets in MMMs for gas separation applications.[18, 19, 32-34] Gascon and co-workers[18] synthesized 2D copper 1,4-benzenedicarboxylate (CuBDC) nanosheets with the thicknesses of 5 – 25 nm and added them into Matrimid membranes. The resultant MMMs display an improved CO_2/CH_4 selectivity (30 – 80%) compared to the neat polymer. Moreover, the presence of the nanosheets counteracts the plasticization due mainly to the superior separation performance of the 2D structure. It is worth mentioning that the MMMs containing bulk or nanocrystal CuBDC do not display this enhanced performance. Under the same conceptual framework, Zhao et al. also found similar results in membranes comprising of PBI and $[Cu_2(ndc)_2(dabco)]$ nanosheets for H_2/CO_2 separation.[20] Wang and co-workers employed two-dimensional ZIF-L into polyimides; the incorporation of ZIF-L into the membrane greatly improved both the H_2 permeability and H_2/CO_2 selectivity.[31]

The above studies have revealed the great potential of MMMs with lamellar MOFs as nanofillers. Up to now, most of the MOF nanosheets were prepared via a top-down or bottom-up approach.[29] The top-down method normally refers to exfoliating lamellar MOF sheets from bulky MOFs by mechanical forces (e.g., ultrasonication), while the bottom-up approach means a direct synthesis of lamellar MOFs to precisely control the reaction conditions (e.g., adjusting solvents or employing surfactants). Despite the diversity of synthesis methods developed for lamellar MOFs, a facile and economical way of synthesis lamellar MOFs with controllable thickness and morphology is still highly desirable.

Hence, in this work, a simple fabrication method for ZIF cuboids (ZIF-Cs) nano-sheets was developed for the first time. The reaction was conducted in an aqueous solution at room temperature with the presence of poly(vinyl alcohol) (PVA) in addition to the ZIF precursors (zinc ions and imidazolate ligands). The material properties of the as-synthesized ZIF-Cs were analyzed by various characterization approaches: Scanning Electron Microscope (SEM), Atomic Force Microscopy (AFM), Fourier-Transform Infrared (FTIR) Spectroscopy, X-ray Photoelectron Spectroscopy (XPS), N_2 adsorption and X-Ray Crystallography (XRD). Later, these ZIF-Cs were incorporated into Pebax 1657 to study their influences on morphology, chemistry nature and crystallinity of MMMs. Mixed gas permeation tests were conducted to reveal the impact of nanocuboids thicknesses on the CO_2 separation performance of resultant MMMs.

EXPERIMENT

MATERIALS

$Zn(NO_3)_2{\cdot}6H_2O$ and 2-methylimidazole (Hmim) were purchased from Sigma, Norway. Poly(vinyl alcohol) (PVA, Mn 30000 – 70000, 72000, and 85000 – 124000 g/mol) were ordered from Sigma, Germany. Pebax 1657 pellets were ordered from Arkema, France. Ethanol (96%) was purchased from VWR, Norway. All the chemicals were used without further treatment.

ZIF-C SYNTHESIS

In brief, PVA was dissolved in DI water at 80 °C with reflux to prepare 1 wt.% PVA solution. After the solution cooled down to room temperature, 0.59 g $Zn(NO_3)_2{\cdot}6H_2O$ and 1.32 g of Hmim were added into 40 ml PVA solution, respectively. After the $Zn(NO_3)_2{\cdot}6H_2O$ and Hmim had been fully dissolved, the two solutions were mixed, and the reaction was carried out at room temperature for 3 hours. Afterwards, the ZIF-C was separated using a centrifuge with 10000 rpm for 10 mins. Obtained ZIF-C particles were re-dispersed in DI water and centrifuged two times more to remove the residual PVA. Finally, the ZIF-C particles were dispersed in DI water to prevent possible aggregation. The ZIF-C content in the dispersion was calculated by drying 0.5g of the dispersion at 40 °C in a vacuum oven for 1 night. Three PVAs with different molecular weights have been used; hence the ZIF-Cs prepared from PVA with a molecular weight of XX are defined as "ZIF-C XX".

MEMBRANE PREPARATION

MMMs were prepared through a knife-casting method similar to those in the literature.[35] Typically, Pebax 1657 was dissolved in $EtOH/H_2O$ mixture (70/30 vol%) with reflux at 80 °C for ~ 3 hours with a concentration of 8 wt.%. Pebax solution was mixed with the desired amount of ZIF-C aqueous dispersion under stirring for at least 6 hours. The mixture was then cast on a glass plate using a casting knife (PA-4302, BYK-CHEMIE GMBH, Germany) with a wet gap of ~ 600 μm. The cast membrane was then placed in a ventilated oven at 40 °C for at least 6 hours. After the membrane was removed from the glass plates, it was dried in a vacuum oven at 60 °C for another 6 hours before further characterization.

CHARACTERIZATION

The topography of ZIF-C nanosheets was characterized by an AFM (Dimension Icon, Bruker) using the ScanAsyst mode. The as-prepared nanosheets were dispersed in ethanol and dried on cover glasses for AFM analysis. An SEM (TM3030 tabletop microscope, Hitachi) was also employed for the morphology study of these ZIF-C nanosheets and the resultant MMMs. For MMMs, cross-section specimens were obtained by breaking the samples in liquid N_2. A sputter coating with gold (2 mins) was conducted for all samples before SEM characterization.

The thermal stability tests for the ZIF-C nanosheets and the MMMs were performed by employing a TGA (TG 209F1 Libra, Netzsch). Samples with a weight of 10 – 20 mg were used. All samples were heated from room temperature to 800 °C with a heating rate of 10 °C / min. N2 was used as both protective and sweep gas.

A Tristar II 3020 (Micromeritics Instruments, USA) was used for N_2 sorption isotherms. Before the measurements, ZIF-C samples were degassed at room temperature overnight with vacuum.

The crystallinity of the prepared nanosheets and MMMs was analyzed by a Bruker D8 A25 DaVinci X-ray Diffractometer (Bruker) with characteristic wavelength λ=1.54 Å (Cu Kα radiation). The scans were taken in the 2θ range from 5° to 75°.

FTIR spectroscopy was performed employing a Thermo Nicolet Nexus spectrometer. The obtained spectra were an average of 16 scans with wavenumber from 550 cm^{-1} to 4000 cm^{-1}.

X-ray photoelectron spectroscopy (XPS) was performed on a PHI-560 ESCA (Perkin Elmer) using a nonmonochromatic Mg Kα excitation source at 15 kV. The C 1s peak position was set to 284.6 eV as an internal standard.

Gas permeation performance of MMMs was conducted using a mixed-gas permeation setup reported elsewhere.[35, 36] Feed gas was the CO_2/N_2 (10/90 vol%) gas mixture, whereas pure CH_4 was used as the sweep gas. The water vapor was introduced by humidified feed and sweep gas, and the humid gases were mixed with dry gases with accurate flow ratio to achieve the desired humidity. All gas permeation tests were carried out at room temperature with a feed pressure and sweep pressure of 2.0 and 1.05 bar, respectively. The compositions of permeate and retentate streams were analyzed by a calibrated gas chromatograph (490 Micro GC, Agilent) throughout the tests.

The permeability coefficient (Pi) of the ith penetrant species can be calculated from equation (1):

$$P_i = \frac{N_{perm}(1 - y_{H_2O})y_i}{A(p_{i,feed} - p_{i,perm})} \quad (1)$$

where N_{perm} is the total permeate flow measured by a bubble flow meter (ml/min), y_{H2O} refers to the molar fraction of the water in the permeate flow (calculated according to the relative humidity value and the vapor pressure at the tested temperature), y_i is the molar fraction of the gas i in the permeate flow (%), and $p_{i,feed}$ and $p_{i,perm}$ stand out the partial pressures of the gas i in feed and permeate streams, respectively. In the present work, the gas permeability is expressed in the unit of Barrer (1 Barrer = 10^{-10} $cm^3(STP)\cdot cm\cdot cm^{-2}\cdot s^{-1}\cdot cmHg^{-1}$). The separation factor was determined from equation (2):

$$\alpha_{AB} = \frac{y_A/y_B}{x_A/x_B} \quad (2)$$

y_A and y_B are the mole ratio of gas A and B in the permeate stream, while x_A and x_B are the mole ratio of gas A and B in the feed side.

RESULTS AND DISCUSSION

ZIF-C SYNTHESIS AND CHARACTERIZATION

It is well-known that additives, such as small molecules,[37] surfactants,[38-41] or polymers, [42-44] play a very important role on nanoparticle morphology because of the competition of the reactants between other reactants and the additives, the adjusted pH, and the restricted regions for crystal growth or selective absorption.[45] To investigate the effect of PVA addition on the formation of ZIF-Cs, the morphologies and material properties of the as-prepared ZIF-Cs were characterized via various technics, and the results are shown in **Figure 1** and **Table S1**. The XRD curves of these ZIF-C generated in PVA solution have almost identical patterns with the one from H_2O,[46] as shown in **Figure 1 (F)**, suggesting that the obtained product has the same crystal structure with the ZIF-L, and the presence of PVA does not affect the crystal structure. The only difference between these XRD results is that the ZIF-C 85-124 has slightly higher intensity, followed by ZIF-72 and ZIF-C 30-70, indicating its highest crystallinity. N_2 adsorption results (**Figure S1**) show that insignificant pores exist inside these ZIF-Cs, indicating ZIF-Cs' non-porous crystal structure similar to that of the leaf-like ZIF-C. The presence of PVA seems to have insignificant influence from this respect.

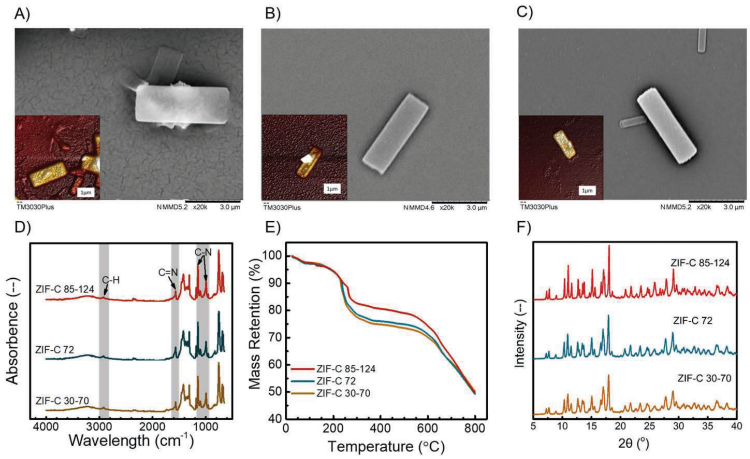

Figure 1 The morphology of A) ZIF-C 30-70, B) ZIF-C 72 and C) ZIF-C 85-124 nanosheets, and D) FTIR spectra, E) TGA curves and F) XRD results of ZIF-C nanosheets prepared in PVA solutions.

However, all ZIF-Cs synthesized in PVA solutions display cuboid morphology, different from the leaf-like ZIF-L reported by Wang *et al.*.[46] In addition, all these ZIF-Cs have a similar size compared with their analogue prepared in H_2O, except for the different thickness. For example, the dimensions for ZIF-C 30-70 are 5 μm × 2 μm × 70 nm, as listed in **Table S1**, while the leaf-like ZIF-L has the same size but larger thickness (150 nm).[46] Moreover, the length and width of these cuboid ZIF-Cs are negatively related with the molecular weight of the used PVA, even though the same concentration was used. On the other hand, with respect to the thickness, a totally opposite trend is observed that, the longer PVA chain is used in synthesis solution, the thicker the ZIF-Cs are (85-124: 170 nm, 72: 120 nm and 30-70: 70 nm). Moreover, the difference between the thickness of these ZIF-Cs prepared in PVA solution and the one from H_2O (150 nm) is much less. It is speculated that the PVA chains may attach on the surface of small crystals by the interaction between the dangling Zn center[32] and OH groups[33] and inhibit the growth among certain directions, leading to the cuboid 2D morphology. In addition, the results indicate that the shorter PVA chains have the higher possibility to attach on the surface of ZIF-Cs as a result of the higher mobility in solution, generating more inhibition and thus the thinner ZIF-C. To confirm this speculation, XPS tests were conducted and the results are present in **Figure S2-3**. The main peak in the C 1s spectra of the ZIF-C 3070 has been correlated to the C-C bond at 284.8 eV. The shoulder peak at higher binding energy is assigned to PVA (**Figure S2 (A)**). Significant peak shifts in Zn 2p and N 1s spectra have been observed when compare with pure ZIF benchmark, suggesting the formation of coordination bond between Zn and O. Similar behavior has been also reported in the lierature.[47]

The chemistry of the ZIF-Cs synthesized in PVA solutions are evaluated by FT-IR, and the resultant spectra are shown in **Figure 1 (D)**. Considering the chemical structure of ZIF-Cs, their characteristic peaks are mainly derived by the imidazole ring. For example, the one at 1565 cm^{-1} associates with the vibrations of C=N bond in imidazole ring, as well as the peaks at 1143, 992 cm^{-1} (C-N) and 2925 cm^{-1} (C-H).[48, 49] All these peaks are agreed with the spectrum of the ZIF-L synthesized in H_2O. Moreover, a board peak between 3500 – 3100 cm^{-1} and the peaks at 1420 and 1375 cm^{-1} exist in three ZIF-Cs spectra, usually referring to the presence of OH bonds, CH_2 blend, and C-H deformation, respectively, which suggest the remaining PVA inside the ZIF-Cs nanosheets.[50]

The thermal properties of 2D ZIF-Cs prepared in different PVA solutions are also evaluated by TGA, and the results are shown in **Figure 1 (D)**. As can be seen, all the ZIF-Cs synthesized in PVA solution have similar three-stage decomposition curves. The first one is shown below 100 ºC, and only < 3% weight is observed from the weight profiles, which corresponds to the removal of the remaining solvent (H_2O). Following a small plateau between 100 and 200 ºC, a steep reduction in the weights of these ZIF-Cs occurred at around 220 – 260 ºC. The possible reason may be loss of the structural water molecules[37] and the residual PVA. During crystal growth, because of the interaction between zinc ions and the OH groups, PVA polymeric chains may be absorbed on the surface of the developing crystals, then inlaid inside the later growing ZIF-C crystal and change the shape. In addition, it is worth mentioning that the remaining weight of ZIF-Cs at around 220 ºC (85-124 > 72 > 30-70) matches with the order of PVA molecular weight, indicating longer PVA polymeric chains have less mobility and absorb less onto ZIF-C crystals; hence less PVA is contained in ZIF-C nanosheets. All ZIF-C nanosheets begin to collapse and are carbonized from 500 ºC, which fits the profile of ZIF-L crystal reported in the literature.[51-53] These results are also in agreement with the FTIR results.

PEBAX/ZIF-C MEMBRANE CHARACTERIZATION

For mixed matrix membranes, the interfacial relationship between the polymeric matrix and inorganic fillers is crucial for the overall performance.[2] For example, the poor interface between fillers and polymeric chains may cause nanoscale interface voids, further causing the lower transport resistance and low or even non-selectivity in the membrane. Inorganic fillers, especially nano-fillers, may be more easily aggregated, which also leads to the formation of pinholes inside the membrane, thus resulting in the deteriorated selectivity.

The surface and cross-section SEM images of MMMs with various ZIF-C 85-124 loading are present in **Figure 2 (A-D)**. The neat Pebax membranes have smooth, defect-free surface and cross-section, as expected. For the ones containing ZIF-C 85-124 of up to 20 wt.%, the ZIF-C 85-124 is uniformly dispersed in the membrane without noticeable agglomeration. Similar morphology of MMMs with the other ZIF-Cs were also observed from SEM, as shown in **Figure S2** and **Figure S3**. These images demonstrate the good polymer-filler contact between the ZIF-C prepared from PVA solution and Pebax matrix, which may be attributed by the PVA chains around ZIF-Cs. The influence of different ZIF-C on the morphology of MMMs was also investigated, as shown in **Figure 2 (D-E)**. The membrane contained ZIF-C 30-70 has the smallest nanofillers, while the fillers in MMMs with ZIF-C 85-124 has the biggest size among these three, which matched the morphology of ZIF-Cs. Moreover, these three ZIF-Cs are generally uniformly distributed on the surface and cross-section of MMMs with a loading of 20 wt. %. However, few ZIF-C 30-70 sheets are observed to be stacked from the cross-section, due probably to the trend of aggregation of very thin nanosheets.

The chemistry nature of these MMMs with different ZIF-Cs is studied by FT-IR. The typical peaks of neat polymer (3303 cm-1 for N-H, 2871 cm-1 for C-H, 1731 cm-1 for C=P, 1638 cm-1 for –C=O and 1095 cm-1 for C-O) are apparent in the spectrum of Pebax membrane, as evidenced in Figure S4 (C), which is in accordance with its chemical structure and the peaks reported in the literature.27 With the increasing ZIF-C 85-124 content, the intensities of these peaks decrease while those from ZIF-Cs, like C-N bond in imidazole ring (1143 and 992 cm-1), become more and more significant in the FTIR curves, as present in Figure 3 (A), indicating that the content of ZIF-Cs 85-124 inside MMMs increases as expected. The other MMMs containing ZIF-C 72 or ZIF-30-70 have a similar trend with the addition of ZIF-C nanosheets and the spectra are presented in Figure S4. Meanwhile, no peaks have been generated or disappeared in the spectra of MMMs compared with those of the neat polymer or the ZIF-Cs; hence we conclude there is no chemical reaction between ZIF-C 85-124 and the Pebax polymeric matrix. The ZIF-C nano-sheets are physically embedded into the Pebax polymeric matrix. For the MMMs containing different ZIF-Cs with the same loading, their spectra are found to be almost identical, demonstrating the chemical similarity of these ZIF-C nano-sheets and thus the resultant MMMs, as shown in **Figure 3 (D)**.

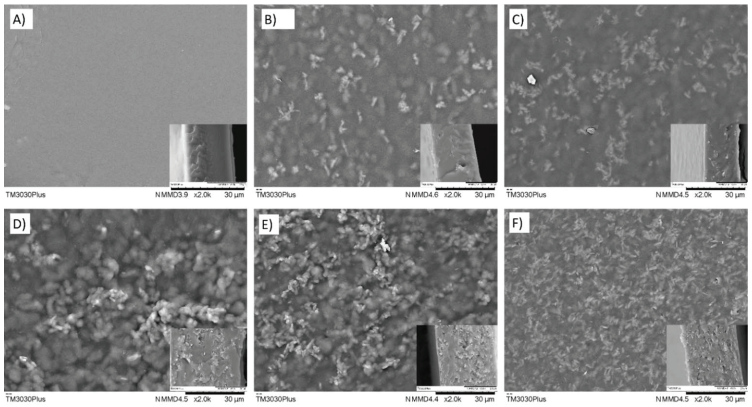

Figure 2. Morphology of MMMs with A) 0%, B) 5%, C) 10% and D) 20% ZIF-C 85-124, E) 20% ZIF-C 72 and F) 20% ZIF-C 30-70.

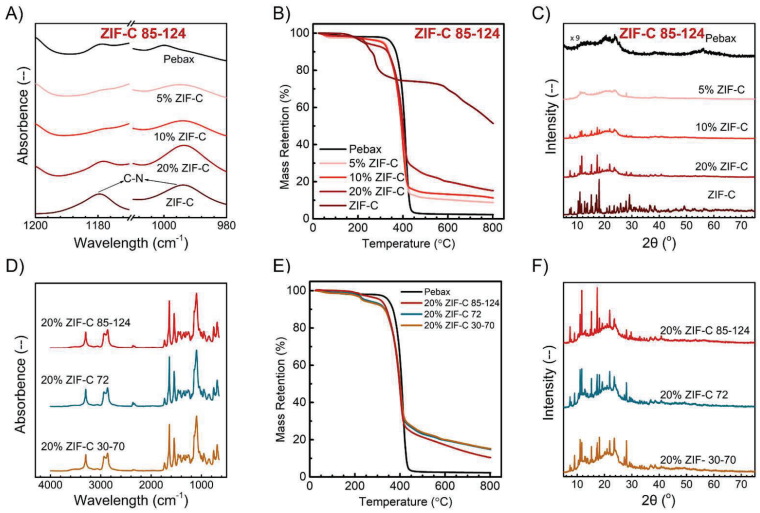

Figure 3. The A) FTIR spectra, B) TGA curves and C) XRD results of Pebax +ZIF-C 85-124 MMMs with different ZIF-C content, and D) FTIR spectra, E) TGA curves and F) XRD results of MMMs with 20% different ZIF-C nanosheets. The scale of Pebax' XRD results are 9 times smaller than the others.

The thermal stability of MMMs containing ZIF-C nanosheets has been investigated by TGA. The neat polymer starts decomposed around 330 °C with a single-stage behavior, which is higher than that of ZIF-Cs. As a result, the thermal stability of MMMs deteriorates with the increasing content of ZIF-Cs, as shown in **Figures 3(B)** and **Figure S5**. For the MMMs with 5% ZIF-C 85-124, the T_{onset} is still higher than 300 °C, but the value for MMMs with 20% ZIF-C decreases to around 200 °C with only 4% loss at this stage. From these results, the addition of ZIF-C into Pebax matrix is also confirmed, agreed with the FTIR results. However, most of the membranes for post-combustion CO_2 capture are operated at a temperature lower than 80 °C, depending on the process. Therefore, these membranes are still qualified in terms of thermal stability. For the membranes containing different ZIF-Cs, their thermal stabilities are very similar, as shown in **Figure 3 (E)**. The only difference is the slightly lower weight loss between 200 and 300 °C in the one with ZIF-C 85-124 because of the marginally better thermal stability of ZIF-C 85-124 compared with the other ZIF-Cs.

The crystallinity analysis of the MMMs was also conducted by XRD, as shown in **Figure 3(C), (F)** and **Figure S6**. The XRD pattern of Pebax displays an amorphous structure, as expected, with the broad pattern shape from 9° to 27°. From **Figure 3(C)**, it is clearly observed that the incorporation of ZIF-C 85-124 into MMMs introduces sharp peaks into the broad curve of the neat polymer. These peaks become clearer with the increasing ZIF-C loading. A similar trend is also observed for MMMs with different ZIF-Cs. The one with ZIF-C 85-124 has slightly sharper ZIF-C peaks compared with the MMMs containing the other ZIF-Cs because of the higher intensity of ZIF-C 85-124.

GAS PERMEATION PROPERTIES

The mixed gas permeation tests are conducted to study the effects of different ZIF-C nanosheets on the CO_2 separation performance of Pebax + ZIF-C MMMs. As shown in **Figure 4**, the CO_2 permeability ($P(CO_2)$) of neat Pebax 1657 membrane under dry condition is 71.3 Barrer with a CO_2/N_2 selectivity of around 30, which is in agreement with the literature value.[35] Regardless of the different morphologies, the addition of these ZIF-C nanosheets increases the $P(CO_2)$ and CO_2/N_2 separation factor of MMMs under dry condition within ZIF-Cs contents of up to 10 wt.%. The CO_2 permeability of MMMs with 10 wt.% ZIF-C 85-124 is found to be 141.7 Barrer, almost twice of that of the neat Pebax membrane, with a slightly enhanced CO_2/N_2 selectivity of 32.8. These results may be explained from several aspects. Firstly, the interlayer channels inside ZIF-C endows a fast transportation shortcut for CO_2 and therefore benefits the CO_2 permeability.[54] Meanwhile, for N_2, the presence of ZIF-C rigidifies the polymer chains[55, 56] and increases tortuosity and thus the transport pathway for gases, leading to enhanced CO_2/N_2 selectivity. In addition, the increment in CO_2/N_2 selectivity implies the absence of interface voids between polymer and filler phases at low ZIF-C loading.[6] However, the existence of interface voids was observed with further addition of ZIF-C,[57] as the result of the decreased CO_2 permeability and CO_2/N_2 in all MMMs. In the case of CO_2 permeability, the contribution of this pathway counteracts the benefit from the selective sorption of ZIF-Cs, causing a slight loss in CO_2 permeability rather than a further increment.

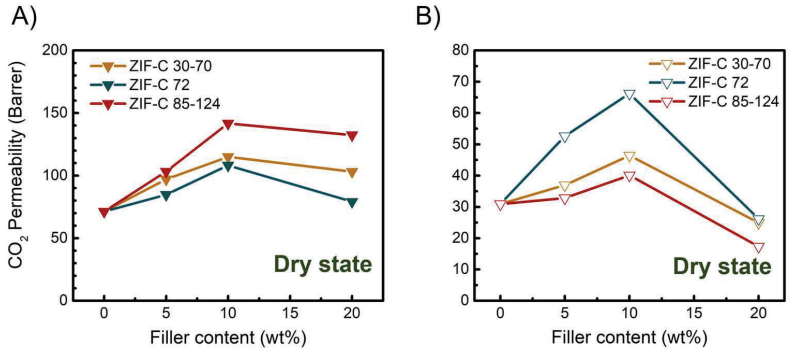

Figure 4. The (A) CO_2 permeability and (B) CO_2/N_2 selectivity of Pebax + ZIF-C MMMs as a function of filler content at the dry state.

In addition to the nanofiller loading, the morphology of these ZIF-C nanosheets also affects the final performances of MMMs. The membranes with ZIF-C 85-124 show the highest CO_2 permeability within all studied filler contents in this work, followed by ZIF-C 30-70 and ZIF-C 72, while the selectivities show a reverse order. The highest improvement in CO_2 permeability may be explained by the greater effect of the selective CO_2 adsorption of thicker ZIF-C nanosheets due to the more available pathway for gases between layers. Moreover, the membranes containing thicker 2D nanosheets may have lower tortuosity and thus lower gas transport resistance, leading to higher gas permeability. On the other hand, lower tortuosity is usually less favorable to the selectivity, so as the relative lower CO_2/N_2 selectivity of MMMs with ZIF-C 85-124 compared to the other membranes. These facts also explain the lower permeability and higher selectivity of MMMs with ZIF-C 72. However, for MMMs with the ZIF-C 30-70, the lower CO_2 permeability and the lower CO_2/N_2 selectivity may be ascribed to the stacked nanosheets inside MMMs, as observed from SEM images, leading to the less selective voids between nanosheets.

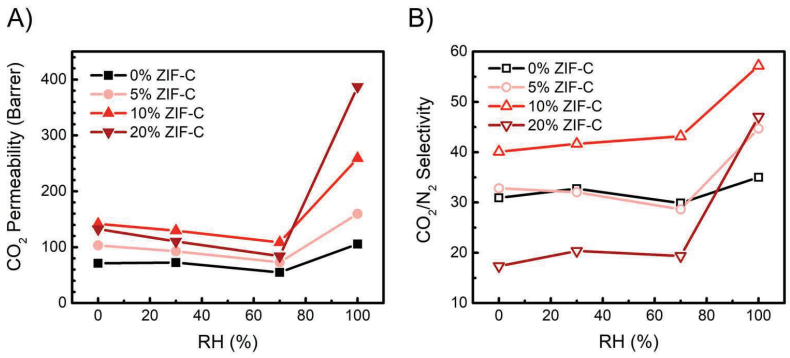

Figure 5. (A) CO_2 permeability and (B) CO_2/N_2 selectivity of Pebax + ZIF-C 85-124 MMMs as a function of RH.

As a hydrophilic material, the gas separation performance of Pebax is greatly affected by the relative humidity of the tested gases. The CO_2 permeability of the neat Pebax membrane decreases and then increases with the increasing relative humidity, and a similar trend is also observed for CO_2/N_2 selectivity, as shown in **Figure 5**. Water vapor first occupies the original free volume, leading to the decreased gas permeability and then swells Pebax polymeric chains, resulting in enhanced gas flux. The fully swollen polymer matrix also benefits the solubility and diffusivity of CO_2, thereby obtaining the simultaneous increment in CO_2 permeability and CO_2/N_2 selectivity. This trend is also observed in MMMs containing ZIF-Cs nanosheets, as presented in **Figure 5**. For instance, the Pebax + 10% ZIF-C 85-124 membrane has a CO_2 permeability of 141.7 Barrer with a selectivity of 40.1 at dry condition. With humidity increasing to 70 RH%, the CO_2 permeability decreases to 108.6 Barrer. However, further humidification from 70 RH% to 100 RH% leads to an around 2-fold increment in CO_2 permeability (259.2 Barrer) and the CO_2/N_2 selectivity (57.2). Apart from the benefits as mentioned, the rigidification of Pebax chains around ZIF-C MMMs could be eased due to the increased flexibility at the swollen state. However, despite the low CO_2 permeability and CO_2/N_2 selectivity under dry condition, the membrane with 20% ZIF-C 85-124 has the most significant increase in CO_2 permeability (4.6-flod, 387.2 Barrer) and CO_2/N_2 selectivity (2.4-fold, 47.1) when the separated gas is fully saturated with water vapor. This is because that the swollen Pebax chains fill the interfacial voids between polymeric matric and ZIF-C nanosheets, which reduces the nonselective elements and increases the selectivity. In addition to the benefit from humidified membranes, the selective adsorption via ZIF-Cs also benefits the CO_2 permeation, while the transportation of N_2 only depends on the solution-diffusion mechanism. Similar results are obtained for MMMs with ZIF-C 30-70 and ZIF-C 72, as shown in **Figure S7** and **S8**.

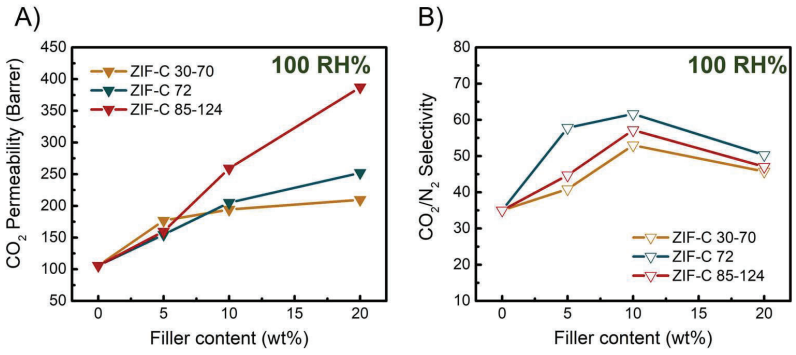

Figure 6. The (A) CO_2 permeability and (B) CO_2/N_2 selectivity of Pebax + ZIF-C MMMs as a function of filler content at 100 RH%

Therefore, under the fully water vapor saturated condition, CO_2 separation performance of the Pebax + ZIF-Cs nanosheets has different behavior compared with that under the dry condition. Increment has been observed in both CO_2 permeability and selectivity for all MMMs as shown in **Figure 6**. The influence of morphology for CO_2 separation performance under the fully water vapor saturated condition is quite similar to that under the dry condition. But due to the presence of more stacked nanosheets, the MMMs with ZIF-C 30-70 display the lowest CO_2 permeability and CO_2/N_2 selectivity when the ZIF-C nanosheets loading is higher than 5 wt.% even though they are the median under the dry condition.

These performances are evaluated in comparison with the 2008 Robeson bound,[5] as shown in **Figure 7**, and some Pebax

1657-based MMMs in the literature [1-3, 27, 35, 58-67], as presented in **Table 1**. It is clearly seen that the incorporation of ZIF-C 85-124 pushes the performance close to the upper bound with the loading of up to 10 wt.%, and then move along the upper bound with the higher ZIF-C loading. In addition, it is clearly shown that the membranes reported in this work have a higher permeability with lower CO_2/N_2 selectivity.

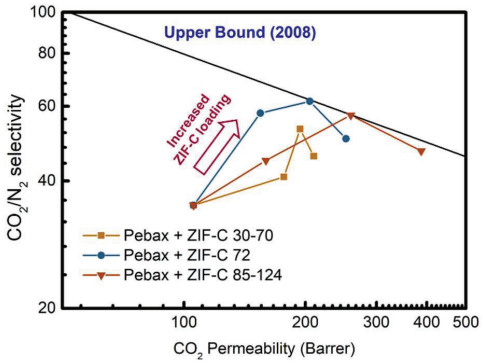

Figure 7. CO_2/N_2 separation performances of Pebax 1657-based MMMs at 100% RH condition separation.

Table 1 The start-of-art CO_2 separation performance of the Pebax 1657-based MMMs

Fillers	P(CO_2) / Barrer	CO_2/N_2 selectivity	Tested condition	Ref
Zeolite-4A[a]	129.5	94.2	Single gas, 24.5 Bar, R.T.	[59]
Fumed silica	74.12	101.53	Mixed gas, 12 Bar, 25 °C	[67]
ZIF-8 (90 nm)	99.7	59.6	Single gas, 1 Bar, 20 °C	[27]
MIL-53	95.7	49.9	Single gas, 10 Bar, 35 °C	[65]
Attapulgite	~ 170	52	Single gas, 35 °C	[64]
Graphene oxide (GO)	100	91	Single, 3 Bar, 25 °C	[68]
Porous reduced GO	119	104	2 Bar, 30 °C	[62]
Imidazole functionalized GO	76.2	105	Single gas, 8 Bar, 25 °C	[63]
MoS_2	64	93	Single gas, 2 Bar, 30 °C	[69]
Multi-walled carbon nanotubes (MWCNTs) (33 %)	361	52	Single gas, 7 Bar, 35 °C	[60]
MWCNTs (5 %)	262.15	58.5	Single gas, 1 Bar, R.T.	[58]
ZIF-C 85-124 (20 %)	387.2	47.1	Humid mixed gas, 2 Bar, 24 °C	This work
ZIF-C 72k (10 %)	205.1	61.6		
ZIF-C 30-70 (10 %)	194.2	53.0		

CONCLUSIONS

In this work, a simple preparation method for cuboid ZIF-C nanosheets with controllable morphology has been developed. Three PVA with different molecular weights were employed to investigate its effect on the morphology of the nanosheets. The results show that the molecular weight of the additive PVA has a significant influence on the thickness and size of the as-synthesized ZIF-C nanosheets, as well as the material properties. The higher MW the PVA has, the thicker and smaller in both length and width the ZIF-C nanosheets are formed. The crystal structure of the ZIF-C is proven by the N_2 adsorption experiment and XRD tests. During the growth of crystals, PVA chains are selectively attached to the surface of the crystals and inhibit the growth along with the particular directions. Thus, the shape and the size of these nanosheets can be manipulated. The existence of PVA inside the ZIF-C nanosheets is confirmed by FTIR and TGA analysis. In addition, the one made from PVA 85-124 solution has the best

thermal stability and highest crystallinity among the as-synthesized ZIF-C nanosheets.

With the Pebax 1657 as the polymeric matrix, the effect of these ZIF-C nanosheets in mixed matrix membranes has been systemically studied by various techniques. The results from FTIR, XRD, and TGA tests confirm the successful incorporation of the ZIF-C nanosheets into the Pebax phase. The surface and cross-section images from SEM analysis show that these nanosheets are generally well-dispersed in the MMMs. However, stacked ZIF-C 30-70s, the thinnest nanosheet obtained in this work, are noticeable from SEM images. Moreover, the mixed gas permeation results show that the addition of the ZIF-C nanosheets increases the permeability and CO_2/N_2 selectivity, regardless of the kind or the content of the nanosheets. ZIF-C 85-124, the thickest nanosheet prepared in this work, is found to be the most efficient nanofiller in promoting CO_2 transport compared with the others because of the selective adsorption of CO_2 inside the ZIF-C nanosheets. Furthermore, the presence of water vapor significantly enhances the gas transport property, and the CO_2 separation efficiency of these MMMs. The highest CO_2 permeability (387.2 Barrer) with a CO_2/N_2 selectivity of 47.1 is obtained from the Pebax + 20% ZIF-C 85-124 MMM.

Overall, this method provides a facile approach to the fabrication of ZIF-C nanosheets with controllable size and thickness. The as-synthesized ZIF-C nanosheets can be used as promising nano-fillers in MMMs to enhance CO2 separation performance. The preparation methods reported here may be further studied by using different additives to form other shapes of nanoparticles, or to better understand the effect of the additives on the crystal formation and growth, and the morphology of the nanoparticles. Other polymers may also be applied as the membrane polymer phases for MMMs with even better CO_2 separation performance or for different applications.

ASSOCIATED CONTENT

Supporting Information

The Supporting Information is available free of charge on the ACS Publications website. Detailed information about the size and the curves obtained from N_2 absorption and XPS of the as-synthesized ZIF-C were listed in supporting information (Table S1 to Figure S4). The SEM images, FTIR spectra, TGA curves, XRD results and the permeation results of the MMMs containing ZIF-C 72 and ZIF-C 30-70 could be found from Figure S5-S11.

AUTHOR INFORMATION

Corresponding Author

Email: deng@nt.ntnu.no

Author Contributions

The manuscript was written through the contributions of all authors. All authors have given approval to the final version of the manuscript.

Funding Sources

This work is supported by the Research Council of Norway through the CLIMIT program ("POLYMEM" project, No. 254791).

Notes

There are no conflicts to declare.

ACKNOWLEDGMENT

This work is supported by the Research Council of Norway through the CLIMIT program ("POLYMEM" project, No. 254791). The authors highly acknowledge Mr Yizhi Zhuo (Department of Structural Engineering, NTNU) and Dr. Weixin Qian (School of Chemical Engineering, East China University of Science and Technology) for their kind help in the AFM and BET characterization.

REFERENCES

1. Seoane, B.; Coronas, J.; Gascon, I.; Etxeberria Benavides, M.; Karvan, O.; Caro, J.; Kapteijn, F.; Gascon, J., Metal-organic framework based mixed matrix membranes: a solution for highly efficient CO_2 capture? *Chem. Soc. Rev.* **2015,** 44, (8), 2421-54.
2. Chung, T.-S.; Jiang, L. Y.; Li, Y.; Kulprathipanja, S., Mixed matrix membranes (MMMs) comprising organic polymers with dispersed inorganic fillers for gas separation. *Prog. Polym. Sci.* **2007,** 32, (4), 483-507.
3. Kang, Z.; Fan, L.; Sun, D., Recent advances and challenges of metal–organic framework membranes for gas separation. *J. Mater. Chem. A* **2017,** 5, (21), 10073-10091.
4. Moghadam, P. Z.; Li, A.; Wiggin, S. B.; Tao, A.; Maloney, A. G. P.; Wood, P. A.; Ward, S. C.; Fairen-Jimenez, D., Development of a Cambridge Structural Database Subset: A Collection of Metal–Organic Frameworks for Past, Present, and Future. *Chem. Mater.* **2017,** 29, (7), 2618-2625.
5. Robeson, L. M., The upper bound revisited. *J. Membr. Sci.* **2008,** 320, (1), 390-400.
6. Park, H. B.; Kamcev, J.; Robeson, L. M.; Elimelech, M.; Freeman, B. D., Maximizing the right stuff: The trade-off between membrane permeability and selectivity. *Science* **2017,** 356, (6343), eaab0530.
7. Liu, M.; Gurr, P. A.; Fu, Q.; Webley, P. A.; Qiao, G. G., Two-dimensional nanosheet-based gas separation membranes. *J. Mater. Chem. A* **2018,** 6, (46), 23169-23196.
8. Lin, R.; Villacorta Hernandez, B.; Ge, L.; Zhu, Z., Metal organic framework based mixed matrix membranes: an overview on filler/polymer interfaces. *J. Mater. Chem. A* **2018,** 6, (2), 293-312.
9. Mon, M.; Bruno, R.; Tiburcio, E.; Grau-Atienza, A.; Sepúlveda-Escribano, A.; Ramos-Fernandez, E. V.; Fuoco, A.; Esposito, E.; Monteleone, M.; Jansen, J. C.; Cano, J.; Ferrando-Soria, J.; Armentano, D.; Pardo, E., Efficient Gas Separation and Transport Mechanism in Rare Hemilabile Metal–Organic Framework. *Chem. Mater.* **2019,** 31, (15), 5856-5866.
10. Bux, H.; Feldhoff, A.; Cravillon, J.; Wiebcke, M.; Li, Y.-S.; Caro, J., Oriented Zeolitic Imidazolate Framework-8 Membrane with Sharp H_2/C_3H_8 Molecular Sieve Separation. *Chem. Mater.* **2011,** 23, (8), 2262-2269.
11. Chen, S.; Lucier, B. E. G.; Boyle, P. D.; Huang, Y., Understanding The Fascinating Origins of CO_2 Adsorption and Dynamics in MOFs. *Chem. Mater.* **2016,** 28, (16), 5829-5846.
12. Anderson, R.; Rodgers, J.; Argueta, E.; Biong, A.; Gómez-Gualdrón, D. A., Role of Pore Chemistry and Topology in the CO_2 Capture Capabilities of MOFs: From Molecular Simulation to Machine Learning. *Chem. Mater.* **2018,** 30, (18), 6325-6337.
13. Bien, C. E.; Liu, Q.; Wade, C. R., Assessing the Role of Metal Identity on CO2 Adsorption in MOFs Containing M–OH Functional Groups. *Chem. Mater.* **2019**.

14. Hess, S. C.; Grass, R. N.; Stark, W. J., MOF Channels within Porous Polymer Film: Flexible, Self-Supporting ZIF-8 Poly(ether sulfone) Composite Membrane. *Chem. Mater.* **2016,** 28, (21), 7638-7644.
15. Dechnik, J.; Gascon, J.; Doonan, C. J.; Janiak, C.; Sumby, C. J., Mixed-Matrix Membranes. *Angew. Chem. Int. Ed.* **2017,** 56, (32), 9292-9310.
16. Bae, T.-H.; Lee, J. S.; Qiu, W.; Koros, W. J.; Jones, C. W.; Nair, S., A High-Performance Gas-Separation Membrane Containing Submicrometer-Sized Metal–Organic Framework Crystals. *Angew. Chem. Int. Ed.* **2010,** 49, (51), 9863-9866.
17. Hwang, S.; Chi, W. S.; Lee, S. J.; Im, S. H.; Kim, J. H.; Kim, J., Hollow ZIF-8 nanoparticles improve the permeability of mixed matrix membranes for CO_2/CH_4 gas separation. *J. Membr. Sci.* **2015,** 480, 11-19.
18. Rodenas, T.; Luz, I.; Prieto, G.; Seoane, B.; Miro, H.; Corma, A.; Kapteijn, F.; Llabrés i Xamena, F. X.; Gascon, J., Metal–organic framework nanosheets in polymer composite materials for gas separation. *Nature Materials* **2014,** 14, 48.
19. Sabetghadam, A.; Seoane, B.; Keskin, D.; Duim, N.; Rodenas, T.; Shahid, S.; Sorribas, S.; Le Guillouzer, C.; Clet, G.; Tellez, C.; Daturi, M.; Coronas, J.; Kapteijn, F.; Gascon, J., Metal Organic Framework Crystals in Mixed-Matrix Membranes: Impact of the Filler Morphology on the Gas Separation Performance. *Adv. Funct. Mater.* **2016,** 26, (18), 3154-3163.
20. Kang, Z.; Peng, Y.; Hu, Z.; Qian, Y.; Chi, C.; Yeo, L. Y.; Tee, L.; Zhao, D., Mixed matrix membranes composed of two-dimensional metal–organic framework nanosheets for pre-combustion CO_2 capture: a relationship study of filler morphology versus membrane performance. *J. Mater. Chem. A* **2015,** 3, (41), 20801-20810.
21. Galizia, M.; Chi, W. S.; Smith, Z. P.; Merkel, T. C.; Baker, R. W.; Freeman, B. D., 50th Anniversary Perspective: Polymers and Mixed Matrix Membranes for Gas and Vapor Separation: A Review and Prospective Opportunities. *Macromolecules* **2017,** 50, (20), 7809-7843.
22. Jeong, H.-K.; Krych, W.; Ramanan, H.; Nair, S.; Marand, E.; Tsapatsis, M., Fabrication of Polymer/Selective-Flake Nanocomposite Membranes and Their Use in Gas Separation. *Chem. Mater.* **2004,** 16, (20), 3838-3845.
23. Ahmadi, M.; Janakiram, S.; Dai, Z.; Ansaloni, L.; Deng, L., Performance of mixed matrix membranes containing porous two-dimensional (2D) and three-dimensional (3D) fillers for CO_2 separation: a review. *Membranes* **2018,** 8, (3), 50.
24. Janakiram, S.; Ahmadi, M.; Dai, Z.; Ansaloni, L.; Deng, L., Performance of nanocomposite membranes containing 0D to 2D nanofillers for CO_2 separation: A review. *Membranes* **2018,** 8, (2), 24.
25. Japip, S.; Xiao, Y.; Chung, T.-S., Particle-Size Effects on Gas Transport Properties of 6FDA-Durene/ZIF-71 Mixed Matrix Membranes. *Ind. Eng. Chem. Res.* **2016,** 55, (35), 9507-9517.
26. Sánchez-Laínez, J.; Zornoza, B.; Friebe, S.; Caro, J.; Cao, S.; Sabetghadam, A.; Seoane, B.; Gascon, J.; Kapteijn, F.; Le Guillouzer, C.; Clet, G.; Daturi, M.; Téllez, C.; Coronas, J., Influence of ZIF-8 particle size in the performance of polybenzimidazole mixed matrix membranes for pre-combustion CO_2 capture and its validation through interlaboratory test. *J. Membr. Sci.* **2016,** 515, 45-53.
27. Zheng, W.; Ding, R.; Yang, K.; Dai, Y.; Yan, X.; He, G., ZIF-8 nanoparticles with tunable size for enhanced CO_2 capture of Pebax based MMMs. *Sep. Purif. Technol.* **2019,** 214, 111-119.
28. Knebel, A.; Friebe, S.; Bigall, N. C.; Benzaqui, M.; Serre, C.; Caro, J., Comparative Study of MIL-96(Al) as Continuous Metal–Organic Frameworks Layer and Mixed-Matrix Membrane. *ACS Appl. Mater. Interfaces* **2016,** 8, (11), 7536-7544.
29. Zhao, M.; Huang, Y.; Peng, Y.; Huang, Z.; Ma, Q.; Zhang, H., Two-dimensional metal–organic framework nanosheets: synthesis and applications. *Chem. Soc. Rev.* **2018,** 47, (16), 6267-6295.
30. Johnson, J. R.; Koros, W. J., Utilization of nanoplatelets in organic–inorganic hybrid separation materials: Separation advantages and formation challenges. *Journal of the Taiwan Institute of Chemical Engineers* **2009,** 40, (3), 268-275.
31. Kim, S.; Shamsaei, E.; Lin, X.; Hu, Y.; Simon, G. P.; Seong, J. G.; Kim, J. S.; Lee, W. H.; Lee, Y. M.; Wang, H., The enhanced hydrogen separation performance of mixed matrix membranes by incorporation of two-dimensional ZIF-L into polyimide containing hydroxyl group. *J. Membr. Sci.* **2018,** 549, 260-266.
32. Yang, Y.; Goh, K.; Wang, R.; Bae, T.-H., High-performance nanocomposite membranes realized by efficient molecular sieving with CuBDC nanosheets. *Chem. Commun.* **2017,** 53, (30), 4254-4257.
33. Shete, M.; Kumar, P.; Bachman, J. E.; Ma, X.; Smith, Z. P.; Xu, W.; Mkhoyan, K. A.; Long, J. R.; Tsapatsis, M., On the direct synthesis of Cu(BDC) MOF nanosheets and their performance in mixed matrix membranes. *J. Membr. Sci.* **2018,** 549, 312-320.
34. Cheng, Y.; Tavares, S. R.; Doherty, C. M.; Ying, Y.; Sarnello, E.; Maurin, G.; Hill, M. R.; Li, T.; Zhao, D., Enhanced Polymer Crystallinity in Mixed-Matrix Membranes Induced by Metal–Organic Framework Nanosheets for Efficient CO_2 Capture. *ACS Appl. Mater. Interfaces* **2018,** 10, (49), 43095-43103.
35. Dai, Z.; Deng, J.; Peng, K.-J.; Liu, Y.-L.; Deng, L., Pebax/PEG Grafted CNT Hybrid Membranes for Enhanced CO_2/N_2 Separation. *Ind. Eng. Chem. Res.* **2019,** 58, (27), 12226-12234.
36. Dai, Z.; Aboukeila, H.; Ansaloni, L.; Deng, J.; Giacinti Baschetti, M.; Deng, L., Nafion/PEG hybrid membrane for CO_2 separation: Effect of PEG on membrane micro-structure and performance. *Sep. Purif. Technol.* **2019,** 214, 67-77.
37. Lo, Y.; Lam, C. H.; Chang, C.-W.; Yang, A.-C.; Kang, D.-Y., Polymorphism/pseudopolymorphism of metal–organic frameworks composed of zinc(ii) and 2-methylimidazole: synthesis, stability, and application in gas storage. *RSC Advances* **2016,** 6, (92), 89148-89156.
38. Yang, F.; Mu, H.; Wang, C.; Xiang, L.; Yao, K. X.; Liu, L.; Yang, Y.; Han, Y.; Li, Y.; Pan, Y., Morphological Map of ZIF-8 Crystals with Five Distinctive Shapes: Feature of Filler in Mixed-Matrix Membranes on C_3H_6/C_3H_8 Separation. *Chem. Mater.* **2018,** 30, (10), 3467-3473.
39. Pan, Y.; Heryadi, D.; Zhou, F.; Zhao, L.; Lestari, G.; Su, H.; Lai, Z., Tuning the crystal morphology and size of zeolitic imidazolate framework-8 in aqueous solution by surfactants. *CrystEngComm* **2011,** 13, (23).
40. Yao, J.; He, M.; Wang, H., Strategies for controlling crystal structure and reducing usage of organic ligand and solvents in the synthesis of zeolitic imidazolate frameworks. *CrystEngComm* **2015,** 17, (27), 4970-4976.
41. Zheng, G.; Chen, Z.; Sentosun, K.; Pérez-Juste, I.; Bals, S.; Liz-Marzán, L. M.; Pastoriza-Santos, I.; Pérez-Juste, J.; Hong, M., Shape control in ZIF-8 nanocrystals and metal nanoparticles@ZIF-8 heterostructures. *Nanoscale* **2017,** 9, (43), 16645-16651.
42. Fu, H.; Wang, Z.; Wang, X.; Wang, P.; Wang, C.-C., Formation mechanism of rod-like ZIF-L and fast phase transformation from ZIF-L to ZIF-8 with morphology changes controlled by polyvinylpyrrolidone and ethanol. *CrystEngComm* **2018,** 20, (11), 1473-1477.
43. Porel, S.; Singh, S.; Radhakrishnan, T. P., Polygonal gold nanoplates in a polymer matrix. *Chem. Commun.* **2005**, (18), 2387-2389.
44. Sang, W.; Fang, Y.; Fan, J.; He, Y.; Min, J.; Qian, Y., Novel synthesis method of ZnO nanorods by ion complex transformed PVA-assisted nucleation. *J. Cryst. Growth* **2007,** 299, (2), 272-276.
45. Tao, A. R.; Habas, S.; Yang, P., Shape Control of Colloidal Metal Nanocrystals. *Small* **2008,** 4, (3), 310-325.
46. Chen, R.; Yao, J.; Gu, Q.; Smeets, S.; Baerlocher, C.; Gu, H.; Zhu, D.; Morris, W.; Yaghi, O. M.; Wang, H., A two-dimensional zeolitic imidazolate framework with a cushion-shaped cavity for CO_2 adsorption. *Chem. Commun.* **2013,** 49, (82), 9500-2.

47. Gao, S.; Hou, J.; Deng, Z.; Wang, T.; Beyer, S.; Buzanich, A. G.; Richardson, J. J.; Rawal, A.; Seidel, R.; Zulkifli, M. Y., Improving the Acidic Stability of Zeolitic Imidazolate Frameworks by Biofunctional Molecules. *Chem* **2019**.

48. Tian, Z.; Yao, X.; Ma, K.; Niu, X.; Grothe, J.; Xu, Q.; Liu, L.; Kaskel, S.; Zhu, Y., Metal–Organic Framework/Graphene Quantum Dot Nanoparticles Used for Synergistic Chemo- and Photothermal Therapy. *ACS Omega* **2017,** 2, (3), 1249-1258.

49. Wu, C.; Liu, Q.; Chen, R.; Liu, J.; Zhang, H.; Li, R.; Takahashi, K.; Liu, P.; Wang, J., Fabrication of ZIF-8@SiO_2 Micro/Nano Hierarchical Superhydrophobic Surface on AZ31 Magnesium Alloy with Impressive Corrosion Resistance and Abrasion Resistance. *ACS Appl. Mater. Interfaces* **2017,** 9, (12), 11106-11115.

50. Dai, Z.; Deng, J.; Yu, Q.; Helberg, R. M. L.; Janakiram, S.; Ansaloni, L.; Deng, L., Fabrication and Evaluation of Bio-Based Nanocomposite TFC Hollow Fiber Membranes for Enhanced CO_2 Capture. *ACS Appl. Mater. Interfaces* **2019,** 11, (11), 10874-10882.

51. Zhao, M.; Wang, Y.; Ma, Q.; Huang, Y.; Zhang, X.; Ping, J.; Zhang, Z.; Lu, Q.; Yu, Y.; Xu, H.; Zhao, Y.; Zhang, H., Ultrathin 2D Metal–Organic Framework Nanosheets. *Adv. Mater.* **2015,** 27, (45), 7372-7378.

52. James, J. B.; Lin, Y., Kinetics of ZIF-8 thermal decomposition in inert, oxidizing, and reducing environments. *J. Phys. Chem. C* **2016,** 120, (26), 14015-14026.

53. Yin, H.; Kim, H.; Choi, J.; Yip, A. C. K., Thermal stability of ZIF-8 under oxidative and inert environments: A practical perspective on using ZIF-8 as a catalyst support. *Chem. Eng. J.* **2015,** 278, 293-300.

54. Zhu, W.; Li, X.; Sun, Y.; Guo, R.; Ding, S., Introducing hydrophilic ultra-thin ZIF-L into mixed matrix membranes for CO_2/CH_4 separation. *RSC Advances* **2019,** 9, (40), 23390-23399.

55. Ahn, J.; Chung, W.-J.; Pinnau, I.; Guiver, M. D., Polysulfone/silica nanoparticle mixed-matrix membranes for gas separation. *J. Membr. Sci.* **2008,** 314, (1), 123-133.

56. Moaddeb, M.; Koros, W. J., Gas transport properties of thin polymeric membranes in the presence of silicon dioxide particles. *J. Membr. Sci.* **1997,** 125, (1), 143-163.

57. Rodenas, T.; van Dalen, M.; García-Pérez, E.; Serra-Crespo, P.; Zornoza, B.; Kapteijn, F.; Gascon, J., Visualizing MOF Mixed Matrix Membranes at the Nanoscale: Towards Structure-Performance Relationships in CO_2/CH_4 Separation Over NH_2-MIL-53(Al)@PI. *Adv. Funct. Mater.* **2014,** 24, (2), 249-256.

58. Yu, B.; Cong, H.; Li, Z.; Tang, J.; Zhao, X. S., Pebax-1657 nanocomposite membranes incorporated with nanoparticles/colloids/carbon nanotubes for CO_2/N_2 and CO_2/H_2 separation. *J. Appl. Polym. Sci.* **2013,** 130, (4), 2867-2876.

59. Surya Murali, R.; Ismail, A. F.; Rahman, M. A.; Sridhar, S., Mixed matrix membranes of Pebax-1657 loaded with 4A zeolite for gaseous separations. *Sep. Purif. Technol.* **2014,** 129, 1-8.

60. Zhao, D.; Ren, J.; Li, H.; Li, X.; Deng, M., Gas separation properties of poly(amide-6-b-ethylene oxide)/amino modified multi-walled carbon nanotubes mixed matrix membranes. *J. Membr. Sci.* **2014,** 467, 41-47.

61. Jomekian, A.; Behbahani, R. M.; Mohammadi, T.; Kargari, A., Utilization of Pebax 1657 as structure directing agent in fabrication of ultra-porous ZIF-8. *J. Solid State Chem.* **2016,** 235, 212-216.

62. Dong, G.; Hou, J.; Wang, J.; Zhang, Y.; Chen, V.; Liu, J., Enhanced CO_2/N_2 separation by porous reduced graphene oxide/Pebax mixed matrix membranes. *J. Membr. Sci.* **2016,** 520, 860-868.

63. Dai, Y.; Ruan, X.; Yan, Z.; Yang, K.; Yu, M.; Li, H.; Zhao, W.; He, G., Imidazole functionalized graphene oxide/PEBAX mixed matrix membranes for efficient CO_2 capture. *Sep. Purif. Technol.* **2016,** 166, 171-180.

64. Xiang, L.; Pan, Y.; Zeng, G.; Jiang, J.; Chen, J.; Wang, C., Preparation of poly(ether-block-amide)/attapulgite mixed matrix membranes for CO_2/N_2 separation. *J. Membr. Sci.* **2016,** 500, 66-75.

65. Meshkat, S.; Kaliaguine, S.; Rodrigue, D., Mixed matrix membranes based on amine and non-amine MIL-53(Al) in Pebax® MH-1657 for CO_2 separation. *Sep. Purif. Technol.* **2018,** 200, 177-190.

66. Sutrisna, P. D.; Hou, J.; Zulkifli, M. Y.; Li, H.; Zhang, Y.; Liang, W.; D'Alessandro, Deanna M.; Chen, V., Surface functionalized UiO-66/Pebax-based ultrathin composite hollow fiber gas separation membranes. *J. Mater. Chem. A* **2018,** 6, (3), 918-931.

67. Aghaei, Z.; Naji, L.; Hadadi Asl, V.; Khanbabaei, G.; Dezhagah, F., The influence of fumed silica content and particle size in poly (amide 6-b-ethylene oxide) mixed matrix membranes for gas separation. *Sep. Purif. Technol.* **2018,** 199, 47-56.

68. Shen, J.; Liu, G.; Huang, K.; Jin, W.; Lee, K.-R.; Xu, N., Membranes with Fast and Selective Gas-Transport Channels of Laminar Graphene Oxide for Efficient CO_2 Capture. *Angew. Chem.* **2015,** 127, (2), 588-592.

69. Shen, Y.; Wang, H.; Zhang, X.; Zhang, Y., MoS_2 Nanosheets Functionalized Composite Mixed Matrix Membrane for Enhanced CO_2 Capture via Surface Drop-Coating Method. *ACS Appl. Mater. Interfaces* **2016,** 8, (35), 23371-23378.

Table of Contents

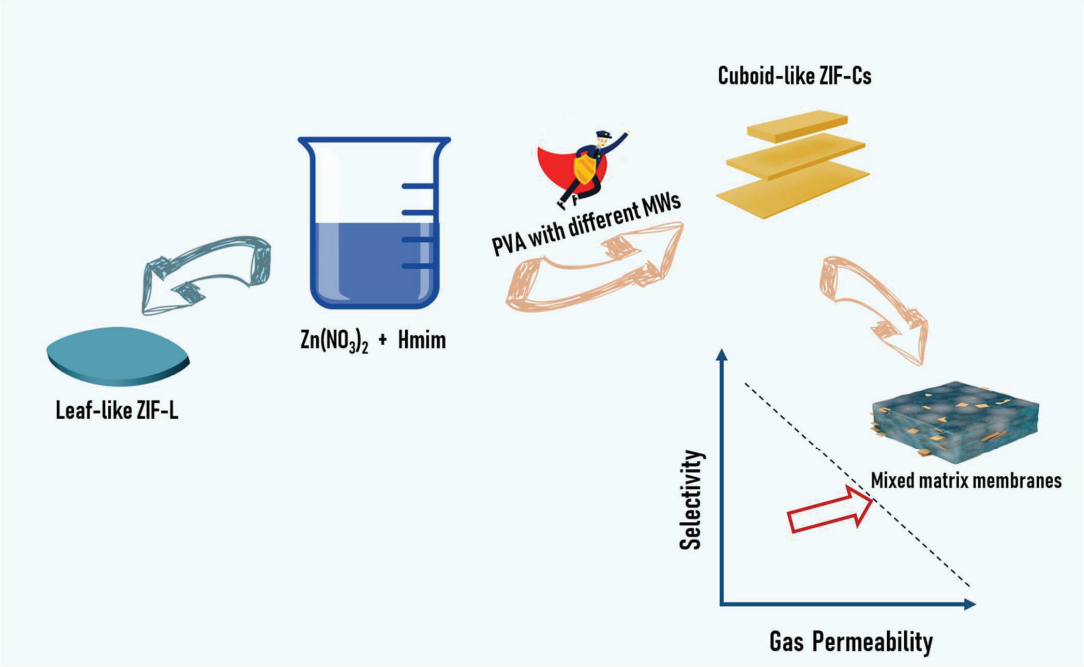

Novel MOF nanosheets with tunable thickness and their application in mixed matrix membranes for CO_2 application

Supporting Information

Jing Deng[†1], Zhongde Dai[†1], Jingwei Hou[2] and Liyuan Deng[*1]

[1]Department of Chemical Engineering, Norwegian University of Science and Technology Trondheim, 7491, Norway

[2]School of Chemical Engineering, Faculty of Engineering, Architecture and Information Technology, the University of Queensland, Brisbane, Queensland, Australia

† These authors contributed equally

Table of contents

Table S1 The size of the as-synthesized ZIF-C obtained from AFM

MOFs	Length (μm)	Width (μm)	Thickness (nm)
ZIF-C 30-70	5.0	2.0	70
ZIF-C 72	4.3	1.4	120
ZIF-C 85-124	4.1	1.1	170
Leaf-like ZIF-C[1]	5.0	2.0	150

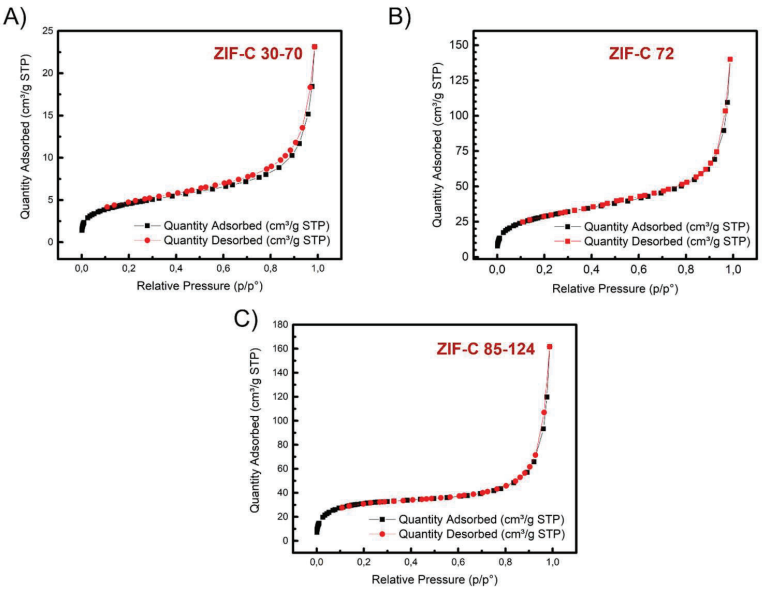

Figure S1 The N_2 adsorption experiment results of ZIF-C prepared in PVA solution

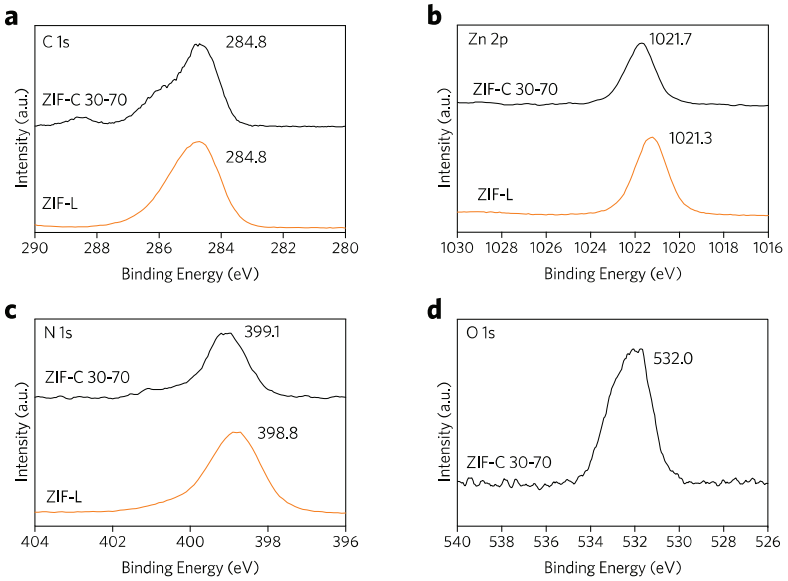

Figure S2 XPS C 1s, Zn 2p, N 1s and O 1s spectra of ZIF-C 30-70 and benchmark ZIF-L.

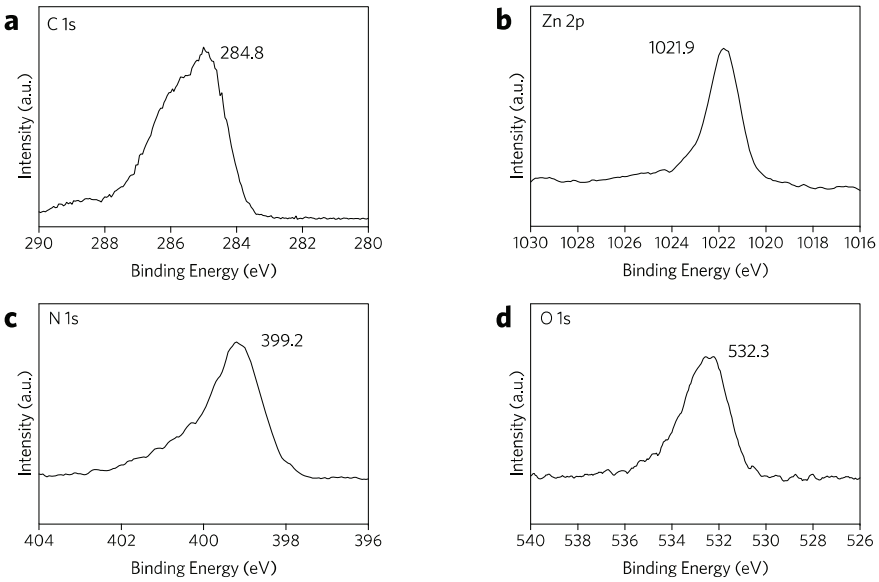

Figure S3 XPS C 1s, Zn 2p, N 1s and O 1s spectra of ZIF-C 72.

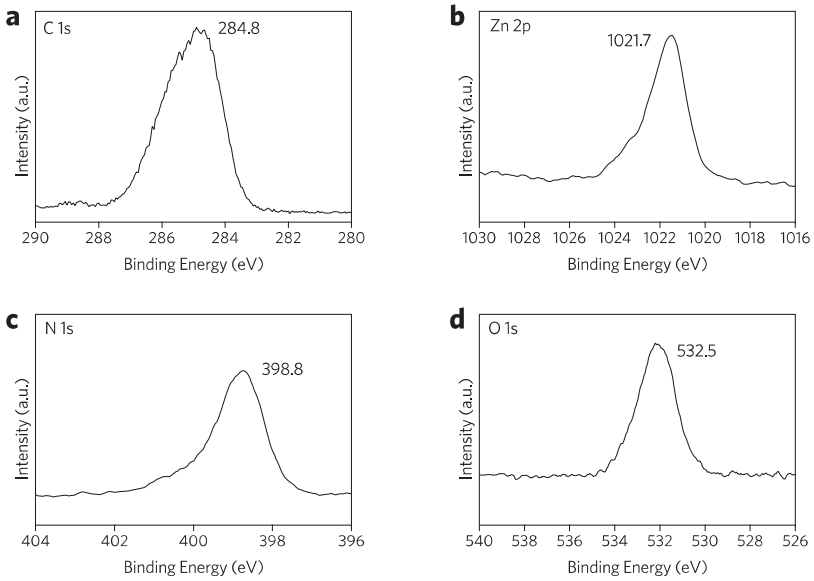

Figure S4. XPS C 1s, Zn 2p, N 1s and O 1s spectra of ZIF-C 85-124.

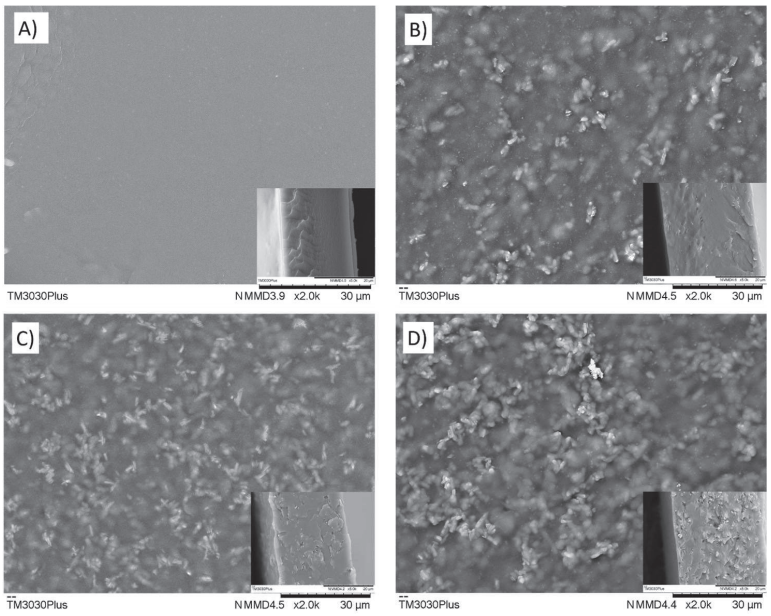

Figure S5 MMMs morphology with A) 0%, B) 5%, C) 10% and D) 20% ZIF-C 72.

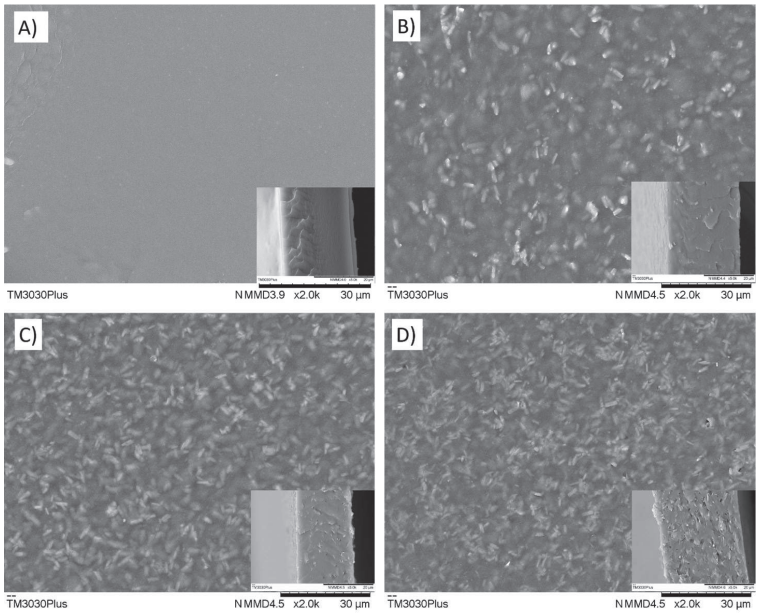

Figure S6 MMMs morphology with A) 0%, B) 5%, C) 10% and D) 20% ZIF-C 30-70

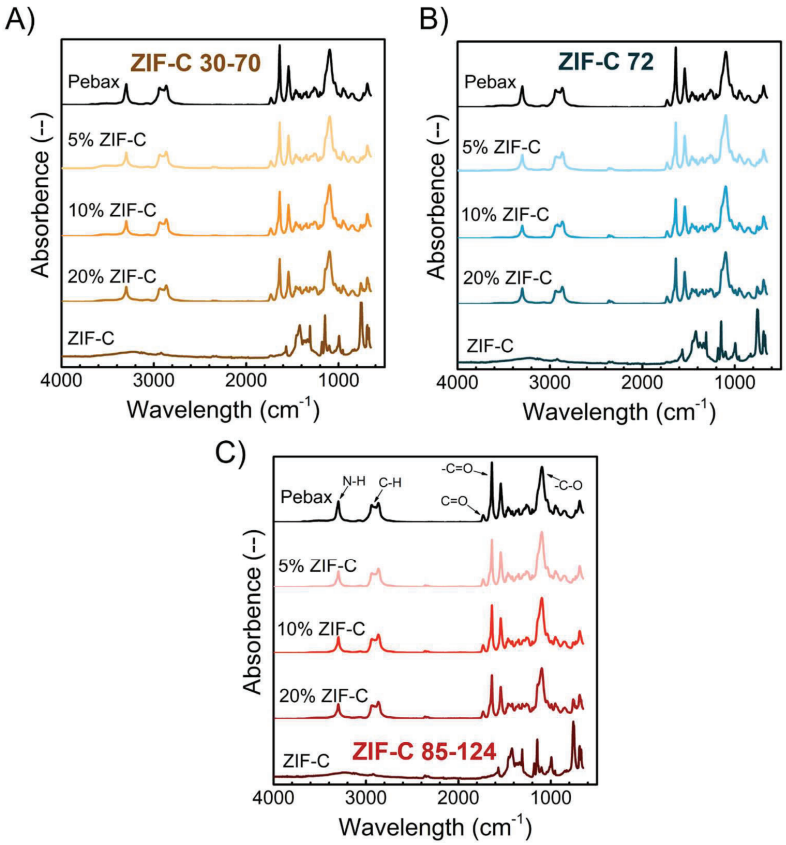

Figure S7 FTIR spectra of MMMs containing A) ZIF-C 30-70, B) ZIF-C 72 and C) ZIF-C 85-124 with a function of filler content.

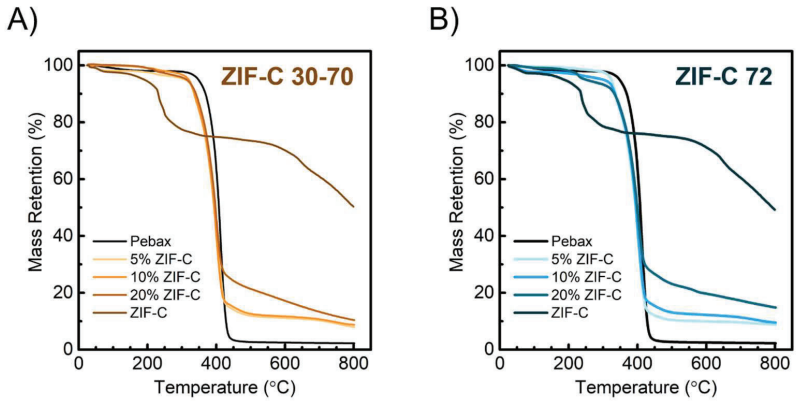

Figure S8 TGA curves of MMMs containing A) ZIF-C 30-70 and B) ZIF-C 72 with a function of filler content.

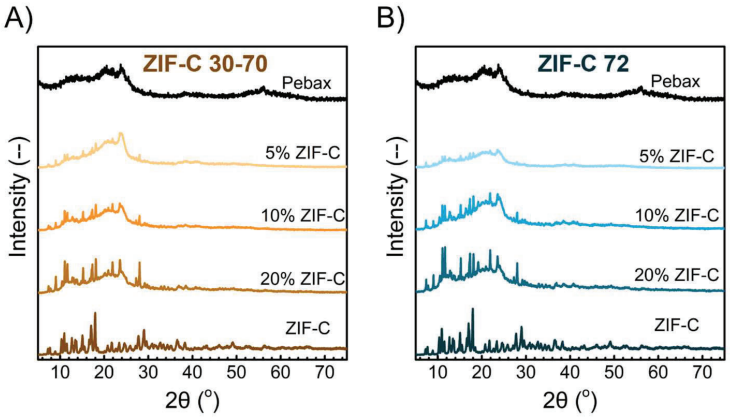

Figure S9 XRD results of MMMs containing A) ZIF-C 30-70 and B) ZIF-C 72 with different content.

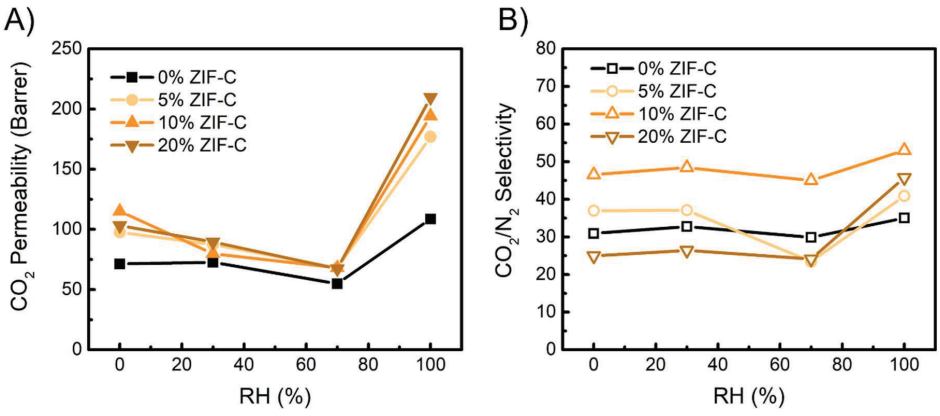

Figure S10 (A) CO_2 permeability and (B) CO_2/N_2 selectivity of Pebax + ZIF-C 30-70 MMMs as a function of RH.

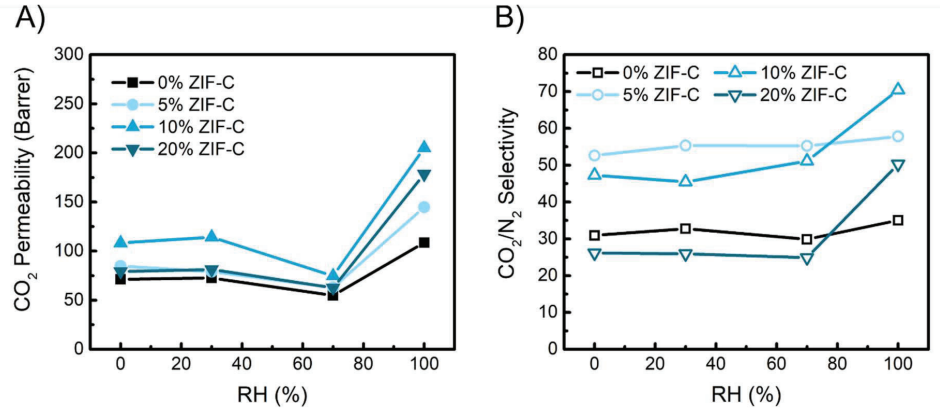

Figure S11 (A) CO_2 permeability and (B) CO_2/N_2 selectivity of Pebax + ZIF-C 72 MMMs as a function of RH.

REFERENCE

1. Chen, R.; Yao, J.; Gu, Q.; Smeets, S.; Baerlocher, C.; Gu, H.; Zhu, D.; Morris, W.; Yaghi, O. M.; Wang, H., A two-dimensional zeolitic imidazolate framework with a cushion-shaped cavity for CO_2 adsorption. *Chem. Commun.* **2013,** 49, (82), 9500-2.

Effects of the ZIFs' Morphology on the CO_2 Separation Performance of MMMs

This paper is to be submitted to
ACS Applied Materials & Interfaces.

Paper V

Effects of the Morphology of the ZIF on the CO_2 Separation Performance of MMMs

*Jing Deng†, Zhongde Dai† and Liyuan Deng**

Department of Chemical Engineering, Norwegian University of Science and Technology, 7491 Trondheim, Norway

† These authors contributed equally.

KEYWORDS:

Mixed matrix membranes; effects of filler morphology; ZIFs, Pebax 2533; CO_2/N_2 separation.

ABSTRACT

In this study, three zeolitic imidazolate frameworks (ZIFs) with different shapes – particles (0D), microneedles (1D) and leaves (2D) - were synthesized by tuning the polymeric additive. These ZIFs have been dispersed into Pebax 2533 matrix with a loading varying from 0 to 20 wt.%. The resultant mixed matrix membranes (MMMs) have been systemically characterized by various techniques. Mixed gas permeation experiment was also employed to evaluate the CO_2 separation performance. The results show that there exists an optimal ZIF loading for these three series of membranes, but the values are highly dependent on the morphologies of the added ZIFs. The membranes containing ZIF particles and microneedles display the highest CO_2 permeability and CO_2/N_2 selectivity simultaneously at 10 wt.% loading, while a much lower loading, i.e., ~ 5 wt.% is the optimized value for ZIF leaves. Moreover, the increment in CO_2 permeability is related to the ZIFs' morphology and the order is 0D < 1D < 2D. On the other hand, the effects of the morphology on selectivity seems to be the opposite, with ZIF of 0D structure showing the highest selectivity. Moreover, the influences of adding ZIF fillers on the performances of the resultant MMMs under varied operating temperatures and the feed pressures were also investigated. The membrane with 10 wt.% 1D ZIF shows the highest increment in CO_2 permeability (727.4 Barrer) with acceptable CO_2/N_2 selectivity at 60 ^oC.

1. INTRODUCTION

The market size of gas separation membranes in various applications, like air separations and natural gas sweetening/dehydration, has been expanding greatly [1-3] and is estimated to reach $1.1 billion by 2024 according to a very recent research report.[4] Among plenty of the membrane materials, polymers have dominated due to their low cost, excellent processability and easy scale-up. But in most fields, especially for CO_2 separation, one of the biggest markets, the current polymeric membrane materials still cannot meet the desirable performance to replace the conventional separation technology (i.e., absorption/adsorption), which usually are energy-intensive processes. The present polymeric materials either have high gas permeabilities with low gas selectivity, or vice versa, known as the "Upper Bound".[5]

On the other hand, the inorganic membrane materials usually have high gas transport properties and selectivity at the same time. However, their high cost and poor processability hinder them from gaining wide application. Hence, an alternative that potentially combines the benefits and avoids the disadvantages of both polymeric and inorganic membranes, known as mixed matrix membranes (MMMs),[6-7] has been proposed by incorporating inorganic fillers into polymeric matrix. Generally speaking, the incorporation of inorganic fillers could have a positive effect in the gas diffusivity. Song et al. has blended ZIF-8 (zeolitic imidazolate framework) nanoparticles into Matrimid and observed a monotonous increment in gas permeability with increasing ZIF-8 content.[8] Further analysis suggests that the enhanced CO_2 permeability is mainly due to the increased CO_2 diffusivity, which comes from the higher free volume created by the rigidified polymeric matrix due to the presence of the ZIF-8, as well as the extra transport path inside ZIF-8 particles. Moreover, the angstrom-scale pores or special channels inside the ZIF fillers offer not

only extra transport paths, but also work as a molecular sieve and thus promote the separation performance. Another research documented that the interlayer channels inside graphene oxide could work as fast and selective pathways for CO_2, and only 1 wt.% graphene oxide could realize significant increments in both CO_2 permeability and CO_2/N_2 selectivity, thereby surpassing the "Upper Bound".[9] In addition, the rich diversity in the polymer-inorganic filler pairs offers great probability of achieving better membranes.

Despite these encouraging results, there still exists lots of problem that are yet not to be fully understood. Researchers have noticed that incorporating inorganic nano-fillers into polymeric matrix could also result in deteriorated performance. Various factors, such as fillers' pore size / shapes, the size / shape / chemical composition of the fillers, the pairing selection of fillers and polymeric matrix, preparation methods, could affect the morphology of the resultant MMMs and thus the performances. Very recently, it has been reported that the altering filler's geometry may result in different performances, even with the same pairing (polymer-fillers). [10] For instance, several studies have found that increasing filler size has negative effects on the gas permeabilities [11-13] with the same loading, since the smaller fillers could offer more external surface area. On the other hand, larger particles have less tendency to form agglomeration and may benefit the gas transport properties of the resultant membranes. [12, 14-15]

Apart from the size effect, the filler shape is also considered as one of crucial factors, which would affect greatly the interfacial contact between fillers and the polymeric matrix. However, only a few related researches have been conducted. Sabetghadam and co-workers [16] prepared NH_2-MIL-53(Al)s nanoparticles (46 × 15 nm), nanorods (64 × 15 nm) and microneedles (4000 × 80 nm) by different preparation methods and incorporated them into Matrimid to investigate the effect of MOF's morphology on the performance of the resultant MMMs. The gas permeation results show

that the nanoparticles could benefit the gas permeability, while the addition of the other MOFs leads to a loss in CO_2 permeability. The better dispersion of nanoparticles inside polymeric matrix is believed to be the main reason, since the nanorods and microneedles have higher aspect ratio and thus less closer to the ideal sphere. The same group also demonstrated that the presence of copper 1,4-benzenedicarboxylate (CuBDC) nanosheets in Matrimid matrix increases the CO_2/CH_4 selectivity while the nanoparticles or bulk-type analogies worsen the separation ability of the polymeric matrix.[17]

In another work by our group, a simple method to prepare ZIF cuboids with different thicknesses has been reported. These ZIFs were then incorporated into Pebax matrix for gas separation. Results show the ZIFs with different thicknesses could result in considerably distinct impacts on the CO_2 separation performance: the thickest one brings about the highest CO_2 permeability.[18] In the current work, following the same ideas, the influences of the filler shapes on the properties of the ZIF + Pebax matrix were investigated by employing ZIF nanoparticles (0D), needles (1D) and leaves (2D). These ZIFs were prepared using different methods at room temperature, and then analyzed by various characterization techniques: scanning electron microscope (SEM), fourier-transform infrared (FTIR) spectroscopy and X-ray crystallography (XRD). Afterwards, these methods were also used to evaluate the properties of the resultant MMMs together with thermal analysis (TGA) and differential scanning calorimetry (DSC). Finally, the CO_2/N_2 separation performance was studied by mixed gas permeation tests and the correspondence between the morphologically properties of the nanofillers and the permeation properties of the MMMs are discussed.

2. Experimental Section

2.1. Materials

$Zn(NO_3)_2 \cdot 6H_2O$, 2-methylimidazole (Hmim), Poly(vinyl alcohol) (PVA, M_n 89000-98000 g/mol, 99% hydrolyzed) and polyethylene glycol (400g/mol, PEG 400) were ordered from Sigma, Norway. Pebax 2533 pellets were purchased from Arkema. Ethanol (96%) was bought from VWR, Norway. All the chemicals were used without further treatment.

2.2. ZIFs preparation

The ZIFs synthesized in PEG 400, PVA and additive-free solution have a morphology of particles, microneedles and leaves, which are named as 0D ZIF, 1D ZIF and 2D ZIF, respectively. The 0D ZIF and 1D ZIF were prepared via the following procedure: 0.59g $Zn(NO_3) \cdot 6H_2O$ was dissolved in 40 mL 1 wt.% PVA or PEG solution, while 1.32 g Hmim was added into another 40 mL same polymeric solution (1 wt.%). Then two solutions were mixed and stirred at room temperatures and solution gradually became whitish. 2D ZIF was prepared according to the same procedure but in DI water. After 3 hours, the solution was centrifuged at 10000 rpm for 10 mins and then the precipitate was as-synthesized ZIFs. The obtained ZIFs were washed twice by dispersing in DI water and centrifuging to remove residual reactants and the polymeric additives. Finally, the ZIFs were placed in vacuum oven at 60 ^oC until fully dried.

2.3. Membrane preparation

Pebax 2533 + ZIFs membranes were fabricated by the knife-casting method. Typically, 8 wt.% Pebax 2533 / ethanol solution was prepared at 80 °C with reflux for around 2 hours. Meanwhile, a certain amount of ZIFs was added into ethanol to prepare the 8 wt.% ZIF / ethanol suspension. Afterwards, the Pebax solution was added into the ZIF / ethanol suspension, accompanied by stirring, overnight. The mixture was cast on a glass plate using a casting knife (PA-4302, BYK-CHEMIE GMBH, Germany) with a wet gap of around 600 μm. The cast membrane was then dried

in a ventilated oven at 40 °C and then moved to a vacuum oven at 60 °C until fully dry. The obtained membranes were stored in a desiccator to avoid the absorption of moisture from air.

2.4. Characterization

The FTIR spectroscopy was performed for all ZIFs and resultant membranes with a Nicolet Nexus spectrometer, Thermo. The obtained spectra of all samples were an average of 16 scans with wavenumber from 550 cm^{-1} to 4000 cm^{-1}.

The morphologies of ZIFs and the resultant MMMs were analyzed using a SEM (TM3030 tabletop microscope, Hitachi). The cross-section specimens of MMMs were prepared by breaking the samples in liquid N_2. A sputter coating with gold (2 mins) was conducted for all samples before SEM characterization.

The thermal stability tests of ZIFs and the MMMs were performed by a TGA (TG 209F1 Libra, Netzsch). Samples of around 10 – 20 mg were used. All samples were heated from room temperature to 700 °C at a heating rate of 10 °C / min under N_2 atmosphere. Differential scanning calorimetry (DSC) analysis was also conducted to study the phase transition behavior of the MMMs (DSC 214 Polyma, NETZSCH-Gerätebau GmbH, Germany). Samples of around 10 - 20 mg were placed in a covered standard aluminum pan and heated at the rate of 10 °C/min in N_2 atmosphere.

The crystalline information of the as-prepared ZIFs and MMMs was obtained from XRD tests using Bruker D8 A25 DaVinci X-ray Diffractometer, Bruker. The characteristic wavelength λ is 1.54 Å (Cu Kα radiation), and all samples were scanned with the 2θ range from 5° to 75°.

2.5. Gas permeation tests

Mixed gas permeation experiments were conducted by an in-house permeation setup reported elsewhere [19-20]. The CO_2/N_2 (10/90 v/v%) gas mixture was employed as the feed gas, whereas the sweep gas was pure CH_4. The sweep pressure was kept around 1 bar, while the feed pressure was adjusted based on the required test conditions. The operating temperatures were controlled by a ventilated oven, inside which a larger part of the gas permeation setup was mounted. The compositions of both permeate and retentate streams were real-time monitored by a gas chromatograph (490 Micro GC, Agilent). The gas permeability (P_i) of the ith penetrant species is calculated using equation (1):

$$P_i = \frac{N_{perm} y_i}{A\left(p_{i,ret} - p_{i,perm}\right)} \quad (1)$$

where N_{perm} is the permeate flow measured by a bubble flow meter (mL/min), y_i is the molar fraction of the gas i in the permeate flow (%), $p_{i,ret}$ and $p_{i,perm}$ stand for the partial pressures of the gas i in retentate and permeate streams (bar), respectively, and A is the effective membrane area (cm^2). In the present work, the unit of gas permeability is Barrer (1 Barrer = 10^{-10} $cm^3(STP)*cm*cm^{-2}*s^{-1}*cmHg^{-1}$). The separation factor was determined from equation (2):

$$\alpha_{ij} = \frac{y_i/y_j}{x_i/x_j} \quad (2)$$

where y_i and y_j are the mole ratio of gas i and j in permeate stream, respectively, while x_i and x_j present the mole ratio of gas i and j in the retentate side, respectively.

3. Results and discussion

3.1. Properties and morphology studies of ZIFs

Three ZIFs with different shapes were fabricated with the same Hmim/Zn^{2+} ratio in aqueous solution at room temperatures, without the polymeric additive. It is well known that additives play

an important role in crystal formation and the growth of the inorganic crystals, and then tune the ZIFs' morphologies, like shapes and sizes.[18, 21] The crystals of the ZIFs generated in PEG solution have a rhombic dodecahedron appearance with a size of around 2 μm , as shown in **Figure 1 (A)**. While the ones generated from PVA 89-98 solution are sharp needles with a length of 6 μm and a width of 0.6 μm (as shown in **Figure 1(B)**). On the other hand, the 2D ZIF has a leaf-like shape (1.3 × 5.4 μm, shown in **Figure 1(C)**), in agreement with a previous report. [22] In addition to the differences in the shapes of the fillers, the XRD characterization results suggests that the crystal structure of these three ZIFs are not the same. The XRD pattern of 1D ZIF matches that of leaf ZIF-L, which is the 2D ZIF in this work. This suggests that the existence of PVA during ZIF synthesis seems to have a negligible effect on the crystal structure [18]. Unexpectedly, the 0D ZIF has similar XRD pattern with ZIF-8, [23] despite having the same Him/Zn^{2+} ratio (8:1) as ZIF-L [22], which is much lower than the typical ratio for synthesizing ZIF-8 particles (70:1) [24]. It is well-known that the Him/Zn^{2+} ratio has great impact on the crystal structure of the resultant particles, especially in aqueous solutions. [25] While the presence of PEG seems to stabilize the Him-Zn coordination structure and allows for the formation of ZIF-8 at low Him/Zn^{2+} ratio [26].

TGA was employed to investigate the thermal stabilities of the ZIF. As shown in **Figure 1 (E)**, all the samples lost a small amount of H_2O when the temperature reaches around 100 ºC. With increasing temperature, the 0D and 1D ZIF starts decomposing, followed by the 2D ZIF. The relatively lower thermal stability of the ZIFs synthesized in polymeric solution is probably due to the polymeric chains entangling with the crystal cells. The ZIF formed in additive-free condition has relatively higher decomposition temperature. During this stage, the loss in weight mainly comes from the losing the structural water molecules and unreacted compounds [23]. All the samples presented a significant weight loss within the temperature range of 200 -300 ºC. The 0D

ZIF has relatively smaller slop, which is mainly due to the decomposition of the ligand. Afterwards, the residual masses of these three ZIFs remain almost unchanged with increasing temperature, indicating that the crystal structure of the ZIFs have been destroyed and changed to the ZnO form [21]. FTIR spectroscopy was also used to analyze the chemical composition of the as-synthesized ZIFs and the results are presented in **Figure 1 (F)**. Since the ionic bonds cannot be detected by FTIR, the only bonding observed are those in Hmim molecules, like C-N and C=N bonds, which has characteristic peaks around 1310 and 1130 cm^{-1}, and 1568 cm^{-1} [27-28], respectively. These peaks are clearly noticed in the spectra of the three ZIFs, suggesting the presence of organic linkers. Combined with other characterization results, these as-synthesized ZIFs' crystal cells are composed of the Hmim and Zn^{2+}, but in different construction ways

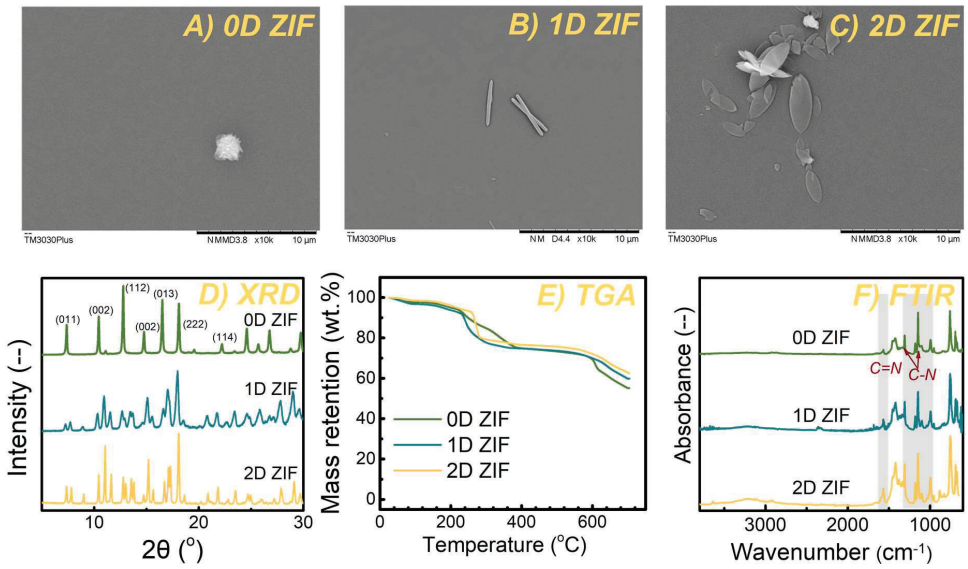

Figure 1 The SEM images of A) 0D ZIF, B) 1D ZIF and C) 2D ZIF, and D) XRD curves, E) TGA results and F) the FTIR spectra of these ZIFs.

3.2.Properties and morphology studies of MMMs

3.2.1. Chemical property

The FTIR spectroscopy was employed to analyze the chemical properties of the Pebax 2533 + 1D ZIFs MMM and the results are presented in **Figure 2** and **Figure S1**. The peaks located around 3300 cm^{-1}, 1640 cm^{-1} and 1100 cm^{-1} are associated with the amine (N-H) in polyamide segments, carbonyl (C=O) and ether (C-O) groups in polyether chains, respectively. This matches with the chemical structure of the neat Pebax 2533 and peak information in the previous literature [29-30]. For the MMMs containing ZIFs, these aforementioned peaks become weaker with increasing ZIF loadings, as shown in **Figure 2 (A)**, due mainly to the decreasing Pebax content inside the membranes. On the other hand, the intensity of the peak corresponding to ZIFs (1310 cm^{-1}) increases with the addition of the ZIF, as shown in **Figure 2 (B)**. It is worth noting that no new peaks or peak shifting has been observed. These results suggest that the ZIFs indeed were physically blended into the Pebax matrix as expected.

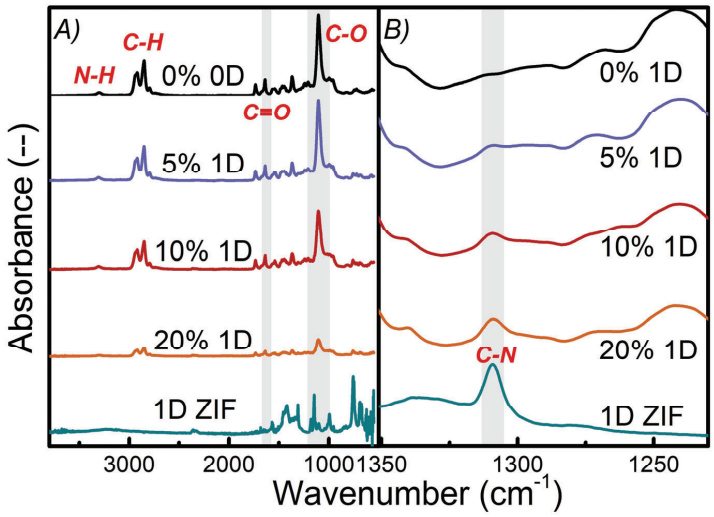

Figure 2 The FTIR spectra of the MMMs containing 1D ZIFs with a range of A) 4000 – 500 cm^{-1} and B) 1350 – 1230 cm^{-1}

3.2.2. Thermal properties

The thermal characterizations are very important and useful in understanding the hybrid materials and thus their properties. The thermal stability of MMMs were investigated by TGA, and the results are shown in **Figure 3** and **S3**. The neat Pebax 2533 has single-stage decomposition behavior with a T_{onset} of ~ 370 °C, which is much higher than those of the three ZIFs used in the current study. Naturally, adding ZIFs results in left-shifted decomposition temperature of the MMMs, despite the ZIFs' morphologies. With increasing ZIF loading in MMMs, the T_{onset} of the hybrid materials decreases and the residual mass increases, as shown in **Figure 4**, indicating that the actual amount of ZIFs in MMMs is increasing as expected. In addition to the changes in T_{onset}, the decomposition behavior of the MMMs is also affected by the ZIFs: the one-step decomposition curve turns to multi-stage curves. The low filler loading leads to at least three stages: 300 - 330 °C, 330 - 360 °C and 360 - 470 °C, which corresponds to the ZIFs and Pebax 2533 chains, respectively. The higher loading causes less clear boundaries between stages.

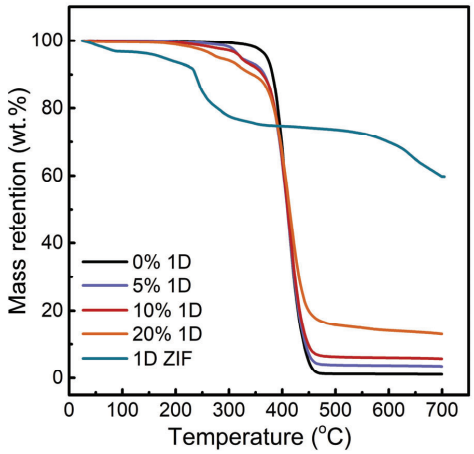

Figure 3 The TGA results of the MMMs with various loading of 1D ZIFs.

In addition, DSC was also employed to characterize the MMMs, and the second heating curve of the different membranes are displayed in **Figure 4** and **S4**. Two distinct peaks are observed in all curves: one located around 15 ºC and the other near 138 ºC. Considering the chemical structure of the Pebax 2533, the peak around 15 ºC is believed to be the melting peak of the soft PE chains, while the second one belongs to the hard PA segment, which are in good agreement with the results previously reported. [30-32] In addition to the melting temperatures, the peak area is theoretically related to the amount of required heat during melting process, which is proportional to content of the corresponding compound. Firstly, for neat Pebax 2533, the melting peak of PE segment is much bigger than the one of PA blocks, which agrees with the composition of Pebax 2533 (86 mol% PE and 14 mol% PA). [29] Secondly, with incorporating ZIFs, both melting peaks become increasingly smaller, and the T_m of the PA blocks shifts to lower values, which indicate the decreasing amount of the polymeric chains in the MMMs. In addition to the influences of the fillers' content, the morphology of the fillers also has influences on the final thermal properties. The MMMs containing 20 wt.% 0D and 1D ZIF have T_ms of PA segment around 132 ºC, while the T_m of the one with 2D decreases to 126 ºC. The lower melting temperature may be because the leaf ZIF-L could break the PA zones and thus interrupt the formation of crystalline zones, [33] leading to less required energy for melting the crystalline and the amorphous chains.

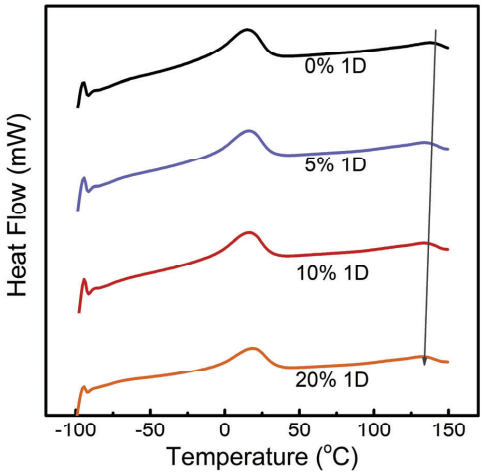

Figure 4 The DSC results of the MMMs with various loading of 1D ZIFs.

3.2.3. Crystallinity

Crystallization has great influence on the various properties of the polymers, such as mechanical properties and gas separation performance. XRD tests were performed for all MMMs and the neat Pebax 2533 membranes as shown in **Figure 5** and **S5**. The neat polymer membrane has two broad peaks locating at 11.7° and 19.8°, respectively, corresponding to the semi-crystalline nature of the Pebax 2533. [34-36] On the other hand, incorporating the highly crystalline materials introduces the sharp and narrow peaks originating from the ZIFs and shrinks the broad peaks of the Pebax 2533. Meanwhile, with the increasing ZIF loading, the sharp peaks become more obvious while these amorphous peaks diminish significantly. This presents the increasing content of ZIF and the decreasing amount of Pebax in these MMMs, greatly agreeing with previous characterization results.

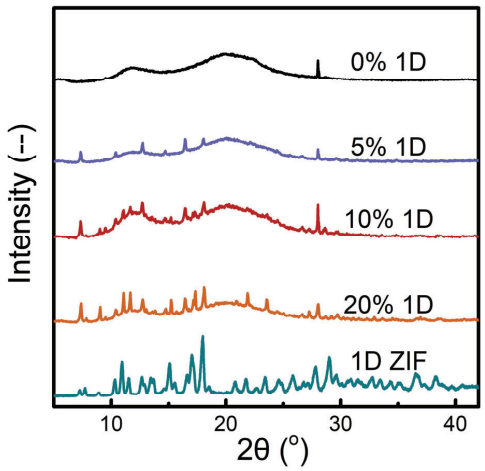

Figure 5 The XRD results of the MMMs with various loading of 1D ZIFs.

3.2.4. Morphology study

As discussed previously, the incorporation of inorganic fillers into the polymeric matrix may cause unideal dispersion in the resultant MMMs, which may be observed by a SEM. The surface and cross-section images of all Pebax + ZIF MMMs are presented in **Figure 6** and **S6.** The neat polymeric membranes have smooth surfaces and void-free cross-sections (**Figure 6 (A)**). While the surfaces and cross-sections of all MMMs become rougher with increasing filler contents, despite the morphology of the ZIFs. Moreover, all the three ZIFs seems to be dispersed well in the resultant MMMs and no obvious aggregation of ZIFs has been seen, except for the one containing 20 wt.% 2D ZIF. The membranes with 20 wt.% ZIF-L clearly have phase-separation from both surface and cross-section images, due probably to the ZIF-L aggregation during membrane fabrication. The reason for this much higher agglomeration trend of ZIF-L is probably its leaf-like shape, compared to the other ZIFs studied in the current work. It is well-known that inorganic fillers tend to aggregate at high filler loadings, and many factors could lead to this unpleasant result, such as particle size, bad compatibility with the polymeric matrix and the shape of the fillers.

Several research works have reported that for inorganic fillers with high aspect ratio (> 10), the low loading may be more attractive [37] because of the greater possibility of stack and aggregation. Moreover, they could offer the same or even better performances at lower loadings compared to the typical spheres.

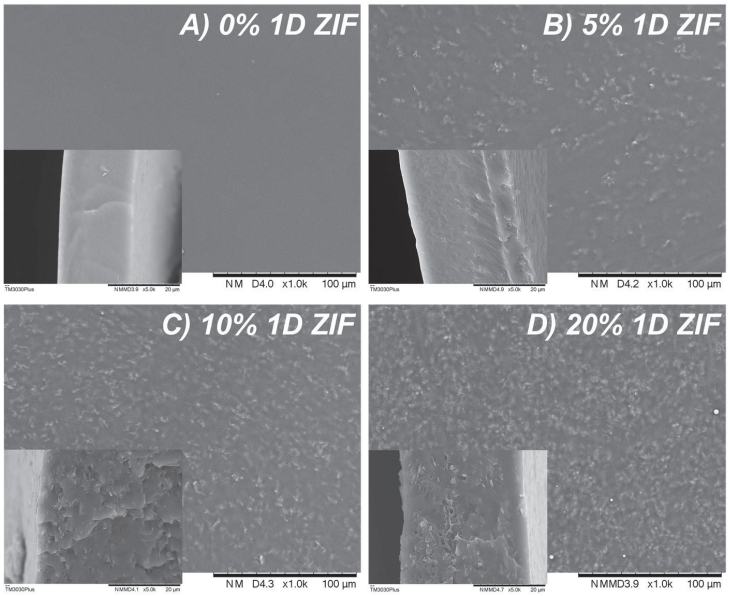

Figure 6 The SEM images of the MMMs containing 1D ZIFs with various loading.

3.2.5. Permeation study

Effect of filler

The CO_2/N_2 separation performance of the resultant MMMs with three ZIFs fillers was evaluated by the mixed gas permeation tests at room temperature with a feed pressure of 2 bar. The CO_2 permeability and CO_2/N_2 separation factor of the resultant MMMs as a function of filler content are presented in **Figure 7**.

The neat Pebax 2533 have a CO_2 permeability of ~ 220 Barrer with a CO_2/N_2 separation factor of 26, in good agreement with previously reported values.[38] A clear increment in CO_2 permeability was observed with the addition of all ZIF fillers, despite the difference in particle shapes. This enhancement may be explained by several factors. First, the addition of ZIFs disrupts the packing way of polymeric chains and then rises the free volume of the resultant membranes. Meanwhile, the pores of these ZIFs act as molecular sieves, allowing the small specimens, like CO_2 in the current work, pass through but not the big ones, which offers the extra transport paths for CO_2 and hence benefiting their permeabilities. However, further increasing the ZIF loading has negative effects on the CO_2 permeability, probably due to the aggregation of fillers inside MMMs, [39-40] although it is only observed in the membranes containing 2D ZIF under microscopy. Despite this similar trend, there exists some difference between the influences of adding each ZIF. The optimal ZIF loadings are related to the morphologies of the employed ZIF: the peaks are located at 10 wt.% for 0D and 1D, while 5 wt.% for 2D. Several researches have inferred that the high aspect ratio of 2D nanomaterials endows similar or better performance at lower loading compared to the spherical ones, the most common filler shape [17, 41-42], in accordance with the results of the current work. It is worth mentioning that the membrane with 5 wt.% 2D ZIF has the highest CO_2 permeability (425.0 Barrer), followed by the one with 10 wt.% 1D ZIF (411.4 Barrer) and 0D ZIF (376.7 Barrer). Moreover, the reason of that the membranes containing 1D ZIFs is more permeable than that with 0D ZIF at same loading is probably because that the interface between the polymeric matrix and microneedles is slightly better than that between the polymeric materials with the microparticles. One of our previous studies found that the ZIFs synthesized in PVA solutions may entangle with PVA chains during the formation of crystal cells, and as a result, achieve good compatibility with

Pebax [18]. This may be one of the reasons the microneedle-shaped ZIFs, prepared in PVA solution, have better interfaces with Pebax phase.

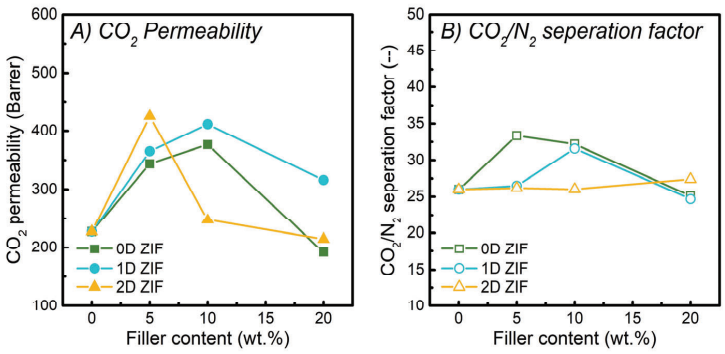

Figure 7 The A) CO_2 permeability and B) CO_2/N_2 separation factor of the MMMs with different filler loading (tested at dry condition and room temperature with a feed pressure of 2 bar).

In addition to the gas permeability, the ZIFs' morphologies also play a role in the CO_2/N_2 separation factor (as shown in **Figure 7 (B)**). The incorporation of 0D or 1D into Pebax lifts the CO_2/N_2 selectivity from 26 to above 30. The presence of ZIFs leads to more tortuous transport paths for larger gases, while in the meantime, the pores inside these ZIFs may work as molecular sieves, allowing the small CO_2 to pass through. Therefore, the selectivity is reinforced by adding ZIFs. However, further addition provokes deterioration, as a result of filler aggregation. On the other hand, the CO_2/N_2 separation factor of membranes with 2D ZIFs stay almost unchanged. This probably is because the interfaces between Pebax and ZIF-L is not ideal, which generates the non-selective gaps (sieve-in-a-cage) and then fails to improve the selectivity at low loading. At high loading, the ZIFs agglomerate, as shown in SEM image (**Figure S6 (H)**) and thus fail separating gas mixtures.

These aforementioned performances were compared with the 2008 upper bound, as shown in **Figure 8** The MMMs with 0D and 1D ZIF move towards the upper right corner, while the membrane with 5 wt.% 2D ZIF only shifts towards the right side. The incorporation of these ZIFs does push the separation performance closer to the 2008 upper bound but still does not surpass it. Considering the improved performances, these three membranes were chosen for further studies.

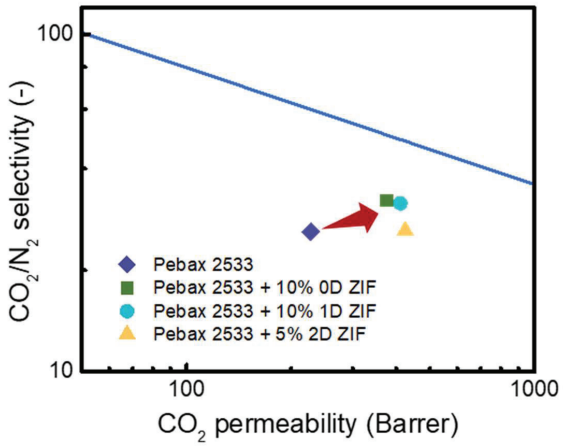

Figure 8 Comparison of the CO_2/N_2 separation performance of Pebax + ZIFs membranes with the 2008 Upper bound.

Effect of operating temperature

The effects of the operating temperature have been investigated by conducting mixed gas permeation experiments at different temperatures: 24, 40 and 60 ºC (**Figure 9**). The CO_2 permeabilities of all membranes increase significantly, while the CO_2/N_2 separation factors decrease with increasing operating temperature. The higher operating temperature facilitates the diffusion of gas molecules, which benefits the enhancement in gas permeability. Moreover, the polymeric chains become more flexible at higher temperatures, and then form more free volume

for gas transporting through membranes, consequently leading to higher gas permeability. While the increment in CO_2 permeability with the increasing temperature seems to be negatively affected by the added ZIFs, indicating by the less slope of the membranes containing ZIFs compared to the neat Pebax. The presence of ZIFs inside membranes may hinder the chain mobility at higher temperature, and hence results in less increments in gas permeability. Among them, the 2D ZIF seems to have more influence on the polymeric chain packing because of its greater decrease in CO_2 permeability.

On the other hand, for most of polymeric membranes, increasing operating temperatures usually leads to decreasing CO_2/light gas selectivity, as a result of the wider pore element distribution at higher temperature. This agrees with the results of neat Pebax, as illustrated in **Figure 9 (B)**. For the membranes containing ZIFs, the separation factors also decrease, as expected, since the Pebax still is the main ingredient (90 or 95 %) of these MMMs. In addition, the loss in the CO_2/N_2 separation factor of these four membranes are similar, which at 60 ^oC, only have remained 50% of the values at R.T.. Therefore, it could be concluded that these decreases are mainly caused by the behavior of the neat Pebax.

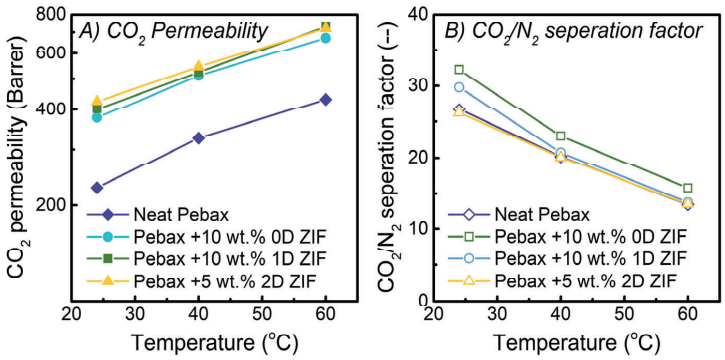

Figure 9 The A) CO_2 permeability and B) CO_2/N_2 separation factor of the MMMs as a function of operation temperature. (Tested at dry condition with a feed pressure of 2 bar.)

Effect of feed pressure

The influences of the feed pressure were also studied, and the results are presented in **Figure 10**. The CO_2 permeability and the CO_2/N_2 separation factor of the neat Pebax membrane decrease slightly (~ 5%) with the increasing feed pressure, in consistence with the previous studies [43-44]. One possible reason is that the feed pressure compresses the polymeric chains and then reduces the free volume, as well as the CO_2 permeability [37]. For the MMMs, the decrease rate of CO_2 permeability is close to that of the neat Pebax, while the changes in CO_2/N_2 separation factor are dependent on the filler. The membrane with 0D ZIF has almost unchanged selectivity with increasing feed pressure. However, the CO_2/N_2 selectivity of the membrane containing 10% 1D ZIF reduces from 28 to 14 when feed pressure increases from 2 bar to 6 bar. The membranes containing 1D ZIFs are much less robust compared to the neat polymeric one: the pore elements generated by adding ZIFs may merge together thus reduce the molecular-sieving effect at higher operation pressure. This result indicates that the Pebax + 1D ZIF membranes may not be a good candidate for higher-pressure application. Unexpectedly, the Pebax + 5% 2D ZIF membranes have

better resistance to the feed pressure compared to the other two MMMs in terms of CO_2/N_2 selectivity.

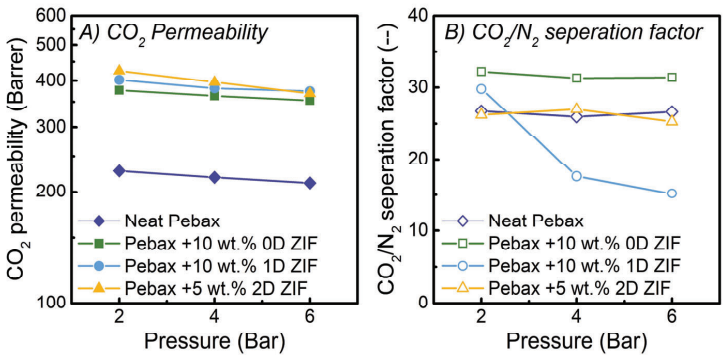

Figure 10 The A) CO_2 permeability and B) CO_2/N_2 separation factor of the MMMs with a function of feed pressure. (Tested at dry condition and room temperature)

4. Conclusions

In present work, three ZIFs with three different morphologies (particles, microneedles and leaves) were prepared. The presence of polymeric additives (PEG 400 and PVA) play an important role on the construction and the structures of the ZIF crystals. The characterization results indicate that the ZIF particles synthesized in PEG 400 solution have the same crystal structure with ZIF-8, while the microneedle-shaped ZIF from PVA solution is closer to that of the ZIF-L, although the shapes of the fillers are quite different.

The influence of the ZIFs with different morphology on the Pebax 2533 + ZIF MMMs were systemically evaluated by several characterization approaches. The chemical, thermal and the crystalline properties of the resultant MMMs have proved the presence of the aforementioned ZIFs, indicating the successful incorporation of ZIFs into Pebax matrix. Further morphology analysis also confirms the well-dispersion of these fillers inside the MMMs at low ZIF loading, based on

both surface and cross-section images. However, the addition of 20 wt.% 2D ZIF leads to clear agglomeration, but this is not observed for the 0D or 1D.

The mixed gas permeation results show that the incorporation of these ZIFs firstly increases and then decreases the CO_2 permeability, regardless of the morphology of the filler. But the optimal ZIF contents are dependent on the filler morphology: 10 wt.% for 0D and 1D ZIF, while 5 wt.% for 2D. Similar influences of the filler loading were found for the CO_2/N_2 selectivity of the membranes with 0D or 1D ZIFs, and the optimal ZIF loadings for selectivity are the same as those for CO_2 permeability. Moreover, the comparison of the best CO_2 separation performance among the three MMMs shows that the increment in CO_2 permeability is associated with the ZIFs' morphologies in the order: 0D < 1D < 2D, despite the lower loading of 2D ZIFs. An opposite trend was observed for CO_2/N_2 selectivity. Therefore, these three optimized MMMs were chosen to study the effects of the operating temperature and the feed pressure. The increasing operating temperature results in greatly enhanced CO_2 permeability and reduced CO_2/N_2 selectivity for all membranes, while this difference in the impact on the operating temperature for the investigated MMMs are similar to that of neat Pebax membrane. The change in feed pressure results in a more different behavior: the CO_2/N_2 selectivity of the membranes with 10 wt.% 1D deteriorates largely (reduced almost by 50 %) with rising feed pressure compared to the results of the other membranes. Similar observation has been found for the CO_2 permeability of the Pebax + 5 wt.% 2D ZIF.

ASSOCIATED CONTENTS

SUPPORTING INFORMATION

The results of FTIR, TGA, DSC, XRD and SEM images of membranes containing 0D and 2D ZIF were presented in Supporting Information.

AUTHOR INFORMATION

Corresponding Author

* Liyuan Deng.

E-mail: deng@nt.ntnu.no, Tel.: +47 73594112,

ORCID:

Zhongde Dai: 0000-0002-3558-5403

Jing Deng: 0000-0003-3680-3799

Liyuan Deng: 0000-0003-4785-4620

Author Contributions

The manuscript was written through contributions of all authors. All authors have given approval to the final version of the manuscript.

Notes

The authors declare no competing financial interest.

ACKNOWLEDGEMENTS

This work is supported by the Research Council of Norway through CLIMIT program ("POLYMEM" project, No. 254791).

REREFENCES

(1) Wu, Z. Inorganic Membranes for Gas Separations. In *Membrane Separation Principles and Applications*; Ismail, A. F.; Rahman, M. A.; Othman, M. H. D.; Matsuura, T., Eds.; Elsevier: 2019; pp 147-179.

(2) Kim, J. F.; Jung, J. T.; Wang, H. H.; Lee, S. Y.; Moore, T.; Sanguineti, A.; Drioli, E.; Lee, Y. M. Microporous PVDF membranes via thermally induced phase separation (TIPS) and stretching methods. *J. Membr. Sci.* **2016,** *509*, 94-104, DOI: https://doi.org/10.1016/j.memsci.2016.02.050.
(3) Zhu, L.; Yin, D.; Qin, Y.; Konda, S.; Zhang, S.; Zhu, A.; Liu, S.; Xu, T.; Swihart, M. T.; Lin, H. Sorption-Enhanced Mixed Matrix Membranes with Facilitated Hydrogen Transport for Hydrogen Purification and CO_2 Capture. *Adv. Funct. Mater.* **2019,** *29* (36), 1904357, DOI: 10.1002/adfm.201904357.
(4) *Gas Separation Membranes Market by Material type (Polyimide & Polyaramide, Polysulfone, and Cellulose Acetate), Application (Nitrogen Generation & Oxygen Enrichment, Carbon Dioxide Removal, and Hydrogen Recovery), and Region - Global Forecast to 2024*; MarketsandMarkets™: 2019.
(5) Robeson, L. M. The upper bound revisited. *J. Membr. Sci.* **2008,** *320* (1-2), 390-400.
(6) Seoane, B.; Coronas, J.; Gascon, I.; Etxeberria Benavides, M.; Karvan, O.; Caro, J.; Kapteijn, F.; Gascon, J. Metal-organic framework based mixed matrix membranes: a solution for highly efficient CO_2 capture? *Chem. Soc. Rev.* **2015,** *44* (8), 2421-54, DOI: 10.1039/c4cs00437j.
(7) Galizia, M.; Chi, W. S.; Smith, Z. P.; Merkel, T. C.; Baker, R. W.; Freeman, B. D. 50th Anniversary Perspective: Polymers and Mixed Matrix Membranes for Gas and Vapor Separation: A Review and Prospective Opportunities. *Macromolecules* **2017,** *50* (20), 7809-7843, DOI: 10.1021/acs.macromol.7b01718.
(8) Song, Q.; Nataraj, S.; Roussenova, M. V.; Tan, J. C.; Hughes, D. J.; Li, W.; Bourgoin, P.; Alam, M. A.; Cheetham, A. K.; Al-Muhtaseb, S. A. Zeolitic imidazolate framework (ZIF-8) based polymer nanocomposite membranes for gas separation. *Energy Environ. Sci.* **2012,** *5* (8), 8359-8369.
(9) Shen, J.; Liu, G.; Huang, K.; Jin, W.; Lee, K.-R.; Xu, N. Membranes with Fast and Selective Gas-Transport Channels of Laminar Graphene Oxide for Efficient CO_2 Capture. *Angew. Chem.* **2015,** *127* (2), 588-592, DOI: 10.1002/ange.201409563.
(10) Lin, R.; Villacorta Hernandez, B.; Ge, L.; Zhu, Z. Metal organic framework based mixed matrix membranes: an overview on filler/polymer interfaces. *J. Mater. Chem. A* **2018,** *6* (2), 293-312, DOI: 10.1039/C7TA07294E.
(11) Ayas, İ.; Yilmaz, L.; Kalipcilar, H. The Gas Permeation Characteristics of Ternary Component Mixed Matrix Membranes Prepared Using ZIF-8 with a Large Range of Average Particle Size. *Ind. Eng. Chem. Res.* **2018,** *57* (47), 16041-16050, DOI: 10.1021/acs.iecr.8b02440.
(12) Sánchez-Laínez, J.; Zornoza, B.; Friebe, S.; Caro, J.; Cao, S.; Sabetghadam, A.; Seoane, B.; Gascon, J.; Kapteijn, F.; Le Guillouzer, C.; Clet, G.; Daturi, M.; Téllez, C.; Coronas, J. Influence of ZIF-8 particle size in the performance of polybenzimidazole mixed matrix membranes for pre-combustion CO_2 capture and its validation through interlaboratory test. *J. Membr. Sci.* **2016,** *515*, 45-53, DOI: https://doi.org/10.1016/j.memsci.2016.05.039.
(13) Bae, T.-H.; Lee, J. S.; Qiu, W.; Koros, W. J.; Jones, C. W.; Nair, S. A High-Performance Gas-Separation Membrane Containing Submicrometer-Sized Metal–Organic Framework Crystals. *Angew. Chem. Int. Ed.* **2010,** *49* (51), 9863-9866, DOI: 10.1002/anie.201006141.
(14) Japip, S.; Xiao, Y.; Chung, T.-S. Particle-Size Effects on Gas Transport Properties of 6FDA-Durene/ZIF-71 Mixed Matrix Membranes. *Ind. Eng. Chem. Res.* **2016,** *55* (35), 9507-9517, DOI: 10.1021/acs.iecr.6b02811.
(15) Zheng, W.; Ding, R.; Yang, K.; Dai, Y.; Yan, X.; He, G. ZIF-8 nanoparticles with tunable size for enhanced CO_2 capture of Pebax based MMMs. *Sep. Purif. Technol.* **2019,** *214*, 111-119, DOI: https://doi.org/10.1016/j.seppur.2018.04.010.

(16) Sabetghadam, A.; Seoane, B.; Keskin, D.; Duim, N.; Rodenas, T.; Shahid, S.; Sorribas, S.; Le Guillouzer, C.; Clet, G.; Tellez, C.; Daturi, M.; Coronas, J.; Kapteijn, F.; Gascon, J. Metal Organic Framework Crystals in Mixed-Matrix Membranes: Impact of the Filler Morphology on the Gas Separation Performance. *Adv. Funct. Mater.* **2016,** *26* (18), 3154-3163, DOI: 10.1002/adfm.201505352.
(17) Rodenas, T.; Luz, I.; Prieto, G.; Seoane, B.; Miro, H.; Corma, A.; Kapteijn, F.; Llabrés i Xamena, F. X.; Gascon, J. Metal–organic framework nanosheets in polymer composite materials for gas separation. *Nat. Mater.* **2014,** *14*, 48, DOI: 10.1038/nmat4113

https://www.nature.com/articles/nmat4113#supplementary-information.
(18) Deng, J.; Dai, Z.; Deng, L. Novel MOF nanosheets with tunable thickness and their application in mixed matrix membranes for CO_2 application. *sumbitted to J. Mater. Chem. A*.
(19) Dai, Z.; Aboukeila, H.; Ansaloni, L.; Deng, J.; Giacinti Baschetti, M.; Deng, L. Nafion/PEG hybrid membrane for CO_2 separation: Effect of PEG on membrane micro-structure and performance. *Sep. Purif. Technol.* **2019,** *214*, 67-77, DOI: https://doi.org/10.1016/j.seppur.2018.03.062.
(20) Dai, Z.; Deng, J.; Peng, K.-J.; Liu, Y.-L.; Deng, L. Pebax/PEG Grafted CNT Hybrid Membranes for Enhanced CO_2/N_2 Separation. *Ind. Eng. Chem. Res.* **2019,** *58* (27), 12226-12234, DOI: 10.1021/acs.iecr.9b01466.
(21) Yang, F.; Mu, H.; Wang, C.; Xiang, L.; Yao, K. X.; Liu, L.; Yang, Y.; Han, Y.; Li, Y.; Pan, Y. Morphological Map of ZIF-8 Crystals with Five Distinctive Shapes: Feature of Filler in Mixed-Matrix Membranes on C_3H_6/C_3H_8 Separation. *Chem. Mater.* **2018,** *30* (10), 3467-3473, DOI: 10.1021/acs.chemmater.8b01073.
(22) Chen, R.; Yao, J.; Gu, Q.; Smeets, S.; Baerlocher, C.; Gu, H.; Zhu, D.; Morris, W.; Yaghi, O. M.; Wang, H. A two-dimensional zeolitic imidazolate framework with a cushion-shaped cavity for CO_2 adsorption. *Chem. Commun.* **2013,** *49* (82), 9500-9502, DOI: 10.1039/C3CC44342F.
(23) Zhou, K.; Mousavi, B.; Luo, Z.; Phatanasri, S.; Chaemchuen, S.; Verpoort, F. Characterization and properties of Zn/Co zeolitic imidazolate frameworks vs. ZIF-8 and ZIF-67. *J. Mater. Chem. A* **2017,** *5* (3), 952-957, DOI: 10.1039/C6TA07860E.
(24) Pan, Y.; Liu, Y.; Zeng, G.; Zhao, L.; Lai, Z. Rapid synthesis of zeolitic imidazolate framework-8 (ZIF-8) nanocrystals in an aqueous system. *Chem. Commun.* **2011,** *47* (7), 2071-2073, DOI: 10.1039/C0CC05002D.
(25) Kida, K.; Okita, M.; Fujita, K.; Tanaka, S.; Miyake, Y. Formation of high crystalline ZIF-8 in an aqueous solution. *CrystEngComm* **2013,** *15* (9), 1794-1801.
(26) Fan, X.; Wang, W.; Li, W.; Zhou, J.; Wang, B.; Zheng, J.; Li, X. Highly Porous ZIF-8 Nanocrystals Prepared by a Surfactant Mediated Method in Aqueous Solution with Enhanced Adsorption Kinetics. *ACS Appl. Mater. Interfaces* **2014,** *6* (17), 14994-14999, DOI: 10.1021/am5028346.
(27) Tian, Z.; Yao, X.; Ma, K.; Niu, X.; Grothe, J.; Xu, Q.; Liu, L.; Kaskel, S.; Zhu, Y. Metal–Organic Framework/Graphene Quantum Dot Nanoparticles Used for Synergistic Chemo- and Photothermal Therapy. *ACS Omega* **2017,** *2* (3), 1249-1258, DOI: 10.1021/acsomega.6b00385.
(28) Wu, C.; Liu, Q.; Chen, R.; Liu, J.; Zhang, H.; Li, R.; Takahashi, K.; Liu, P.; Wang, J. Fabrication of ZIF-8@ SiO_2 micro/nano hierarchical superhydrophobic surface on AZ31 magnesium alloy with impressive corrosion resistance and abrasion resistance. *ACS Appl. Mater. Interfaces* **2017,** *9* (12), 11106-11115.

(29) Armstrong, S.; Freeman, B.; Hiltner, A.; Baer, E. Gas permeability of melt-processed poly(ether block amide) copolymers and the effects of orientation. *Polymer* **2012,** *53* (6), 1383-1392, DOI: https://doi.org/10.1016/j.polymer.2012.01.037.
(30) Dai, Z.; Bai, L.; Hval, K. N.; Zhang, X.; Zhang, S.; Deng, L. Pebax®/TSIL blend thin film composite membranes for CO_2 separation. *Sci. China. Chem.* **2016,** *59* (5), 538-546, DOI: 10.1007/s11426-016-5574-3.
(31) Estahbanati, E. G.; Omidkhah, M.; Amooghin, A. E. Preparation and characterization of novel Ionic liquid/Pebax membranes for efficient CO_2/light gases separation. *Journal of Industrial and Engineering Chemistry* **2017,** *51*, 77-89.
(32) Guan, P.; Luo, J.; Li, W.; Si, Z. Enhancement of gas permeability for CH_4/N_2 separation membranes by blending SBS to Pebax polymers. *Macromolecular Research* **2017,** *25* (10), 1007-1014.
(33) Dong, L.; Chen, M.; Wu, X.; Shi, D.; Dong, W.; Zhang, H.; Zhang, C. Multi-functional polydopamine coating: simultaneous enhancement of interfacial adhesion and CO_2 separation performance of mixed matrix membranes. *New J. Chem.* **2016,** *40* (11), 9148-9159.
(34) Dong, L.; Zhang, C.; Bai, Y.; Shi, D.; Li, X.; Zhang, H.; Chen, M. High-Performance PEBA2533-Functional MMT Mixed Matrix Membrane Containing High-Speed Facilitated Transport Channels for CO_2/N_2 Separation. *ACS Sustainable Chemistry & Engineering* **2016,** *4* (6), 3486-3496, DOI: 10.1021/acssuschemeng.6b00536.
(35) Han, J.; Bai, L.; Yang, B.; Bai, Y.; Luo, S.; Zeng, S.; Gao, H.; Nie, Y.; Ji, X.; Zhang, S.; Zhang, X. Highly Selective Oxygen/Nitrogen Separation Membrane Engineered Using a Porphyrin-Based Oxygen Carrier. *Membranes* **2019,** *9* (9), DOI: 10.3390/membranes9090115.
(36) Yu, S.; Jiang, Z.; Yang, S.; Ding, H.; Zhou, B.; Gu, K.; Yang, D.; Pan, F.; Wang, B.; Wang, S.; Cao, X. Highly swelling resistant membranes for model gasoline desulfurization. *J. Membr. Sci.* **2016,** *514*, 440-449, DOI: https://doi.org/10.1016/j.memsci.2016.05.015.
(37) Zhu, W.; Li, X.; Sun, Y.; Guo, R.; Ding, S. Introducing hydrophilic ultra-thin ZIF-L into mixed matrix membranes for CO_2/CH_4 separation. *RSC Adv.* **2019,** *9* (40), 23390-23399.
(38) Bondar, V. I.; Freeman, B. D.; Pinnau, I. Gas transport properties of poly(ether-b-amide) segmented block copolymers. *J. Polym. Sci., Part B: Polym. Phys.* **2000,** *38* (15), 2051-2062, DOI: 10.1002/1099-0488(20000801)38:15<2051::AID-POLB100>3.0.CO;2-D.
(39) Bachman, J. E.; Smith, Z. P.; Li, T.; Xu, T.; Long, J. R. Enhanced ethylene separation and plasticization resistance in polymer membranes incorporating metal–organic framework nanocrystals. *Nat. Mater.* **2016,** *15*, 845, DOI: 10.1038/nmat4621

https://www.nature.com/articles/nmat4621#supplementary-information.
(40) Md. Nordin, N. A. H.; Ismail, A. F.; Mustafa, A.; Murali, R. S.; Matsuura, T. Utilizing low ZIF-8 loading for an asymmetric PSf/ZIF-8 mixed matrix membrane for CO_2/CH_4 separation. *RSC Adv.* **2015,** *5* (38), 30206-30215, DOI: 10.1039/C5RA00567A.
(41) Johnson, J. R.; Koros, W. J. Utilization of nanoplatelets in organic–inorganic hybrid separation materials: Separation advantages and formation challenges. *Journal of the Taiwan Institute of Chemical Engineers* **2009,** *40* (3), 268-275, DOI: https://doi.org/10.1016/j.jtice.2009.03.003.
(42) Karunakaran, M.; Shevate, R.; Kumar, M.; Peinemann, K. V. CO_2-selective PEO–PBT (PolyActive™)/graphene oxide composite membranes. *Chem. Commun.* **2015,** *51* (75), 14187-14190, DOI: 10.1039/C5CC04999G.

(43) Isfahani, A. P.; Ghalei, B.; Wakimoto, K.; Bagheri, R.; Sivaniah, E.; Sadeghi, M. Plasticization resistant crosslinked polyurethane gas separation membranes. *J. Mater. Chem. A* **2016,** *4* (44), 17431-17439.
(44) Hou, J.; Li, X.; Guo, R.; Zhang, J.; Wang, Z. Mixed matrix membranes with fast and selective transport pathways for efficient CO_2 separation. *Nanotechnology* **2018,** *29* (12), 125706.

TOC

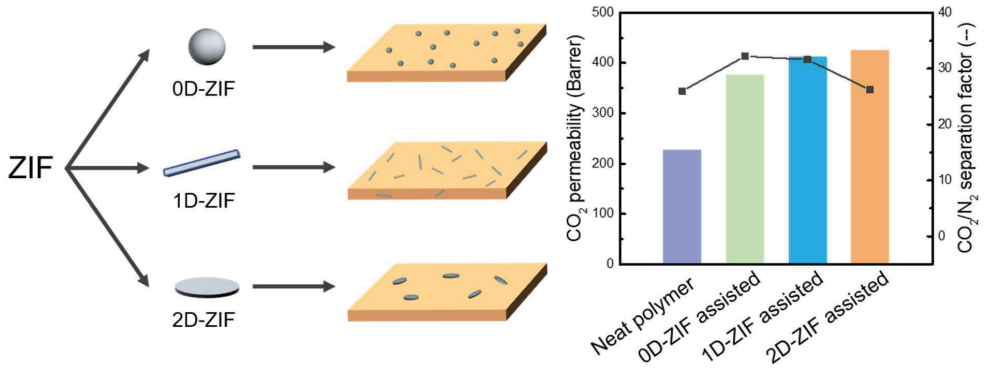
ZIF
0D-ZIF
1D-ZIF
2D-ZIF
CO2 permeability (Barrer)
CO2/N2 separation factor (--)
0
100
200
300
400
500
0
10
20
30
40
Neat polymer
0D-ZIF assisted
1D-ZIF assisted
2D-ZIF assisted

Effects of the ZIFs' Morphology on the CO_2 Separation Performance of MMMs

Supporting Information

*Jing Deng†, Zhongde Dai† and Liyuan Deng**

Department of Chemical Engineering, Norwegian University of Science and Technology, 7491 Trondheim, Norway

† These authors contributed equally.

Table of Contents

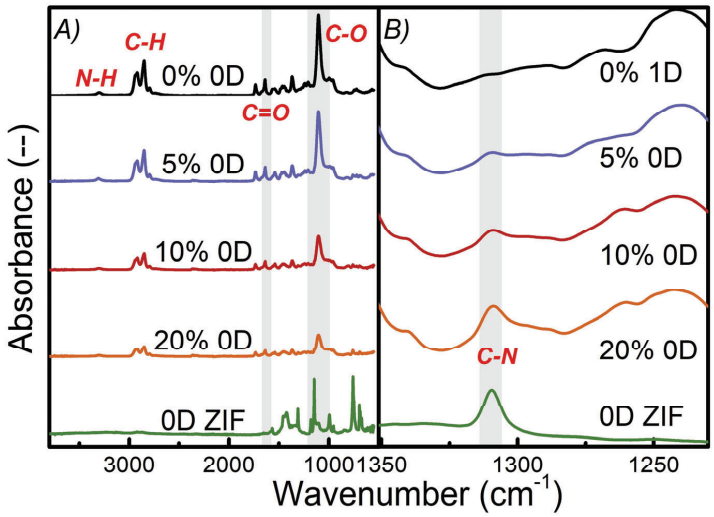

Figure S1 The FTIR spectra of the MMMs containing 0D ZIFs with a range of A) 4000 – 500 cm^{-1} and B) 1350 – 1230 cm^{-1}

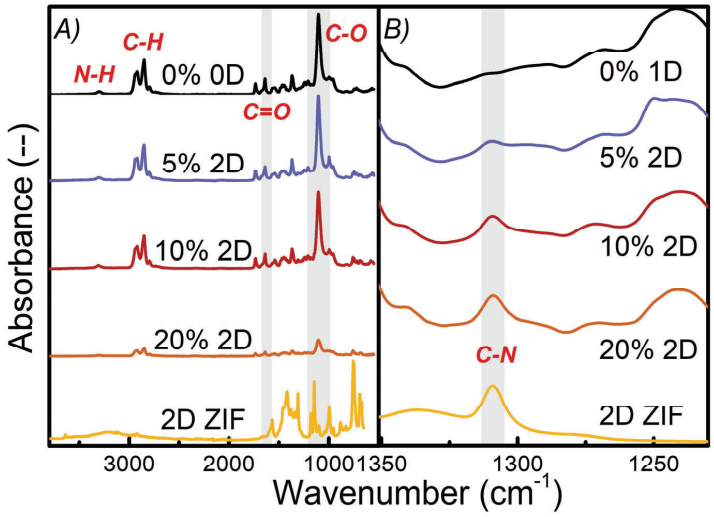

Figure S2 The FTIR spectra of the MMMs containing 2D ZIFs with a range of A) 4000 – 500 cm^{-1} and B) 1350 – 1230 cm^{-1}

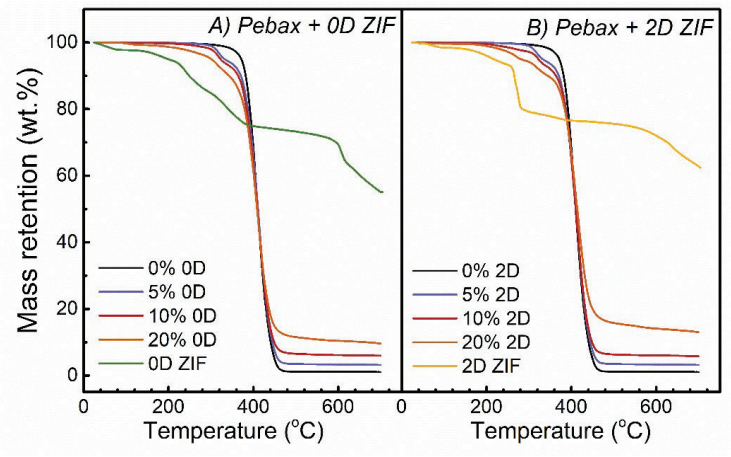

Figure S3 The TGA results of the MMMs with various loading of A) 0D ZIFs and B) 2D ZIF.

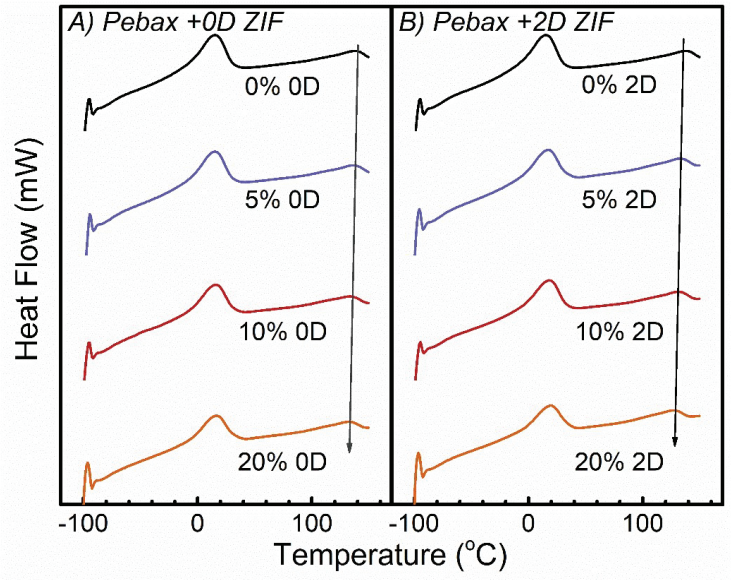

Figure S4 The DSC results of the MMMs with various loading of A) 0D ZIFs and B) 2D ZIF.

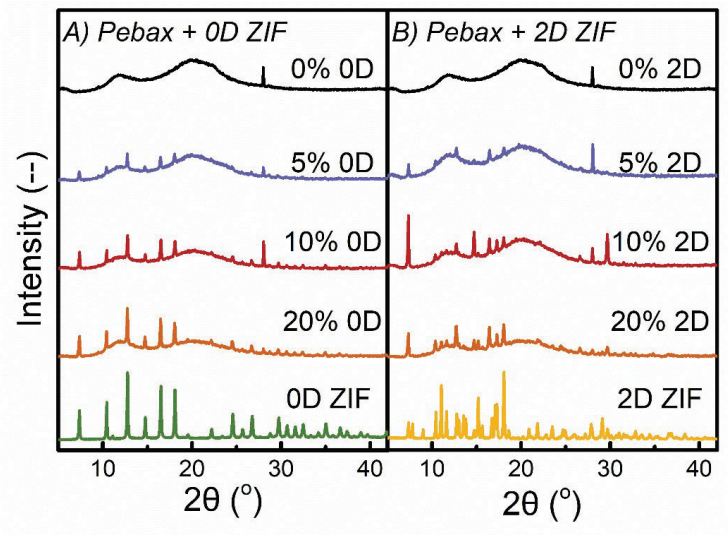

Figure S5 The XRD results of the MMMs with various loading of A) 0D ZIFs, B) 1D ZIFs and C) 2D ZIFs

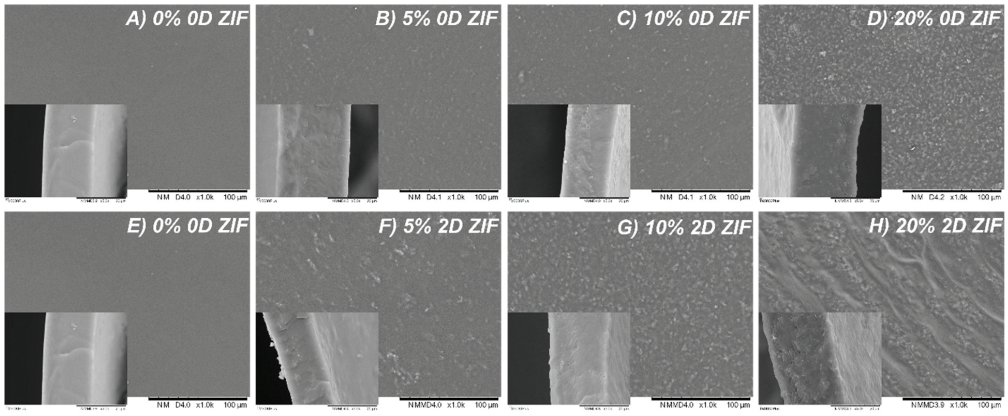

Figure S6 The SEM images of the MMMs containing A-D) 0D ZIFs and E-H) 2D ZIFs with various loading.

H_2-selective Mixed Matrix Membranes Enhanced by 2D MOFs

This paper has been submitted to

Journal of Membrane Science.

Paper VI

H_2-selective Mixed Matrix Membranes Enhanced by 2D MOFs

Jing Deng†, Zhongde Dai† and Liyuan Deng*

Department of Chemical Engineering, Norwegian University of Science and Technology, 7491 Trondheim, Norway

E-mail: deng@nt.ntnu.no, Tel.: +47 73594112

† These authors contributed equally.

Abstract

In this work, two two-dimensional (2D) leaf-like ZIFs (ZIF-L-Zn and ZIF-L-Co) were incorporated into the microporous Troger's base (TB)-based polymers for hydrogen separation. Various characterization results have documented the good dispersion of leaf ZIFs in the resultant mixed matrix membranes (MMMs), thanks to the good compatibility between polymeric matrix and nanoleaves. The addition of both leaf ZIFs greatly enhances the gas permeabilities of all investigated species within the studied loading. Thanks to the interlayer channels in the laminated 2D ZIFs, small molecules like H_2 obtain additional fast transport pathway and, thus, a remarkable increase in gas permeability up to 4 times. A H_2 permeability of 1235.5 Barrer was achieved in the presence of only 20 wt.% ZIF-L-Co. Compared with ZIF-L-Zn, ZIF-L-Co is more efficient in promoting gas permeabilites with similar selectivities for all gas pairs. The MMMs with ZIF-L-Co have displayed excellent hydrogen separation performances which surpass all Upper Bounds of H_2/CO_2, H_2/N_2 and H_2/CH_4. Further increasing the operating temperature enhances the gas transport properties, and the membrane with 20 wt.% ZIF-L-Co at 60 ^oC gives a H_2 permeability up to 1985.9 Barrer, which is 6.8 times greater than that given by the neat polymers.

Keywords:

Leaf ZIFs; troger's base polymer; mixed matrix membranes; hydrogen separation

Highlights

- The addition of leaf ZIFs greatly enhances the gas transport properties of the MMMs;
- The ZIF-L-Co is more efficient in promoting gas permeabilities than ZIF-L-Zn;
- H_2 permeability was increased to up to 1235.5 Barrer with 20 wt.% ZIF-L-Co at R.T.;
- The separation performances exceed the Upper Bounds of H_2/CO_2, H_2/CH_4 and H_2/N_2;
- Increasing temperature leads to an increment in $P(H_2)$ by a factor of 4.3 (1985.9 Barrer).

1 Introduction

Hydrogen (H_2), recognized as one of the cleanest energy sources, has been utilized as an energy source in fuel cells or the starting materials for the syntheses of various chemicals [1-3]. The demands for clean and sustainable energy have grown exponentially, and the hydrogen market, which was valued at around $108.1 billion in 2016, has been estimated to reach $180.2 billion by 2025 [4]. Despite its abundance on earth, H_2 cannot be obtained naturally, and the major production technique currently is the steam methane reforming based on fossil fuel or natural gas [5-7]. The synthesized H_2 needs to be purified from the H_2/CO_2 mixture before being used in various industrial applications (e.g., methanol or ammonia production). Generally speaking, in these applications, the reactant H_2 needs to be separated from the product mixture and re-cycled to ensure a high process efficiency and a high product yield. Therefore, H_2 separation from various gas mixture is extremely crucial. Considering the huge market size, any improvement in H_2 purification will bring significant benefits.

The gas membrane technology has a much lower energy consumption rate, smaller footprints and simpler operation than the major conventional separation method (i.e., liquid absorption). However, current H_2-selective polymeric membranes are limited to a few materials, since most polymeric materials usually have very low H_2 permeabilities (< 100 Barrer) or H_2 selectivities (H_2/N_2 selectivity of ~ 2 for PTMSP and ~ 10 for PIM-1; H_2/CH_4 selectivity of ~ 1 for PTMSP and ~ 10 for PIM-1) [8, 9]. According to the solution-diffusion theory, materials with high free volume and narrow porous element distribution may achieve high H_2 permeability and high H_2 selectivity at the same time. Therefore, recently developed materials with more free volume elements have been intensively employed to realize higher gas diffusion and, thus, higher gas permeability without sacrificing high selectivity. Based on the polymer structure, decreasing chain mobility by introducing bulky and contorted units could generate more free volume and thus lead to better separation performance [10]. This is mostly seen in polymers with intrinsic microporosity (PIM). Since the excellent separation performance of PIMs was first reported [11], many contorted and inflexible units have been developed and incorporated into polymer structure for membrane separation purposes [12]. In 2013, Mckeown and coworkers found that PIMs containing bridged bicyclic amine, usually called Troger's base (TB), could have particularly high gas permeability and considerably high gas selectivity, which exceed or are close to the Upper Bounds for several gas pairs [13]. Further analysis was carried out and the results show that the dihedral angle at the

center of the TB (120°) is much higher than that at the center of the spirobisindane (~ 90 °), usually known as units of PIM-1, thus resulting in more rigid chains, less efficient packing and higher gas permeability. It is worth noting that the synthesis of TB units is relatively easy and simple, and the resultant polymers are usually soluble in many organic solvents. Recent studies have enlarged the family of TB-based polymers to include polyimide copolymer [14-18], or polymers containing only TB units [19, 20]. These TB-based polymers generally have high gas permeability for small molecules because of the contorted chains. In addition, due to their narrow distribution of free volume elements, their selectivities for various gas pairs (e.g.: H_2/N_2: ~ 50) are rather high compared to other polymers with high gas permeabilities.

Recently, introducing inorganic materials into polymeric matrix has aroused plenty of attention as it combines the excellent H_2 separation performance of the inorganic materials and the good processability of polymeric matrix [21-24]. Some studies have reported this method's effectiveness in promoting the H_2 separation performance. Song *et al.* reported that by mixing two different nanoparticles (nonporous SiO_2 and microporous ZIF-8) with PIM-1, H_2 permeability was enhanced from around 3361 Barrer to 5456 Barrer with a slight increase in H_2/N_2 and H_2/CH_4 selectivities [22]. The large increment in H_2 permeability is mainly as a result of the increased diffusion, which could be explained by several factors. First, the incorporation of nanofillers disrupts the packing arrangement of rigid polymer and, thus, changes the porous elements in the membranes. The interfaces between the inorganic particles and the polymeric matrix also enhance the gas diffusion. Moreover, the well-designed structure of these inorganic fillers may contribute extra transport channels for H_2 transport. The authors compared two different nanoparticles and found that the porous ZIF-8s could offer extra transport channels for small molecules like H_2, thus obtaining higher H_2 permeabilities, compared with the nonporous silica. The overall performances surpass the Upper Bounds for several gas pairs, like H_2/N_2 and H_2/CH_4. But some well-designed nonporous nanoparticles could also provide great benefits for this application. Wang and coworkers incorporated the ZIF-Ls into a polyimide (PI) matrix for gas separation [23]. The gas permeation results show this combination offers a greatly increased H_2 permeability and selectivity, and these enhancements are mainly caused by the aligned interlayer channels in the 2D ZIF-L with a size of 3.1 Å, which could block the bigger molecules (i.e., CO_2), but not the smaller ones (i.e., H_2) that can pass freely.

Hence, in this work, the heterocyclic TB-based polymer was chosen as the polymeric matrix. Two leaf-like ZIFs (ZIF-L-Zn and ZIF-L-Co) were incorporated into the TB-based polymer to prepare a series of TB + leaf-like ZIFs MMMs. The influence of these leaf-like ZIFs on the material properties and the H_2 separation performance of the resultant MMMs were studied. Various methods, like thermal gravimetric analysis (TGA), Fourier-transform infrared spectroscopy (FTIR), scanning electron microscope (SEM) and single gas permeation experiments, were employed. The gas transport properties, with respect to H_2, CO_2, N_2, and CH_4, of the resultant MMMs were systematically assessed, and the ideal selectivity for various gas pairs were also studied. Moreover, the effects of permeation operating temperature were studied.

2 Experimental section

2.1. Materials

$Zn(NO_3)_2{\cdot}6H_2O$, $Co(NO_3)_2{\cdot}6H_2O$ and 2-methylimidazole (Hmim) were ordered from Sigma, Norway. Tolidine, dimethoxymethane (DMM), trifluoroacetic acid (TA), ammonium hydroxide solution (28%) and methylpyrrolidone (NMP) were also purchased from Sigma, Norway. Methanol was bought from VWR, Norway. All the chemicals were used without further treatment.

2.2. Leaf ZIFs and TB polymer synthesis

The preparation of ZIF-L-Zn followed the method developed by Wang et al. [25]. Typically, 0.59 g of $Zn(NO_3)_2{\cdot}6H_2O$ and 1.30 g of Hmim were dissolved in 40 mL deionized (DI) water respectively, and then the two solutions were mixed and stirred for 3 h at room temperature. For the preparation of ZIF-L-Co, 0.7275g of $Co(NO_3)_2{\cdot}6H_2O$ was dissolved in 50 mL DI water for 10 min, and 2.4025g of Hmim was dissolved in another 50 ml DI water for 10 min. Afterwards, the two solutions were mixed and stirred for 30 min. White ZIF-L-Zn and purple ZIF-L-Co leaf were obtained by filtering the respective mixtures using a vacuum filtration assembly (VWR) equipped with a PVDF filter membrane (pore size of 0.65 μm). The obtained ZIFs were dried in vacuum oven for 12 hours at 60 °C.

The TB polymer was synthesized, according to a procedure reported previously by Li et al. [19, 20], as shown in **Scheme 1**. Under a N_2 atmosphere, 20 g o-Tolidine and 36 g DMM were mixed in a 500 mL three-necked flask, which was placed in an ice-water bath. Afterwards, 200 mL of trifluoroacetic acid (TFA) was added in drops into the mixture within 30 min. Thereafter, the mixture was stirred at ambient conditions for 48 h. Then the polymerization was stopped by slowly

pouring the solution into 2L aqueous ammonium hydroxide solution (5 wt. %). The precipitated polymer was washed with excess DI water until the pH was close to 7, and then dried in a vacuum oven for 12 hours at 80 °C. The polymer was further purified by dissolving in NMP (~10 wt.%) and re-precipitating twice in methanol. Finally, the polymer was dried again in a vacuum oven for 12 hours at 80 °C.

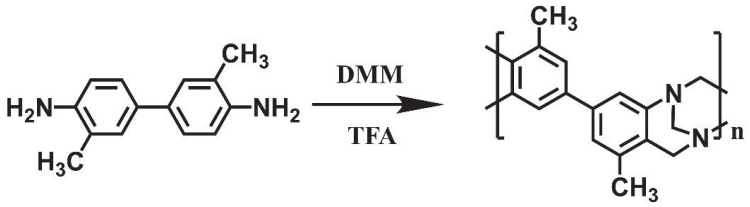

Scheme 1 The polymerization of TB polymer.

2.3. MMMs fabrication

MMMs were prepared through a knife casting method. Typically, the desired amount of dried leaf-like ZIFs were added into 5 ml NMP and stirred overnight until a well-dispersed suspension was obtained. Then the desired amount of TB polymer was added into the ZIF suspension and the total solid (i.e., TB + ZIFs) concentration was around 10 wt. %. Thereafter, the membrane solution was cast on a glass plate using a casting knife (PA-4302, BYK-CHEMIE GMBH, Germany), with a wet gap of ~ 600 μm. The cast membrane was then heated to 80 ^{o}C in vacuum for 24 h to evaporate NMP. To completely remove the solvent, the resulting membranes were immersed in methanol for 12 h at room temperature. Finally, the membranes were dried overnight in a vacuum oven at 60 ^{o}C.

2.4. Characterization

The morphology of the leaf ZIFs and MMMs was studied using a SEM (TM3030 tabletop microscope, Hitachi High Technologies). Surface samples of MMMs were prepared using scissors and cross-section specimens were prepared by breaking the samples in liquid N_2. All the samples were sputter-coated with gold for 2 minutes before SEM experiments to ensure good electrical conductivity.

The thermal stability of the leaf ZIFs and the resultant MMMs was evaluated by TGA (TG 209F1 Libra, Netzsch). Samples with 10 ~ 20 mg were tested from room temperature to 800 °C in N_2 atmosphere.

XRD (D8 A25 DaVinci, Bruker) was employed for the analysis of the crystallinity of the leaf ZIFs, as well as that of the resultant MMMs. The source was offered by Cu (Kα radiation) and the characteristic wavelength λ is 1.54 Å. The scans were taken in the 2θ range from 5° to 75°.

FTIR spectroscopy was carried out using a Thermo Nicolet Nexus spectrometer with a smart endurance reflection cell. The spectra averaged over 16 scans at a wavenumber resolution of 4 cm^{-1} from 550 cm^{-1} to 4000 cm^{-1}.

Single gas permeation tests were performed by the constant-volume variable-pressure method, with a feed pressure of around 2 bar at various temperatures. The gas permeabilities (*P*) were calculated as shown in equation (1):

$$\mathrm{P} = \left[\left(\frac{\mathrm{dp_d}}{\mathrm{dt}}\right)_{\mathrm{t}\to\infty} - \left(\frac{\mathrm{dp_d}}{\mathrm{dt}}\right)_{\mathrm{leak}}\right] \cdot \frac{\mathrm{V_d}}{\mathrm{A}\cdot\mathrm{R}\cdot\mathrm{T}} \cdot \frac{\mathrm{l}}{(\mathrm{p_u} - \mathrm{p_d})} \quad (1)$$

where *P* is the permeability (in Barrer), p_d and p_u are the downstream and upstream pressure, respectively, *t* refers to time, V_d is the downstream volume, *A* means the effective permeation area of membrane, *R* and *T* are the ideal gas constant and temperature, respectively, and *l* is the thickness of membrane. The leakage rate dp_d/dt was measured by isolating the membrane cell under vacuum condition for a certain period. The thicknesses of all membranes were measured by an ABS Digimatic Indicator (Mitutoyo, Suzhou, China). They were given by the average of more than 10 measurements for each membrane. The permeability was the average values obtained from at least 2 samples with a relative error of less than 10%.

The ideal selectivity of gas A over gas B ($\alpha_{A/B}$) was calculated using equation 2:

$$\alpha_{A/B} = \frac{\mathrm{P}_A}{\mathrm{P}_B} \quad (2)$$

3 Results and discussion

3.1. Characterization of Leaf ZIFs

The SEM images of the morphology of the two as-prepared leaf ZIFs are shown in **Figure 1 (A)-(B)**. These ZIF-L-Zn and ZIF-L-Co display a leaf-like shape with a size of 1.3 × 5.4 μm and 1.6 × 5.6 μm, respectively, similar with a previous report [25]. A BET surface area of 162.9 m^2/g and 12.5 m^2/g was obtained for ZIF-L-Zn and ZIF-L-Co, respectively, from N_2 adsorption experiments, and these results are comparable to the values reported in the previous literature (BET surface area lower than 200 m^2/g for ZIF-L-Zn [25-27] and 20 m^2/g for ZIF-L-Co [28]). Interestingly, both

adsorbed N_2 amount (**Figure 1(C)**), and the surface area of ZIF-L-Co are lower than that of ZIF-L-Zn. Regarding the identical structure and arrangement of the crystal units, the possible reason may be the narrower interlayer channels of ZIF-L-Co. To further confirm the structure of these as-prepared ZIFs, XRD analysis was employed. As shown in **Figure 1(D)**, the obtained XRD curves of both ZIFs are very similar to the reported experimental or simulated pattern by Wang and co-workers. [25]. Because of the same crystal construction, the crystal units of both leaf ZIFs are theoretically the same, which result in almost identical XRD patterns. The chemical nature of the ZIFs is evaluated by FTIR spectroscopy, and the resultant spectra are displayed in **Figure 1(E).** The main characteristic peaks of these ZIFs are associated with the Hmim units: the peaks at 1567 cm^{-1}, 1305 cm^{-1} and 995 cm^{-1} refer to the C=N bonds and C-N bond, respectively, and the broad ones at 3500 – 2500 cm^{-1} suggest the N–H···N hydrogen bonds between Hmim units. Since these ZIFs have the same organic ligand, their spectra are almost identical despite the different metal ions. That is because that the absorbance peak of metal ions – Hmim is reported to be around 400 cm^{-1} [29], which exceeds the tested range of the used FTIR.

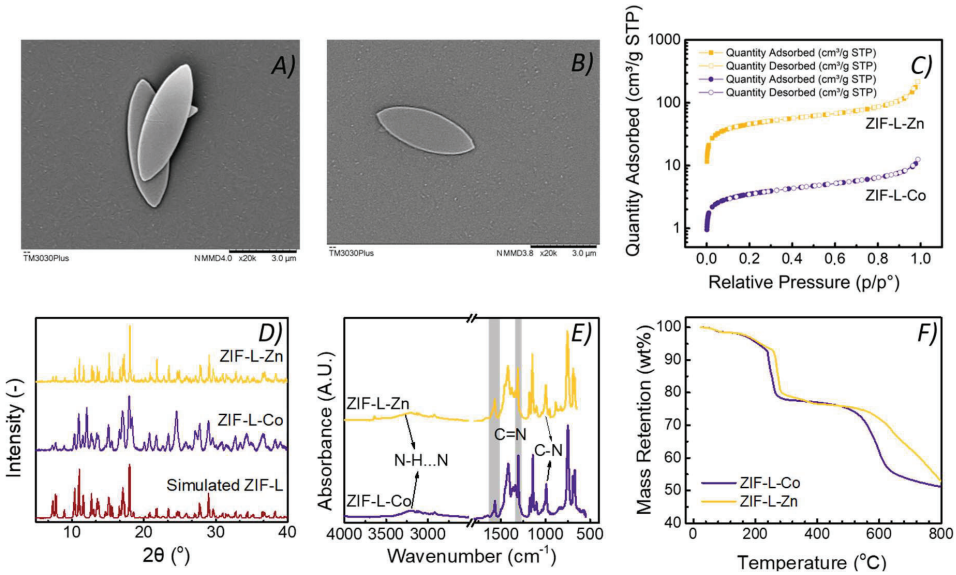

Figure 1 SEM image of A) ZIF-L-Zn and B) ZIF-L-Co, and the C) N_2 adsorption, D) XRD, E) FTIR and F) TGA results of ZIF-L-Zn and ZIF-L-Co.

The thermal decomposition behaviors of both ZIFs are quite similar, as shown in **Figure 1(F)**. A small weight loss (< 3 %) is observed at temperature below 100 ºC because of the remaining

solvent, followed by loss of structural water molecules and Hmim in the ZIFs [26, 27], which explains the sharp decrease at temperature around 230 - 250 ºC. Then there is a collapse in the crystal structure of the ZIFs when the temperature reaches 500 ºC, presented by the second sharp slope. Generally speaking, the ZIF-L-Co starts losing structural units slightly earlier than the ZIF-L-Zn. Considering that most applications of membrane gas separation have an operating temperature of 60 ºC or even lower, both ZIFs could fulfill the temperature requirements as membrane materials.

3.2. Characterization of the MMMs

3.2.1. Physical and chemical property characterization

FTIR

FTIR analysis was employed to study the chemical nature of the as-synthesized polymer and the resultant MMMs, and the results are presented in **Figure 2**. For the neat TB polymer, the absorbance bands at 2900 – 3000 cm^{-1} and 1450 - 1600 cm^{-1} are associated with the C-H vibration and the C=C vibration of the benzene ring, respectively. The C-N bonds in the heterocycles are observed at 1320 cm^{-1} [30], and no obvious peaks have been detected above 3000 cm^{-1}, suggesting the absence of the amine groups and thus the desired formation of the heterocycles during polymerization, which proves the successful synthesis of TB polymer. With the addition of leaf ZIFs, these peaks become weaker, while those from ZIFs are more significant: the C=N bond and C-N of Hmim ligand (1305 and 995 cm^{-1} respectively). These results represent the successful blend of the leaf ZIFs into TB polymer matrix.

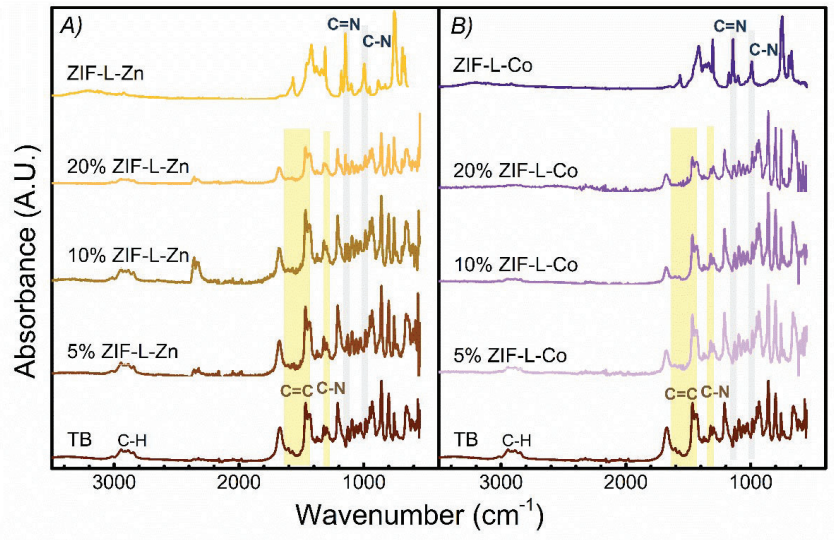

Figure 2 FTIR spectra of MMMs with different loading of A) ZIF-L-Zn and B) ZIF-L-Co.

XRD

In addition to the FTIR spectra, XRD results can provide valuable information for the MMMs containing crystalline particles. Generally, in XRD results, the sharp and narrow peaks imply higher crystallinity, while the broad and wide ones are usually associated with amorphous materials. In **Figure 3**, the neat TB polymer has two broad peaks at 5° – 30° and around 41°, which are the typical results for amorphous polymers. After the leaf ZIFs were introduced, some sharp and narrow peaks appear, and the intensities of these peaks continue to increase with further addition of ZIFs. Moreover, in the curves of the MMMs with low ZIFs loading, only a few peaks related to the ZIFs are clear, like those at 7.3° and 29.5 °, while with further increase in ZIF content, more peaks from the ZIFs can be observed, such as peaks at 10.4 °, 12.8 ° and 18.0 °. All these peaks can be found in the pattern of the neat leaf ZIFs. The ones at 7.3 ° and 18.0 ° are assigned with the (200) and (004) planes of leaf ZIFs [31]. These findings match the results of the FTIR analysis, implying that these leaf ZIFs have been blended into the polymeric matrix.

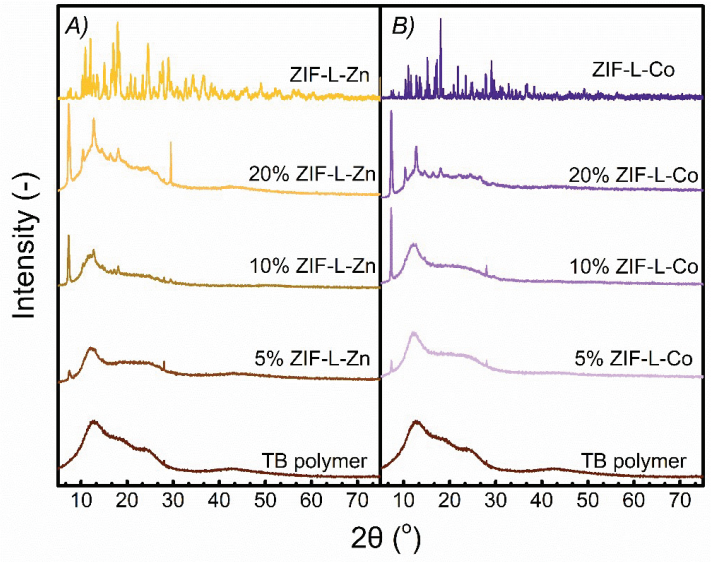

Figure 3 XRD results of MMMs with different loading of A) ZIF-L-Zn and B) ZIF-L-Co

SEM

In addition to the presence of the ZIFs, the dispersion of the ZIFs in the MMMs plays a great role on the final performance, which can be observed using the SEM. The surface and cross-section images of the MMMs with leaf ZIFs are displayed in **Figure 4**. The neat TB membrane (0% ZIFs) has a uniform and homogenous surface, as well as the cross-section, and no visible defects can be found. After adding leaf ZIFs, these presence of particles changes the morphology of the resultant membranes, making the surface and cross-section more heterogeneous. The leaf ZIFs are wrapped by the polymer chain in the membranes and have been found in the cross-section of the MMMs, even at low ZIF loading (as shown in **Figure 4(B)**). The dispersion of the ZIFs are quite homogenous in the membranes since no apparent aggregation has been found. Moreover, from the SEM images, no clear agglomeration has been detected, suggesting the relatively good compatibility between these leaf ZIFs and TB polymer.

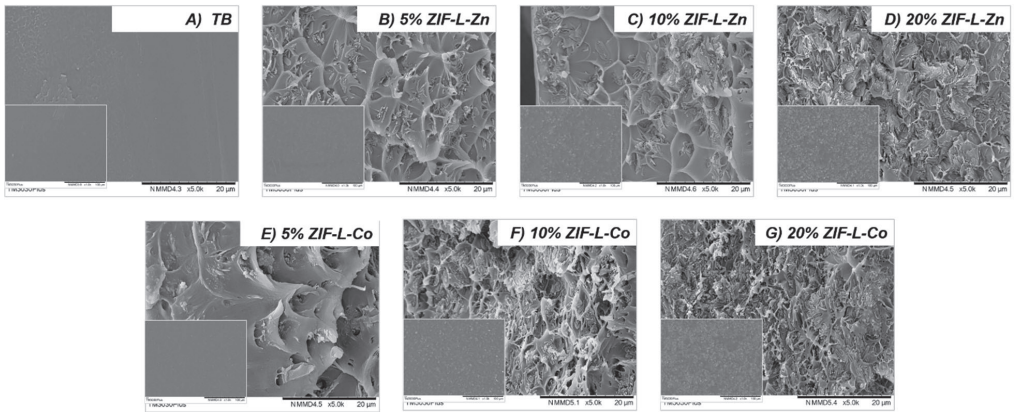

Figure 4 SEM images of MMMs containing A-D) ZIF-L-Zn and E-G) ZIF-L-Co.

TGA

The thermal stability of the membranes with leaf ZIFs was studied by TGA, and the results are displayed in **Figure 5**. For the neat TB polymer, a small amount of weight loss (< 2%) is observed at a low temperature range (R.T. to 100 ºC), mainly because of the remaining methanol. Afterwards, the mass remains constant until the temperature reaches ~ 400 ºC, denoting the superior thermal stability of the neat polymer. These MMMs have similar decomposition behavior to the neat polymer: a small weight loss at low temperature due to the remaining methanol, followed by a plateau (100 - 400 ºC) and then the steep slope starting around 400 ºC. The T_{onset} decreases with ZIF addition, due to the relative lower decomposition temperature of the ZIFs. However, the changes in T_{onset} are very small, especially for the one with 20 wt.% ZIFs. Considering that the first compound to decompose in ZIFs is the structural water, referring to the weight loss at 150 – 250 ºC, this enhanced thermal stability may be explained by the removal of structural water inside ZIFs during methanol immersion step, thus leading to an increase in T_{onset}.

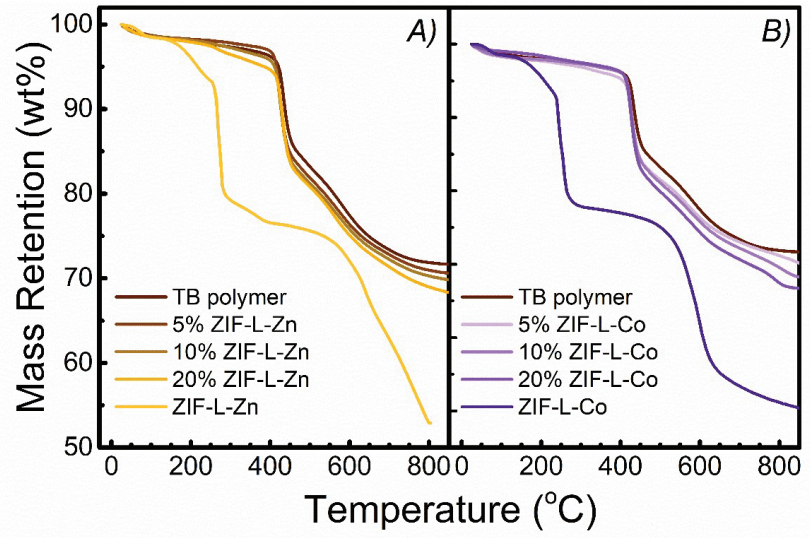

Figure 5 TGA results of MMMs with different loading of A) ZIF-L-Zn and B) ZIF-L-Co.

3.2.2. Gas permeation study

The effect of leaf ZIF loading

The gas separation performances of the MMMs containing leaf ZIFs were evaluated by single gas permeation tests at room temperature with a feed pressure of 2 bar. The gas permeabilities of the membranes with various ZIFs loading are presented in **Figure 6**. The neat polymeric membrane has a H_2 and CO_2 permeability of 290.2 and 148.3 Barrer, respectively, in agreement with the values reported in the literature [20]. With the addition of leaf ZIFs, the permeabilities of all investigated gases increase monotonously with ZIF loading. For instance, the addition of ZIF-L-Co (20 wt.%) leads to a 326% and a 272% increase in H_2 (1235.5 Barrer) and CO_2 permeability (551.6 Barrer), respectively. This significant increment in gas permeability is mainly contributed by the lamellar structure inside these leaf-like ZIFs [25]. Theoretically, the lamellar gaps in 2D ZIFs work as fast shortcuts for those gases small enough to pass through, while for the bulky gases, roundabout pathways must be taken to detour these barriers. As a result, the enhancement in permeability should be negatively related to the gas size, which means smaller gases, like H_2 (2.89 Å) and CO_2 (3.3 Å), benefit more from the addition of leaf ZIFs than N_2 (3.64 Å) or CH_4 (3.8 Å) [23]. This explains the large enhancement in H_2 and CO_2 permeability. However, the permeation results follow the opposite trend. The increment in permeability for larger gases is higher than that

for their smaller counterparts. For example, still for membranes with 20 wt.% ZIF-L-Co, 7.5-fold and 8.1-fold increments in N_2 and CH_4 permeability are observed, respectively. These results imply the presence of micro-void between the fillers and the polymeric matrix, and the nonselective pathway leads to decreased selectivities, as shown in **Figure 7**. The H_2/N_2 and H_2/CH_4 selectivities decrease from 49 to 27 and 50 to 25, respectively, in the presence of 20 wt.% ZIF-L-Co. For CO_2/N_2 and CO_2/CH_4 selectivities, the values decrease by around 50 %, from 24 to 12 and 25 to 11, respectively, while for H_2/CO_2 pair, both gases have similar transport mechanisms, so the selectivity remains almost unchanged.

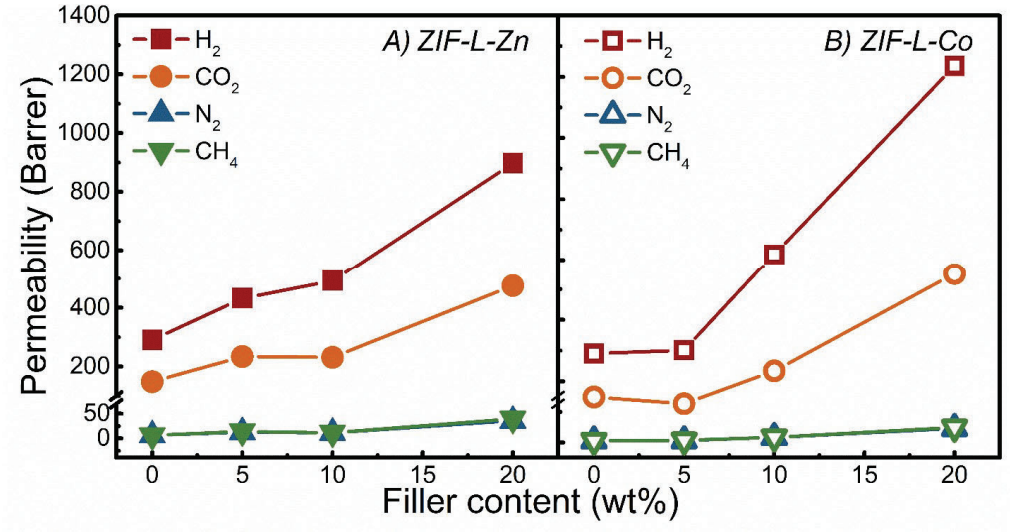

Figure 6 Gas permeabilities of MMMs with different loading of A) ZIF-L-Zn and B) ZIF-L-Co.

It is well known that, in addition to the filler content, different ZIFs in MMMs will lead to different gas separation performances, mainly due to the different crystal structure, the chemical nature, the interaction with gas species and the compatibility with the polymeric matrix. In this work, although both leaf ZIFs have identical crystal structure and similar chemical compositions, there still exists some difference between the gas separation performance of MMMs containing ZIF-L-Zn and that of those containing ZIF-L-Co. For all gases, the permeabilities of membranes with ZIF-L-Co are obviously higher than those of membranes containing ZIF-L-Zn. For instance, the membrane containing 20 wt.% ZIF-L-Zn only has H_2 and CO_2 permeabilities of 897.5 and 475.4 Barrer, respectively. MMMs with the same amount of ZIF-L-Co display a H_2 and CO_2 permeabilities of 1235.5 and 551.6 Barrer, which is 37% and 16% higher than the MMM with Zn-based ZIF,

respectively. These increments in gas permeability of MMMs may be explained by the interlay channels existing in these 2D leaf-like ZIFs, working as shortcuts for transport of small molecules through the membranes [23, 25, 32]. The higher gas permeability of the MMMs containing ZIF-L-Co may be explained by several factors. First, despite the same crystal structure and organic linker, the Co-N bonding is stiffer than Zn-N bonds, and thus results in a more rigid framework and smaller aperture (3.3 Å of ZIF-67 compared with 3.4 Å of ZIF-8) [33]. Hence, the pores of the molecular sieve of Co-based ZIFs is smaller than that of Zn-based ZIFs, promoting more benefits for H_2 and CO_2. Moreover, it has been reported that the interactions between CO_2 and Zn^{2+} are stronger than those between CO_2 and Co^{2+}, and hence slow down CO_2 transport inside the MMMs containing ZIF-L-Zn, as reported in a very recent work [34]. On the other hand, there are far less differences in the effects of the addition of these two ZIFs on gas selectivities. The membranes with ZIF-L-Co display slightly higher, or almost same, selectivities for all investigated gas pairs than the ones with ZIF-L-Zn, suggesting that the differences in the chemical compositions of leaf ZIFs have little effects on the N_2 or CH_4 permeabilites. These results suggest that the N_2 or CH_4 diffuse mainly through the polymeric matrix; therefore, the microstructure of ZIFs has negligible influences on their permeabilites.

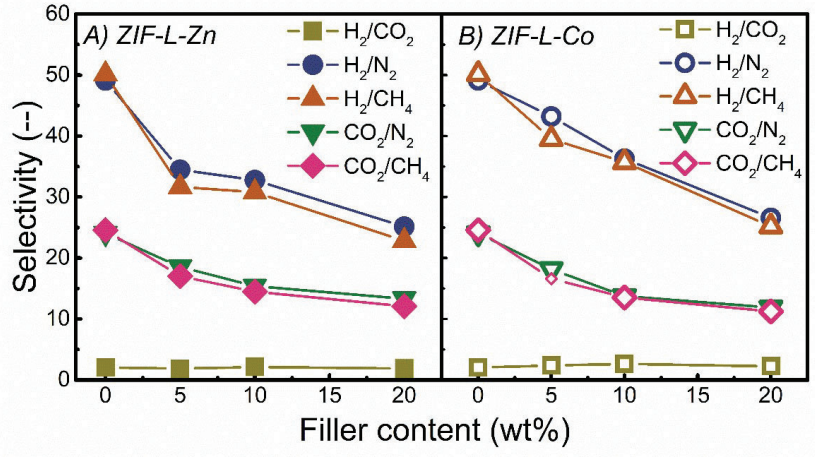

Figure 7 Gas selectivities of TB + A) ZIF-L-Zn and B) ZIF-L-Co membranes with a function of filler content

To confirm these speculations, the diffusivity and solubility of these MMMs were calculated, and are presented in **Figure 8** and **9**, respectively. Because of the extremely fast transport, the time-lag curves of H_2 are unnoticeable, and hence the related results are not included here. For the other

gases, increased gas diffusivities are observed with the addition of both leaf-like ZIFs. But the ZIF-L-Co brings about larger increment in the diffusivities of these gases (i.e., CO_2, N_2, and CH_4), especially CO_2, compared with ZIF-L-Zn. However, there are less obvious differences in the effects of adding these two ZIFs on the solubility of the gases. The added ZIF-Ls generally decrease the solubility, but these changes are much less compared with the changes in gas diffusion. These results suggest that the main reason for higher gas permeability of MMMs with ZIF-L-Co is the greatly enhanced diffusivity, which agrees with previous discussion. However, considering that the sizes of N_2 and CH_4 are larger than the pore size of the ZIF-L-Co, higher diffusivities of N_2 and CH_4 were found in TB + ZIF-L-Co membranes than in TB + ZIF-L-Zn membranes. This may be explained by the gate-opening effects [21, 35, 36], which assumes that these MOFs are flexible and would allow some of the large molecules to pass through, in agreement with the fact that the increment in CH_4 diffusivity is less than the gains of N_2 diffusivity.

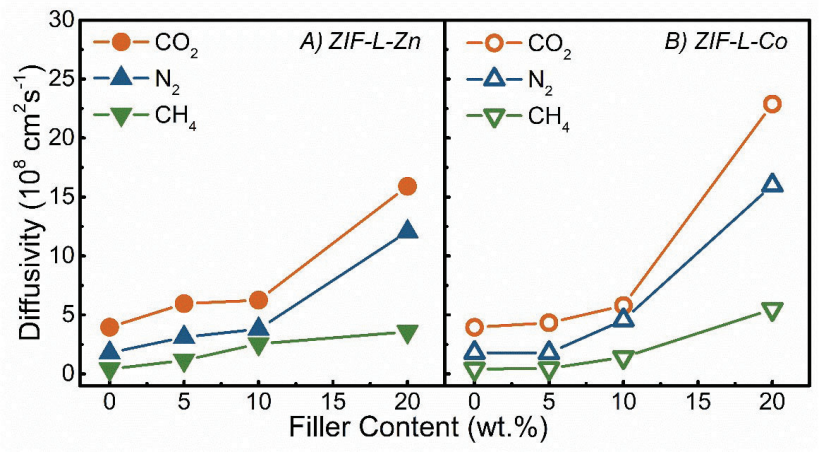

Figure 8 Gas diffusivity of TB + A) ZIF-L-Zn and B) ZIF-L-Co membranes with a function of filler content

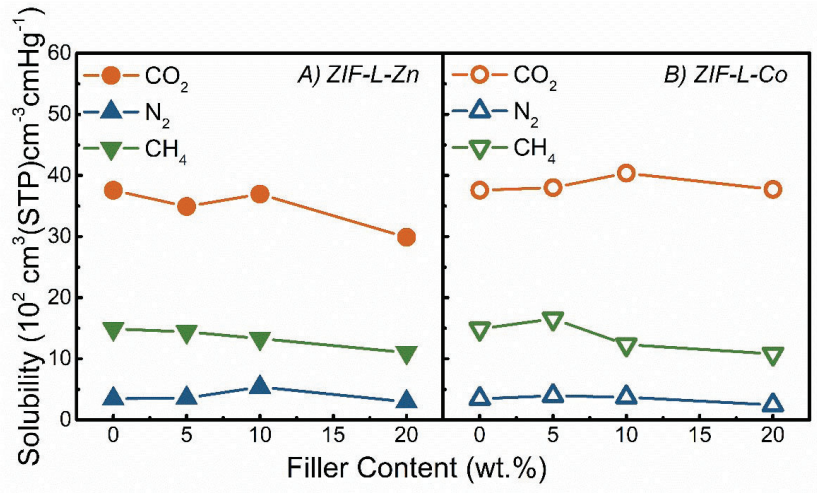

Figure 9 Gas solubility of TB + A) ZIF-L-Zn and B) ZIF-L-Co membranes with a function of filler content

The effect of operating temperature

The ability to efficiently separate gas mixture at relatively high temperature is of great value to some applications, especially for hydrogen separation, which can greatly reduce energy consumption. Moreover, increasing operating temperature usually results in an enhancement in gas diffusivity and thus gas permeability. Due to the high gas permeabilities, the membrane with 20 wt.% ZIF-L-Co was chosen to investigate the effect of temperature.

The permeabilities of all the gases increase greatly with temperature for TB + 20 wt.% ZIF-L-Co membrane, as shown in **Figure 10 (A)**, and this is a typical behavior of diffusion-dominated gas transport in the membrane. At 60 °C, the H_2 permeability increases to 1985.9 Barrer, which is 161% of the value obtained at room temperature. It is worth mentioning that the effect of temperature on gas permeability of TB polymer was studied by Fan *et al*., and the results revealed that an increment of ~ 120 % was obtained [20]. Therefore, it is believed that the high value obtained in the present study was mainly because of the fast transport channel brought about by the leaf ZIF-L-Co. All of the gas selectivities in the same work reported by Fan *et al*. decrease with increasing temperature, except for H_2/CO_2 selectivity which showed a marginal increase [20]. Neat TB polymer only retains around 65 – 84 % of selectivities of these gas pairs at 65 °C, compared with the values at 35 °C [20]. A similar trend has been observed in our case; selectivities of almost all the gas pairs decreased as temperature increased from RT to 60 °C. The activation energy of gas

permeabilities (E_p), shown in **Table 1**, was calculated using Arrhenius equation. The E_p is composed of two parts: the activation energy of diffusion (E_d) and the heat of sorption (H_s), which are usually positive and negative in value, respectively. Hence, the positive E_p means that E_d is higher than H_s. Moreover, the activation energy increases with the kinetic diameter of gases, signifying that the larger molecules obtain more benefits from the increased temperature, and that explains the decreased selectivities.

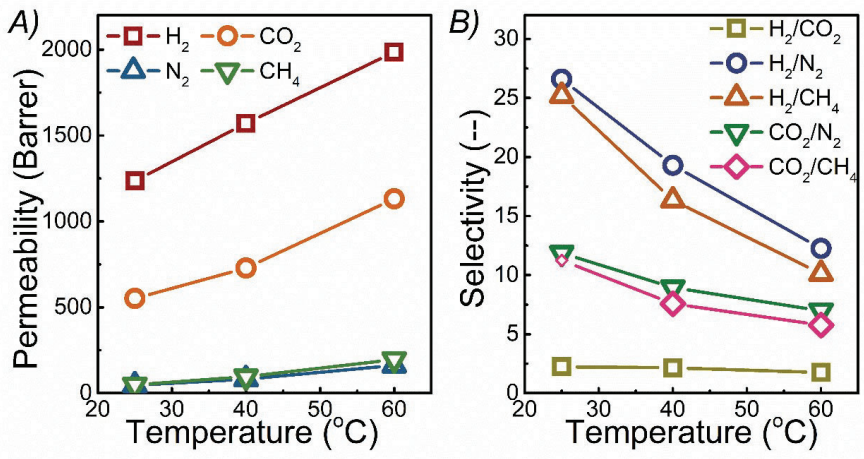

Figure 10 A) Gas permeabilities and B) selectivities of TB + 20% ZIF-L-Co as a function of operating temperature

Table 1 Activation energy of permeability of the different gases in TB + 20 % ZIF-L-Co membranes.

Gas	H_2	CO_2	N_2	CH_4
E_p (kJ/mol)	11.2	17.0	28.8	32.6

Comparison with the Upper Bounds

The Robeson Upper Bounds have been widely used as benchmarks for the newly developed membrane materials. The gas separation performances of each membrane obtained in this work have been compared with the corresponding Upper Bounds, as shown in **Figure 11**, as well as the performances of some representative MMMs, as presented in **Table 2**. As discussed previously, the addition of leaf ZIFs results in enhanced gas permeability and reduced selectivities. Therefore, in all figures, the data points move to the bottom right corner with increasing ZIF content or operating temperature. Despite the decreased selectivity, the TB + ZIF-L-Zn membranes seem to

be more promising for H_2 separation applications (e.g., H_2/CO_2, H_2/CH_4, and H_2/N_2), since all obtained H_2 separation performances are close to or even surpassed the Upper Bounds, while for CO_2 separation applications, even though a rather high CO_2 permeability was obtained, the relatively low CO_2/N_2 and CO_2/CH_4 selectivities (10 ~ 20) result in separation performance lower than the Upper Bounds.

Another interesting finding in this study is that the MMMs with ZIF-L-Co are more efficient in H_2 separation than MMMs with ZIF-L-Zn because they have both higher H_2 permeability and selectivity. However, for CO_2 separation, this difference is almost negligible.

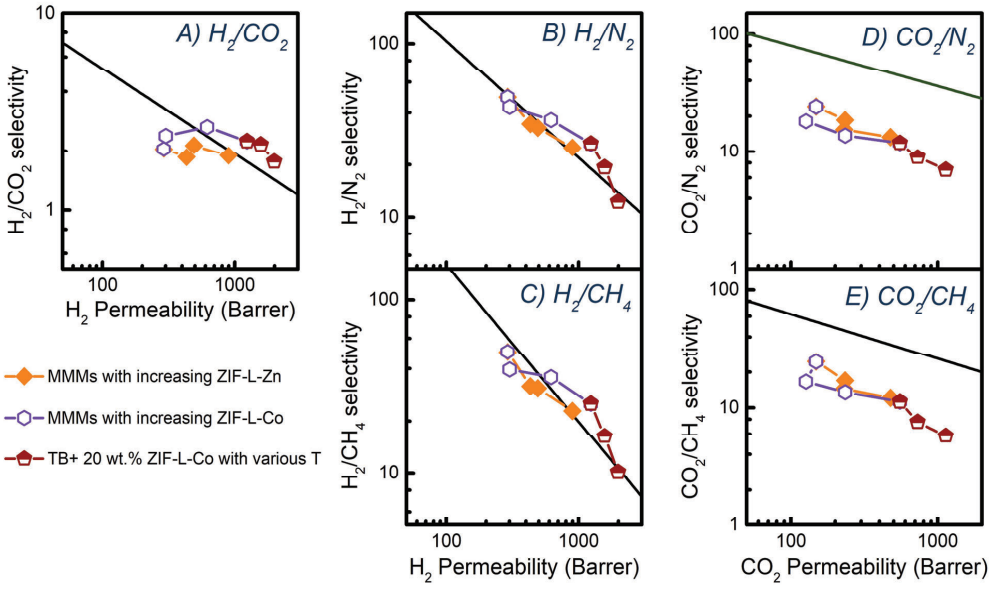

Figure 11. Comparison of the pure gas permeation results of the MMMs in this work with the Robeson Upper Bounds (2008).

Table 2. H_2 separation or CO_2 separation of relevant mixed matrix membranes reported in literature

Membranes	Permeability (Barrer)		Selectivity (--)					Reference
	H_2	CO_2	H_2/CO_2	H_2/N_2	H_2/CH_4	CO_2/N_2	CO_2/CH_4	
6FDA-DAM + 20 wt% ZIF-11 [a]	272.4	-	1.1	-	32.8	-	-	[37]
PIM-1 + 30 wt.% ZIF-8 [b]	5456	6424	0.8	17.9	14.8	21.1	17.4	[22]

TOX-PIM-1 + 20 wt.% ZIF-8 [b]	3465	3944	0.9	24.9	23.6	28.3	26.8	
PIM-1 + 40 wt.% SiO_2 [b]	5544	8505	0.6	9.5	6.7	14.6	10.2	
TOX- PIM-1 + 20 wt.% SiO_2 [b]	2816	2615	1.1	28	35	26.0	32.5	
Matrimid + 15 wt% ZIF-11 [c]	535	-	9.1	-	-	-	-	[38]
6FDA-DAM + 8 wt% Mg-MSS [d]	794	1214 (CO_2/N_2) 1245 (CO_2/CH_4)	-	-	21.8	24.4	31.5	[39]
6FDA-Durene + 10 wt.% ZIF-71 [e]	540	-	62.5	-	-	-	-	[21]
6FDA-DAM/HAB + 20 wt% ZIF-L [f]	260	19.4	13.4	41.4	61.6	3.1	4.6	[23]
TB-PI + 30 wt.% ZIF-8 [g]	2585	1437	1.8	22	28	12	16	[24]
TB-PI + 30 wt.% PD@ZIF-8 [g]	1858	1056	4.3	27	36	14	20	
PBI 58 wt.% Pd [h]	66	-	33	-	-	-	-	[40]
TB + 20 wt% ZIF-L-Zn [j]	897.5	475.4	1.9	25	23	13	12	
TB + 20 wt% ZIF-L-Co [j]	1235.5	551.6	2.2	27	25	12	11	This work
TB + 20 wt% ZIF-L-Co [j]	1985.9	1131.5	1.8	12	10	7	6	

[a]: single gas permeation test, feed pressure: 4 bar, 30 ºC

[b]: single gas permeation test, feed pressure: 4 bar, 22 ºC

[c]: mixed gas permeation test, feed: H_2/CO_2 (25/75 vol), 3.3 bar; sweep: Ar, 1.24 bar; 200 ºC

[d]: Mg-MSS: Grignard surface functionalized mesoporous silica MCM-41 spheres; mixed gas permeation test, feed: 50/50 vol for all gas pair, 3.0 bar; sweep: Ar or He, 1.0 bar; 35 ºC

[e]: mixed gas permeation test, feed: H_2/CO_2 (50/50 vol), 7 atm; vacuum; 35°C- 150°C.

[f]: single gas permeation test, feed pressure: 1 bar, room temperature

[g]: single gas permeation test, feed pressure: 1 bar, 35 ºC

[h]: mixed gas permeation test, feed: H_2/CO_2 (50/50), 10 bar; sweep: N_2, 1 bar; 200 ºC

[j]: single gas permeation test, feed pressure: 2 bar, room temperature

4 Conclusions

In this work, a series of heterocyclic TB-based polymeric membranes, with two 2D leaf ZIFs (ZIF-L-Zn and ZIF-L-Co) incorporated, have been fabricated and systematically studied using various characterization methods. The relevant characterization results show that both leaf ZIFs have good compatibility with the TB membranes. In addition, all resultant MMMs have excellent thermal stability.

The incorporation of 2D leaf ZIFs results in great enhancement in gas permeabilities for all investigated gases. The addition of 20 wt.% ZIF-L-Co brings about a highly permeable membrane with H_2 and CO_2 permeability of 1235.5 Barrer and 551.6 Barrer, respectively, which are 4.3 times and 3.7 times of the corresponding gas permeabilities in the neat polymeric membranes. It has also been noticed that the metal centers of the ZIFs could affect their microstructure and therefore the gas transport properties of the resultant MMMs. The Co-based ZIF results in larger increments in gas permeabilites without sacrificing the selectivities, especially for H_2, the smallest gas studied in this work, compared with the Zn-based ZIF. Due to the largely increased H_2 permeability, all MMMs fabricated using both ZIFs exhibited H_2 separation performances close to or surpassing the 2008 Robeson Upper Bounds.

The effects of operating temperature (R.T. to 60 ^oC) on the gas transport properties of the MMMs with 20% ZIF-L-Co were also evaluated. The increasing temperature could further raise the gas permeabilites: at 60 ^oC, the H_2 permeability reaches 1985.9 Barrer, which is 684% of the values of the neat polymer. In view of the economic consideration and previous process simulation analysis, these highly permeable membranes with moderate selectivity may be an excellent candidate for some industrial applications.

Overall, this work reveals that the metal centers of the ZIFs affect not only the material properties, but also the gas separation performances of the resulting MMMs. Hence, more in-depth studies related to the effects of the chemical structures, especially the metal ions, of the ZIFs on the gas separation performance of the corresponding MMMs are worth undertaking, from which the ZIFs with better gas separation performances could be developed.

Conflicts of interest

There are no conflicts to declare.

Acknowledgements

This work is supported by the Research Council of Norway through the CLIMIT program ("POLYMEM" project, No. 254791). The authors highly acknowledge Dr. Weixin Qian (School of Chemical Engineering, East China University of Science and Technology) for the kind help in N_2 adsorption characterization.

References

[1] J.A. Turner, Sustainable Hydrogen Production, Science, 305 (2004) 972.
[2] H. Lin, Z. He, Z. Sun, J. Vu, A. Ng, M. Mohammed, J. Kniep, T.C. Merkel, T. Wu, R.C. Lambrecht, CO_2-selective membranes for hydrogen production and CO_2 capture – Part I: Membrane development, J. Membr. Sci., 457 (2014) 149-161.
[3] P. Li, Z. Wang, Z. Qiao, Y. Liu, X. Cao, W. Li, J. Wang, S. Wang, Recent developments in membranes for efficient hydrogen purification, J. Membr. Sci., 495 (2015) 130-168.
[4] Hydrogen Generation Market Size, Share & Trends Analysis Report By Application (Coal Gasification, Steam Methane Reforming), By Technology, By System (Merchant, Captive), And Segment Forecasts, 2018 - 2025, in, Grand View Research, Inc., 2018.
[5] M. Omidvar, C.M. Stafford, H. Lin, Thermally stable cross-linked P84 with superior membrane H_2/CO_2 separation properties at 100 °C, J. Membr. Sci., 575 (2019) 118-125.
[6] W. Mei, Y. Du, T. Wu, F. Gao, B. Wang, J. Duan, J. Zhou, R. Zhou, High-flux CHA zeolite membranes for H_2 separations, J. Membr. Sci., 565 (2018) 358-369.
[7] A. Naderi, A. Asadi Tashvigh, T.-S. Chung, H_2/CO_2 separation enhancement via chemical modification of polybenzimidazole nanostructure, J. Membr. Sci., 572 (2019) 343-349.
[8] S. Thomas, I. Pinnau, N. Du, M.D. Guiver, Pure- and mixed-gas permeation properties of a microporous spirobisindane-based ladder polymer (PIM-1), J. Membr. Sci., 333 (2009) 125-131.
[9] L.M. Robeson, The upper bound revisited, J. Membr. Sci., 320 (2008) 390-400.
[10] Y.B. Zhuang, J.G. Seong, Y.M. Lee, Polyimides containing aliphatic/alicyclic segments in the main chains, Prog. Polym. Sci., 92 (2019) 35-88.
[11] P.M. Budd, B.S. Ghanem, S. Makhseed, N.B. McKeown, K.J. Msayib, C.E. Tattershall, Polymers of intrinsic microporosity (PIMs): robust, solution-processable, organic nanoporous materials, Chem. Commun., (2004) 230-231.
[12] Z.X. Low, P.M. Budd, N.B. McKeown, D.A. Patterson, Gas Permeation Properties, Physical Aging, and Its Mitigation in High Free Volume Glassy Polymers, Chem. Rev., 118 (2018) 5871-5911.
[13] M. Carta, R. Malpass-Evans, M. Croad, Y. Rogan, J.C. Jansen, P. Bernardo, F. Bazzarelli, N.B. McKeown, An efficient polymer molecular sieve for membrane gas separations, Science, 339 (2013) 303-307.
[14] Z.G. Wang, X. Liu, D. Wang, J. Jin, Troger's base-based copolymers with intrinsic microporosity for CO2 separation and effect of Troger's base on separation performance, Polym. Chem., 5 (2014) 2793-2800.
[15] Z.G. Wang, D. Wang, F. Zhang, J. Jin, Troger's Base-Based Microporous Polyimide Membranes for High-Performance Gas Separation, Acs Macro Lett., 3 (2014) 597-601.
[16] J.G. Seong, Y.B. Zhuang, S. Kim, Y.S. Do, W.H. Lee, M.D. Guiver, Y.M. Lee, Effect of methanol treatment on gas sorption and transport behavior of intrinsically microporous polyimide membranes incorporating Troger's base, J. Membr. Sci., 480 (2015) 104-114.
[17] Y. Zhuang, J.G. Seong, Y.S. Do, W.H. Lee, M.J. Lee, M.D. Guiver, Y.M. Lee, High-strength, soluble polyimide membranes incorporating Troger's Base for gas separation, J. Membr. Sci., 504 (2016) 55-65.
[18] Y. Zhuang, J.G. Seong, Y.S. Do, W.H. Lee, M.J. Lee, Z. Cui, A.E. Lozano, M.D. Guiver, Y.M. Lee, Soluble, microporous, Troger's Base copolyimides with tunable membrane performance for gas separation, Chem. Commun., 52 (2016) 3817-3820.
[19] S.S. Zhao, J.Y. Liao, D.F. Li, X.D. Wang, N.W. Li, Blending of compatible polymer of intrinsic microporosity (PIM-1) with Troger's Base polymer for gas separation membranes, J. Membr. Sci., 566 (2018) 77-86.

[20] Y.F. Fan, C. Li, X.S. Zhang, X.M. Yang, X.Y. Su, H.M. Ye, N.W. Li, Troger's base mixed matrix membranes for gas separation incorporating NH_2-MIL-53(Al) nanocrystals, J. Membr. Sci., 573 (2019) 359-369.
[21] S. Japip, K.-S. Liao, T.-S. Chung, Molecularly Tuned Free Volume of Vapor Cross-Linked 6FDA-Durene/ZIF-71 MMMs for H2/CO2 Separation at 150 °C, Adv. Mater., 29 (2017) 1603833.
[22] Q. Song, S. Cao, R.H. Pritchard, H. Qiblawey, E.M. Terentjev, A.K. Cheetham, E. Sivaniah, Nanofiller-tuned microporous polymer molecular sieves for energy and environmental processes, J. Mater. Chem. A, 4 (2016) 270-279.
[23] S. Kim, E. Shamsaei, X. Lin, Y. Hu, G.P. Simon, J.G. Seong, J.S. Kim, W.H. Lee, Y.M. Lee, H. Wang, The enhanced hydrogen separation performance of mixed matrix membranes by incorporation of two-dimensional ZIF-L into polyimide containing hydroxyl group, J. Membr. Sci., 549 (2018) 260-266.
[24] Z. Wang, D. Wang, S. Zhang, L. Hu, J. Jin, Interfacial Design of Mixed Matrix Membranes for Improved Gas Separation Performance, Adv. Mater., 28 (2016) 3399-3405.
[25] R. Chen, J. Yao, Q. Gu, S. Smeets, C. Baerlocher, H. Gu, D. Zhu, W. Morris, O.M. Yaghi, H. Wang, A two-dimensional zeolitic imidazolate framework with a cushion-shaped cavity for CO_2 adsorption, Chem. Commun., 49 (2013) 9500-9502.
[26] Y. Lo, C.H. Lam, C.-W. Chang, A.-C. Yang, D.-Y. Kang, Polymorphism/pseudopolymorphism of metal–organic frameworks composed of zinc (II) and 2-methylimidazole: synthesis, stability, and application in gas storage, RSC Adv., 6 (2016) 89148-89156.
[27] A.M. Nasir, N.A.H. Md Nordin, P.S. Goh, A.F. Ismail, Application of two-dimensional leaf-shaped zeolitic imidazolate framework (2D ZIF-L) as arsenite adsorbent: Kinetic, isotherm and mechanism, J. Mol. Liq., 250 (2018) 269-277.
[28] X. Li, Z. Li, L. Lu, L. Huang, L. Xiang, J. Shen, S. Liu, D.R. Xiao, The Solvent Induced Inter-Dimensional Phase Transformations of Cobalt Zeolitic-Imidazolate Frameworks, Chem. Eur. J., 23 (2017) 10638-10643.
[29] Z.-X. Low, J. Yao, Q. Liu, M. He, Z. Wang, A.K. Suresh, J. Bellare, H. Wang, Crystal transformation in zeolitic-imidazolate framework, Cryst. Growth Des., 14 (2014) 6589-6598.
[30] Y. Cui, Y. Liu, J. Liu, J. Du, Y. Yu, S. Wang, Z. Liang, J. Yu, Multifunctional porous Tröger's base polymers with tetraphenylethene units: CO_2 adsorption, luminescence and sensing properties, Polym. Chem., 8 (2017) 4842-4848.
[31] H. Mao, H.-G. Zhen, A. Ahmad, S.-H. Li, Y. Liang, J.-F. Ding, Y. Wu, L.-Z. Li, Z.-P. Zhao, Highly selective and robust PDMS mixed matrix membranes by embedding two-dimensional ZIF-L for alcohol permselective pervaporation, J. Membr. Sci., 582 (2019) 307-321.
[32] J. Shen, G. Liu, K. Huang, W. Jin, K.-R. Lee, N. Xu, Membranes with Fast and Selective Gas-Transport Channels of Laminar Graphene Oxide for Efficient CO_2 Capture, Angew. Chem., 127 (2015) 588-592.
[33] P. Krokidas, M. Castier, I.G. Economou, Computational study of ZIF-8 and ZIF-67 performance for separation of gas mixtures, The Journal of Physical Chemistry C, 121 (2017) 17999-18011.
[34] S. Meshkat, S. Kaliaguine, D. Rodrigue, Comparison between ZIF-67 and ZIF-8 in Pebax® MH-1657 mixed matrix membranes for CO_2 separation, Sep. Purif. Technol., 235 (2020) 116150.
[35] D. Fairen-Jimenez, S.A. Moggach, M.T. Wharmby, P.A. Wright, S. Parsons, T. Düren, Opening the Gate: Framework Flexibility in ZIF-8 Explored by Experiments and Simulations, J. Am. Chem. Soc., 133 (2011) 8900-8902.
[36] L. Zhang, Z. Hu, J. Jiang, Sorption-Induced Structural Transition of Zeolitic Imidazolate Framework-8: A Hybrid Molecular Simulation Study, J. Am. Chem. Soc., 135 (2013) 3722-3728.
[37] M. Safak Boroglu, A.B. Yumru, Gas separation performance of 6FDA-DAM-ZIF-11 mixed-matrix membranes for H_2/CH_4 and CO_2/CH_4 separation, Sep. Purif. Technol., 173 (2017) 269-279.
[38] J. Sánchez-Laínez, B. Zornoza, Á. Mayoral, Á. Berenguer-Murcia, D. Cazorla-Amorós, C. Téllez, J. Coronas, Beyond the H_2/CO_2 upper bound: one-step crystallization and separation of nano-sized ZIF-11 by centrifugation and its application in mixed matrix membranes, J. Mater. Chem. A, 3 (2015) 6549-6556.
[39] B. Zornoza, C. Téllez, J. Coronas, O. Esekhile, W.J. Koros, Mixed matrix membranes based on 6FDA polyimide with silica and zeolite microsphere dispersed phases, AlChE J., 61 (2015) 4481-4490.
[40] L. Zhu, D. Yin, Y. Qin, S. Konda, S. Zhang, A. Zhu, S. Liu, T. Xu, M.T. Swihart, H. Lin, Sorption-Enhanced Mixed Matrix Membranes with Facilitated Hydrogen Transport for Hydrogen Purification and CO2 Capture, Adv. Funct. Mater., 29 (2019) 1904357.